Instituto de Geociências
Programa de Pós-Graduação em Geociências

**UNIVERSIDADE FEDERAL DO RIO GRANDE DO SUL**
**INSTITUTO DE GEOCIÊNCIAS**
**PROGRAMA DE PÓS-GRADUAÇÃO EM GEOCIÊNCIAS**

# EVOLUÇÃO GEOTECTÔNICA DOS COMPLEXOS VILA NOVA E TUMUCUMAQUE NA PORÇÃO NORDESTE DO CRÁTON AMAZÔNICO, AMAPÁ

CRISTIANO BORGHETTI

ORIENTADOR – Prof. Dr. Ruy Paulo Philipp

Porto Alegre – 2018

Programa de Pós-Graduação em Geociências - UFRGS
Av. Bento Gonçalves 9500 - Agronomia - Cx. P. 15.001 - Prédio 43.113 S-207B - 91509-900 - Porto Alegre - RS
Tel.: (051) 316-6340 Ramais 6340/6332 FAX: (051) 316-6340
E-mail: ppggeo@ufrgs.br

**UNIVERSIDADE FEDERAL DO RIO GRANDE DO SUL**
**INSTITUTO DE GEOCIÊNCIAS**
**PROGRAMA DE PÓS-GRADUAÇÃO EM GEOCIÊNCIAS**

# EVOLUÇÃO GEOTECTÔNICA DOS COMPLEXOS VILA NOVA E TUMUCUMAQUE NA PORÇÃO NORDESTE DO CRÁTON AMAZÔNICO, AMAPÁ

CRISTIANO BORGHETTI

ORIENTADOR – Prof. Dr. Ruy Paulo Philipp

BANCA EXAMINADORA
Prof. Dr. Edinei Koester - Instituto de Geociências, Universidade Federal do Rio Grande do Sul (UFRGS)
Prof. Dr. Marcos V.D. Remus - Instituto de Geociências, Universidade Federal do Rio Grande do Sul (UFRGS)
Prof. Dr. Wilson Teixeira - Instituto de Geociências, Universidade de São Paulo (USP)

Tese de Doutorado apresentada como
requisito parcial para a obtenção do
Título de Doutor em Ciências

Porto Alegre – 2018

Borghetti, Cristiano

Evolução geotectônica dos Complexos Vila Nova e Tumucumaque na porção nordeste do Cráton Amazônico, Amapá. / Cristiano Borghetti. - Porto Alegre: IGEO/UFRGS, 2018.
[211 f.] il.

Tese (Doutorado). - Universidade Federal do Rio Grande do Sul. Programa de Pós-Graduação em Geociências. Instituto de Geociências. Porto Alegre, RS - BR, 2018.

Orientador: Ruy Paulo Philipp

1. Geocronologia U-Pb. 2. Paleoproterozóico. 3. Evolução Crustal. 4. Arqueano. I. Título.

CDU 551.24

Catalogação na Publicação
Biblioteca Instituto de Geociências - UFRGS
Sônia Teresinha Duarte de Oliveira CRB 10/2310

Universidade Federal do Rio Grande do Sul - Campus do Vale Av. Bento Gonçalves, 9500 - Porto Alegre - RS - Brasil
CEP: 91501-970 / Caixa Postal: 15001.
Fone: +55 51 3308-6329 Fax: +55 51 3308-6337
E-mail: bibgeo@ufrgs.br

**AGRADECIMENTOS**

Agradeço a minha Família pela presença e apoio. Ao meu orientador Prof. Dr. Ruy Paulo Philipp, pela dedicação, empenho e paciência no direcionamento deste trabalho. Ao Programa de Pós-Graduação em Geociências do Instituto de Geociências da UFRGS e a PETROBRÁS pelo acolhimento e amparo deste projeto. Ao Prof. Dr. Miguel A.S. Basei, aos geólogos Heiny Paim Kloss e Gustavo Zvirtes pelo auxílio nas análises geocronológicas. A geóloga Itiana Hoffmann pela análise petrográfica e geoquímica das rochas do Complexo Vila Nova. Aos técnicos do Centro de Pesquisas Geocronológicas (CEPEGEO) do Instituto de Geociências da Universidade de São Paulo, Walter Maurício Sproesser e Solange Lucena de Souza pela cooperação na obtenção das análises geocronológicas. A Mineração Amapari SA pelo suporte e fornecimento de dados. Agradeço também a todos que ajudaram de alguma maneira na realização deste trabalho.

**RESUMO**

Esta tese investigou as relações estratigráficas entre as rochas metavulcano-sedimentares do Complexo Vila Nova (CVN) e os ortognaisses do Complexo Tumucumaque (CT) na região da Vila Nova, Amapá. As relações entre os complexos foram definidas através do mapeamento geológico e estrutural integrado com dados geofísicos (aeromagnetometria e aerogamaespectroscopia), análise petrográfica e geocronologia. O CVN é uma sequencia do tipo *greenstone belt* localizada na porção sudeste do Escudo das Guianas, nordeste do Cráton Amazônico. Esta região está inserida na Província Maroni-Itacaiúnas, cinturão móvel paleoproterozóico que circunda o núcleo arqueano da Província Amazônia Central. A integração dos dados permitiu definir as principais unidades litológicas e estruturas, que foram representadas nos mapas geológicos nas escalas 1:100.000 e 1:50.000. As relações estratigráficas foram suportadas por análises geocronológicas pelos métodos U-Pb e Lu-Hf em zircão através da técnica de LA-ICP-MS, aplicada em zircões detríticos de metassedimentos do CVN e em cristais ígneos de rochas dos Complexos Vila Nova e Tumucumaque. O contato entre os complexos são definidos por zonas de cisalhamentos dúcteis. O CVN é composto por metassedimentos clásticos intercalados com metabasaltos e meta-andesitos, contendo camadas subordinadas de formações ferríferas e manganesíferas, xistos calci-silicáticos e mármores. Estas unidades foram afetadas por um metamorfismo orogênico sob condições de baixo a médio grau, entre as fácies Xistos Verdes Superior e Anfibolito Médio, sob pressão intermediária. O CT é constituído por gnaisses tonalíticos a granodioríticos, anfibolitos, metagranitóides e gabros intrusivos, com registro metamórfico entre a fácies Anfibolito Médio a Superior. Levantamentos estruturais sugerem que os complexos foram afetados pelos mesmos processos de deformação e metamorfismo, que resultaram em uma foliação regional $S_{1-2}$ orientada segundo a direção N70-85ºW. Esta foliação está afetada por uma fase de deformação mais tardia, que gerou dobras $F_3$ de escala regional e com formas abertas a fechadas, e com eixos direcionados segundo a direção NW-SE. Os zircões detríticos dos metassedimentos do CVN apresentaram idades arqueanas (entre 3.6 e 2.7 Ga), com participação muito subordinada de idades paleoproterozóicas (entre 2.5 e 2.37 Ga). As idades Neo- a Meso-arqueanas, entre 2.85 e 2.67 Ga, foram identificadas em ortognaisses e gabros do CT, enquanto idades Paleoarqueanas, entre 3.0 e 3.5 Ga, foram descritas em ortognaisses das regiões de Tartarugalzinho (3.48 Ga) e da Vila Nova (3.3 Ga). Os resultados U-Pb das amostras do CT apontam para dois

episódios magmáticos, um Meso-arqueano (2.85-2.81Ga) e um Neo-arqueano (2.67 Ga). Os dados de Lu-Hf também confirmam a existência de uma ampla área de embasamento Arqueano na região estudada. A idade máxima de deposição da bacia é definida pela idade de 2.170 ±9 Ma, representando a cristalização dos metandesitos do CVN. As rochas metavulcânicas do *greenstone belt* Vila Nova foram depositadas durante o Riaciano sobre um embasamento arqueano e apresentam composição geoquímica semelhante a das rochas de arcos de ilhas e bacias de retro-arco. A justaposição tectônica destas unidades esteve associada, provavelmente, ao fechamento de um antigo oceano, culminando com um evento de metamorfismo regional orogênico colisional que estruturou as rochas da Província Maroni-Itacaiúnas.

**ABSTRACT**

This work investigated the stratigraphic relationships between metavolcano-sedimentary rocks of the Vila Nova Complex (CVN) and the orthogneisses from Tumucumaque Complex (CT) in the Vila Nova region, Amapá. The relationships among the complexes were defined through geological and structural mapping integrated with geophysical data (aeromagnetometry and aerogamaespectroscopy), petrographic analysis and geochronology. The CVN is an association of greenstone belt type located in the southeastern portion of the Guiana Shield, northeastern of the Amazonian Craton.This region is inserted in the Maroni-Itacaiúnas Province, a paleoproterozoic mobile belt that surrounds the archean core of the Central Amazon Province. The integration of the data allowed us define the main lithological units and structures, which were represented in the geological maps presented in the 1:100.000 and 1:50.000 scales. The stratigraphic relationships were supported by geochronological analysis by U-Pb and Lu-Hf methods in zircon using the LA-ICP-MS technique, applied on detrital zircons from metasediments of the CVN and igneous crystals from Tumucumaque and Vila Nova Complexes. The contact between the complexes are defined by ductile shear zones. The CVN is composed of clastic metasedimentary rocks interspersed with metabasalts and meta-andesites, containing subordinate layers of iron and manganese formations, calci-silicate schists and marbles. These units were affected by an orogenic metamorphism under low to medium degree conditions, between the upper green schist and middle amphibolites facies, under intermediate pressure. The CT is constituted by granodioritic tonalitic gneisses, amphibolites, metagranitoids and intrusive gabbros, with metamorphic registration between the amphibolite medium to superior facies. Structural surveys suggest that the complexes were affected by the same processes of deformation and metamorphism, which resulted in a regional foliation $S_{1-2}$ oriented according to the N70-85ºW direction. This foliation is affected by a later deformation phase, which generated $F_3$ folds of regional scale and with open to closed forms and with axis according to the direction NW-SE. The detrital zircons of the CVN metassediments indicated Archaean ages (between 3.6 and 2.7 Ga), with very subordinate participation of Paleoproterozoic ages (between 2.5 and 2.37 Ga). The Neo- to Mesoarchaean ages between 2.85 and 2.67 Ga, were identified in orthogneisses and gabbros of the CT, while Paleoarquean ages between 3.0 and 3.5 Ga, were found in gneiss of the Tartarugalzinho (3.48 Ga) and Vila Nova regions (3.3 Ga). The U-Pb results obtained from samples of the CT indicate two magmatic episodes, one

Mesoarchean (2.85-2.81 Ga) and one Neoarchean (2.67 Ga). The Lu-Hf data also confirm the existence of a large Archaean basement area in the studied region. The maximum deposition age of the basin is defined by the age of 2.170 ± 9 Ma, representing the crystallization of the metandesites of the CVN . The metavulcanic rocks of the Vila Nova greenstone belt were deposited during the Rhyacian on an Archean basement and present a geochemical composition similar to the rocks of the island arc and retro arc basin. The tectonic overlap of these units was probably associated with the closure of an ancient ocean, culminating in a collisional orogenic regional metamorphism event that structured the rocks of the Maroni-Itacaiúnas Province.

# SUMÁRIO

**Estrutura da Tese**

Esta tese de Doutorado está estruturada na forma de três artigos científicos submetidos à publicação nas revistas científicas Boletim de Geociências da USP, Journal of South American Earth Sciences (JSAES) e Precambrian Research, em que o presente canditado é o primeiro autor. Um quarto artigo em tema associado a esta tese, foi aceito para publicação no JSAES. Desta maneira a organização deste trabalho compreende as seguintes etapas:

a) Introdução sobre o tema, contendo a localização da área, o Contexto Geotectônico e a descrição do objeto da Tese de Doutorado, onde estão sumarizados os objetivos e os métodos desenvolvidos nesta pesquisa.

b) Discussão integradora e Conclusões contendo os principais resultados e interpretações deles derivados.

c) Cópia dos três artigos científicos submetidos às revistas especializadas com corpo editorial permanente, revisores independentes, precedidos pela respectiva carta de recebimento do artigo.

d) Anexo, contendo artigo aceito para publicação no Journal of South American Earth Sciences em tema relacionado à tese.

## 1. INTRODUÇÃO

O Cráton Amazônico representa uma das principais unidades tectônicas da Plataforma Sul-Americana, englobando o Escudo das Guianas, ao norte, e o Escudo Brasil Central, ao sul da bacia do Amazonas-Solimões. Situado no norte da América do Sul, abrange uma área de aproximadamente 4.500.000 km$^2$, que compreende parte do Brasil, Guiana Francesa, Guiana, Suriname, Venezuela, Colômbia e Bolívia **(Figura 1)**. A área de estudo está localizada na porção sudeste do Escudo das Guianas, nordeste do Cráton Amazônico, e é recoberta por uma densa floresta equatorial e por um espesso perfil de solos lateríticos, desenvolvidos sobre substrato rochoso pré-cambriano. As grandes dificuldades de acesso, somadas aos poucos levantamentos geológicos sistemáticos, mantiveram esta região com poucas informações geológicas, mesmo sendo reconhecida como uma área de grande potencial metalogenético.


**Figura 1**. Localização dos escudos das Guianas e do Brasil Central no Cráton Amazônico, destacando no retângulo vermelho a localização da área estudada.

A região da Vila Nova apresenta muitos depósitos minerais, incluindo diferentes tipos de depósitos de ouro, vários corpos de cromititos estratiformes contendo jazidas de Cr e V, minério de ferro e manganês, além de ocorrências e garimpos de tantalita e diamante, todos localizados 90 km a sudeste dos depósitos

de manganês de Serra do Navio, que denotam a concentração anômala de depósitos minerais nesta região.

A integração de ferramentas científicas tradicionais, como mapeamento geológico, petrografia e geologia estrutural, com métodos indiretos como a geofísica, geocronologia U-Pb, e dados isotópicos de Lu-Hf em zircões, permitiram avaliar a continuidade e a extensão das unidades geológicas e o seu posicionamento estratigráfico. Estes recursos são fundamentais em áreas de difícil acesso, de vegetação densa, com manto de alteração espesso e com exposições limitadas. Os dados geofísicos permitiram a identificação de falhas e zonas de cisalhamento, a definição das unidades litológicas da sequencia metavulcano-sedimentar do Complexo Vila Nova e a separação destas, das unidades ortognaissicas e metagranitóides do embasamento representados pelo Complexo Tumucumaque. Os dados geocronológicos obtidos pelo método U-Pb em zircão providenciaram as idades de cristalização das rochas do embasamento e das rochas metavulcânicas, bem como a proveniência dos metassedimentos através da análise de zircões detríticos. Os dados isotópicos Lu-Hf indicaram a origem dos magmas e a idades das fontes formadoras das rochas ígneas do CT e CVN.

A presente tese de doutorado tem como objetivo definir as relações estratigráficas entre as rochas metassedimentares e metavulcânicas do Complexo Vila Nova (CVN) e as unidades metaplutônicas do Complexo Tumucumaque (CT), embasamento da bacia.

As relações geológicas foram estabelecidas a partir do mapeamento geológico e geofísico, integrados com a caracterização estrutural, análise petrográfica, geoquímica, geocronológica e isotópica das unidades do CVN e do CT. Os dados de aeromagnetometria e aerogamaespectromoetria foram interpretados e associados aos dados estruturais obtidos na interpretação de imagens de satélite e nos trabalhos de campo. A integração destes dados foi representada nos mapas geológicos em escalas 1:100.000 e 1:50.000 produzidos. A definição da estratigrafia foi estabelecida a partir das relações observadas em campo e na petrografia, com os dados U-Pb e Lu-Hf em zircões obtidos pela técnica de LA-MC-ICP-MS (Laser Ablation-Multi-Collector-Inductively Coupled Plasma-Mass Spectrometry).

A área estudada está situada entre as localidades de Cupixi e Vila Nova, nos municípios de Porto Grande e Mazagão, sudeste do Estado do Amapá **(Figura 2)**. Nesta área situam-se as principais ocorrências de rochas do CVN, do Complexo Máfico-Ultramáfico Bacuri e do embasamento cristalino, representado pelas

unidades do CT. As rochas do embasamento foram estudadas com o intuito de obter as idades de cristalização dos zircões e as relações estruturais e metamórficas com o CVN. Esta investigação foi importante para contribuir com a definição da extensão das rochas arqueanas na porção nordeste do Cráton Amazônico, tema em debate no cenário regional.

As rochas do CVN e que caracterizam o *greenstone belt* Vila Nova, constituem uma espessa sequência de quartzitos com camadas subordinadas de metaconglomerados e metapelitos, seguidos por rochas metamórficas de origem química que incluem xistos calci-silcáticos, BIF's (formação ferrífera bandada), com intercalação de camadas contínuas de hematita filitos, hematita xistos e quartzitos ferruginosos. As fontes dos metassedimentos da bacia do CVN foram estabelecidas a partir da determinação das razões U-Pb em zircões detríticos de duas amostras de metaconglomerado e quartzito. A idade do vulcanismo e provavelmente da idade máxima de deposição da bacia do CVN foi estabelecida a partir da datação de duas amostras de meta-andesitos. Na região do Cupixi e da Vila Nova, o CVN ainda apresenta ocorrência de diversos granitos intrusivos num contexto relacionado ao período pós-colisional ao clímax do metamorfismo orogênico.

A determinação das idades U-Pb em zircões detríticos e ígneos pertencentes as unidades metassedimentares e metavulcânicas do CVN e do embasamento representado pelo Complexo Tumucumaque, integrados ao mapeamento geológico e geofísico (1:00.000 e 1:50.000) com análise petrográfica e estrutural, determinaram as inter-relações destas rochas, a idade máxima para deposição dos metassedimentos na bacia do Vila Nova, definindo os protólitos, o período da atividade vulcânica, bem como a idade de cristalização do embasamento.

Com base nos trabalhos desenvolvidos juntamente com a Mineração Amapari Sa, que pesquisa as ocorrências de ouro e ferro na região, e que compreendeu mapeamento geológico e estrutural, descrição de furos de sondagem e interpretação geofísica dos alvos de ouro e ferro, foi possível integrar os resultados para gerar a base das relações estratigráficas e a confecção de um novo mapa geológico para a região da Vila Nova (1:50.000), que posteriormente foi expandido até a região da Serra do Navio (1:100.000), com base nos dados aerogeofísicos disponíveis.

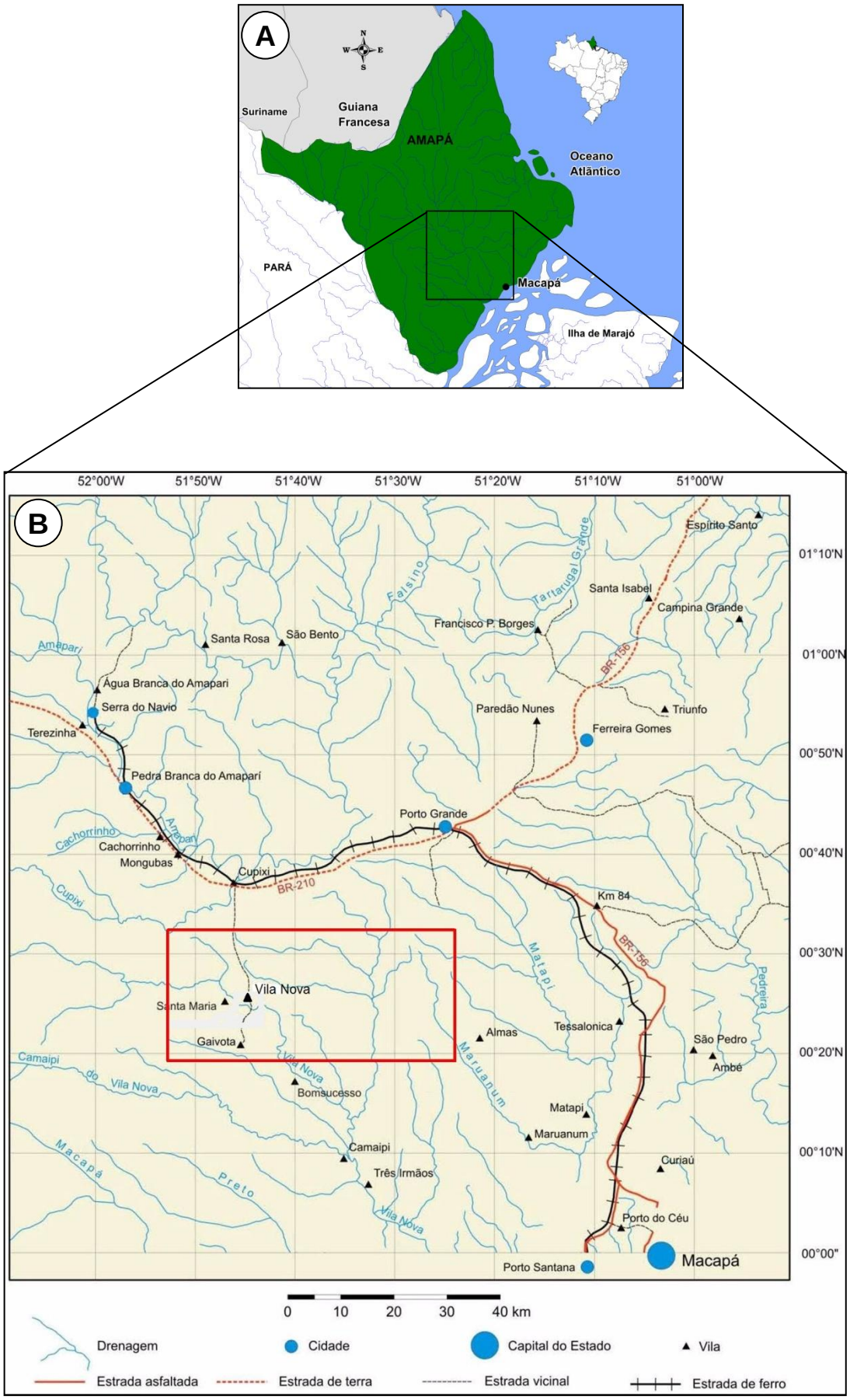


**Figura 2**. A) Localização da área de estudo regional com relação ao Estado do Amapá, B) Mapa geográfico com as principais vias de acesso ferroviário e rodoviários e a localização da área de estudo de semi-detalhe.

A seguir é apresentada a experiência desenvolvida nesta tese, dentro da ótica de integração de escalas e de ferramentas geológicas como aerogeofísica, mapeamento geológico e estrutural, análise petrográfica e geocronologia U-Pb e Lu-Hf. Inicialmente é apresentada uma revisão da evolução do conhecimento sobre o Complexo Vila Nova. Posteriormente é apresentada uma síntese do contexto tectônico e significado do Complexo Vila Nova em relação ao Complexo Tumucumaque e a Província Maroni-Itacaiúnas.

## 1.1 Trabalhos Anteriores

Os trabalhos pioneiros sobre a geologia da região sudeste do Amapá derivam do final da década de quarenta, quando Paiva (1946) descreveu a sequência de metassedimentos próximos a Serra do Navio, em que distinguiu três camadas de manganês (Serra do Navio, Espigio e Espigão do Chumbo), e da localidade de Santa Maria, onde descreveu quartzitos intercalando itabiritos e lentes de hematita.

A denominação Série de Vila Nova foi proposta por Ackermann (1948) para descrever o conjunto de rochas pré-cambrianas pertencentes ao Complexo Fundamental, estando às mesmas "perturbadas, dobradas e em posição subvertical". Os levantamentos de Ferreira (1949) caracterizam as ocorrências e jazidas de manganês na bacia do rio Amapari na publicação "Jazimentos de Minerais Metálicos no Brasil".

No reconhecimento aerofotogeológico da região centro-leste do Amapá, os pesquisadores da empresa LASA (1958, *in* Projeto Radam Brasil, 1974), dividiram as rochas do pré-cambriano em três categorias, sendo a última, os metassedimentos pertencentes à Série Vila Nova, composta por quartzitos e xistos.

A subdivisão dos metassedimentos em três grupos foi proposta por Nagell & Silva (1961), que descreveram da base para o topo uma constituição caracterizada por quartzitos, anfibolitos e biotita-granada xistos. A foliação dos metassedimentos tem direção NW-SE e no seu interior ocorrem dobras isoclinais e intrafoliais. Os autores salientam que a foliação metamórfica é paralela a das jazidas de manganês e mergulha para NE no flanco oeste do distrito da Serra do Navio. Posteriormente, Nagell (1962), redefiniu a Série Vila Nova em Série Amapá e incluiu uma sequência de conglomerado, itabirito e quartzo-mica xisto e quartzito, o qual denominou de Grupo Santa Maria (**Tabela 1**).

Na região sudeste do Estado do Amapá, Scarpelli (1966) reconheceu dois grupos dos três propostos anteriormente por Nagel (1962), subdividindo a Série Amapá em Grupo Jornal, constituído de anfibolitos, e Grupo Serra do Navio, formado de xistos, gonditos, anfibolitos e lentes de mármore (**Tabela 2**). Os metassedimentos situados a oeste do Distrito de Serra do Navio, em contato com o embasamento, são descritos como pertencentes a Série Vila Nova por Marotta (1966).

Os levantamentos realizados na porção sudoeste do estado por Neves & Menezes (1967) e Carvalho & Silva (1969) descreveram ocorrências de quartzitos, clorita-xisto e sericita xistos na região situada a oeste da Vila Nova, no rio Jari. As exposições de minério de manganês foram incluídas nos metassedimentos do Grupo Vila Nova por Carvalho & Silva (1969).

A ocorrência de uma sequência metassedimentar no rio Cupixi e na bacia do rio Vila Nova foi descrita por Leal & Pinheiro (1971), que incluíram os mesmo como pertencendo aos grupos Jornal e Serra do Navio. Os metassedimentos ocorrentes no Amapá foram inseridos no Grupo Vila Nova por Lima et al. (1974), que inserem no Grupo Vila Nova, todos os metassedimentos ocorrentes no Estado do Amapá. Posteriormente, João *et al.* (1979) consideraram esta unidade como sendo um cinturão do tipo *greenstone belt*.

| | | | |
|---|---|---|---|
| Pré-Cambriano | | | Pegmatitos<br>Diques de Diabásio |
| | Série Amapá<br>(Vila Nova) | Grupo Serra do Navio | Biotita-granada-xisto<br>Quartzito-granatífero<br>Quartzo-biotita-gnaisse<br>Xisto-grafítico<br>Gondito (protominério)<br>Carbonato de manganês<br>(protominério)<br>Rocha c/diopsídio-granada-calcita<br>Anfibolito |
| | | Grupo Jornal | Anfibolito |
| | | Grupo Santa Maria | Quartzito<br>Quartzo-mica-xisto<br>Itabirito (formação ferrífera)<br>Quartzo conglomerado |
| | | Embasamento | Granito-Gnaisse |

**Tabela 1**. Estratigrafia da Série Amapá proposta por Nagell (1962).

| | | | | |
|---|---|---|---|---|
| Pré-Cambriano | Intrusivas | Veios Hidrotermais<br>Diques de Diabásio | | |
| | Intrusivas | Pegmatito e Veios de Quartzo<br>Granito Sintectônico | | |
| | Série Amapá (Vila Nova) | Grupo Serra do Navio | Xistos | Cumingtonita-biotita-xisto<br>Paranfibolito<br>Quartzito-granada<br>Quartzo-bioitita-granada-xisto, com lentes de gondito e lentes de mármore |
| | | Grupo Jornal | | Anfibolito |
| | Embasamento | | | Granito-Gnaisse |

**Tabela 2**. Estratigrafia da Série Amapá proposta por Scarpelli (1966).

Montalvão (1985) em estudo petrológico caracterizou o Grupo Vila Nova como uma sequencia metavulcano-sedimentar do tipo *greenstone belt*. Os autores definiram a composição toleítica a komatiítica para as rochas metavulcânicas e sugeriram uma origem a partir da fusão do manto superior. Os *greenstone belts* ocorriam como grandes cinturões alongados segundo a direção NW-SE e repousavam discordantemente sobre o embasamento gnáissico arqueano. As relações entre os eventos de deformação e o metamorfismo regional que afetaram o Grupo Vila Nova, e as condições metamórficas entre a fácies Xistos Verdes e Anfibolito foram descritas por Costa & Hasui, (1997).

Mais recentemente, McReath & Faraco (2006), baseado em Carvalho *et al.* (1995), Coelho Filho *et al.* (1998) e em Spier & Ferreira Filho (1999), reconheceram cinco unidades litológicas no Grupo Vila Nova: (1) intercalação de rochas metavulcânicas e metassedimentares indiferenciadas; (2) anfibolitos e xistos mafico/ultramáficos; (3) rochas metaplutônicas máfica/ultramáficas; (3) quartzito, xisto, gnaisse e anfibolito (antigo Grupo Serra da Lombarda, de Veiga *et al.*, 1985 e Ferran, 1988); (4) xistos e metavulcânicas que ocorrem na região de Tartarugalzinho (Jorge João *et al.*, 1978); (5) metaconglomerado, quartzito conglomerático, quartzito, formação ferrífera e manganesífera bandada, mármores e metapelitos.

Na região da Serra do Navio, ocorre uma sequência basal de ortoanfibolito capeado por xisto e mármore manganesífero. A oxidação dos carbonatos produziu os depósitos de manganês lavrados pela Empresa ICOMI S.A. desde 1957 até

1997, sendo extraídas no total 61 milhões de toneladas de minério de manganês (Coelho Filho, 1998).

O Grupo Vila Nova nos estados do Amapá e Pará está distribuído em diferentes cinturões de rochas metavulcano-sedimentares separados por terrenos granito-gnáissicos (McReath & Faraco, 2006) (**Figura 3**). Partindo do sudoeste do Estado do Amapá, os cinturões da Serra de Ipitinga, e da Serra de Tumucumaque ao da Serra do Navio não apresentam continuidade no Suriname e na Venezuela, e talvez representem depósitos penecontemporâneos formados em margens continentais passivas e bacias oceânicas (Faraco, 1990, 1997; Lafon *et al.* 2008). Seguindo para nordeste, os cinturões da Serra Lombarda até Tartarugalzinho e Oiapoque são continuações de cinturões presentes nas Guianas onde as características geoquímicas, tanto das rochas metavulcânicas máficas como das félsicas plutônicas posteriores, apontam para origens em zonas de supra-subducção (Delor *et al.* 2003; Rosa-Costa *et al.* 2003, 2006).

No cinturão de Ipitinga, Faraco (1997) caracteriza as rochas metavulcânicas como basaltos toleíticos de fundo oceânico e, subordinadamente, como basaltos komatiíticos de bacias de back-arc, indicando uma origem associada a processos de subducção de crosta oceânica. Os dados geoquímicos caracterizaram as rochas metavulcânicas máficas da região de Ipitinga como basaltos toleíticos de fundo oceânico e subordinamente a basaltos komatiíticos associados a bacias de back-arc.

A idade Paleoproterozóica foi referida inicialmente por Montalvão & Tassinari (1984), que obtiveram idades K-Ar de 2.028 ±93 Ma, 2.046 ±63 Ma e 1.971 ±51 Ma em anfibólios de três amostras de anfibolitos do Grupo Vila Nova da região da Serra do Navio. Estes autores interpretaram esses valores como a idade do resfriamento regional dessas rochas, durante o Ciclo Transamazônico. As idades de 2.26 Ga, obtidas para o Rio Santo Antônio Diorito, intrusivo nas unidades do Grupo Vila Nova na região da Serra do Navio sugerem que a sequencia metavulcano-sedimentar tenha sido formada durante um evento plutônico eo-riaciano. Essas idades sugerem que as rochas do Grupo Vila Nova são contemporâneas as rochas máficas do Grupo Ipitinga, situado na porção sudoeste do Estado do Amapá, e do Complexo de "*l´ile de Cayenne*", na Guiana Francesa. Dessa forma, o Grupo Vila Nova na Serra do Navio não é relacionado às sequencias *greenstones* meso-riacianas do sudeste do Escudo das Guianas e constitui mais uma testemunha do estágio eoriaciano de formação de crosta oceânica que deu inicio à evolução Transamazônica da Província Maroni-Itacaiúnas. Estudos isotópicos pelo método Sm-Nd nas rochas

metavulcânicas do Cinturão Ipitinga reforçam a idade paleoproterozóica dessas rochas, revelando idades modelos ($T_{DM}$) entre 2.26 e 2.19 Ga (Faraco, 1997, McReath & Faraco, 2006). Através do método Sm-Nd, a isócrona rocha total-granada em anfibolitos do Grupo Vila Nova indicou a idade de 2.08 Ga para o metamorfismo regional, que coincide com o magmatismo tardi-orogênico na Província Maroni-Itacaiúnas (Pimentel *et al.*, 2002).

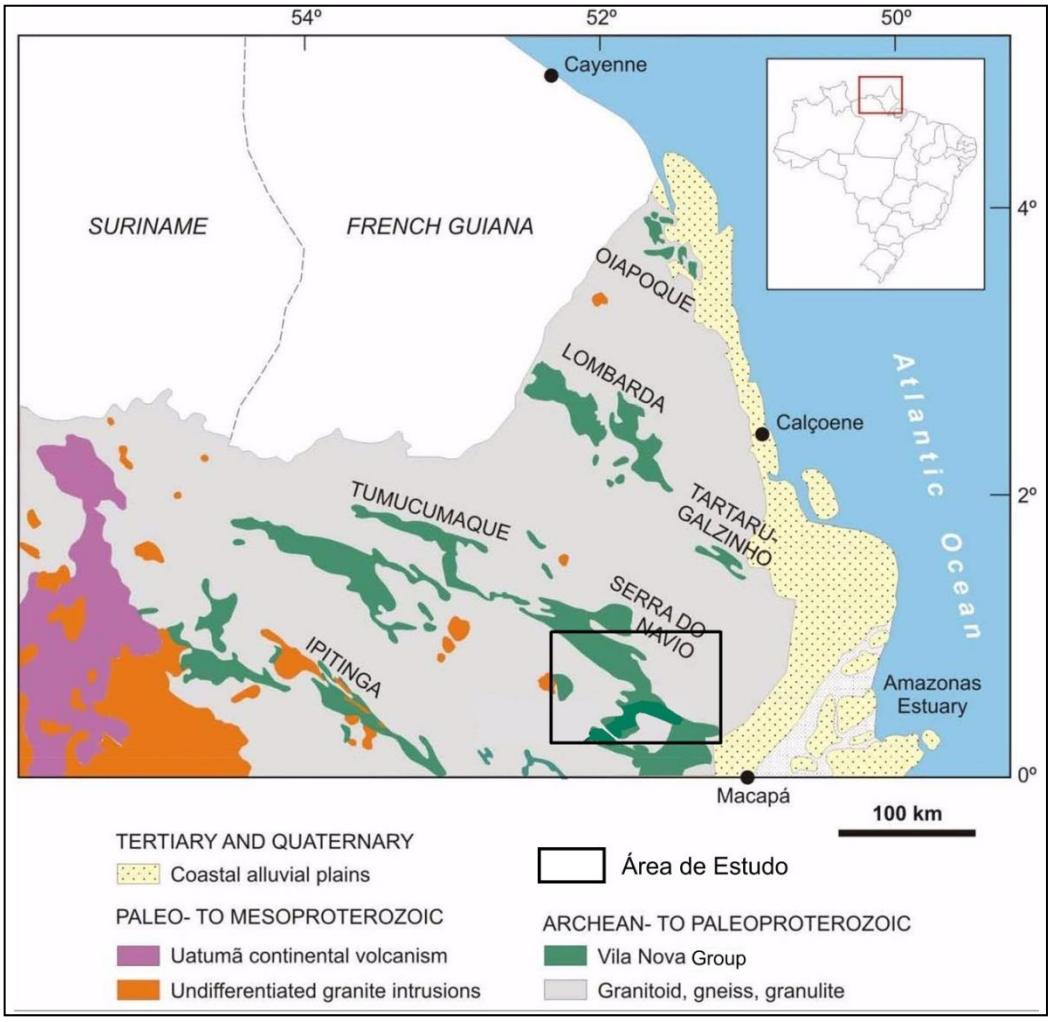


**Figura 3**. Mapa geológico de uma parte do estado do Amapá com os nomes dos diversos cinturões que compõe o Complexo Vila Nova. A área de estudo está representada pelo retângulo preto. Modificado de McReath & Faraco (2006).

As idades paleoproterozóicas do Grupo Vila Nova na região de Ipitinga permitiram correlacionar as unidades desse grupo com aquelas do Grupo Paramacá, na Guiana Francesa (Gruau *et al*., 1985, Vanderhaege *et al.,* 1998, Delor *et al*., 2003a) e do Grupo Barama-Mazaruni, na República da Guiana (Gibbs & Olszewski 1982).

Na região sudeste do Amapá, o Grupo Vila Nova foi dividido em uma unidade máfica-ultramáfica e outra metassedimentar (e.g. Scarpelli *et al*., 1963; Carvalho *et al*., 1995; McReath & Faraco, 2006). A unidade mafica-ultramáfica é composta principalmente por anfibolitos e actinolita-xistos, que apresentam uma fonte caracterizada por assinatura isotópica mantélica com significativa contaminação crustal arqueana (Lafon *et al*., 2008; Tavares, 2009). A unidade metassedimentar, na região da Serra do Navio, que sobrepõe a mafica-ultramáfica, é composta por quartzitos, intercalados com lentes de rochas calco-silicáticas, biotita xistos e xistos grafitosos, além de mármores manganesíferos e formações ferríferas bandadas com ocorrência local que incluem as facies óxido e óxido-silicato (Melo *et al*., 2003).

Neste trabalho, será utilizada a designação Complexo Vila Nova em substituição ao Grupo Vila Nova para o conjunto de rochas igneas e sedimentares metamorfisadas que constituem o *greenstone be*lt Vila Nova, de idade Paleoproterozóica, conforme descrito por Hoffman *et al.* (2018). Esta opção tem como base as definições e recomendações do Código de Estratigrafia da *International Commission on Stratigraphy* da IUGS *(International Union of Geological Sciences)*. Esta comissão ressalta que a designação grupo deve ser utilizada para designar associações de rochas com estrutura acamadada e pouco deformadas, que ainda mantém sua estratigrafia preservada, com relações de topo e base e continuidade lateral dos estratos.

## 1.2 Contexto Geotectônico

O Cráton Amazônico consiste de um núcleo de idade Arqueana, envolto por faixas móveis alongadas segundo a direção NW-SE de idades Paleo- e Meso-proterozóica (Cordani *et al.*1979; Cordani & Neves 1982; Teixeira *et al*., 1989; Santos *et al*., 2000; Tassinari *et al*., 2000; Avelar *et al.,* 2003; Tassinari & Macambira 2004; Rosa-Costa *et al.,* 2006). O embasamento policíclico na porção norte do Craton Amazônico abrange dois segmentos principais da crosta, caracterizados por unidades geológicas Arqueanas e Paleoproterozóicas, respectivamente. A integração mostra um vasto domínio do núcleo arqueano de ortognaisses, granitos e gabros. As faixas móveis paleoproterozóicas estão constituídas por extensas bacias do tipo back-arc associadas a arcos magmáticos, compondo trilhas descontínuas de *greenstone belts*, e por associações graníticas do tipo TTG (Avelar *et al.* 2003; Mc Reath & Faraco, 2006). A porção norte do Cráton Amazônico representa o Escudo

das Guianas, enquanto a porção sul é denominada Escudo Guaporé ou Brasil Central, separados pela cobertura sedimentar das bacias do Solimões e do Amazonas. (**Figura 4**).

A porção sudeste do Escudo das Guianas está inserida na Província Maroni-Itacaiúnas, que contorna a Província Amazônia Central, definindo uma larga faixa na borda norte-nordeste do Cráton Amazônico, com evolução relacionada ao Ciclo Orogênico Transamazônico, no período entre 2.26 Ga e 1.95 Ga (Tassinari & Macambira, 1999; Tassinari *et al*. 2000, Avelar *et al.* 2003; Tassinari & Macambira 2004, Cordani *et al*. 2009).

A região da Vila Nova está situada na porção sudeste do Escudo das Guianas, porção nordeste do Cráton Amazônico. O Complexo Vila Nova foi a designação usada para denominar as associações metavulcano-sedimentares que ocorrem na região da Vila Nova e do Cupixi e são correlatas às outras associações do tipo *greenstone belts* denominados regionalmente por McReath & Faraco (2006) como Ipitinga, Tumucumaque, Serra do Navio, Tartarugalzinho, Lombarda e Oiapoque (**Figura 3 e 5A**).

Segundo Oliveira *et al*. (2008), o estado do Amapá pode ser dividido em dois domínios: ao norte, predominam granitóides e ortognaisses paleoproterozóicos, e na porção centro-sul, predominam as rochas arqueanas retrabalhadas durante o Ciclo Orogênico Transamazônico (Montalvão & Tassinari 1984, Sato & Tassinari 1997, Avelar 2002, Avelar *et al.* 2003, Rosa Costa *et al*. 2006). Na região norte e na fronteira com a Guiana Francesa, os ortognaisses e granitóides são essencialmente relacionados à evolução neoriaciana da Orogênese Transamazônica (Nogueira *et al*. 2000; Lafon *et al*. 2001; Avelar, 2002; Lafon *et al.* 2003). Nesta região, testemunhos de crosta arqueana foram registrados principalmente em zircões detríticos (3.2-2.7 Ga) de rochas metassedimentares, em zircões herdados (2.9-2.6 Ga) e em idades modelo $T_{DM}$ (2.75-2.40 Ga) de granitóides e ortognaisses paleoproterozóicos (Lafon *et al*. 2000, Avelar *et al*. 2001, 2003).

Na porção centro-sul do Amapá, há predomínio de rochas arqueanas retrabalhadas (Rosa Costa *et al*., 2006). Estudos geocronológicos pelo método Pb-Pb em zircão e novos dados gerados nesta tese para os gnaisses tonalíticos e granodioríticos, metagranitos e gabros do Complexo Tumucumaque da região sudeste do Amapá apresentaram idades U-Pb entre 2.85 e 2.6 Ga, confirmando a existência de uma ampla área de embasamento arqueano nesta região, conforme hipóteses apresentadas Montalvão & Tassinari (1984), Lafon *et al*. (2001), Avelar

(2002), Ricci *et al*. (2002), Avelar *et al*. (2003), Rosa-Costa *et al*. (2003, 2006, 2012), Barbosa *et al*. (2013) e Borghetti *et al.* (2014). Rosa Costa *et al*. (2012) encontraram idades Pb-Pb em zircão de 3.48 Ga em ortognaisses da região de Tartarugalzinho. Em rochas gnáissicas encaixantes na região de Vila Nova, Pimentel *et al*. (2002) definiram pelo método Sm-Nd em rocha total idades modelo $T_{DM}$ entre ca. 3.31 e 3.13 Ga e devem representar os contaminantes crustais para os ortognaisses do Complexo Tumucumaque.

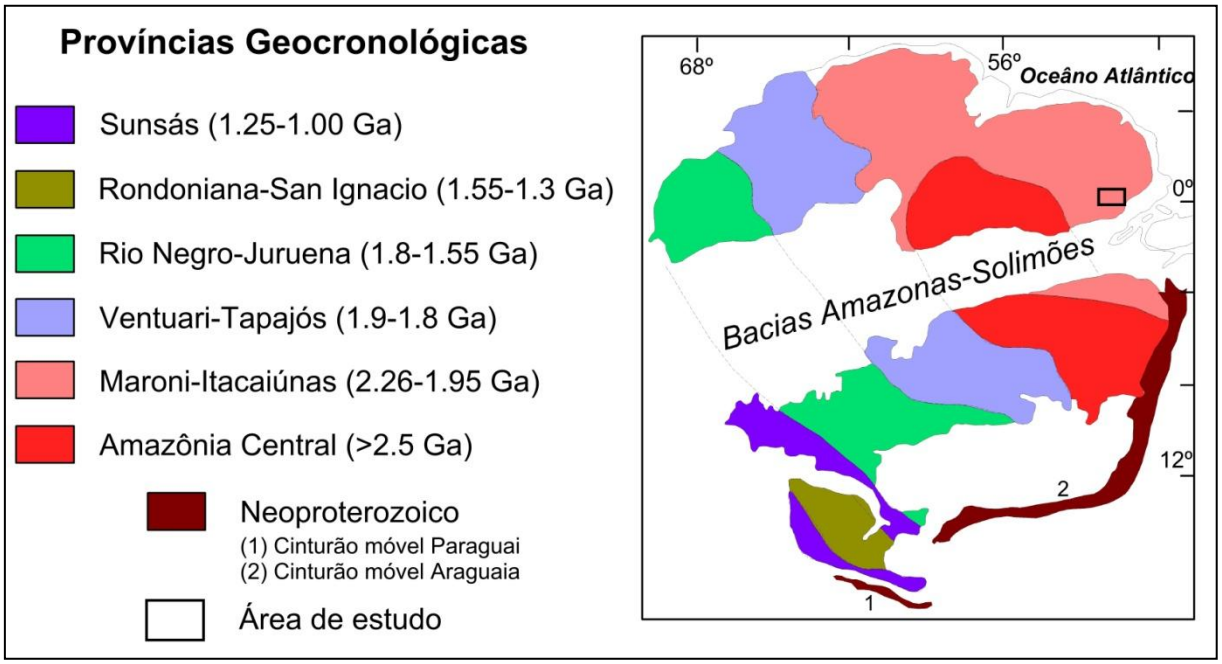


**Figura 4**. Distribuição das Províncias Geocronológicas do Cráton Amazônico de acordo com Tassinari & Macambira (2004).

Os dados Pb-Pb em zircão e Sm-Nd obtidos por Rosa-Costa *et al.* (2003, 2006) permitiu aos autores definir um bloco continental de idade Arqueana denominado de Terreno Amapá. Este terreno foi subdividido nos domínios Paru, Jari e Cupixi, estando o primeiro inserido no Domínio Carecuru de idade Paleoproterozóica. Ao norte as rochas arqueanas do Terreno Amapá estão e contato tectônico com rochas paleoproterozóicas do Domínio São Lourenço **(Figura 5B)**. Estas idades sugerem a correlação proposta por Rosa-Costa *et al.* (2006) entre os blocos Imataca (Venezuela) e Amapá. Na região central do Amapá e nordeste do Pará, evidências de crosta continental arqueana estão registradas em rochas de alto grau metamórfico, caracterizando um forte retrabalhamento metamórfico de idade Paleoproterozóica (Montalvão & Tassinari 1984, Tassinari *et al*. 2000, Pimentel *et al*. 2002, Avelar *et al*. 2003, Rosa-Costa *et al*. 2003, 2006).

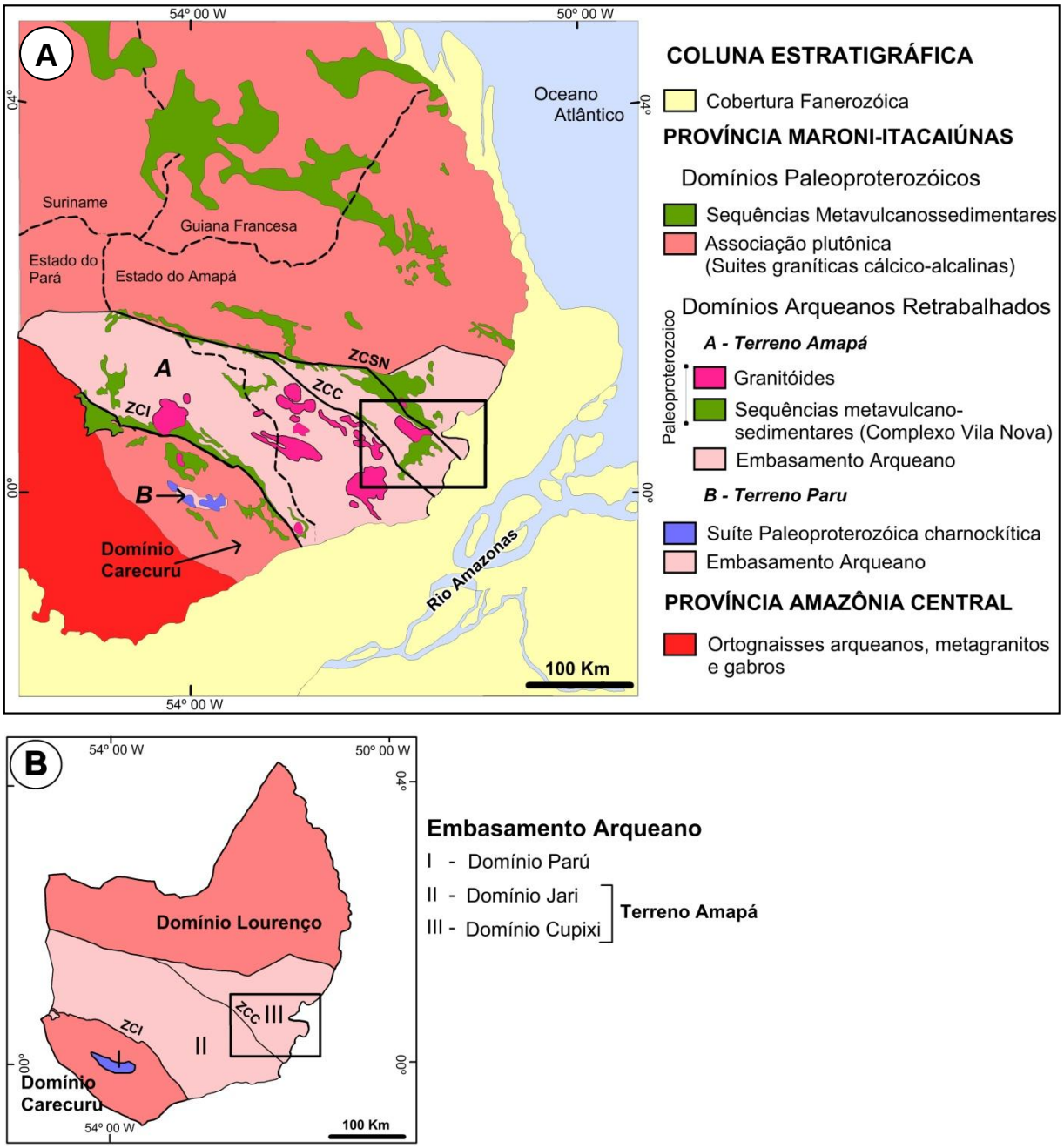


**Figura 5**. **A)** Mapa geotectônico da porção sudeste do Escudo das Guianas com a representação das unidades das províncias Amazônia Central e Maroni-Itacaiúnas, modificado de Rosa-Costa *et al.* (2006). As províncias geocronológicas estão de acordo com Tassinari & Macambira (2004). A área de estudo está localizada no retângulo preto. **B)** Domínios geotectônicos dos estados do Amapá e Pará, de acordo com Ricci *et al*. (2001) e Rosa Costa *et al*. (2012). Zonas de Cizalhamento: ZCSN = Serra do Navio; ZCC = Cupixi; ZCI = Ipitinga.

As seqüências metavulcano-sedimentares e os granitos associados constituem cinturões que formam a Província Maroni-Itacaiúnas, de idade Riaciana, disposta entre o Escudo Guianense e o Cráton Oeste-Africano (Delor *et al.* 2003; Avelar *et al.* 2003; Velasquez *et al.* 2011). Os cinturões guianenses e do oeste-africano apresentam muitas feições e características semelhantes. A evolução desta província paleoproterozóica ocorreu por etapas, com atividades a partir de 2.3 Ga e

diminuição após 2.11 Ga. Velasquez *et al.* (2011) propuseram um modelo de desenvolvimento caracterizado por dois eventos principais de adição crustal. O primeiro está relacionado a uma fase inicial com desenvolvimento de arcos juvenis e o segundo com a formação de arcos continentais mais maturos envolvendo o retrabalhamento de crosta continental antiga.

Estas unidades estão caracterizadas em campo por complexos metavulcanossedimentares e por associações graníticas tipo TTG, pouco ou totalmente metamorfizadas (Avelar *et al*. 2003; Delor *et al*. 2003; Rosa-Costa *et al*. 2003, 2006; Velasquez *et al*. 2011). A maioria dos autores sugere que a deformação mais tardia e de natureza transcorrente, foi responsável pela estrutura atual dos cinturões (Avelar *et al*. 2003; Delor *et al*. 2003; McReath & Faraco, 2006). Exemplos de zonas de cisalhamento transcorrentes regionais são os lineamentos Cupixi e Ipitinga (Rosa Costa, 2006).

A análise petrográfica, composição geoquímica e isotópica das rochas metavulcânicas do *greenstone belt* Vila Nova permitiu a caracterização de duas associações de rochas metavulcânicas, de metabasaltos toleíticos de fundo oceânico e de metabasaltos komatiíticos de bacias de back-arc (Hoffmann, 2017; Hoffmann *et al.* 2018). Os autores indicaram uma origem associada a processos de subducção de crosta oceânica, relacionando as atuais relações estratigráficas, aos eventos de deformação e metamorfismo associados a colisão das unidades arqueanas do embasamento.

## 1.3 Análise Integradora

Os trabalhos de pesquisa desenvolvidos para a elaboração desta tese resultaram nos três artigos apresentados e que se mostram interligados, servindo um de suporte ao outro. O ARTIGO 1 apresenta os resultados da análise dos dados geofísicos, que associado aos trabalhos de campo resultaram no mapa geológico regional (escala 1:100.000) e de semi-detalhe da área estudada (escala 1:50.000) e na identificação das principais zonas de cisalhamento dúcteis responsáveis pelo contato entre as unidades do embasamento e do complexo metavulcano-sedimentar. Com base nestes novos mapas geológicos foram estabelecidas as relações estratigráficas obtidas através da integração das relações observadas em campo e nos furos de sondagem, com os dados estruturais, petrográficos e geocronológicos da área. Com base nestes resultados, o ARTIGO 2 nos permitiu

reconstruir e entender o embasamento da bacia do CVN, representado pelos ortognaisses e metagranitóides do Complexo Tumucumaque. O ARTIGO 3 apresentou as relações estratigráficas e a caracterização petrográfica, estrutural e geoquímica das unidades do Complexo Vila Nova. A estes dados foram incorporados os dados obtidos pelos métodos U-Pb e Lu-Hf em zircões detríticos e ígneos, para determinar as áreas fontes e a idade do vulcanismo da bacia.

.

**ARTIGO 1**

Borghetti, C. & Philipp, R.P. (2017). Geologia e geofísica do *greenstone belt* Vila Nova, porção NE do Cráton Amazônico, Amapá, Brasil. Publicado na Revista do Instituto de Geociências, USP, Série Científica, São Paulo, v. 17, n. 1, p. 109-127, Março 2017.

Neste primeiro artigo é apresentada a base estratigráfica do *greenstone belt* Vila Nova, definida através da integração de dados geofísicos (aeromagnetometria e aerogamaespectroscopia) com os dados obtidos durante o mapeamento geológico. Com base no trabalho de campo desenvolvido juntamente com a Mineração Amapari SA que compreendeu, mapeamento geológico e estrutural, descrição de furos de sondagem e interpretação dos levantamentos geofísicos dos alvos de ouro e ferro foi possível integrar os resultados para determinar as relações estratigráficas e confeccionar os novos mapas geológicos da região da Vila Nova e da Serra do Navio em escalas 1:100.000 e 1:50.000.

O uso da geofísica na caracterização de terrenos Pré-cambrianos com ocorrência de *greenstone belts,* tem assumido grande destaque no cenário nacional e internacional. Os *greenstone belts* são sequências metavulcano-sedimentares que ocorrem associados a terrenos granito-gnáissicos, compondo grande parte dos terrenos arqueanos e paleoproterozóicos que constituem os crátons. Os *greenstones* são constituídos por uma sucessão de rochas metavulcânicas máficas a ultramáficas com ocorrência subordinada de metavulcânicas ácidas, intercaladas com rochas metasedimentares clásticas e químicas. Estas sequências são formadas numa diversidade de ambientes, sempre relacionados a vulcanismo submarino, sendo muito comuns no Arqueano e no Paleoproterozóico. De acordo com Grant (1984) os *greenstone belts* são responsáveis por grande número de depósitos minerais de metais preciosos, principalmente ouro, prata, chumbo, cobre, níquel, cromo, zinco e a associação Pb-W-Zn-Ag-(Cu).

O *greenstone belt* Vila Nova apresenta mineralizações de ouro (como nos garimpos de Vila Nova e Santa Maria) e ferro (UNAMGEM Mineração e Metalurgia SA) associado aos metassedimentos, e ainda jazidas de cromo e vanádio (Mineração Vila Nova Ltda) associados às rochas ultramáficas e máficas do Complexo Bacuri, bem como ocorrência de Tantalita em diversos pegmatitos espalhados pela região associados a granitos intrusivos. O resultado obtido pelos trabalhos de pesquisa foi a definição cartográfica e geológica de novos corpos litológicos, com a definição das unidades metassedimentares e metavulcânicas do Complexo Vila Nova e os ortognaisses, anfibolitos e metagranitos do Complexo Tumucumaque. Também foram caracterizadas as principais zonas de cisalhamento responsáveis pelas relações de contato entre as unidades basais e superiores do *greenstone belt* Vila Nova para a região estudada.

**ARTIGO 2**

Borghetti, C., Philipp, R.P., Mandetta, P., Hoffmann, I.B. (2018a). Geochronology of the Archean Tumucumaque Complex, Amapá Terrane, Amazonian Craton, Brazil. Submetido ao *Journal of South American Earth Sciences* em 06 de Abril de 2018 e aceito para publicação em 01 de Maio de 2018.

A partir da definição da estratigrafia da região da Vila Nova através do mapeamento geológico, as rochas do embasamento foram estudadas e coletas 05 amostras de ortognaisses, granitóides e gabros intrusivos do Complexo Tumucumaque que compõe o embasamento da bacia que gerou o Complexo Vila Nova. As análises geocronológicas pelo método U-Pb e Lu-Hf em zircão através de LA-ICP-MS permitiram determinar as idades e as fontes das unidades do embasamento e verificar as suas relações estratigráficas com o Complexo Vila Nova. Inicialmente, devido as relações de contato entre as rochas do CVN e o CT, imaginava-se que os metagranitos sendo sin- ou pós-tectônicos pudessem ser a fonte termal da mineralização de ouro que ocorre no Garimpo da Vila Nova. O resultado das amostras analisadas, porém mostrou que, pelo menos, os metagranitos estudados apresentaram idades Meso- a Neo-arqueana, com fontes de idade paleo-arqueanas.

Os resultados U-Pb encontrados nos zircões das rochas do Complexo Tumucumaque entre 2.85-2.67Ga, bem como os dados Lu-Hf confirmaram a existência do Terreno Arqueano Amapá, conforme proposto por Rosa Costa (2006).

**ARTIGO 3**

Borghetti, C., Philipp, R.P., Mandetta, P., Hoffmann, I.B. (2018b). Geology, U-Pb zircon geochronology and Lu-Hf isotopes of the Vila Nova greenstone belt: arc-related associations of the Rhyacian orogeny in the northern Amazonian Craton, Brazil. Submetido na revista *Precambrian Research* em 17 de abril de 2018.

A partir da delimitação e o reconhecimento em campo das unidades basais e superiores do Complexo Vila Nova, este artigo teve como objetivo apresentar a estratigrafia do *greenstone belt* Vila Nova a partir da perfilagem e dos dados de campo obtidos nas localidades da Vila Nova, Nova Canaã e Pelado, e na amostragem de ambas as unidades. A unidade basal, formada principalmente por rochas metavulcânicas, foi amostrada com o objetivo de determinar a idade do vulcanismo associado ao desenvolvimento da bacia do Complexo Vila Nova. Da unidade superior do CVN, foram amostrados um quartzito e um metaconglomerado, para avaliar a proveniência através de geocronologia de U-Pb em zircões detríticos, e determinar a idade máxima e mínima de deposição da bacia representada pelas rochas do Complexo Vila Nova, bem como determinar as possíveis rochas fontes dos sedimentos que preencheram a mesma.

A delimitação precisa do contato das unidades basais e superiores do CVN e suas relações com os gnaisses e metagranitóides arqueanos do Complexo Tumucumaque foi obtida em trabalho conjunto com a Mineração Amapari. As relações estratigráficas além de ser um dos objetivos desta tese, também era um dos focos da empresa, que incluia também pesquisar as ocorrências de ouro associada aos metaconglomerados da unidade superior e as ocorrências de ferro, intimamente relacionadas às rochas metavulcânicas da unidade basal, justapostas pela Zona de Cisalhamento Vila Nova. Os dados geocronológicos de U-Pb e isotópicos de Lu-Hf foram fundamentais para estabelecer a evolução tectônica das unidades. Os resultados obtidos mostram uma ótima correlação entre as idades arqueanas das unidades do embasamento e as idades encontradas nas unidades metavulcano-sedimentares de cobertura.

**ARTIGO 4 (Em anexo)**

O artigo “Geochemistry and origin of the Rhyacian tholeiitic metabasalts and meta-andesites from the Vila Nova Greenstone Belt, Guiana Shield, Amapá, Brazil”

de autoria de Itiana B. Hoffmann, Ruy P. Philipp & Cristiano Borghetti. Este artigo foi desenvolvido através do Mestrado Acadêmico da primeira autora junto ao PPGGEO-UFRGS e concluído em 2017.

O artigo foi submetido ao Journal of South American Earth Sciences em 27 de novembro de 2017 e aceito para publicação em 09 de março de 2018. Este pesquisa investigou a origem e o significado das rochas metavulcânicas do *greenstone belt* Vila Nova através da integração entre o mapeamento geológico e estrutural, com análises estratigráficas, obtidas pela descrição de furos de sondagem selecionados, e análises petrográficas, litogeoquímicas, geocronológicas e isotópicas.

A parte inferior do VNGB consiste em rochas metavulcânicas que incluem metabasaltos, meta-andesitos, anfibolitos e anfibólios-xistos, suportados por um domínio metassedimentar superior com rochas químicas metavulcânicas e exalativas subordinadas. Os corpos estão deformados e alongados, concordantes com a foliação metamórfica regional de direção NW-SE. Os dados de zircão U-Pb apresentou uma idade Riaciana para a cristalização ígnea do zircões.

Um metamorfismo orogênico seguido de três eventos deformacionais foi reconhecido e caracterizado por dois picos metamórficos distintos: $M_1$ e $M_2$ com temperaturas de 450 e 650 °C, e pressão litoestática entre 4 e 6 kbares. As características litogeoquimicas observadas indicam que as rochas metavulcânicas do VNGB representam a evolução de rochas vulcânicas básicas geradas em bacias back-arc e arcos insulares associados ao Ciclo Orogênico Transamazônico.

## 1.4 Conclusões

A integração dos dados aerogeofísicos com os dados de mapeamento geológico e estrutural permitiram delimitar de forma precisa as principais unidades metassedimentares e metavulcânicas do CVN e estabelecer a relação de contato destas com as unidades do CT. Os mapas geofísicos também indicaram de forma precisa os limites e as formas dos granitóides intrusivos ocorrentes na região. O resultado desta integração de dados esta representado nos mapas geológicos apresentados nesta tese.

O resultado desta integração permitiu entender o significado dos principais lineamentos representados por zonas de cisalhamento dúcteis, estabelecendo a correlação dos dados interpretados com os principais domínios geológicos reconhecidos a partir dos trabalhos de campo realizados na região. Assim, foi

possível separar as áreas do embasamento arqueano compostas pelos ortognaisses, metagranitóides, anfibolitos e gabros do CT, das áreas ocupadas pelas rochas metavulcano-sedimentares do CVN. Dentro das unidades deste último complexo, destacam-se os baixos magnetométricos representando os metassedimentos situados ao sul da Zona de Cisalhamento Vila Nova, quando comparados com os valores elevados das rochas metavulcânicas situadas ao norte desta zona. Esta diferença permitiu reconhecer um Domínio Basal, com predominância de rochas metavulcânicas e um Domínio Superior, composto por metassedimentos clásticos.

Os resultados geocronológicos obtidos pelo método U-Pb para os zircões detríticos dos metassedimentos do Domínio Superior do CVN, com valores entre 3.61 e 2.37 Ga, apontam principalmente rochas paleo-arqueanas a neo-arqueanas com participação subordinada de rochas paleoproterozóicas, como áreas fontes dos metassedimentos analisados. Dentro destes resultados, as idades Neo- a Meso-arqueana, entre 2.85 e 2.67 Ga foram identificadas nas unidades do CT, atestando que o embasamento da bacia está presente na região estudada e que não esta distante de suas rochas fontes. As idades paleo-arqueanas encontradas, entre 3.0 e 3.5 Ga, foram descritas em ortognaisses da região de Tartarugalzinho (3.48 Ga) e da Vila Nova (3.3 Ga) por Rosa Costa *et al*. (2006, 2012) e Pimentel *et al*. (2002). As idades em torno de 3.6 Ga são inéditas e representam rochas ainda não encontradas na região.

Os resultados geocronológicos obtidos para os gnaisses granodioríticos e metagranodioritos do Complexo Tumucumaque, entre 2.85 e 2.81 Ga, apontam idades meso-arquenas, enquando os gabros intrusivos apresentam idade Neo-arqueana (2.67 Ga). Estes resultados indicam um episódio magmático principal de idade Meso-arqueana, e um episódio mais jovem, de idade Neo-arqueana, corroborando os dados obtidos anteriormente por Avelar (2002) e Rosa-Costa *et al*. (2003, 2006) nas porções centro-norte e centro-sul do estado do Amapá.

As idades modelo de Hf ($T_{DM}$) dos gnaisses granodioríticos do CT apresentaram valores Meso- e Paleo-arqueanos, entre 4.69 e 2.9 Ga com epsilon Hf positivos, entre +2.9 and +4.9, corroborando as observações de Barreto *et al*. (2013) que considerou o episódio Meso-arqueano como de crescimento crustal, enquanto o magmatismo Neo-arqueano seria dominantemente de retrabalhamento da crosta Meso-arqueana pré-existente.

Os novos dados de U-Pb em zircões detríticos obtidos em quartzito e metaconglomerado do CVN e as novas idades de cristalização obtidas nas rochas do CT corroboram as hipóteses da existência de um núcleo arqueano na porção sudeste do Escudo das Guianas, como sugerido nos trabalhos de Montalvão & Tassinari 1984, Lafon *et al*. (2001), Avelar (2002), Ricci *et al*. (2002), Avelar *et al*. 2003, Rosa-Costa *et al*. (2003, 2006, 2012), Barbosa *et al*. (2013). As idades U-Pb obtidas em zircões de meta-andesitos, entre 2.17 e 2.15 Ga, sugere que a evolução da bacia do CVN ocorreu durante a parte final do período Riaciano.

Os eventos de metamorfismo orogênico são mais jovens que a deposição da bacia e, portanto, são mais jovens que 2.15 Ga. A idade do metamorfismo de contato é sugerida por poucas idades U-Pb em granitos intrusivos desta região, como a Suíte Intrusiva Igarapé Careta, com 2.06 Ga e pelo Granito Amapari, de 1.99 Ga (Barbosa *et al*, 2013). Os dados do mapeamento geológico e estrutural, e da análise petrográfica e microestrutural, sugerem que os complexos Vila Nova e Tumucumaque foram afetados pelo mesmo evento de metamorfismo orogênico como indicado pelas mesmas feições deformacionais e pelo aumento de grau metamórfico, que varia entre as fácies Xistos Verdes Superior a Anfibolito Médio-Superior. Análises de rocha total em granadas de anfibolitos do Domínio Basal do CVN forneceram idades de 2.08 ±0.02 Ga, indicando que o metamorfismo regional antecedeu o magmatismo tardi-orogênico na Província Maroni-Itacaiúnas (Pimentel *et al.*, 2002). Além disso, datações U-Th-Pb em monazita realizadas em amostras de gnaisses de alto grau indicam que o metamorfismo de fácies granulito ocorreu a cerca de 2.10 e 2.08 Ga, durante o estádio de colisão do orógeno Transamazônico (Rosa-Costa *et al*., 2006). As idades das monazitas também revelam eventos de migmatização pós-colisional entre 2.06 e 2.04 Ga que ocorreram sob condições de fácies Anfibolito e foram contemporâneos com alguns episódios de intrusões graníticas (Rosa Costa *et al*., 2006). As idades isocronicas obtidas por Oliveira *et al*., (2008) pelo método Sm-Nd para o metamorfismo da fácies Granulito em granada-rocha total, situam-se entre 2.02 e 1.98 Ga e estão de acordo com os outros dados disponíveis. Deste modo, o metamorfismo que afetou o CVN é o mesmo que afetou o CT. As idades disponíveis permitem sugerir que este evento de metamorfismo orogênico pode ter ocorrido no intervalo entre 2.15 e 2.06 Ga.

Os dados obtidos permitiram apresentar o modelo esquemático da evolução geodinâmica para a área de estudo, modificado a partir do trabalho de Delor *et al*. (2003a) (**Figura 6**). Neste modelo, a abertura da porção NE do Cráton Amazônico

gerou um proto-oceano durante o Eo-riaciano, com geração de rochas básicas e sedimentos siliciclásticos maturos de margem passiva (Figura 6A). O fechamento deste oceano entre 2.18 e 2.13 Ga, produz um magmatismo orogênico pouco evoluído caracterizado pela formação de arcos intra-oceânicos e sequencias vulcano-sedimentares relacionadas a bacias de arco (Figuras 6B e 6C). O metamorfismo orogênico e a deformação das unidades marca a colisão entre os dois blocos arqueanos e a geração das principais zonas de cisalhamento dúcteis regionais (Figura 6D).

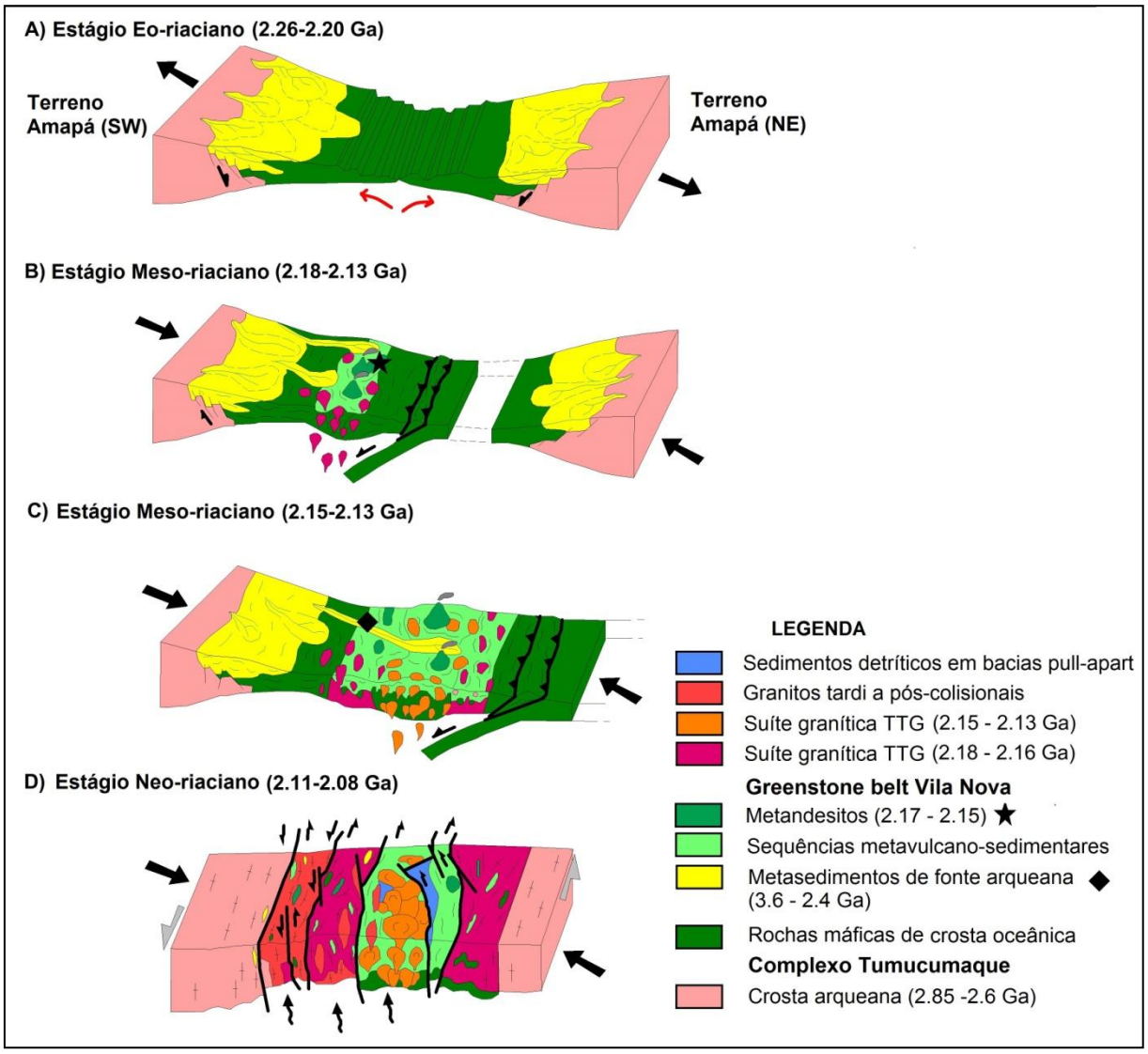


**Figura 6**. Modelo de evolução geotectônica do *greenstone belt* Vila Nova modificado a partir de Delor *et al*. (2003a).

## 1.5 Referências Bibliográficas

ACKERMANN, F.L. 1948. Recursos minerais do Território Federal do Amapá. Rio de Janeiro, Imprensa Nacional, 30 p.

AVELAR, V.G. 2002. *Geocronologia Pb-Pb em zircão e Sm-Nd em rocha total da porção centro- norte do Estado do Amapá – Brasil: Implicações para a evolução geodinâmica do setor oriental do Escudo das Guianas*. (Tese de Doutorado). 213 p. Universidade Federal do Pará, Centro de Geociências, Pós-Graduação em Geologia e Geoquímica, Belém.

AVELAR, V.G.; LAFON, J.M.; DELOR, C. 2001. Geocronologia Pb-Pb em zircão e Sm-Nd em rocha total da porção centro-norte do Estado do Amapá. Implicações pra a evolução geodinâmica do Escudo das Guianas. In: *Simpósio de Geologia da Amazônia, 7*. Resumos Expandidos. Belém, SBG-NO. CD-ROM.

AVELAR, V.G.; LAFON, J.M.; DELOR, C.; GUERROT, C.; LAHONDÈRE, D. 2003. Archean crustal remnants in the easternmost part of the Guiana Shield: Pb-Pb and Sm-Nd geochronological evidence for Mesoarchean versus Neoarchean signatures. *Geologie de la France*, 2-3-4:83-100.

BARBOSA, J.P.O.; COSTA NETO, M.C.; ROSA-COSTA, L.T.; ANJOS, G.C.; CHAVES, C.L., 2013. Projeto Folha Macapá (NA.22-Y-D). Mapa Geológico (1:250.000). CPRM, Belém.

BARRETO, C.J.S.; LAFON, J.M.; ROSA-COSTA, L.T.; DANTAS, E.L. 2013. Paleoproterozoic granitoids from the northern limit of the Archean Amapá block (Brazil), southeastern Guyana Shield: Pb-Pb evaporation in zircons and Sm-Nd geochronology. *Journal of South American Earth Sciences*, 45:97-116.

BORGHETTI, C.; PHILIPP, R.P.; BASEI, M.A.S.; MANDETTA, P. 2014. New ages from Vila Nova and Tumucumaque Complex in the Cupixi region, Porto Grande, Amapá, Brazil. *9th South American Symposium on Isotope Geology*. Boletim de Resumos Expandidos, São Paulo, CPGeo-IGc/USP.

CARVALHO, F.P. de & SILVA, M.R. 1969. Relatório de reconhecimento geo-econômico da ocorrência de magnetita da regiäo de Tracajatuba, município de Amapá, Território Federal do Amapá. Belém, DNPM, 12 p.

CARVALHO, J.M.A.; FARACO, M.T.L.; KLEIN, E.L. 1995. Carta geoquímico-metalogenética de ouro do Amapá/NW do Pará, escala 1:500.000: Mapa e Nota Explicativa. Belém: CPRM, 4 p.

COELHO FILHO, A.C. 1998. Exaustão das Reservas Remanescentes do Distrito Manganesífero de Serra do Navio. ICOMI (Relatório Interno).

CORDANI, U.G. & BRITO NEVES, B.B. 1982. The geologic evolution of South America during the Archean and Early Proterozoic. *Revista Brasileira de Geociências*, 12: 78-88.

CORDANI, U.G.; TASSINARI, C.C.G.; TEIXEIRA, W.; BASEI, M.A.S.; KAWASHITA, K. 1979. Evolução tectônica da Amazônia com base nos dados geocronológicos. In: *Congresso Geológico Chileno, 2*. Actas, p. 137-148. Arica, Chile.

CORDANI, U.G.; TEIXEIRA, W.; D'AGRELLA-FILHO, M.S.; TRINDADE, R.I. 2009. The position of the Amazonian Craton in supercontinents: *Gondwana Research*, 15, 396–407. doi:10.1016/j.gr.2008.12.005.

COSTA, J.B.S. & HASUI, Y. 1997. Evolução geológica da Amazônia. In: COSTA, M.L.C. & ANGÉLICA, R.S. (coords.) Contribuição à Geologia da Amazônia. Belém, SBG-NO, p.15-90.

DELOR, C.; LAHONDÈRE, D.; EGAL, E.; LAFON, J.M.; COCHERIE, A.; GUERROT, C.; ROSSI, P.; TRUFERT, C.; THEVENIAUT, H.; PHILLIPS, D.; AVELAR, V.G. 2003a. Transamazonian crustal growth and reworking as revealed by the 1:500.000 - scale geological map of French Guiana (2nd edition). *Géologie de la France*, 2-3-4: 5-57.

DELOR, C.; ROEVER, E.W.F.; LAFON, J.M.; LAHONDÈRE, D.; ROSSI, P.; COCHERIE, A.; GUERROT, C.; POTREL, A. 2003b. The Bakhuis ultrahigh-temperature granulite belt (Suriname): II. Implications for late Transamazonian crustal stretching in a revised Guiana Shield framework. *Géologie de la France*, 2-3-4: 207-230.

FARACO, M.T.L. 1990. *Evolução petrológico-geoquímica das rochas da Suíte Metamórfica Vila Nova na Serra do Ipitinga (NW do Pará)*. (Dissertação de Mestrado). Centro de Geociências, Universidade Federal do Pará, Belém.

FARACO, M.T.L. 1997. *Evolução petroquímico-metalogenética das rochas e mineralizações associadas à Suíte Vila Nova na Serra do Ipitinga (NW do Pará)*. (Tese de Doutorado). 245p. Universidade Federal do Pará, Centro de Geociências, Pós-Graduação em Geologia e Geoquímica, Belém.

GRANT, F.S. 1984. Aeromagnetic, geology and ore environments: II Magnetite and ore environments. *Geoexploration*, 24, 335-362.

GIBBS, A.K.; OLSZEWSKI, W.J. 1982. Zircon U-Pb ages of Guyana greenstone-gneiss terrane. *Precambrian Research* 17, 199-214.

GRUAU, G.; MARTIN, H.; LEVEQUE, B.; CAPDEVILLA, R. 1985. Rb-Sr and Sm-Nd geochronology of lower Proterozoic granite-greenstone terrains in French Guyana, South America. *Precambrian Research* 30, 63-80.

FERRAN, A. 1988. Depósitos de ouro de Salamangone e Mutum, Calçoene Amapá, In: SCHOBBENHAUS, C.; GOLD, C.E.S. (Coords). *Principais Depósitos Minerais do Brasil*. 3, 581-588. Brasília, DNPM/CVRD.

FERREIRA, E.O. 1949. Jazimentos de minerais metalíferos no Brasil (síntese). Divisão de Geologia e Mineralogia, Rio de Janeiro, 130, 122 p.

HOFFMANN, I. 2017. *Petrologia dos basaltos toleiticos de 2.1 Ga do Greenstone Belt da Vila Nova, Escudo das Guianas, Amapá, Brasil*. (Dissertação de Mestrado). 77p. Universidade Federal do Rio Grande do Sul, Instituto de Geociências, Programa de Pós-graduação em Geociências, Porto Alegre.

HOFFMANN, I.; PHILIPP, R.P.; BORGHETTI, C. 2018 Geochemistry and origin of the Rhyacian tholeiitic metabasalts and meta-andesites from the Vila Nova Greenstone Belt, Guiana Shield, Amapá, Brazil. *Journal of South American earth Sciences*, aceito para publicação.

JORGE JOÃO, X.S.; FRIZZO, S.J.; MARINHO, P.A.; CARVALHO, J.M.A.; SILVA NETO, C.S.; SOUZA, A.N.; GUIMARÃES, L.R. 1978. Projeto Sudoeste do Amapá (Relatório Final). Belém: DNPM/ CPRM. v. 1-A, 224p.

JORGE JOÃO, X.S..; CARVALHO, J.M.A.; VALE, A.G.; FRIZZO, S.J.; MARTINS, R.C. 1979. Projeto Rio Falsino (Relatório Final). Belém, DNPM-CPRM. v.1-A, 199 p.

LAFON J.M.; AVELAR V.G.; ROSSI P.; DELOR C.; GUERROT C.; PIDGEON, R. T. 2000. Geochronological evidence for reworked Neoarchean crust during Transamazonian orogeny (2,1Ga) in the southeastern Guiana Shield. In: *International Geological Congress, 31*. Abstracts. Rio de Janeiro, CD-ROM.

LAFON, J.M.; ROSSI, P.; DELOR, C.; BARBOSA, O.S. 2001. Granulitos tardi-Transamazônicos (2,06Ga) na região norte do Estado do Amapá: o charnoquito de Calçoene. In: *Simpósio de Geologia da Amazônia*, *7*. Resumos Expandidos. Belém, SBG-NO. CD-ROM.

LAFON, J.M.; DELOR, C.; THÉVENIAUT, H.; KRYMSKY, R.; TAVARES, R.P.S.; ROIG, J.Y. 2003. Isotopic deciphering of Rhyacian crustal evolution along the northern Oyapok river: new constraints from Sm-Nd, U-Pb and Pb-Pb geochronology. In: *Simpósio de Geologia da Amazônia*, *8*. Resumos Expandidos. Manaus, SBG-NO. CD-ROM.

LAFON, J.M.; TAVARES, R.P.S.; TASSINARI, C.G.G.; BARROS, C.E.M. 2008. Idade, caracterização geoquímica e isótopos de Nd dos anfibolitos do grupo Vila Nova e granitóides associados na Serra do Navio, borda norte do bloco arqueano Amapá: implicações geodinâmicas. In: *Congresso Brasileiro Geologia*, 44, Curitiba.

LASA, 1958. Levantamento Aerofotogramétricos. In: *Projeto RADAM Brasil*, *1974*. Folha NA/NB 22 Macapá, 120p. Rio de Janeiro.

LEAL, J.W.L. & PINHEIRO, M.M. 1971. Cadastramento dos garimpos de ouro e tantalita do rio Cupixi. Belém, DNPM, 24 p.

LIMA, M.I.C.; MONTALVÃO, R.M.G.; ISSLER, R.S.; OLIVEIRA, A.S.; BASEI, M.A.S.; ARAÚJO, J.F.V.; SILVA, G.G. 1974. Geologia. In: *Projeto RADAM Brasil, 1974.* Folha NA/NB 22 Macapá, 120p. Rio de Janeiro.

MAROTTA, C.A. 1966. Notas sobre o distrito manganesífero da Serra do Navio, território Federal do Amapá - Brasil. Divisão de Geologia e Mineralogia, Rio de Janeiro, 41:57-68.

McREATH I. & FARACO M.T.L. 2006. Paleoproterozoic greenstone-granite belts in northern Brazil and the former Guyana Shield-West African craton province. *Revista do Instituto de Geociências - USP, Série Científica*, 5(2):49-63.

MELO, L.V.; VILLAS, R.N.N.; FARACO, M.T.L.; SOARES, J.W. 2003. Geological setting and mineralization fluids of the Amapari gold deposit, Amapa State, Brazil. *Géologie de la France* 2-3-4, 243-255.

MONTALVÃO, R.M.G. & TASSINARI, C.C.G. 1984. Geocronologia pré-cambriana do Território Federal do Amapá (Brasil). In: *Simpósio de Geologia da Amazônia*, 2, 54-57. Manaus, SBG.

MONTALVÃO, R.M.G. 1985. Petrologia das rochas máfico-ultramáficas do Supergrupo Vila Nova (greestone belt) e Grupo Parima (greenstone belt) e enclaves na região de Parima. *Simpósio Geologia Amazônia*, 2, 110-123. Belém.

NAGELL, R.H. & SILVA, A.R. 1961. O carbonato de manganês como proto-minério do deposito da Serra do Navio, território Federal do Amapá. Brasil. *Sociedade Brasileira de Geologia*, 10 (2):53-59. São Paulo.

NAGELL, R.H. 1962. Geology of the Serra do Navio manganese district, Brazil. Econ. Geol., Lancaster, 57 (4):481-498.

NEVES, S.B. & MENEZES, J.A.L. 1967. Reconhecimento geológico da região nordeste do território Federal do Amapá. Belém, Petrobrás - Renor, 24 p. (Relatório técnico, 84).

NOGUEIRA, S.A.A.; BETTENCOURT, J.S.; TASSINARI, C.C.G. 2000. Geochronology of the Salamangone gold deposit host-rocks, Lourenço district, Amapá, Brazil. *Revista Brasileira de Geociências*, 30(2): 261-264.

OLIVEIRA, E.C.; LAFON, J.M.; GIOIA, S.M.C.L.; PIMENTEL, M.M. 2008. Datação Sm-Nd em rocha total e granada do metamorfismo granulítico da região de Tartarugal Grande, Amapá Central. *Revista Brasileira de Geociências*, 38(1): 114-127.

PAIVA, G. 1946. Províncias Pegmatíticas do Brasil. Rio de Janeiro, DNPM/DFPM, 13-21 (Boletim 78).

PIMENTEL, M.M.; FERREIRA FILHO, C.F.; SPIER, C.A. 2002. Estudo Sm-Nd do Complexo Máfico-Ultramáfico Bacuri, Amapá: idade da intrusão, metamorfismo e natureza do magma original. *Revista Brasileira de Geociências*, 32: 371-376.

PROJETO RADAM BRASIL, 1974. Folha NA/NB. 22 Macapá: geologia, geomorfologia, solos, vegetação e uso potencial da terra (Rio de Janeiro: Departamento Nacional da Produção Mineral). Levantamento de Recursos Naturais, 6.

RICCI, P.S.F.; CARVALHO, J.M.A.; ROSA-COSTA, L.T.; LAFON, J.M. 2002. Plúton charnoenderbítico arqueano intrusivo nos ortognaisses granulíticos do Cinturão Jari

– Terreno Arqueano expressivo do sudeste do Escudo das Guianas. In: *Congresso Brasileiro de Geologia*, 41, p.524. João Pessoa, SBG-NE.

ROSA-COSTA, L.T; RICCI, P.S.F.; LAFON, J.M.; VASQUEZ, M.L.; CARVALHO, J.M.A.; KLEIN, E.L.; MACAMBIRA, E.M.B. 2003. Geology and geochronology of archean and paleoproterozoic domains of the southeastern Amapá and northwestern Pará, Brazil – southeastern Guyana Shield. *Géologie de la France*, 2-3-4:101-120.

ROSA-COSTA, L.T. 2006. *Geocronologia $^{207}Pb/^{206}Pb$, Sm-Nd, U-Th-Pb e $^{40}Ar$-$^{39}Ar$ do Segmento Sudeste do Escudo das Guianas: Evolução Crustal e Termocronologia do Evento Transamazônico*. (Tese de Doutorado). 226p. Universidade Federal do Pará, Curso de Pós-Graduação em Geologia e Geoquímica, Belém.

ROSA-COSTA, L.T.; SILVA, C.M.G.; BARBOSA, J.P.O.; COSTA NETO, M.C. 2012. Projeto Folha Rio Araguari - NA 22-Y-B. Mapa Geológico (1:250.000). CPRM, Belém.

SANTOS, J.O.S.; HARTMANN, L.A.; GAUDETTE, H.E.; GROVES, D.I.; McNAUGHTON, N.J.; FLETCHER, I.R. 2000. A new understanding of the provinces of the Amazon Craton based on integration of field mapping and U-Pb and Sm-Nd geochronology. *Gondwana Research*, 3(4): 453-488.

SATO, K. & TASSINARI, C.C.G. 1997. Principais eventos de acreção continental no Cráton Amazônico baseados em idade-modelo Sm-Nd, calculada em evoluções de estágio único e estágio duplo. In: COSTA, M. L. C. & ANGÉLICA, R.S. (coords.) *Contribuição à Geologia da Amazônia,* 91-142. Belém, SBG-NO.

SCARPELLI, W. 1966. Aspectos genéticos e metamórficos das rochas do distrito da Serra do Navio; Território Federal do Amapá. Divisão de Geologia e Mineralogia, Rio de Janeiro, 41:37-55.

SPIER, C.A. & FERREIRA FILHO, C.F. 1999. Geologia, estratigrafia e depósitos minerais do Projeto Vila Nova, Escudo das Guianas, Amapá, Brasil. *Revista Brasileira de Geociências*, 29:173-178.

TASSINARI, C.C.G. & MACAMBIRA, M.J.B. 1999. Geochronological provinces of the Amazonian Craton. *Episodes*, 22(3): 174-182.

TASSINARI, C.C.G. & MACAMBIRA, M.J.B. 2004. A evolução tectônica do Cráton Amazônico. In: MANTESSO-NETO, V.; BARTORELLI, A.; CARNEIRO, C.D.R.; BRITO NEVES, B.B. (eds.) *Geologia do Continente Sul-Americano: Evolução da Obra de Fernando Flávio Marques de Almeida*, 471-485. São Paulo, Beca.

TASSINARI, C.C.G.; BETTENCOURT, J.S.; GERALDES, M.C.; MACAMBIRA, M. J.B.; LAFON, J.M. 2000. The Amazonian Craton. In: CORDANI, U.G.; MILANI, E.J.; FILHO, A.T.; CAMPOS, D.A. (eds.) *Tectonic Evolution of South America,* 41-95. 31$^{0}$ International Geological Congress, Rio de Janeiro, SBG.

TAVARES, R.P.S. 2009. *Granitóides e anfibolitos da Serra do Navio, borda norte do bloco arqueano Amapá: caracterização petrográfica e geoquímica, geocronologia*

*Pb-Pb em zircão e isótopos de Nd*. (Dissertação de mestrado). 114p. Universidade Federal do Pará, Programa de Pós-graduação em Geociências, Belém.

TEIXEIRA, J.B.G.; MISI, A.; SILVA, M.G. 2007. Supercontinent evolution and the Proterozoic metallogeny of South America. *Gondwana Research*, 11: 346–361.

TEIXEIRA, W.; TASSINARI, C.C.G.; CORDANI, U.G.; KAWASHITA, K. 1989. A review of the geochronology of the Amazonian Craton: Tectonic implications. *Precambrian Research*, 42: 213-227.

VEIGA, A.T.C.; BRAIT FILHO, L.; OLIVEIRA, C.A.C. 1985. Geologia da Província Aurífera de Cassiporé – Amapá. In: *Simpósio de Geologia da Amazônia, 2*. Anais, 135-146. Belém, SBG.

VELÁSQUEZ, G.; BÉZIAT, D.; SALVI, S.; TOSIANI, T.; DEBAT., P. 2011. First occurrence of Paleoproterozoic oceanic plateau in the Guiana Shield: The gold-bearing El Callao Formation, Venezuela. *Precambrian Research,* 186: 181–192.

## 2. CORPO PRINCIPAL DA TESE

**2.1** Geologia e geofísica do greenstone belt Vila Nova, porção NE do Cráton Amazônico, Amapá, Brasil. Revista do Instituto de Geociências, USP, Série Científica, São Paulo, v. 17, n. 1, p. 109-127, Março 2017.

Geologia USP
Série Científica

DOI: 10.11606/issn.2316-9095.v17-372

Revista do Instituto de Geociências - USP
Geol. USP, Sér. cient., São Paulo, v. 17, n. 1, p. 109-127, Março 2017

# Geologia e geofísica do *greenstone belt* Vila Nova, porção NE do Cráton Amazônico, Amapá, Brasil

## *Geology and geophysics of the Vila Nova Greenstone Belt, northeastern portion of the Amazonian Craton, Amapá, Brazil*

Cristiano Borghetti[1] e Ruy Paulo Philipp[2]

[1]Universidade Federal do Rio Grande do Sul – UFRGS, Instituto de Geociências, Programa de Pós-graduação em Geociências – PPGGEO, Avenida Bento Gonçalves, 9500, CEP 91501-970, Porto Alegre, RS, Brasil (cborghetti@terra.com.br)
[2]Universidade Federal do Rio Grande do Sul – UFRGS, Instituto de Geociências, Centro de Estudos em Petrologia e Geoquímica – CPGq, Porto Alegre, RS, Brasil (ruy.philipp@ufrgs.br)

Recebido em 22 de janeiro de 2016; aceito em 10 de outubro de 2016

**Resumo**

Poucos afloramentos e um acentuado intemperismo caracterizam a região do *greenstone belt* Vila Nova, no sudeste do Amapá. Este artigo vale-se de dados aerogeofísicos na interpretação geológica e estrutural durante o mapeamento geológico, objetivando aumentar o entendimento geológico e tectônico dessa porção do Cráton Amazônico. A interpretação qualitativa das imagens magnetométricas e gama-espectrométricas geradas para o projeto foi efetuada em ambiente de Sistema de Informações Geográficas (SIG). O reconhecimento de unidades magnetométricas e gamaespectrométricas presentes na área de estudo teve como base a classificação hierárquica dos polígonos delineados pela interpretação visual. A partir dessa análise foram delimitados os principais domínios geológicos e definidos os traçados geológico-estruturais, em conjunto com dados geológicos de campo, dados geofísicos e da análise petrográfica. Essa integração permitiu delimitar as rochas das áreas do embasamento arqueano composto por ortognaisses e granitóides do Complexo Tumucumaque, as rochas metavulcano-sedimentares do Complexo Vila Nova e os maciços graníticos intrusivos de idade paleoproterozoica. A integração entre os dados geofísicos e de campo resultou no aumento da definição da cartografia geológica, ressaltando-se a importância dessa metodologia para o reconhecimento de tramas estruturais e litológicas complexas em áreas de pouca exposição e dificuldade de acesso.

**Palavras-chave:** Cráton Amazônico; *Greenstone belt* Vila Nova; Aerogeofísica; Geologia estrutural; Mapeamento geológico.

**Abstract**

A few outcrops and strong weathering conditions prevail in the region of the Vila Nova Greenstone Belt in the southeastern Amapá (Brazil). This paper describes the use of airborne geophysical data for geological and structural analysis during geological mapping. This integration aims to improve the geological and tectonic understanding of this portion of the Amazonian Craton. The magnetometric and gamma-spectrometric qualitative interpretation of the images took place in a Geographic Information System (GIS) environment. Recognition of magnetometric and gamma-ray spectrometric units present in the study area was based on the hierarchical classification of polygons outlined by visual interpretation. The major geological domains and the structural patterns were defined by integration of geophysical data, geological mapping and petrographic analysis. The results allowed the recognition of Archean basement rocks composed of orthogneisses and granitoids of the Tumucumaque Complex, the metavolcano-sedimentary rocks of the Vila Nova Complex and Paleoproterozoic granite massifs. The integration of geophysical and field data resulted in the increase of the geological mapping definition, highlighting the importance of this methodology for recognition of complex structural and lithological fabrics in areas of difficult access and scarce fresh rock outcrops.

**Keywords:** Amazonian Craton; Vila Nova Greenstone belt; Aerogeophysics; Structural geology; Geological mapping.

## INTRODUÇÃO

O uso de métodos indiretos para auxiliar na interpretação geológica e estrutural durante o mapeamento geológico é uma ferramenta importante para avaliar a continuidade e a extensão de registros litológicos e estruturais obtidos em campo. Esse recurso é fundamental em áreas de difícil acesso, de vegetação densa, de espessas camadas de solo e com exposições limitadas.

A utilização de métodos geofísicos, como gama-espectrometria e magnetometria, na caracterização de terrenos com ocorrência de *greenstone belts* tem assumido grande destaque no cenário nacional e internacional. Os *greenstone belts* são sequências vulcano-sedimentares que ocorrem associadas a terrenos granito-gnáissicos, compondo grande parte dos terrenos arqueanos e paleoproterozoicos, como aqueles dos crátons Slave (Canadá), Pilbara (Austrália), Kapvaal (Barberton, África do Sul), Madagascar, Groenlândia (Isua) (Vearncombe et al., 1986; McCarthy e Rubidge, 2005; Press et al., 2006; Kearey et al., 2009). Os *greenstone belts* são constituídos por uma sucessão de rochas vulcânicas máficas e ultramáficas, com ocorrência subordinada de rochas ácidas, intercaladas com rochas sedimentares clásticas e químicas. Essas sequências são formadas numa diversidade de ambientes, como riftes continentais evoluídos, bacias marginais, arcos de ilha, bacias de retroarco e ambientes oceânicos gerados por influência de *hot spots*. Sempre relacionados ao vulcanismo submarino, são muito comuns no Arqueano e no Paleoproterozoico e responsáveis por grande número de metais preciosos, principalmente ouro, prata, chumbo, níquel, cromo, zinco e associação de Pb-W-Zn-Ag (Cu) (Grant, 1984).

No Brasil, encontram-se sequências do tipo *greenstone belts* nas áreas dos crátons Amazônico e do São Francisco, com destaque para as importantes mineralizações dos *greenstone belts* do Rio das Velhas, em Minas Gerais, Rio Itapicuru, na Bahia, e associados à província de Carajás, no Pará (Lobato et al., 2001; Noce et al., 2007).

A região sudeste do Amapá, área objeto deste estudo, possui acesso rodoviário restrito, densa cobertura de floresta tropical, solo e regolito muito espesso (entre 10 e 50 metros) e poucas exposições rochosas. Os principais afloramentos são blocos e lajeados encontrados ao longo dos rios Vila Nova, Cupixi, Santa Maria e Piaçacá, raros cortes de estrada muito alterados e exposições de rocha alterada nas áreas do garimpo de ouro da Vila Nova.

O Complexo Vila Nova é uma unidade metavulcano-sedimentar do tipo *greenstone belt* que repousa sobre um embasamento composto por ortognaisses e granitóides do Complexo Tumucumaque, do Complexo Guianense e dos granitos Anauerapucu e Mungubas, estando localizado no sudeste do Escudo das Guianas, nordeste do Cráton Amazônico (Figura 1). A base do Complexo Vila Nova é composta por metabasaltos, metandesitos e raros metadacitos e sua unidade superior é constituída dominantemente por metassedimentos clásticos, intercalados com rochas metavulcânicas máficas e químico-exalativas subordinadas. As rochas metassedimentares caracterizam-se por espesso pacote de quartzitos, quartzitos hematíticos e xistos pelíticos, com níveis subordinados de metaconglomerados e de hematita filitos.

As relações estratigráficas e estruturais e os tipos de contatos entre essas unidades ainda são pouco conhecidos. A região da Vila Nova está localizada na porção centro-sul do Estado do Amapá, nos municípios de Mazagão e Porto Grande, cortada pelo Rio Vila Nova, em seu médio-alto curso, e pelo Rio Piaçacá (Figura 2).

Este trabalho objetiva definir as relações estratigráficas e o arcabouço estrutural do Complexo Vila Nova e suas relações com o terreno granito-gnáissico representado pelas unidades do Complexo Tumucumaque. Essas relações estão apresentadas no mapa geológico da região da Vila Nova em escala 1:50.000, gerado a partir da integração de dados aeromagnetométricos e gama-espectrométricos com os dados obtidos no mapeamento geológico e estrutural. Posteriormente, esse mapa foi expandido (1:100.000) até a região da Serra do Navio, com base nos dados aerogeofísicos disponíveis. Essa integração permitiu o mapeamento de estruturas regionais, a caracterização dos principais lineamentos, definição dos contatos geológicos e avaliação das estruturas do embasamento do Complexo Vila Nova em uma área de domínio de floresta equatorial densa.

## CONTEXTO GEOTECTÔNICO

A área de estudo está localizada na extremidade sudeste do Escudo das Guianas, porção nordeste do Cráton Amazônico, na Província Maroni-Itacaiúnas (Figura 1A). O Cráton Amazônico é constituído por uma extensa faixa central composta por um núcleo arqueano, envolto por faixas móveis alongadas segundo a direção NW-SE de idades paleo e mesoproterozoicas (Cordani et al., 1979, 2009; Cordani e Brito Neves, 1982; Teixeira et al., 1989; Santos et al., 2000; Tassinari et al., 2000; Avelar et al.; 2003; Tassinari e Macambira, 2004) (Figura 1B). As faixas móveis paleoproterozoicas são constituídas por extensas bacias associadas a arcos magmáticos, compondo trilhas descontínuas de *greenstone belts*, e por associações graníticas do tipo TTG (Avelar et al., 2003; McReath e Faraco, 2006; Rosa-Costa et al., 2006).

A região da Vila Nova, situada na porção sudeste do Escudo das Guianas, está inserida dentro da Província Maroni-Itacaiúnas, uma faixa móvel paleoproterozoica com evolução relacionada à Orogênese Transamazônica, entre 2,25 Ga e 2,05 Ga (Tassinari et al., 2000; Delor et al., 2003a, 2003b; Cordani et al., 2009). Nessa região, o embasamento é composto por ortognaisses e granitóides que correspondem a rochas metamorfizadas e parcialmente retrabalhadas

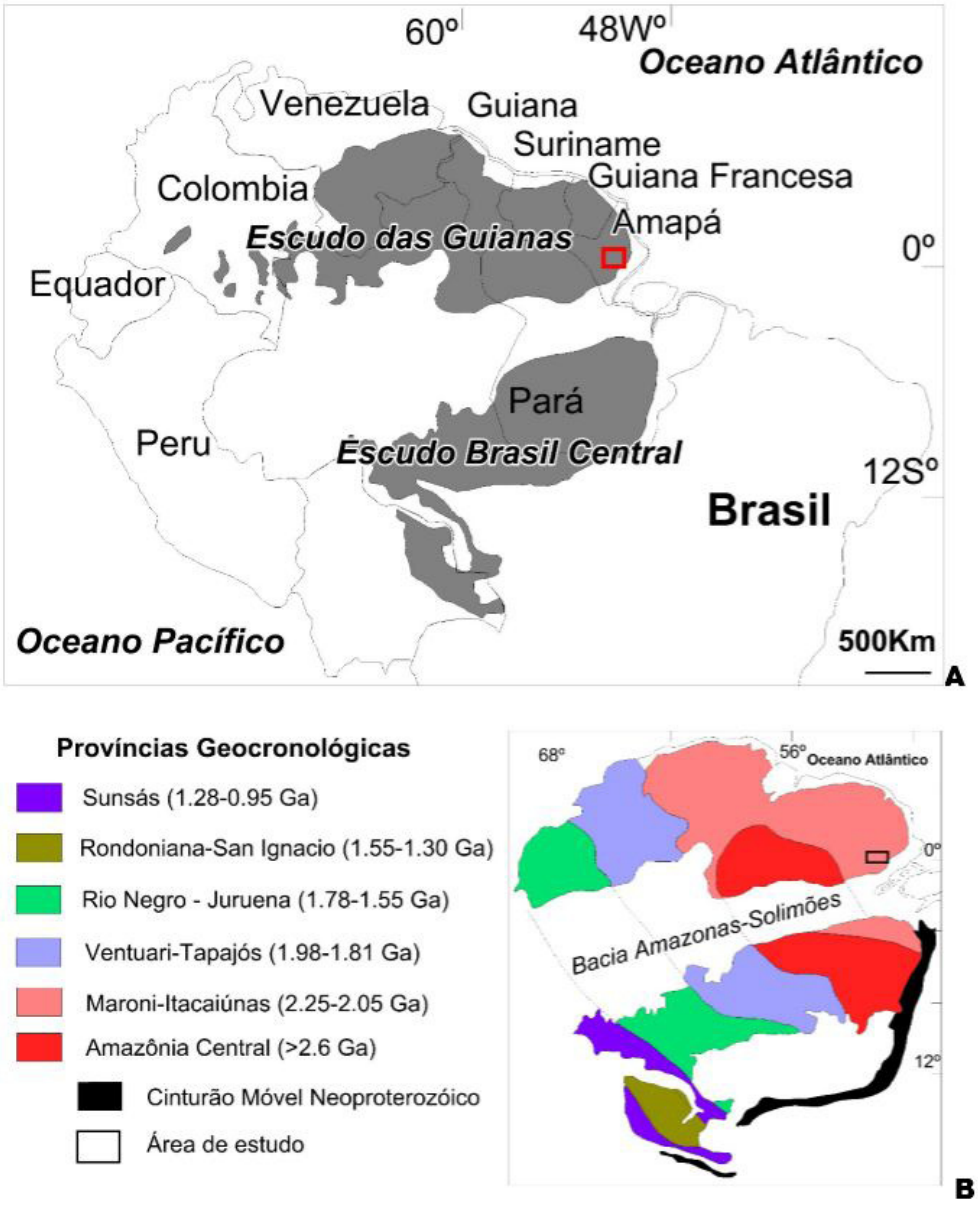


**Figura 1.** A) Localização dos escudos das Guianas e do Brasil Central no Cráton Amazônico, destacando-se no retângulo vermelho a localização da área estudada; B) Distribuição das Províncias Geocronológicas do Cráton Amazônico de acordo com Tassinari e Macambira, (2004). Os intervalos de idades das províncias estão de acordo com Cordani et al. (2009).

durante a Orogênese Transamazônica constituindo um núcleo arqueano disposto como uma faixa alongada segundo a direção NW-SE, envolta por rochas paleoproterozoicas (Rosa-Costa et al., 2006; Rosa-Costa, 2006). O termo Complexo Vila Nova foi usado para designar as unidades metavulcano-sedimentares que ocorrem como *greenstone belts,* denominados regionalmente como Ipitinga, Tumucumaque, Serra do Navio, Tartarugalzinho, Lombarda e Oiapoque (McReath e Faraco, 2006).

Na região da Vila Nova, as unidades mais antigas são representadas pelo Complexo Tumucumaque, pelos granitos Anauerapucu, Mungubas e pelas rochas intrusivas do Complexo Bacuri (Spier, 1999; Spier e Ferreira Filho, 1999; Pimentel et al., 2002; Barbosa et al., 2013). O Complexo Tumucumaque é a unidade mais antiga e está representado por gnaisses tonalíticos a granodioríticos, metagranodioritos e metadioritos/anfibolitos, com ocorrência subordinada de metagabros intrusivos pouco ou indeformados e concordantes ao bandamento gnáissico regional (Rosa-Costa et al., 2006; Borghetti et al., 2014). Esses gnaisses estão metamorfizados em condições da fácies anfibolito médio a superior. As relações estratigráficas indicam que o Complexo Bacuri é intrusivo

no Complexo Tumucumaque, embora o contato esteja encoberto por espessa cobertura de solos (Spier e Ferreira Filho, 1999). Sobre essas unidades repousam as rochas do Complexo Vila Nova, afetadas por baixo a médio grau de metamorfismo orogênico (Figura 2).

O Complexo Máfico-Ultramáfico Bacuri (CMUB) é formado pela intercalação de corpos de anfibolitos com serpentinitos, associados com tremolititos e cromititos. Essas unidades apresentam registro de intensa deformação dúctil sob condições metamórficas de fácies anfibolito. O CMUB constitui um corpo alongado segundo a direção E-W, com estrutura interna estratiforme, que apresenta relações intrusivas com os ortognaisses do Complexo Tumucumaque e contato tectônico com os metassedimentos do Complexo Vila Nova (Spier, 1999). A natureza estratiforme do CMUB é definida por um acamadamento magmático e por texturas cumuláticas, bem como pelas características químicas e texturais dos cromititos e das rochas máfico-ultramáficas hospedeiras (Spier e Ferreira Filho, 1999).

O Complexo Vila Nova é uma unidade metavulcano-sedimentar constituída por rochas metavulcânicas básicas a intermediárias, rochas químico-exalativas e rochas metassedimentares clásticas (Barbosa et al., 2013). Segundo esses mesmos autores, esse complexo é composto pelas seguintes formações, da base

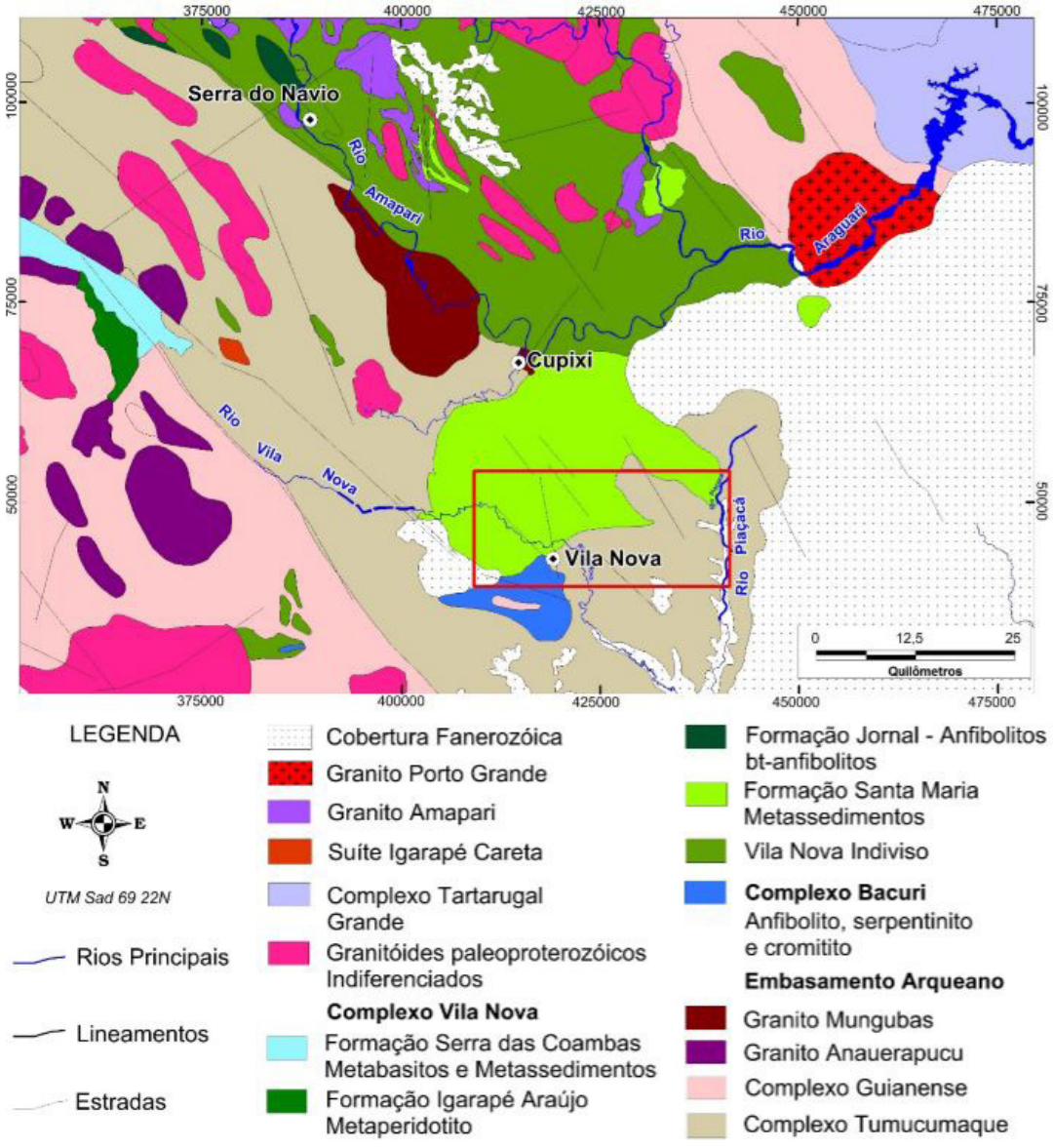


**Figura 2.** Mapa geológico da região da Vila Nova e da Serra do Navio, destacando-se no retângulo a localização da área estudada. Escala 1:100.000. Fonte: extraído de Faraco et al. (2004) e Barbosa et al. (2013).

para o topo: Vila Nova Indiviso, Formação Santa Maria, Formação Jornal, Formação Igarapé Araujo e Formação Serra das Coambas.

A Formação Vila Nova Indiviso compõe-se de um conjunto de anfibolitos, actinolita xistos e xistos paraderivados com metamorfismo em fácies anfibolito, atingindo localmente granulito (Barbosa et al., 2013). A Formação Santa Maria compreende xistos paraderivados com biotita, granada e cordierita, por vezes com muscovita ou sillimanita, além de quartzitos. Inclui faixas isoladas de rochas paraderivadas químicas e clásticas, com BIFs, quartzitos a magnetita e magnetititos contendo depósitos de ferro. A Formação Jornal é composta por actinolita xistos, anfibolitos e clorita-cummingtonita-antofilita xistos. A Formação Igarapé Araujo é composta por metamafitos e metaultramafitos, representados por xistos com plagioclásio e actinolita e anfibolitos e por metadunitos, metaperidotitos e xistos magnesianos com olivina, tremolita, antofilita-talco e serpentina-clorita. A Formação Serra das Coambas é constituída por quartzitos puros e aluminosos, xistos pelíticos e BIFs (formação ferrífera bandada, fácies óxido e aluminoso), com ocorrência subordinada de anfibolitos e metariolitos (Barbosa et al., 2013) (Figura 2). Na área de estudo afloram as rochas correspondentes a Formação Santa Maria, Complexo Bacuri e Complexo Tumucumaque.

Na região ocorrem, ainda, o Complexo Tartarugal Grande e granitoides indiferenciados, esses dominantemente biotita-granitos, ocasionalmente milonitizados. O Complexo Tartarugal Grande compreende uma associação de granulitos de composição enderbítica, charnockítica e charnoenderbítica, com lentes de granulitos máficos, com retrometamorfismo de fácies anfibolito e também com registros de migmatização. A Suíte Igarapé Careta é representada por leucogranitos peraluminosos com biotita e muscovita, com ou sem granada, de composição sienogranítica a granodiorítica. Em geral estão deformados e apresentam estruturas foliadas e portadoras de recristalização dinâmica. O Granito Amapari está representado por álcali-feldspato granito e sienogranitos e monzogranitos com textura inequigranular alotriomórfica média a grossa. O Granito Porto Grande varia de sienogranito a monzogranito, apresenta textura equigranular a porfirítica grossa, textura rapakivi e feições de fluxo magmático (Barbosa et al., 2013).

A cobertura fanerozoica inclui pelitos, arenitos e arenitos conglomeráticos ferruginosos de ambiente fluvial e estuarino, sedimentos areno-argilosos a areno-conglomeráticos friáveis, associados a sistema fluvial.

## MATERIAIS E MÉTODOS

Esta pesquisa foi desenvolvida a partir da interpretação de dados aero-gama-espectrométricos e aero-magnetométricos integrados com dados litológicos e estruturais obtidos no mapeamento geológico associada com análises petrográficas, geoquímicas e de testemunhos de sondagem.

O mapeamento geológico foi realizado com o apoio da Mineração Amapari SA e ocorreu em duas etapas, entre 2011 e 2013. Foram realizados trabalhos sistemáticos de campo com coleta de amostras para petrografia, geoquímica e geocronologia e correlação entre as estruturas interpretadas na geofísica e as feições geológicas observadas no campo (estruturas e litotipos). Os trabalhos de campo na região da Vila Nova objetivaram a caracterização dos principais conjuntos litoestratigráficos e suas relações de contato, sintetizadas através do mapeamento geológico em escala 1:50.000. Foram desenvolvidos perfis geológicos perpendiculares às principais estruturas, com coleta de dados estruturais e confecção de croquis esquemáticos (Figura 3). As atividades de campo foram complementadas pela descrição e interpretação de testemunhos de sondagem disponibilizados pela Mineração Amapari SA.

Os dados aerogeofísicos foram obtidos e processados (nivelamento e micronivelamento) pelo Serviço Geológico do Brasil (CPRM) através dos projetos Rio Araguari (CPRM, 2004) e Amapá (CPRM, 2006), sendo posteriormente reprocessados para a obtenção dos produtos necessários à interpretação e avaliação regional. A obtenção dos dados pela CPRM foi estabelecida com base em voos paralelos com espaçamento entre linhas de 500 metros, com uma medida realizada a cada 70 metros e 7 metros, respectivamente. A direção das linhas de aquisição de dados geofísicos do projeto Rio Araguari foi de N45ºW e a do projeto Amapá N-S. Os dados topográficos foram retirados do levantamento Shuttle Radar Topography Mission (SRTM), com resolução espacial aproximada de 90 metros na região do estudo.

Na execução deste trabalho foram utilizados os seguintes produtos geofísicos: (1) Campo Magnético Total (CMT); (2) Primeira Derivada Magnética do CMT (1DZ); (3) Amplitude do Sinal Analítico (ASA_hd) e (4) Amplitude do Sinal Analítico (ASA_nd); (5) Mapa da Distribuição Radiométrica Ternária (TER) dos rádio-elementos K, U e Th; (6) Mapa de distribuição do Tório (eTh); e do (7) Potássio Anômalo (Kd).

A partir dos dados do campo magnético total derivou-se o mapa de amplitude do sinal analítico (ASA), uma técnica eficiente para determinação do limite e profundidade dos corpos geológicos, como também para a delimitação de feições lineares (Blum, 1999; Thurston e Smith, 1997). As fontes magnéticas são representadas numa mesma superfície, permitindo, dessa forma, o traçado de estruturas lineares, que geralmente representam fraturas e falhas geológicas.

A primeira derivada vertical do campo magnético total (1DZ) foi utilizada na definição de contatos geológicos, descontinuidades e lineamentos, os quais não se destacam nos mapas de campo magnético total. Foram gerados mapas em falsa cor nos quais os baixos e altos magnéticos foram representados em azul e vermelho, respectivamente, realçando as estruturas e as unidades litológicas da área de estudo.

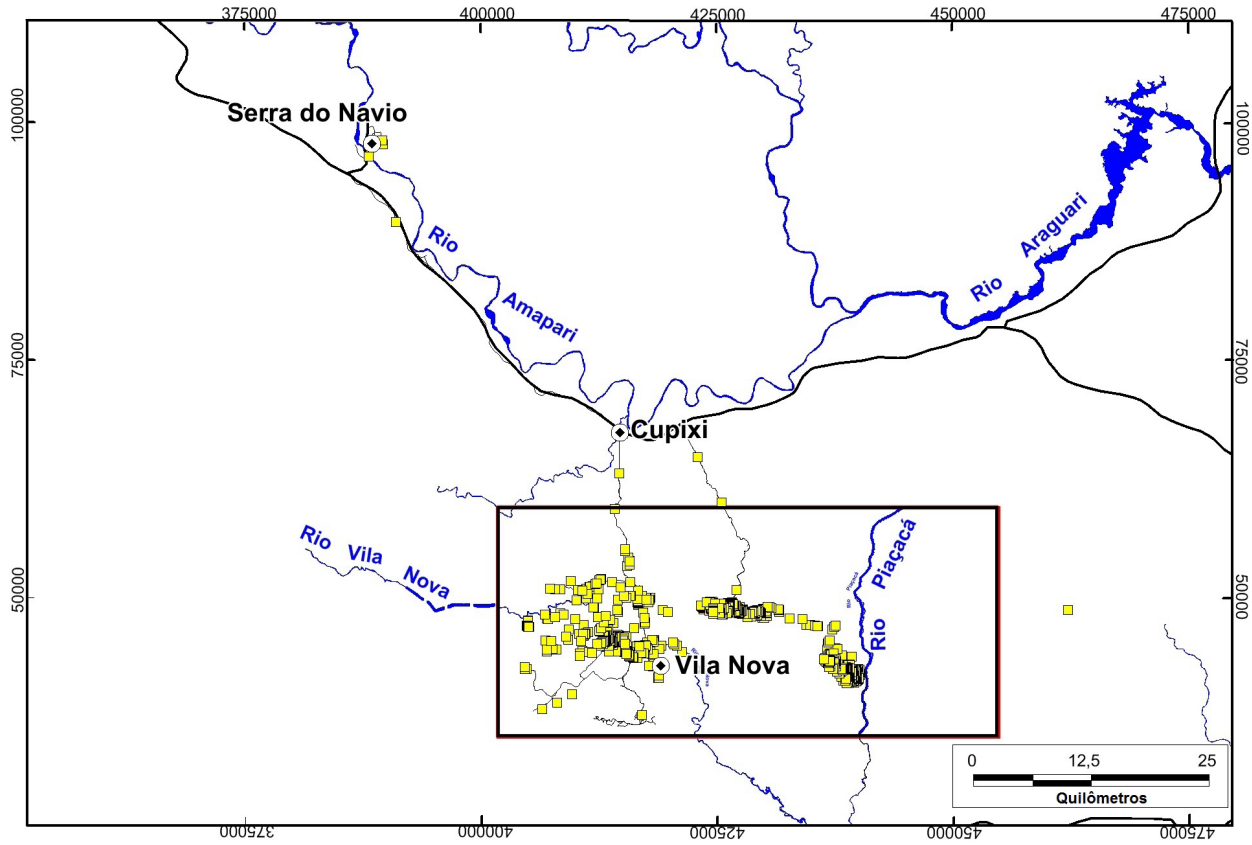


**Figura 3.** Localização da área de estudo (polígono preto) e dos pontos descritos (amarelo) de mapeamento.

Os produtos derivados da magnetometria foram utilizados para delimitar as áreas do embasamento ortognáissico das rochas metavulcano-sedimentares do *greenstone belt* Vila Nova, os granitos intrusivos, as zonas de cisalhamento dúcteis, as dobras regionais e as zonas fraturadas.

A análise individual e integrada das imagens dos canais de radioelementos foi efetuada objetivando a discriminação das principais unidades litoestruturais da região, além da identificação de possíveis áreas com registros de hidrotermalismo, como alterações potássicas. Foram interpretados os mapas de canais individuais do potássio, tório e urânio da composição ternária, além da imagem de contagem total. A interpretação qualitativa dos dados gama-espectrométricos foi efetuada através das composições ternárias RGB (*Red, Green* e *Blue*).

A interpretação qualitativa das imagens magnetométricas e gama-espectrométricas geradas para este trabalho foi efetuada em ambiente de Sistema de Informações Geográficas (SIG). As unidades magnetométricas e gama-espectrométricas presentes na área de estudo foram individualizadas através da classificação hierárquica dos polígonos delineados pela interpretação visual. A partir dessa análise visual e da delimitação dos domínios correspondentes em todas as anomalias dos canais magnéticos e gama-espectrométricos foi possível delinear os traçados geológico-estruturais em conjunto com os demais dados obtidos em campo. A integração dos dados geofísicos e de campo teve como principal produto o mapa geológico (1:50.000) da região da Vila Nova, que posteriormente foi ampliado (1:100.000) com base nos dados aerogeofísicos, englobando a região da Serra do Navio.

## RESULTADOS

### Geologia da região da Vila Nova

O embasamento na região da Vila Nova é constituído pelos ortognaisses, metagranitos e gabros do Complexo Tumucumaque. Sobre o embasamento estão as rochas intrusivas metamáfico-ultramáficas do Complexo Bacuri, o Complexo Vila Nova (CVN) e os granitoides indiferenciados. O Complexo Tumucumaque é a unidade predominante e constitui estruturas dômicas alongadas segundo a direção NW-SE, envoltas por faixas estreitas e muito deformadas constituídas pelas rochas metavulcano-sedimentares do CVN, que apresentam foliação metamórfica com orientação principal E-W, com variações a NW-SE (Figura 4).

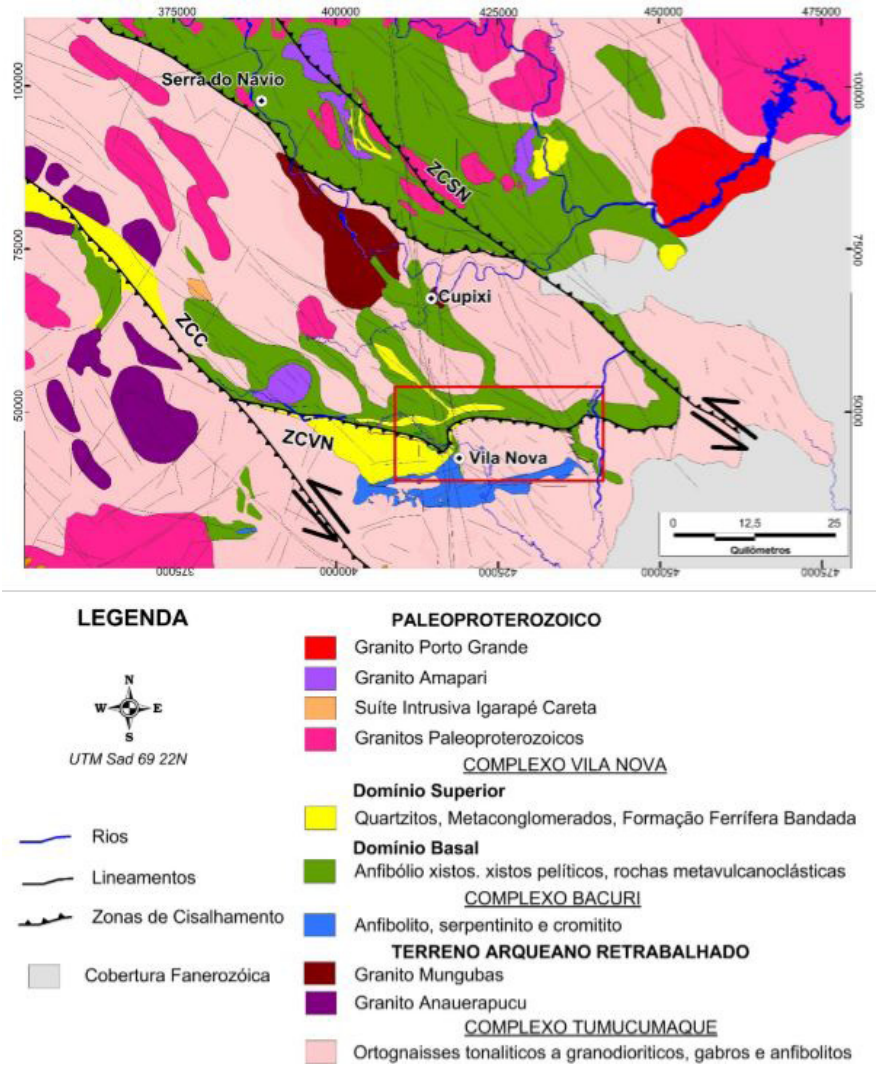


**Figura 4.** Mapa geológico da região da Vila Nova e da Serra do Navio com destaque para a área de estudo, no retângulo vermelho. Fonte: modificado de Faraco et al. (2004) e Barbosa et al. (2013). ZCC = Zonas de Cisalhamento Cupixi; ZCSN = Zonas de Cisalhamento Serra do Navio; CZVN = Zonas de Cisalhamento Vila Nova.

## Complexo Tumucumaque

Essa unidade está representada por gnaisses granodioríticos, tonalíticos e dioríticos, com ocorrência subordinada de corpos anfibolíticos com formas alongadas e concordantes ao bandamento gnáissico. Os ortognaisses apresentam um bandamento irregular e descontínuo, definido pela alternância de níveis máficos à base de biotita e/ou hornblenda, de espessura milimétrica (2 mm e 10 mm), e por níveis félsicos de composição quartzo-feldspática (Figura 5A). Os gnaisses tonalíticos a granodioríticos têm cor cinza clara e textura blasto-equigranular média a grossa (2 mm a 8 mm), envolta por uma textura granoblástica inequigranular interlobada média (0,2 mm a 0,5 mm) nas áreas mais afetadas pela recristalização. Os anfibolitos têm cor preta e estrutura foliada, definida por uma textura netamoblástica média a grossa caracterizada pela orientação de hornblenda. As transformações metamórficas estabelecidas pela recristalização do plagioclásio e da hornblenda indicam condições entre a fácies anfibolito médio e superior.

Os ortognaisses e anfibolitos estão cortados por corpos circunscritos *(stocks)* de gabros com dimensões variando de 100 m até 1.500 m. Os corpos de gabros apresentam formas alongadas segundo as direções E-W e NW-SE, concordantes com as estruturas regionais, principalmente ao longo da Zona de Cisalhamento Vila Nova. O gabro tem cor verde escura a preta, estrutura maciça e textura equigranular média a grossa (2 mm a 6 mm), caracterizada por cristais equidimensionais de plagioclásio e clinopiroxênio, com magnetita como mineral acessório (Figura 5B).

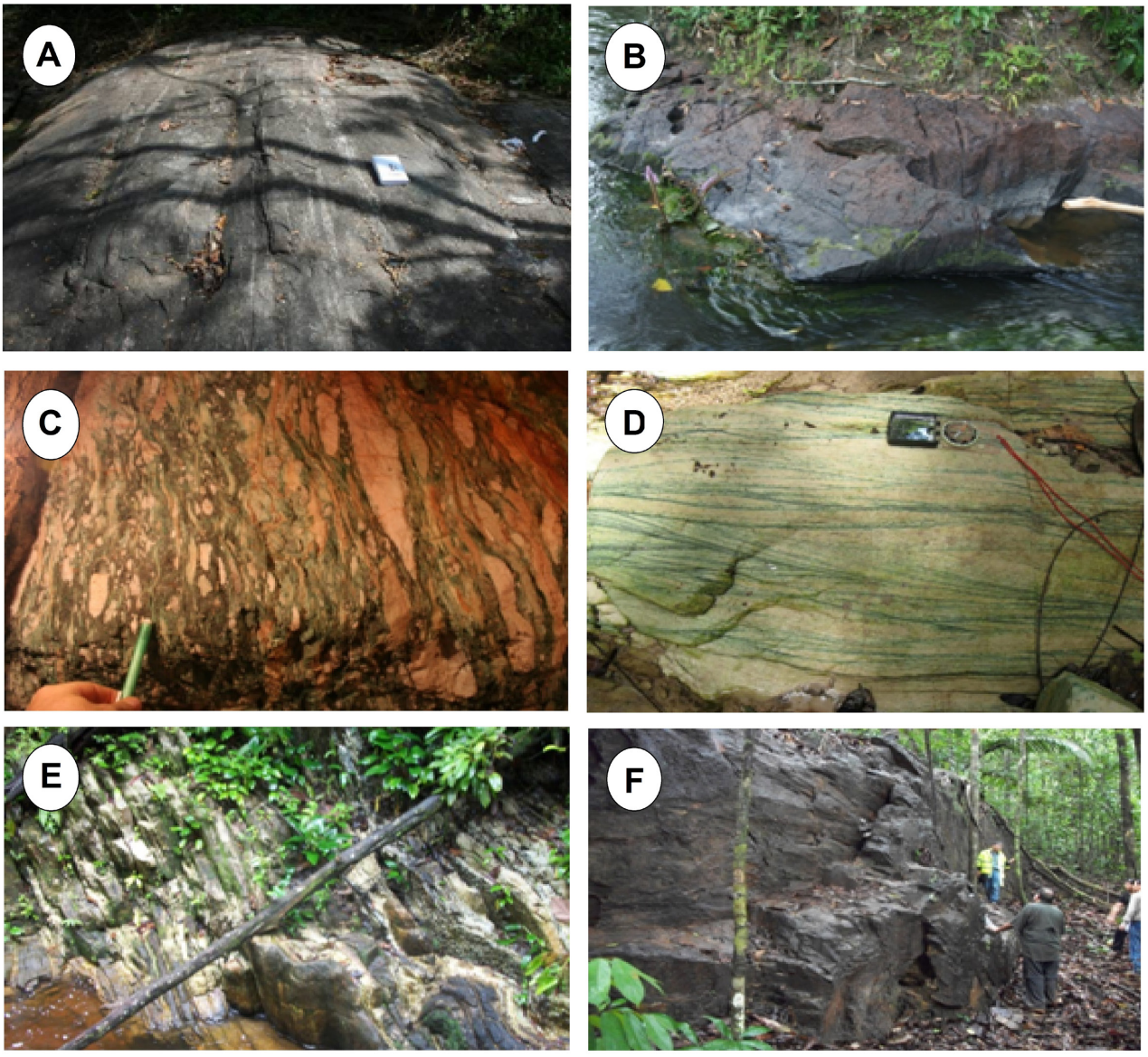


**Figura 5.** Aspectos macroscópicos e estruturais das rochas dos complexos Tumucumaque e Vila Nova. A) Ponto CB-28 – Gnaisse tonalítico com bandamento irregular e descontínuo definido por injeções félsicas de trondhjemitos; B) Ponto CB-12 – Aspecto do afloramento de anfibolito no leito do Rio Vila Nova; C) Ponto CB-03 – Metaconglomerado com seixos de quartzitos de cor branca e veios de quartzo estirados, envoltos por uma matriz de cor verde composta por fuchsita e turmalina do tipo Schorlita; D) Ponto CB-21 – Afloramento de fuchsita quartzito com estratificação cruzada acanalada marcada por níveis de cor verde ricos em fuchsita; E) Ponto CB-04 – Intercalação de quartzito e níveis de metaconglomerado ao longo do Igarapé Santa Maria; F) Ponto CB-30 – Aspecto da Formação Ferrífera Maciça.

## Complexo Bacuri

O Complexo Máfico-Ultramáfico Bacuri (CMUB) está localizado na parte sul da área estudada e constitui um corpo alongado segundo a direção N80°E, intrusivo nos gnaisses do Complexo Tumucumaque e em contato tectônico com os metassedimentos do Complexo Vila Nova (Pimentel et al., 2002) (Figura 4). As rochas máfico-ultramáficas apresentam, da base para o topo, uma zona máfica inferior composta por leucoanfibolitos e uma zona ultramáfica constituída por serpentinitos, tremolititos e cromititos, sendo esses litotipos geralmente foliados segundo a estruturação regional (Spier, 1999). O CMUB está metamorfizado e deformado, apresentando estruturas complexas devido a redobramentos e falhamentos, sendo comum o posicionamento subvertical das camadas. As assembleias minerais das rochas máficas

(Diop+Hbl+PI±Bt±Qtz) indicam metamorfismo em condições da fácies anfibolito médio a superior, sob condições de baixa pressão (Spier, 1999).

## Complexo Vila Nova

O Complexo Vila Nova (CVN) ocorre como uma faixa principal alongada segundo a direção E-W, com quatro faixas subordinadas de direção N40º-50ºW, interligadas na sua porção sul pela Zona de Cisalhamento Vila Nova (ZCVN) (Figuras 4 e 6). O contato do CVN com as rochas do embasamento ao sul é definido por uma falha de empurrão, caracterizada como uma zona de cisalhamento dúctil (ZCVN), originalmente sub-horizontal e de direção E-W. Na porção oeste da área estudada, essa zona de cisalhamento também é responsável pelo contato entre os principais pacotes de rochas metamáficas e metassedimentares. Ao norte, o contato não é observado e foi inferido pela interpretação dos dados aerogeofísicos.

O complexo metavulcano-sedimentar foi subdividido em duas associações petrotectônicas ou domínios rochosos dominantes, um Domínio Basal e um Superior.

No Domínio Basal ocorrem metandesitos, metabasaltos e metadacitos, com predomínio das rochas metavulcânicas máficas, intercaladas com mica xistos, lentes de mármore, xistos cálcio-silicáticos e grafita xistos. Esse domínio se estende como uma faixa alongada segundo a direção E-W por cerca de 50 km, desde Vila Nova, passando pelas localidades de Nova Canaã e Pelado, entre os rios Vila Nova e Piaçacá. As rochas metamáficas estão representadas por bt-anfibólio xistos e anfibolitos, ocorrendo também metabasaltos, metandesitos e metadacitos. Os metaultramafitos são tremolita xistos e actinolita-tremolita xistos. Cornubianitos máficos também foram reconhecidos como produto de metamorfismo termal

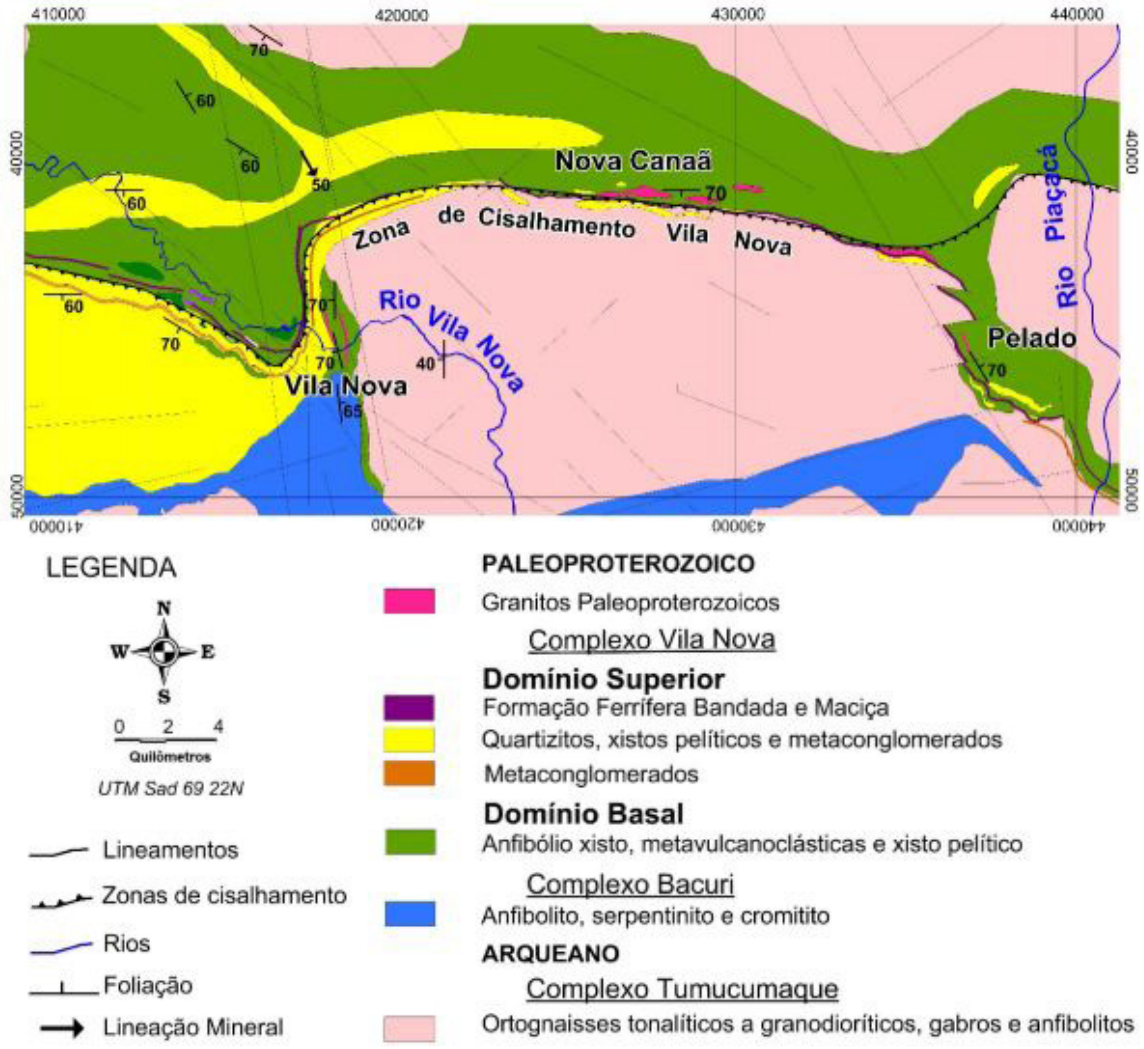


**Figura 6.** Mapa geológico da área estudada. Escala 1:50.000.

associado à colocação de granitos paleoproterozoicos mais jovens.

O Domínio Superior é composto por metassedimentos clásticos, intercalados com rochas metavulcânicas félsicas a máficas e rochas químico-exalativas subordinadas e está mais restrito à porção oeste da área, ocorrendo como três faixas alongadas principais com cerca de 20 km a 25 km de extensão por 1 km a 10 km de largura. As rochas metassedimentares intercalam-se com as rochas metavulcânicas e estão deformadas e dobradas por estruturas regionais. Os metassedimentos clásticos incluem metaconglomerados, quartzitos, quartzitos ferruginosos, fuchsita-quartzo xisto e mica xistos, enquanto as rochas de origem química incluem xistos calci-silcáticos e rochas associadas a BIFs (formações ferríferas bandadas) como hematita filitos, hematita xistos e quartzito ferruginoso (Figura 5C-F).

Levantamentos estruturais indicam que as unidades do Complexo Vila Nova foram deformadas e metamorfizadas conjuntamente, resultando em uma foliação regional orientada segundo a direção N50º-60ºW (Borghetti et al., 2013).

### Granitos intrusivos

Rochas graníticas metamorfizadas e corpos de pegmatito cortam todas as unidades anteriormente descritas. Variam desde diques centimétricos subconcordantes à foliação metamórfica até intrusões com disposição alongada segundo a direção E-W e com poucas centenas de metros de extensão. Os granitoides apresentam cor cinza clara a esbranquiçada, composição tonalítica, granodiorítica e granítica, com textura equigranular variando de fina até pegmatítica. Apresentam estrutura maciça, ocorrendo também corpos deformados e ocasionalmente com foliação milonítica. São compostos por K-feldspato, plagioclásio e quartzo, com baixos teores de biotita, muscovita e granada.

Alguns desses corpos graníticos estão mineralizados, sendo conhecido no limite oeste da área um grande corpo de pegmatito mineralizado a tantalita, explorado por vários anos por garimpeiros. Todos os corpos identificados são concordantes e ocorrem muito próximos ou restritos à Zona de Cisalhamento Vila Nova. Essa zona de cisalhamento está muito bem demarcada nas imagens de satélite e nos levantamentos aerogeofísicos, mas quase não está exposta no terreno.

## DADOS AEROGEOFÍSICOS

### Aeromagnetometria

O padrão de anomalias magnéticas observado nas imagens de campo magnético total mostra a estruturação regional da área de estudo, destacando as estruturas de direção NW-SE representadas pela orientação geral das foliações metamórficas (Figura 7A). Na região da Vila Nova destacam-se as rochas do Complexo Vila Nova, com forma alongada segundo a direção E-W, marcada por anomalias de alta amplitude magnética, com formas alongadas e contínuas que delimitam as rochas metavulcano-sedimentares desse complexo. As áreas de baixa amplitude magnética são ocupadas pelos ortognaisses e granitoides do Complexo Tumucumaque.

Os principais lineamentos magnéticos apresentam direção NW-SE e E-W e, subordinadamente, direção N-S, como evidenciado no mapa da primeira derivada (Figura 7B, e no de amplitude do sinal analítico – ASA nd e ASA hd) (Figura 7C, D). Nesses dois últimos, as anomalias magnéticas de maior amplitude correspondem às rochas metavulcano-sedimentares do CVN, podendo também ser observados os limites dos granitos Amapari, Mungubas e Anauerapucu. O Complexo Máfico-Ultramáfico Bacuri também apresenta uma resposta magnética definida, caracterizando um corpo principal com direção N80ºE (Figura 7C, D).

A partir da análise dos dados aeromagnetométricos observam-se lineamentos magnéticos de grande continuidade que se estendem até a região da Serra do Navio. O padrão estrutural dominante está marcado por lineamentos de direção NW-SE, sendo mais expressivos na faixa central da área, prolongando-se para NW e para SE. Esses lineamentos definem zonas de cisalhamento dúctil que variam em menor proporção para estruturas de direção E-W, apresentando em conjunto um aspecto sigmoidal. Os lineamentos de direção NW-SE estão caracterizados em campo pelas Zona de Cisalhamento Cupixi (ZCC) e Zona de Cisalhamento Serra do Navio (ZCSN), que cortam toda a área e apresentam no seu interior uma grande estrutura de direção E-W, representada pela Zona de Cisalhamento Vila Nova (ZCVN). O *greenstone belt* Vila Nova apresenta uma estruturação principal de direção E-W, caracterizada em campo pelas foliações metamórficas $S_1$ e $S_2$ que, posteriormente, são afetadas por eventos mais tardios de deformação dúctil, resultando em dobramentos regionais.

O *greenstone belt* Vila Nova está inserido entre as zonas de cisalhamento Cupixi (ZCC) e Serra do Navio (ZCSN). A ZCSN limita as rochas do *greenstone belt* Vila Nova na porção nordeste e prolonga-se até o *greenstone belt* Serra do Navio (GBSN), delineando toda sua borda sudoeste. No setor centro-nordeste da área de estudo dominam os lineamentos de direção N-S, expressos por segmentos retilíneos que seccionam os lineamentos anteriormente citados. Os lineamentos N-S são contínuos e bem definidos, cortando as rochas do GBVN na região dos garimpos de ouro da região da Vila Nova. Os lineamentos de direções NE-SW e N-S ocorrem preferencialmente no setor sudoeste e nordeste da área, representando provavelmente uma tectônica rúptil a rúptil-dúctil (Figura 7).

### Aero-gama-espectrometria

Os dados aero-gama-espectrométricos representados pelos mapas de potássio anômalo (Kd) e o mapa radiométrico ternário mostram o enriquecimento de potássio na região central da

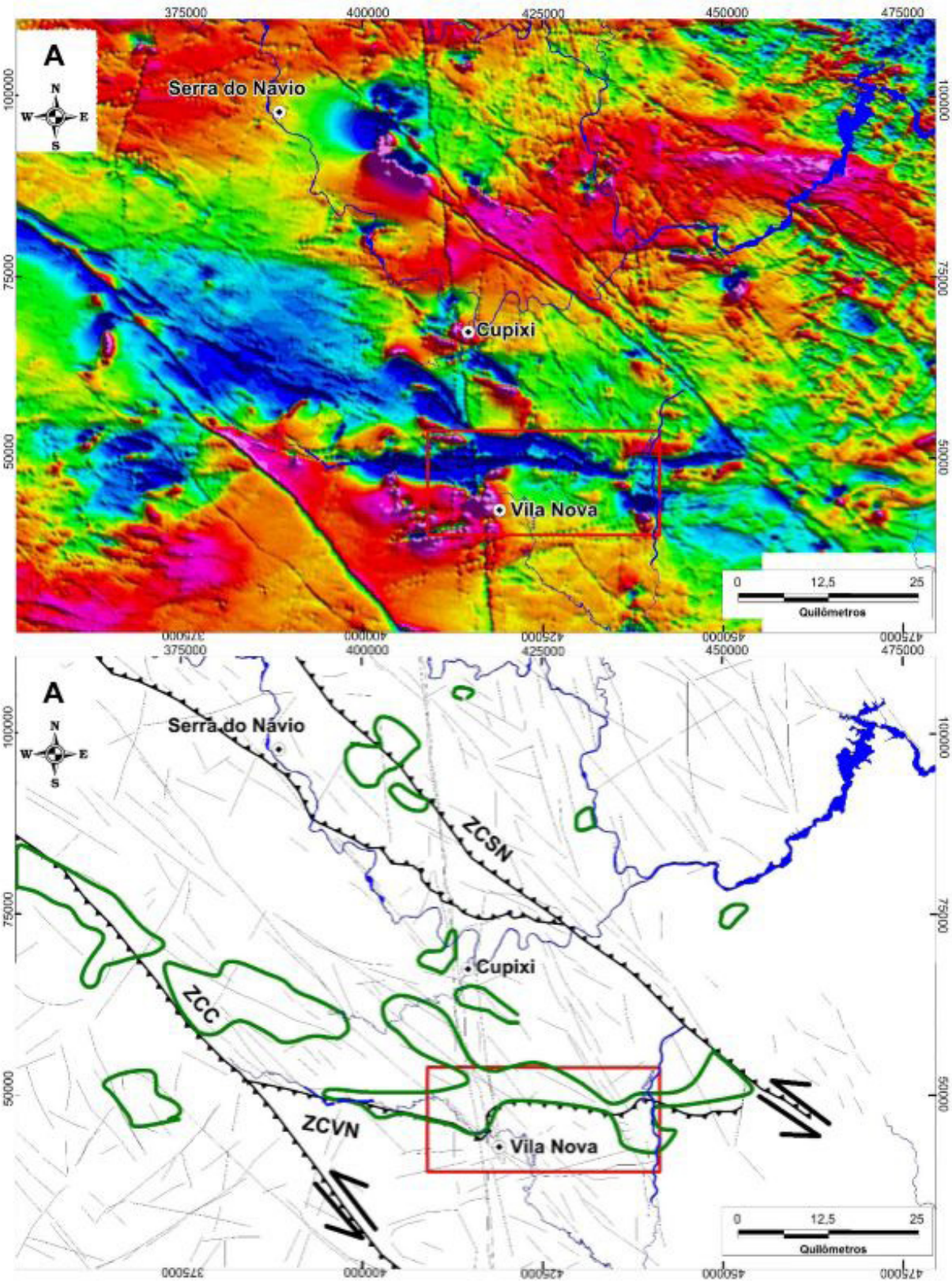


**Figura 7A.** Campo magnético total (CMT) com delimitação das anomalias de grande amplitude magnética (linha verde), correspondente às rochas metavulcano-sedimentares do CVN e dos principais lineamentos estruturais. ZCC = Zona de Cisalhamento Cupixi; ZCSN = Zona de Cisalhamento Serra do Navio; ZCVN = Zona de Cisalhamento Vila Nova.

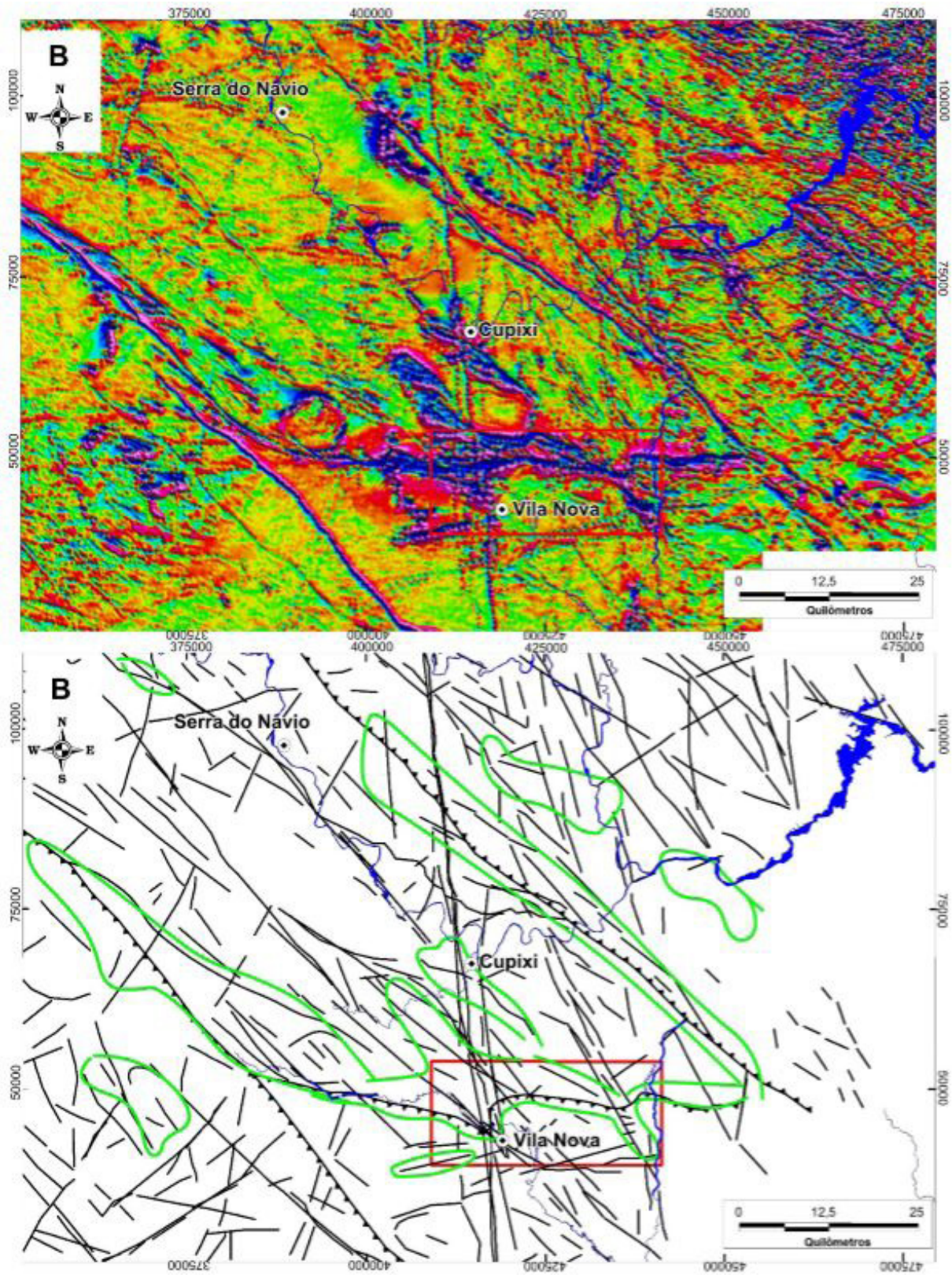


**Figura 7B.** Primeira derivada do campo magnético total (CMT), destacando as feições estruturais e as anomalias magnéticas (linhas verdes). ZCC = Zona de Cisalhamento Cupixi; ZCSN = Zona de Cisalhamento Serra do Navio; ZCVN = Zona de Cisalhamento Vila Nova.

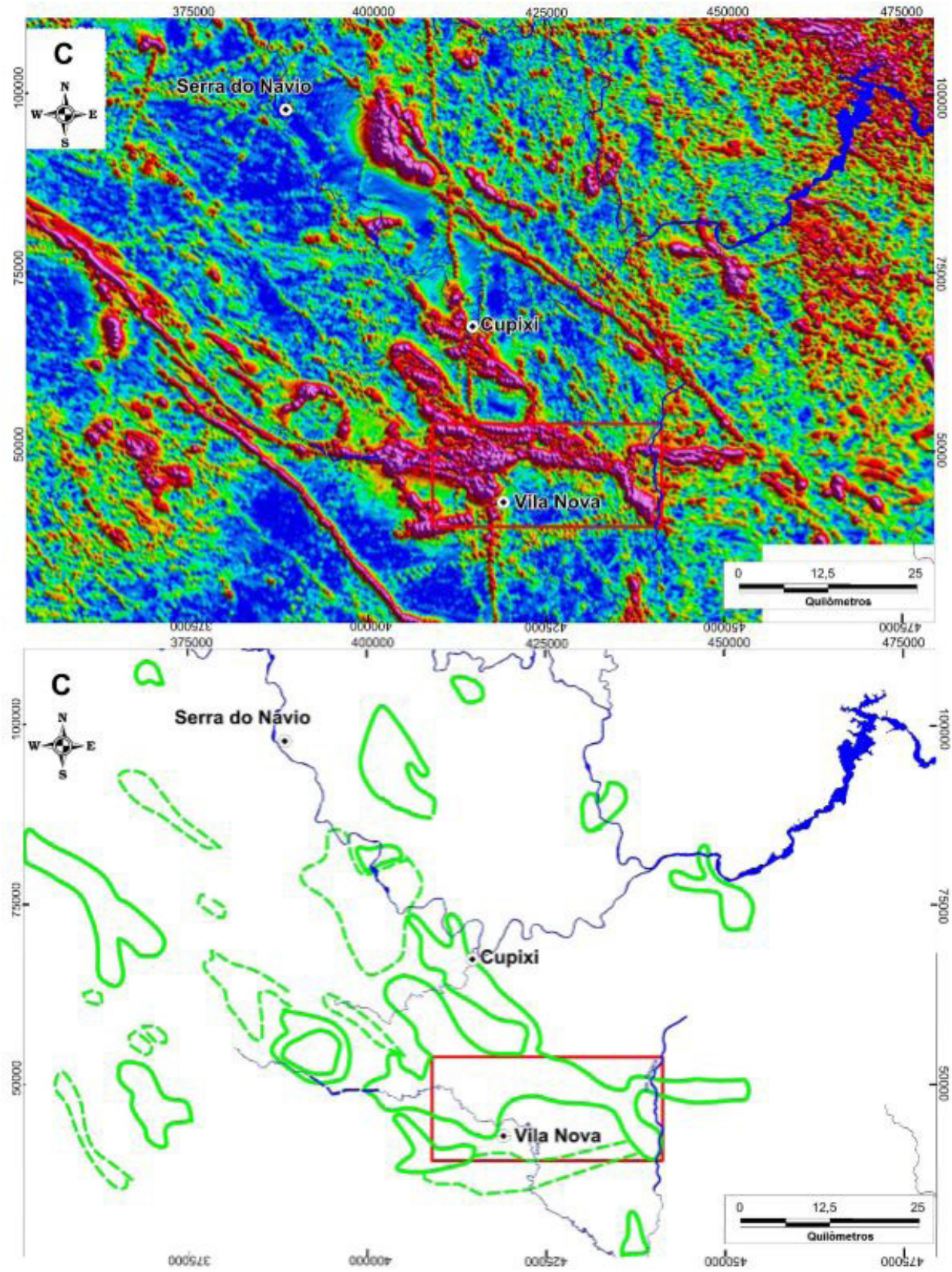


**Figura 7C.** Amplitude do Sinal Analítico (ASA_hd) com as anomalias magnéticas (linhas verdes), destacando-se as ocorrências de rochas metavulcano-sedimentares do Complexo Vila Nova e os limites externos de corpos graníticos.

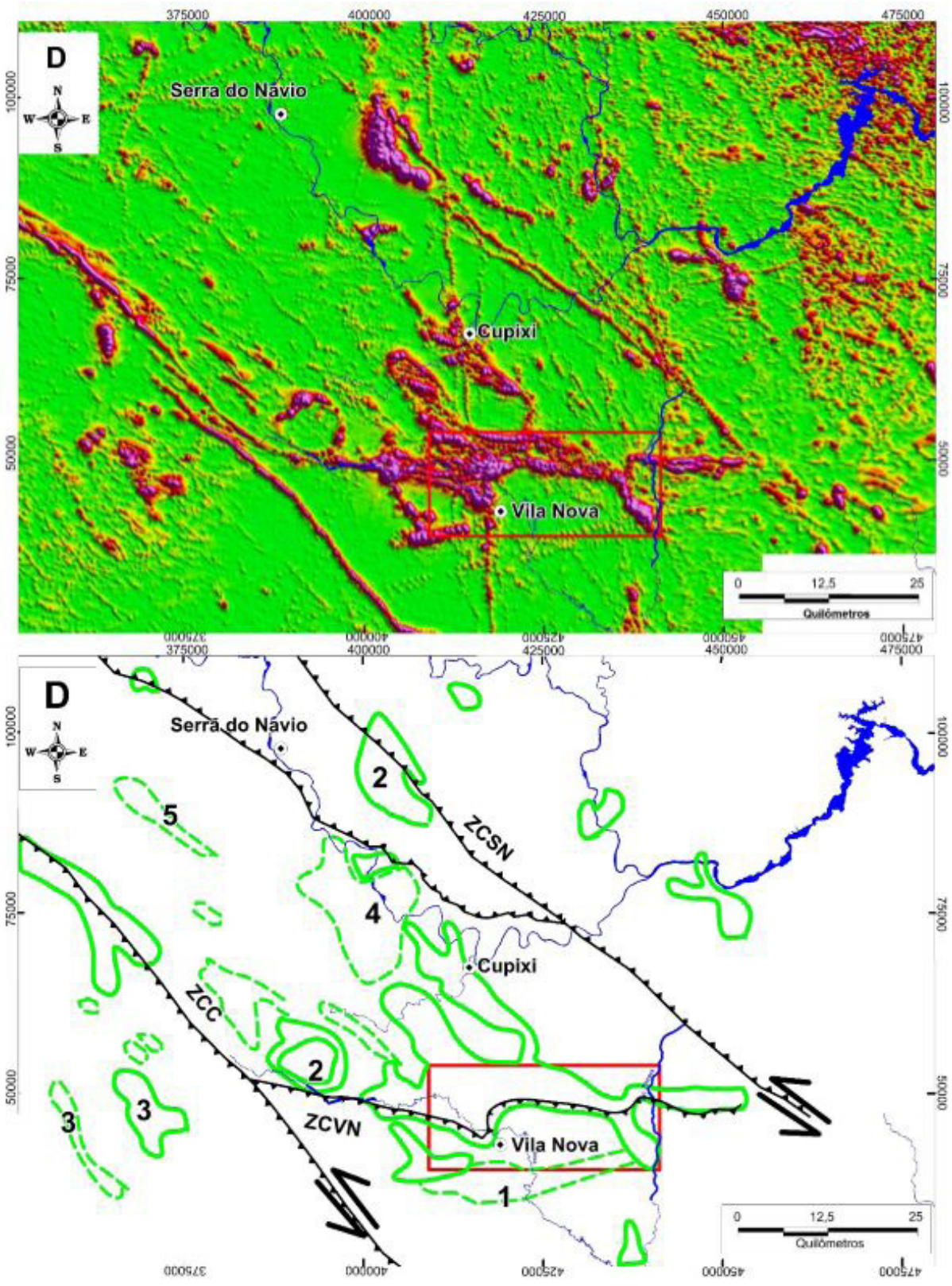


**Figura 7D.** Amplitude do Sinal Analítico (ASA_nd) com delimitação das anomalias magnéticas mais fortes (linhas verdes), que correspondem às rochas do Complexo Vila Nova, e também anomalias correspondentes ao Complexo Bacuri (1), Granito Amapari (2), Granito Anauerapucu (3), Granito Mungubas (4) e granitos paleoproterozoicos indiferenciados (5).

área, coincidente com a anomalia magnética que delimita as rochas do Complexo Vila Nova (Figura 8). Os *greenstones belts* de idades arqueanas e paleoproterozoicas apresentam baixas contagens radiométricas. O enriquecimento de potássio detectado pela aero-gama-espectrometria é causado por zonas de alteração hidrotermal. A associação das mineralizações com veios de quartzo de baixa temperatura sugere que elas podem estar relacionadas a esse tipo de alteração.

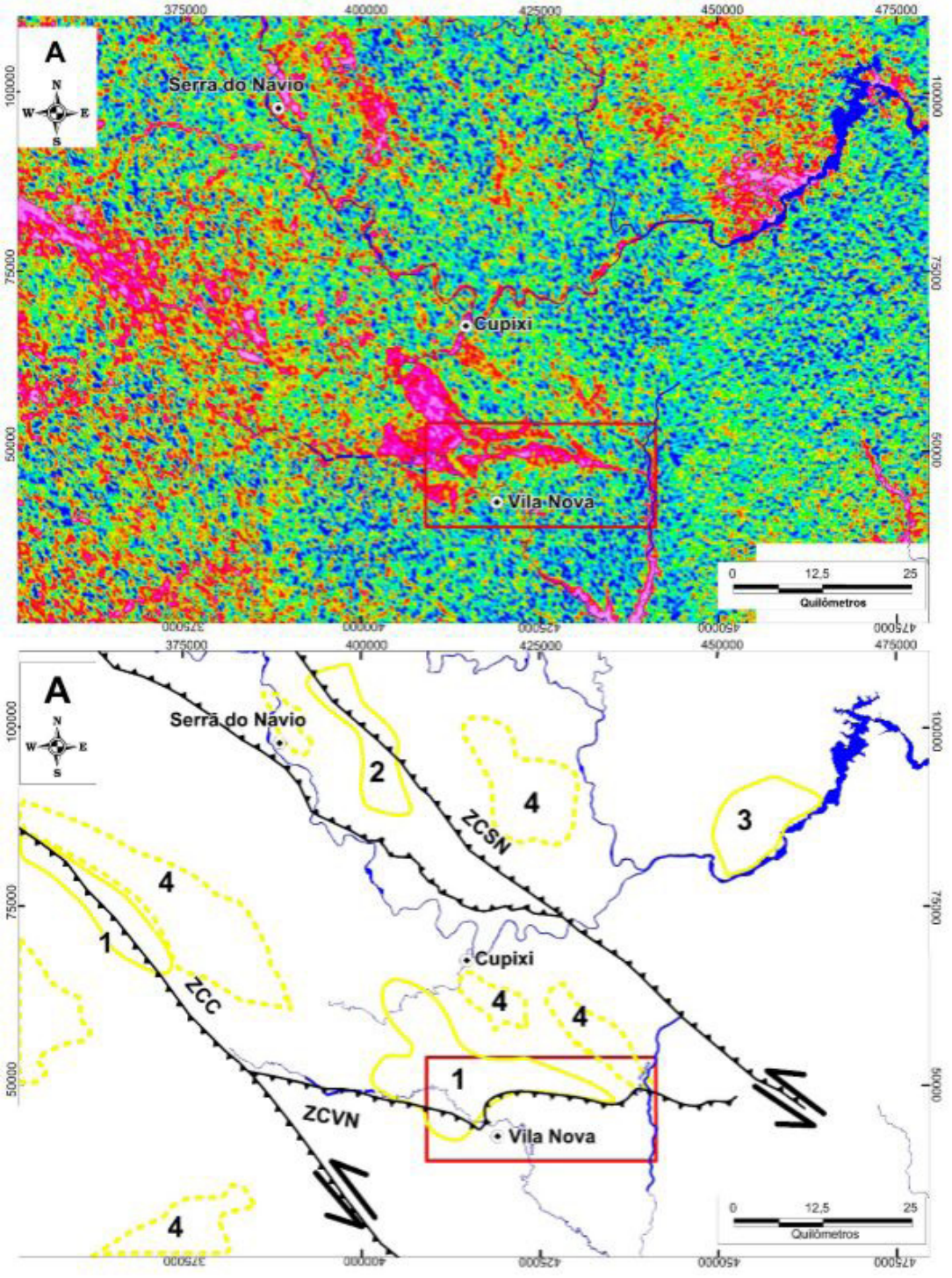


**Figura 8A.** Mapa de Potássio Anômalo evidenciando as principais anomalias (linhas amarelas) sobre as rochas do Complexo Vila Nova (1), Granito Amapari (2) e Granito Porto Grande (3), além de anomalias menores (4), principalmente associadas a zonas preferenciais de percolação de fluídos.

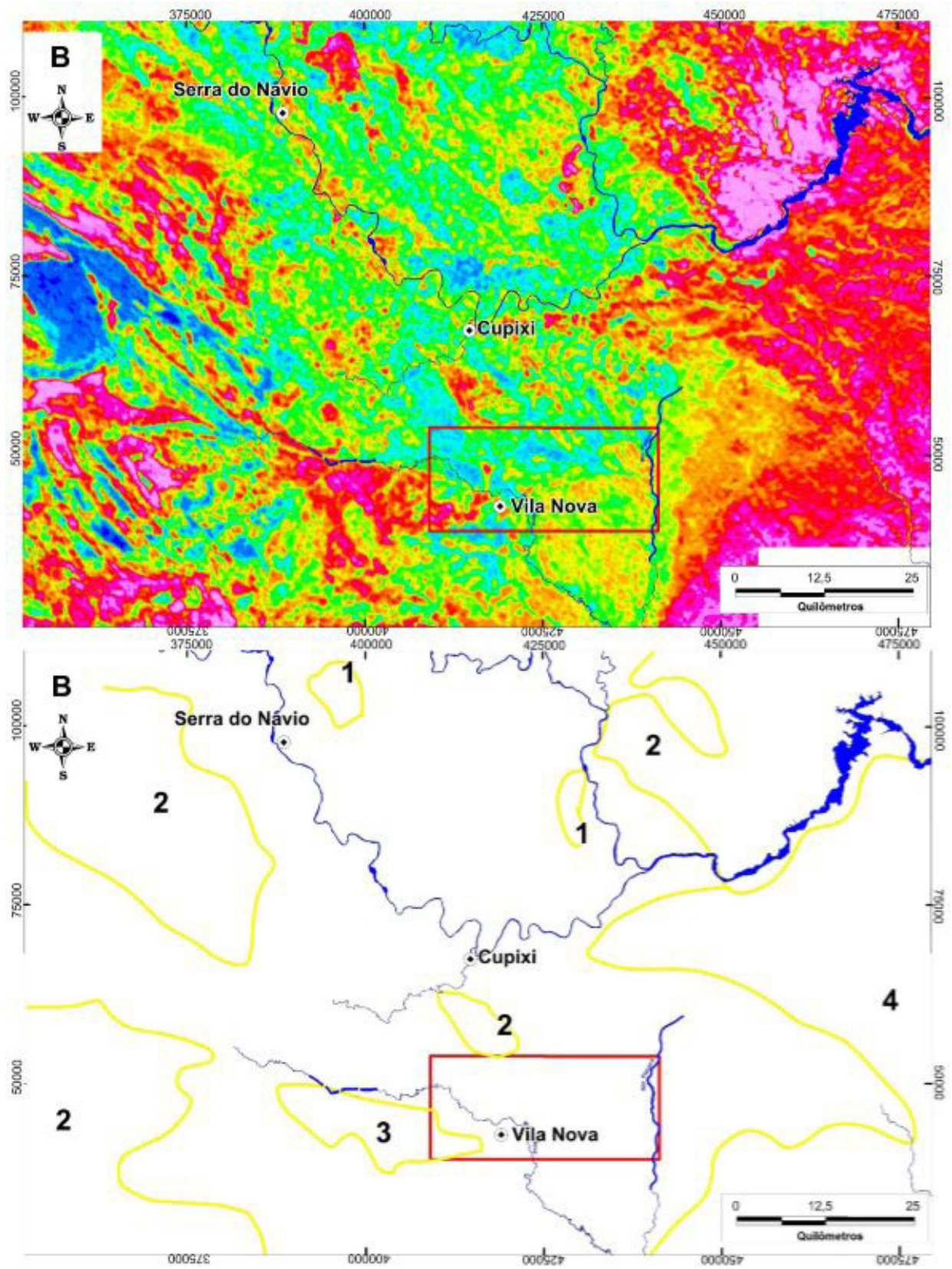


**Figura 8B.** Mapa de distribuição do Tório (Th) destacando as intrusões graníticas como Granito Amapari (1), granitos paleoproterozoicos e Anauerapucu (2), os quartzitos (3) do CVN e a Cobertura Fanerozóica (4).

Além da região abrangida pelas rochas metavulcano-sedimentares do GBVN e GBSN, podem ser diferenciados nos mapas radiométricos os granitos Porto Grande e Amapari, o Complexo Máfico-Ultramáfico Bacuri, o domínio superior metassedimentar do Complexo Vila Nova e as rochas do Complexo Tumucumaque.

A Figura 8A (Potássio Anômalo) evidencia as principais anomalias positivas sobre as unidades do CVN no centro e na porção oeste do mapa, definindo o Granito Amapari em contato com o CVN e também o Granito Porto Grande, além de anomalias menores, essas possivelmente associadas a zonas preferenciais de percolação de fluídos.

No mapa de distribuição do tório, as principais anomalias positivas apresentadas podem ser relacionadas, principalmente, com as rochas graníticas, em especial as intrusões do Granito Amapari no GBSN e à associação dos granitos paleoproterozoicos e Anauerapucu (Figura 8B). Os quartzitos da unidade superior do CVN também apresentam uma anomalia na parte central do mapa, junto ao GBVN, assim como a Cobertura Fanerozoica apresenta enriquecimento em tório.

## DISCUSSÕES E CONCLUSÕES

A correlação entre as anomalias aerogeofísicas (magnéticas e radiométricas), a composição das rochas e as estruturas geológicas é uma ferramenta importante para subsidiar os trabalhos de campo, para caracterizar as principais estruturas do embasamento e na avaliação das relações existentes entre assinaturas aerogeofísicas, padrões de relevo, associações litológicas e padrões estruturais.

A integração dos dados de campo com a interpretação dos dados aerogeofísicos permitiram a definição e delimitação dos complexos Tumucumaque e Vila Nova. Os mapas geológicos regional e da área da Vila Nova gerados neste trabalho representam um importante incremento na cartografia geológica dessa porção do Cráton Amazônico, quando comparados com os mapas apresentados por Spier e Ferreira Filho (1999), Pimentel et al. (2002), Faraco et al. (2004), McReath e Faraco (2006), Rosa-Costa et al. (2006) e Barbosa et al. (2013). A integração dos dados aerogeofísicos e de campo permitiu reconhecer as principais zonas de cisalhamento regionais e delimitar em escala 1:50.000 as unidades metavulcânicas e metassedimentares do Complexo Vila Nova.

Os dados de aeromagnetometria e de aero-gama-espectrometria permitiram separar as áreas do embasamento arqueano e paleoproterozoico, compostas por ortognaisses e granitoides do Complexo Tumucumaque, das áreas ocupadas pelas rochas metavulcano-sedimentares do Complexo Vila Nova. Dentre as unidades desse complexo, destacam-se os baixos magnetométricos apresentados pelos metassedimentos situados ao sul da Zona de Cisalhamento Vila Nova, quando comparados com as rochas metavulcânicas situadas ao norte dessa zona de cisalhamento. Essa diferença permitiu o reconhecimento do Domínio Basal, com predominância de rochas metavulcânicas, e do Domínio Superior, composto por metassedimentos clásticos. As rochas metavulcânicas são compostas por metabasaltos, metandesitos e metadacitos e estão intercaladas com rochas químico-exalativas como xistos cálcio-silicáticos e BIFs. Entre os metassedimentos clásticos destacam-se a intercalação de espessos pacotes de quartzitos e duas camadas principais de metaconglomerados basais.

As principais estruturas da região estão caracterizadas pelas zonas de cisalhamento dúcteis do Cupixi e da Serra do Navio, de direção NE-SW, representando os principais corredores de deformação regionais. Essas duas grandes zonas de cisalhamento estão conectadas através da Zona de Cisalhamento Vila Nova, de direção E-W, responsável pela forma alongada do *greenstone belt* da Vila Nova e pelo contato entre o embasamento e as unidades metavulcano-sedimentares. Os trabalhos de campo permitiram reconhecer uma estruturação complexa, com a caracterização de duas foliações metamórficas principais ($S_1$ e $S_2$) associadas ao desenvolvimento da Zona de Cisalhamento Vila Nova. Essa zona de cisalhamento tem natureza dúctil e controla o posicionamento de diversos granitoides de idade paleoproterozoica. Os granitos apresentam formas alongadas concordantes, caracterizadas por estruturas internas, como foliação magmática, e porções de borda com deformação milonítica. Essas características sugerem que a colocação dos corpos graníticos é sin-cinemática ao desenvolvimento da zona.

Essas estruturas dúcteis são ainda afetadas por uma fase de dobramento mais tardia, que afeta a disposição das foliações metamórficas, gerando um padrão regional de dobras $F_3$ com formas abertas a fechadas e eixos direcionados para a direção SE. As estruturas anteriores ainda são afetadas por zonas de cisalhamento rúpteis de direção N70º-80ºE e mergulhos subverticais.

Os dados apresentados neste trabalho demonstram a importância da integração dos dados aerogeofísicos como uma importante ferramenta para reconhecimento de tramas estruturais e litológicas complexas em áreas de pouca exposição e cujo acesso é muito difícil.

## REFERÊNCIAS

Avelar, V. G., Lafon, J. M., Delor, C., Guerrot, C., Lahondère, D. (2003). Archean crustal remnants in the easternmost part of the Guiana Shield: Pb-Pb and Sm-Nd geochronological evidence for Mesoarchean versus Neoarchean signatures. *Geologie de la France*, 2-3-4, 83-100.

Barbosa, J. P. O., Costa Neto, M. C., Rosa-Costa, L. T., Anjos, G. C., Chaves, C. L. (2013). *Projeto Folha Macapá: NA.22-Y-D.* Mapa Geológico (1:250.000). Belém: CPRM.

Blum, M. L. B. (1999). *Processamento e interpretação de dados de geofísica aérea no Brasil central e sua aplicação à geologia regional e à prospecção mineral*. Tese (Doutorado). Brasília: Universidade de Brasília.

Borghetti, C., Philipp, R. P., Basei, M. A. S., Mandetta, P. (2013). Evolução tectônica do Complexo Vila Nova na região do Cupixi, Porto Grande, Amapá. *XIV Simpósio Nacional de Estudos Tectônicos; VIII Symposium on Tectonics*, Boletim de Resumos Expandidos, Chapada dos Guimarães, SBG, ST-2.

Borghetti, C., Philipp, R. P., Basei, M. A. S., Mandetta, P. (2014). New ages from Vila Nova and Tumucumaque Complex in the Cupixi region, Porto Grande, Amapá, Brazil. *9th South American Symposium on Isotope Geology*, Boletim de Resumos Expandidos. São Paulo: CPGeo-IGc/USP

Cordani, U. G., Brito Neves, B. B. (1982). The geologic evolution of South America during the archean and early proterozoic. *Revista Brasileira de Geociencias*, 12, 78-88.

Cordani, U. G., Tassinari, C. C. G., Teixeira, W., Basei, M. A. S., Kawashita, K. (1979). Evolução da Amazônia com base nos dados geocronológicos. *Actas do II Congresso Geologico Chileno*, 4, 137-148. Arica: Instituto de Investigaciones Geologicas.

Cordani, U. G., Teixeira, W., D'Agrella-Filho, M. S., Trindade, R. I. (2009). The position of the Amazonian Craton in supercontinents. *Gondwana Research*, 15, 396-407. http://dx.doi.org/10.1016/j.gr.2008.12.005.

Delor, C., Lahondère, D., Egal, E., Lafon, J. M., Cocherie, A., Guerrot, C., Rossi, Ph., Trufert, C., Theveniaut, H., Phillips, D., Avelar, V. G. (2003a). Transamazonian crustal growth and reworking as revealed by the 1:500.000: scale geological map of French Guiana (2nd ed.). *Géologie de la France*, 2-3-4, 5-57.

Delor, C., Roever, E. W. F., Lafon, J. M., Lahondère, D., Rossi, P., Cocherie, A., Guerrot, C., Potrel, A. (2003b). The Bakhuis ultrahigh-temperature granulite belt (Suriname): II. Implications for late Transamazonian crustal stretching in a revised Guiana Shield framework. *Géologie de la France*, 2-3-4, 207-230.

Faraco, M. T. L., Marinho, P. A. C., Costa, E. J. S., Vale, A. G., Camozzato, E. (2004). *Carta Geológica do Brasil ao Milionésimo: Sistema de Informações Geográficas (SIG). Folha NA.22 – Macapá. Escala 1:1.000.000*. (CDROM, Programa Geologia do Brasil). Brasília: CPRM.

Grant, F. S. (1984). Aeromagnetic, geology and ore environments: II Magnetite and ore environments. *Geoexploration*, 24, 335-362.

Kearey, P., Klepeis, K. A., Vine, F. J. (2009). *Global tectonics*. (3a ed.), 482 p. New York: Wiley-Blackwell.

Lobato, L. M., Rodrigues, L. C. R., Zuchetti, M., Noce, C. M., Baltazar, O. F., Silva, L. C., Pinto, C. P. (2001). Brazil's premier gold province. Part I: The tectonic, magmatic and structural setting of the Archean Rio das Velhas greenstone belt. *Mineralium Deposita*, 36(3/4), 228-248.

McCarthy, T., Rubidge, B. (2005). *The story of earth and life*, 333 p. Johannesburg: Struik Publishers.

McReath, I., Faraco, M. T. L. (2006). Paleoproterozoic greenstone-granite belts in northern Brazil and the former Guyana Shield-West African craton province. *Geologia USP. Série Científica*, 5(2), 49-63.

Noce, C. M., Pedrosa-Soares, A. C., Silva, L. C., Alkmim, F. F. (2007). O embasamento Arqueano e Paleoproterozóico do Orógeno Araçuaí. *Geonomos*, 15, 15-17.

Pimentel, M. M., Ferreira Filho, C. F., Spier, C. A. (2002). Estudo Sm-Nd do Complexo Máfico-Ultramáfico Bacuri, Amapá: idade da intrusão, metamorfismo e natureza do magma original. *Revista Brasileira de Geociencias*, 32, 371-376.

Press, F., Siever, R., Grotzinger, J., Jordan, T. H. (2006). *Para entender a Terra* (4a ed.), 656 p. Porto Alegre: Bookman.

Rosa-Costa, L. T., Lafon, J. M., Delor, C. (2006). Zircon geochronology and Sm-Nd isotopic study: further constraints for the Archean and Paleoproterozoic geodynamic evolution of the southeastern Guiana Shield, north of Brazil. *Gondwana Research*, 10, 277-300.

Rosa-Costa, L. T. (2006). *Geocronologia 207Pb/206Pb, Sm-Nd, U-Th-Pb e 40Ar-39Ar do Segmento Sudeste do Escudo das Guianas: evolução crustal e termocronologia do evento transamazônico*. Tese (Doutorado). Belém: Curso de Pós-graduação em Geologia e Geoquímica – UFPA.

Santos, J. O. S., Hartmann, L. A., Gaudette, H. E., Groves, D. I., Mcnaughton, N. J., Fletcher, I. R. (2000). A new understanding of the provinces of the Amazon Craton based on integration of field mapping and U-Pb and Sm-Nd geochronology. *Gondwana Research*, 3(4), 453-488.

Serviço Geológico do Brasil (CPRM). (2004). *Programa Geologia do Brasil, Projeto Aerogeofísico Rio Araguari, Relatório Final do levantamento e processamento dos dados magnetométricos e gamaespectrométricos*, 136 p. Rio de Janeiro: Lasa Engenharia e Prospecções S/A. (Texto Técnico, I).

Serviço Geológico do Brasil (CPRM). (2006). *Programa Geologia do Brasil, Projeto Aerogeofísico Amapá, Relatório final do levantamento e processamento dos dados magnetométricos e gamaespectrométricos*, 272 p. Rio de Janeiro: Lasa Engenharia e Prospecções S/A. (Texto Técnico, I).

Spier, C. A. (1999) *Petrologia e metalogênese dos depósitos de cromita associados ao complexo máfico-ultramáfico*

*Bacuri, AP*. Dissertação (Mestrado). Brasília: Instituto de Geociências – UnB.

Spier, C. A., Ferreira Filho, C. F. (1999). Geologia, estratigrafia e depósitos minerais do Projeto Vila Nova, Escudo das Guianas, Amapá, Brasil. *Revista Brasileira de Geociencias*, 29, 173-178.

Tassinari, C. C. G., Bettencourt, J. S., Geraldes, M. C., Macambira, M. J. B., Lafon, J. M. (2000). The Amazonian Craton. In: U. G. Cordani, E. J. Milani, A. T. Filho, D. A. Campos (Eds.), *Tectonic evolution of South America. 31st International Geological Congress*, 41-95. Rio de Janeiro: SBG.

Tassinari, C. C. G., Macambira, M. J. B. (2004). A evolução tectônica do Cráton Amazônico. In: V. Mantesso-Neto, A. Bartorelli, C. D. R. Carneiro, B. B. B. Brito-Neves (Orgs.), *Geologia do continente Sul-Americano: evolução da obra de Fernando Flávio Marques de Almeida*, 471-485. São Paulo: Beca.

Teixeira, W., Tassinari, C. C. G., Cordani, U. G., Kawashita, K. (1989). A review of the geochronology of the Amazonian Craton: tectonic implications. *Precambrian Research*, 42, 213-227.

Thurston, J. B., Smith, R. S. (1997). Automatic conversion of magnetic data to depth, dip and susceptibility contrast using the SPITM method. *Geophysics*, 62, 807-813.

Vearncombe, J. R., Barton Junior, J. M., van Reenen, D. D., Phillips, G. N., Wilson, A. H. (1986). Greenstone belts: their components and structure. In: M. J. Wit, L. D. Ashwal (Eds.), *LPI Technical Report Workshop on Tectonic Evolution of Greenstone Belts*, 86-10. Houston: Lunar and Planetary Institute.

**2.2** Geochronology of the Archean Tumucumaque Complex, Amapá Terrane, Amazonian Craton, Brazil. Artigo aceito para publicação no *Journal of South American Earth Sciences*.

Invitation to revise manuscript SAMES_2018_135

Para: cborghetti@terra.com.br

"Victor A. Ramos (Journal of South American Earth Sciences)" EviseSupport@elsevier.com>

Ter 01/05/18 10:57

Ref: SAMES_2018_135

**Title: Geochronology of t he Archean Tumucumaque Complex, Amapá Terrane, Amazonian Craton, Brazil**

**Journal: Journal of South American Earth Sciences**

Dear Mr. Borghetti, Thank you for submitting your manuscript to Journal of South American Earth Sciences. We have completed the review of your manuscript. A summary is appended below. While revising the paper please consider the reviewers' comments carefully. We look forward to receiving your detailed response and your revised manuscript.

To submit your revised manuscript:

Log into EVISE® at:

http://www.evise.com/evise/faces/pages/navigation/NavController.jspx?JRNL_ACR=SAMES

Locate your manuscript under the header 'My Submissions that need Revisions' on your 'My Author Tasks' view

Click on 'Agree to Revise'

Make the required edits

Click on 'Complete Submission' to approve

What happens next?

After approving your s ubmission you will receive a notification that the submission is complete. To track the status of your paper throughout the editorial process, log into EVISE® at:

http://www.evise.com/evise/faces/pages/navigation/NavController.jspx?JRNL_ACR=SAMES

# Geochronology of the Archean Tumucumaque Complex, Amapá Terrane, Amazonian Craton, Brazil

Cristiano Borghetti[1], Ruy P.Philipp[2], Persio Mandetta[3], Itiana B. Hoffmann[1]

[1]Programa de Pós Graduação em Geociências (PPGGEO), Instituto de Geociências, Universidade Federal do Rio Grande do Sul, UFRGS. Av. Bento Gonçalves 9.500, CEP 91501-970, Porto Alegre, RS, BR, e-mail: cborghetti@terra.com.br
[2]Centro de Estudos em Petrologia e Geoquímica (CPGq), Instituto de Geociências, Universidade Federal do Rio Grande do Sul - UFRGS, Porto Alegre, RS, e-mail: ruy.philipp@ufrgs.br
[3]Amapari Mineração Ltda.

## Abstract

U-Pb and Lu-Hf isotopic studies were performed in igneous zircon crystals from orthogneisses, metagranodiorites and a gabbro of the Tumucumaque Complex (TC), in Vila Nova region, south of Amapá state, Brazil. The complex is located in the southeastern region of the Guyana Shield, northeastern portion of the Amazonian Craton. The TC is represented by tonalitic to granodioritic gneisses and amphibolites, with subordinate metagranites and intrusive gabbros, metamorphosed in conditions of middle to Upper Amphibolite facies. The complex represent the basement of the metavolcano-sedimentary associations of the Vila Nova and Serra do Navio regions, and occur as NW-SE elongated domes. The contact of infra- and supracrustal rocks is defined by N45°-55°W-trending high-angle ductile shear zones. In this contribution we provide U-Pb zircon ages by LA-MC-ICPMS which attest for the presence of a broad area of Archean rocks in the Guyana Shield. In addition, we present stratigraphic relationships and structural data between the TC and the Rhyacian Vila Nova Greenstone Belt. The orthogneisses yielded zircon igneous ages of 2.851 ±37 Ma and 2.852 ±32 Ma and the metagranodiorites of 2.822 ±33 Ma and 2.812 ±17 Ma. Intrusive gabbro present age of 2.671 ±46 Ma. The Lu-Hf data suggest an enriched mantle source and reworking of Paleo-archean crustal rocks. The results obtained suggest a magmatic orogenic episode during the Meso-archean (2.85 to 2.81 Ga) and a later Neo-archean (2.67 Ga) event, probably anorogenic.

**Keywords:**
U-Pb zircon geochronology, granitic magmatism, Archean, Tumucumaque Complex, Amazonian Craton, Guyana Shield.

## 1. Introduction

The Amazonian Craton (AC) consists of an Archean nucleus, bounded by Paleo- and Mesoproterozoic NW-SE trending orogenic belts (Teixeira et al. 1989; Tassinari and Macambira, 1999; Tassinari et al. 2000; Santos et al. 2000; Avelar et al. 2003; Rosa-Costa et al. 2006, 2012). The AC is composed by northern Guyana Shield and the southern Central Brazil Shield and covered by the sediments of the Solimões and Amazonas basins **(Fig.1A)**. The proposed model for the evolution of the Amazonian Craton includes a Archean core (Central Amazonian Province) surrounded by several orogenic belts included in the denominated Maroni-Itacaíunas (2.26-1.95 Ga), Ventuari-Tapajós (1.95-1.85 Ga), Rio Negro-Juruena (1.85-1.55 Ga), Rondoniana-San Ignácio (1.5-1.3 Ga) and the Sunsás (1.25-1.0 Ga) provinces (Tassinari and Macambira, 1999; Tassinari et al. (2000) **(Fig.1B)**. The Paleoproterozoic orogenic belts are composed of greenstone belts and TTG-type granitic associations (Avelar et al. 2003; Mc Reath and Faraco 2006; Borghetti et al. 2017, 2018; Hoffmann et al. 2018).

The historical scarcity of geological information in the Amazon region is related to the difficulty of access and the low availability of rock outcrops, due to the dense tropical forest coverage and by the thick soil layer. On the other hand, AC provides one of the most preserved and complete sequences of Earth's crustal tectonic evolution between the Archean and Mesoproterozoic, including the upper and lower crustal segments (Almeida et al. 2000; Rosa et al. 2016). Despite its size and importance for the South American Platform, the geochronological studies in the AC are still sparse.

The oldest rocks of the Guyana Shield are located in the eastern portion of the Amapá State, where the Tumucumaque Complex (TC) is exposed and in the central-south area, where the metamorphic rocks of the Ananaí, Jari-Guaribas, Baixo Mapari

and Guianense complexes occur. Located in the eastern portion of the Maroni-Itacaiúnas Province, the orthogneisses and amphibolites of the Tumucumaque Complex were initially interpreted as generated in Paleoproterozoic. Previous geochronology studies (Pb-Pb zircon evaporation) developed by Avelar (2002), Avelar et al. (2003) and Rosa-Costa et al. (2003, 2006) provide ages for orthogneisses and metagranites of the Tumucumaque and Guianense complexes between 2.8 and 2.6 Ga, confirming the existence of an Archean basement in this region.

The southeastern portion of the Guyana Shield is located in a remarkable position to understand the Western Gondwana reconstruction, as shown by De Wit et al. (2008). The new U-Pb zircon ages of the basement rocks and the detrital zircon provenance of the metasedimentary rocks of this portion, and their role in the tectonic context is crucial to restore the paleogeography and the pre-drift correlations between South America and West Africa.

The objective of this paper is to integrate geological and structural mapping data with the new U-Pb zircon ages and Lu-Hf isotopic data of rocks of the TC to contribute to the tectonic evolution of the Amazonian Craton.

## 2. Geological Setting

The Amazonian Craton is one of the largest and least known Precambrian areas of the world and the major tectonic unit of the South America, with about 5.6 million km$^2$. In Brazil, the AC comprises an area of around 4.4. million km$^2$, bordered by to the east by the Araguaia Belt, and to the south and southeast by the Paraguay Belt, both related to Neoproterozoic Brasiliano Orogeny (900-540 Ma) (Almeida et al. 2000).

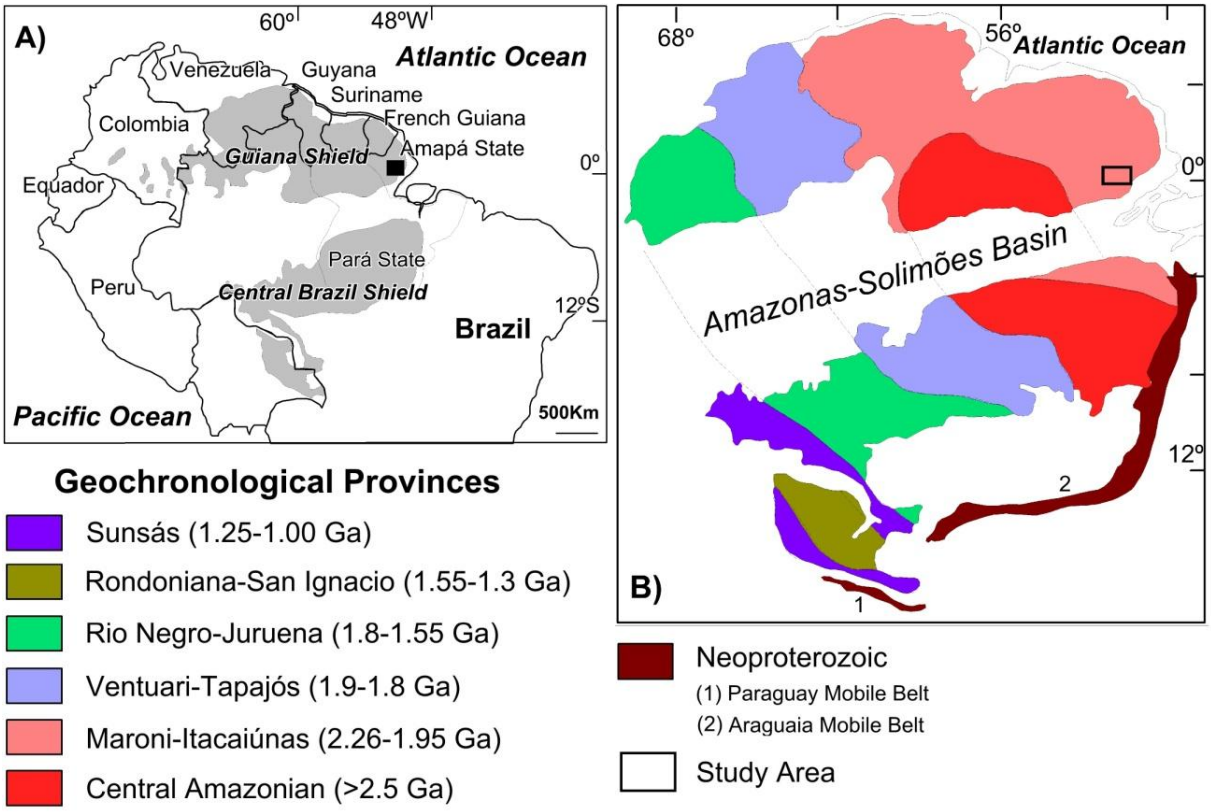


**Figure 1. A)** Map of the Amazonian Craton in South America and location of the Guiana and Central Brazil shields, **B)** Geochronological Provinces of the Amazonian Craton proposed by Tassinari and Macambira (2004) and location of the study area (Black rectangle).

The southeast region of the Guyana Shield is contained in one of the largest orogenic Paleoproterozoic belts in Earth's crust. The Maroni-Itacaiúnas Province (MIP) presents for the AC an evolutionary model that involves a large Archean nucleus of continental crust which is surrounded by Paleo- and Mesoproterozoic orogenic belts (Tassinari and Macambira 1999, 2004; Tassinari et al. 2000; Santos et al. 2000) **(Fig. 1B)**. The MIP surrounds the Archean Central Amazonian Province to the north and northeast, with evolution related to the Rhyacian, between 2.26 and 1.95 Ga (Tassinari et al. 2000; Delor et al. 2003a, b; Rosa-Costa et al. 2006; Tavares, 2009). The **table 1** show a summary of the published geochronological data of the basement units and of the Paleoproterozoic greenstone belts and intrusive granites of Vila Nova and Serra do Navio regions.

## 2.1 Archean basement complexes

The Archean crust of the eastern Guyana Shield is characterized by the accretion of TTG suites (medium to high-grade orthogneisses), clinopyroxene-bearing orthogneisses and granitoid rocks with Pb-Pb zircon ages between 2.85 and 2.58 Ga (Avelar et al. 2003; Rosa-Costa et al. 2003, 2006) (**Table 1**). Zircon geochronology and Nd data define the Neo-archean as a period of intense crustal reworking from Paleo- and Meso-archean protoliths, with subordinate generation of juvenile magmatism (Pimentel et al. 2002; Avelar et al. 2003; Rosa-Costa et al. 2003, 2006).

The geology of the Amapá state is composed by a northern portion dominated by Paleoproterozoic orthogneisses (arc-related granitoids), metavolcano-sedimentary sequences and late-orogenic granitoids, and by the south-central portion, composed by reworked Archean rocks (Avelar et al. 2003; Rosa-Costa et al. 2003, 2006; Tavares, 2009; Barreto et al. 2013; Borghetti et al. 2014). The orthogneisses, metagranitoids and high-grade metamorphic rocks of Archean age that occupy an extensive area in the central portion of the Amapá and north of Pará states constitute the Amapá Block (Rosa-Costa et al., 2006) **(Fig. 2A)**. Based on petrotectonic associations, geophysical signature, metamorphic grade and geochronological data, the Amapá Terrane was subdivided in Jari and Cupixi domains. The Archean Paru Domain occurs inside of the Paleoproterozoic Carecuru Domain (Rosa-Costa et al., 2003, 2006) **(Fig. 2B)**.

The *Jari Domain* is constituted by granulitic orthogneisses of the Jari-Guaribas and Guianense complexes, clinopyroxene-bearing orthogneisses of the Baixo Mapari Complex, charnockitic and enderbitic granites of the Noucouru Suite and monzogranites of the Anauerapucu Granite. The *Cupixi Domain*, where is located the study area, is composed by TTG orthogneisses, amphibolites and metagranites, and

by Rhyacian metavolcano-sedimentary sequences of komatiitic to tholeitic composition and intrusive granitic plutons **(Fig. 2B)**. The *Paru Domain* is surrounded by the Carecuru Domain units, being composed of Archean granulite gneisses, invaded by Paleoproterozoic charnockitic and granites plutons. The *Carecuru Domain* consists of Paleoproterozoic metavolcano-sedimentary sequences of tholeitic to low-K calc-alkaline composition and granitic domes composed by calc-alkaline TTG associations.

The *Jari Domain* represents the largest portion of the Amapá Terrane, most expressive segment of Archean crust of the Guyana Shield. While the juvenile crustal accretion is attributed to Paleo-archean and along the Meso-archean, the data from 2.8 and 2.58 Ga period is related to ensialic reworking of older Archean rocks (Rosa-Costa et al. 2003, 2006) **(Table 1)**. The associations of Neo-archean are considered as a substantial and prolonged crust-forming episode (Cordani & Sato, 1999). In the *Paru Domain* the Neo-archean magmatism dated at 2.59 Ga was generated by the Meso-archean crustal reworking. In addition, juvenile and calc-alkaline magmatism were identified in 2.32 Ga and 2.15 Ga, with late charnockitic magmatism in 2.07 Ga **(Table 1)**. The *Carecuru Domain* is interpreted as an active continental margin magmatic arc system, added to the Amapá Terrane during the Rhyacian. The beginning of juvenile accretion and of the calc-alkaline magmatism developed around 2.28 Ga, with two late pulses of granitic magmatism between 2.19-2.18 Ga and 2.15-2.14 Ga (Rosa-Costa et al., 2003, 2006) **(Table 1)**. The Nd $T_{DM}$ model ages between 2.5 and 2.38 Ga and the negative values of the epsilon Nd isotopes indicate the participation of Archean components.

In the *Cupixi Domain*, the orthogneisses of TC in the Vila Nova region present Pb-Pb zircon ages of 2.849 ±6 Ma and 2.844 ±2 Ma (Avelar et al. 2003) and a Nd $T_{DM}$ model ages of 3.36 to 3.07 Ga (Pimentel et al., 2002) **(Table 1)**. The

orthogneisses of Tartarugalzinho region located northeast of the study area present Pb-Pb zircon ages of 2.58 Ga (Avelar et al. 2003) and 3.48 Ga (Rosa-Costa el al. 2012). This evidence of an Archean crust implies strong metamorphic reworking during the Paleoproterozoic (Tassinari et al. 2000; Pimentel et al. 2002; Avelar et al. 2003; Rosa-Costa et al. 2003, 2006). The definition of the TC was proposed by Scarpelli (1973) to gather the ortho- and paragneisses that occurred from the Jari River to the Lombarda Ridge in north-central Amapá State. Subsequently, Ricci et al. (2001) described this unit as tonalitic to granodioritic gneisses, with minor occurrences of amphibolite bodies concordant to the regional banding. Rosa-Costa et al. (2003, 2006) separated the gneisses of the Guianese Complex, the dominant unit of the Jari Domain and located southwest of the Cupixi Lineament.

The evidence for Archean crust also was recorded by detrital zircons (3.6-2.4 Ga) from metasedimentary rocks of Vila Nova Greenstone Belt (Borghetti et al. 2018), by inherited zircons (2.9-2.6 Ga) and by Nd $T_{DM}$ model ages (3.29-2.24 Ga) yielded by Paleoproterozoic granites and orthogneisses (Lafon et al. 2000; Avelar et al. 2002, 2003; Tavares, 2009; Barreto et al. 2013; Barbosa et al. 2013) **(Table 1)**.

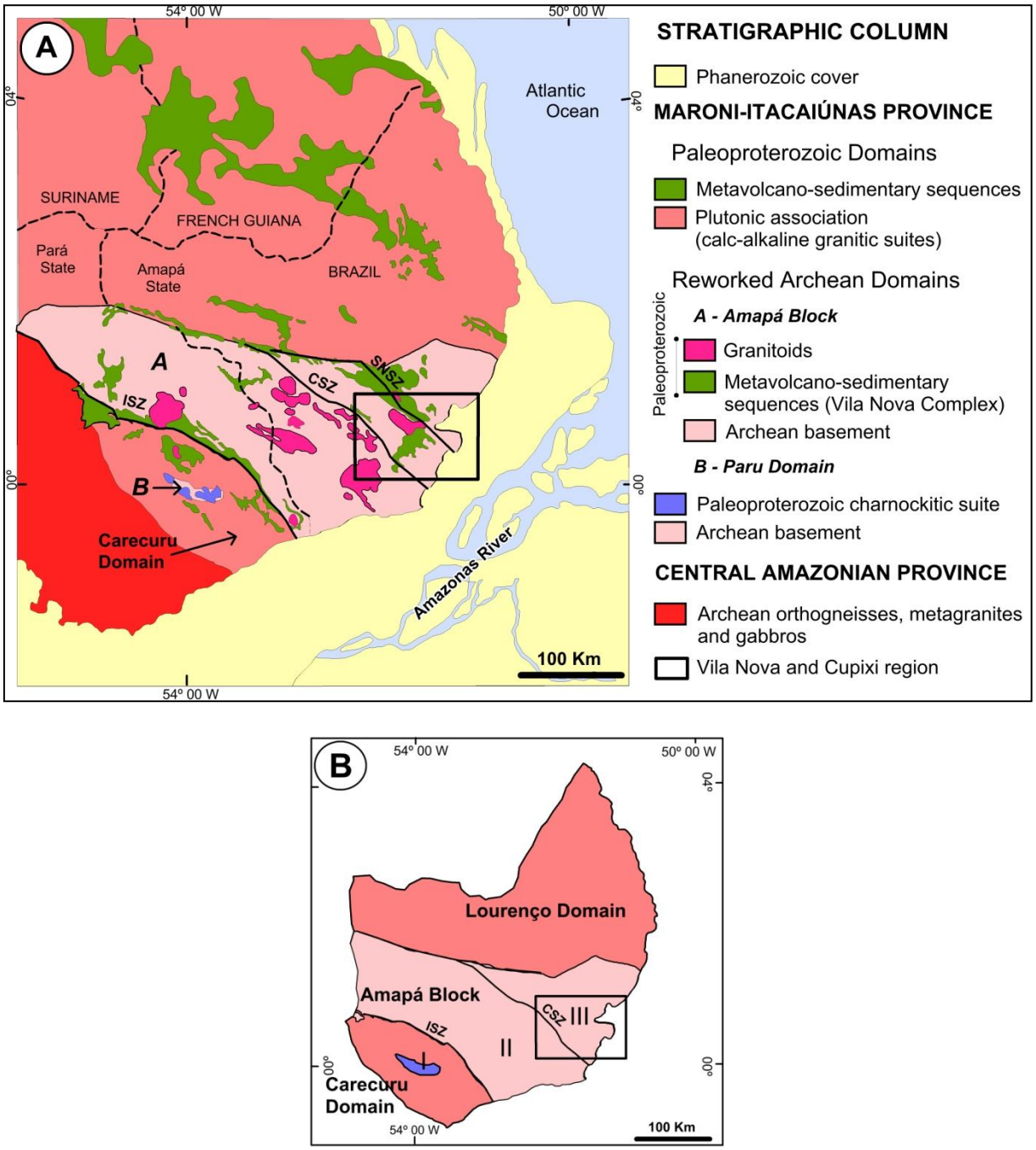


**Figure 2**. **A)** Archean and Paleoproterozoic tectonic-geochronological domains of the southeastern portion of the Guiana Shield, modified from Rosa-Costa et al. (2006). The geochronological provinces are according to Tassinari & Macambira (2004). **B)** The geotectonic domains of the Amapá and north Pará state, according to Ricci et al. (2001) and Rosa Costa et al. (2012). Archean Basement: **I** - Parú Domain; **II** - Jari Domain; **III** - Cupixi Domain. Shear Zones: CSZ = Cupixi; ISZ = Ipitinga.

| STRATIGRAPHIC UNITS | ROCK TYPE | Pb-Pb or U-Pb (Zircon) | $T_{DM}$ (Sm-Nd WR) | References |
|---|---|---|---|---|
| **PALEOPROTEROZOIC LATE-OROGENIC TO ANOROGENIC GRANITES (1.99-1.84 Ga)** | | | | |
| **Porto Grande Granite** | Syenogran./monzogran. | 1.842 ±23 Ma[a] | | Barbosa et al. (2013) |
| **Amapari Granite** | Alkali-feldspar granite | 1.993 ±13 Ma[a] | | Faraco et al. (2004) |
| **Late-orogenic volcanic French Guiana (Uatumã)** | Acid volcanic rock | 1.96 Ga | | Delor et al. (2003a) |
| **Late orogenic granite French Guiana** | Biotite granite | 2.01 Ga | | Delor et al. (2003a) |
| **PALEOPROTEROZOIC COLLISIONAL GRANITES (2.11-2.03 Ga)** | | | | |
| **Undifferentiated granitoids** | Biotite monzogranite | | 2.9 Ga | Rosa-Costa et al. (2012) |
| | Biotite monzogranite | | 2.2 Ga | Barreto et al. (2013) |
| | Tonalite | 2.184 ±13 Ma[b] | | Barreto et al. (2013) |
| | Charnockitic granulites | 2.065 ±5 Ma[a] | | Barreto et al. (2013) |
| | Biotite monzogranite | 2.124 ±21 Ma[a] | | Barreto et al. (2013) |
| | Tonalite | 2.160 ±130 Ma[b] | 2.34-2.24 Ga | Nogueira et al. (2000) |
| **Peraluminous granite** | Two mica granite | 2.030 ±2 Ma[a] | | Rosa-Costa et al. (2006) |
| **Parintins Suite** | Monzogranite | 2.053 ±4 Ma[a] | | Rosa-Costa et al. (2006) |
| **Igarapé Careta Suite (Cupixi Domain)** | Syenogranite | 2.065 ±35 Ma[a] | | Barbosa et al. (2013) |
| **Carrapatinho Granite** | Monzogran./syenogranite | 2.025 ±17 Ma[a] | | Barbosa et al. (2013) |
| | Monzogran./syenogranite | 2.08-2.02 | 2.66 Ga | Barreto et al. (2013) |
| | Monzogran./syenogranite | | 3.68 Ga | Rosa-Costa et al. (2012) |
| **Sucuriju Metagranite (Cupixi Domain)** | Monzogranite | 2.08-2.02 Ga[a] | | Barreto et al. (2013) |
| | Monzogran./syenogranite | | 3.0-2.88 Ga | Barreto et al. (2013) |
| | Monzogran./syenogranite | | 2.59 Ga | Rosa-Costa et al. (2012) |
| **Igarapé Urucu Suite (Cupixi Domain)** | Charnockite | 2.074 ±5 Ma[a] | | Rosa-Costa et al. (2006) |
| **Tartarugal Grande Complex** | Enderbitic to charnockitic | 2.125.±4 Ma[a] | 3.29-2.25 Ga[c] | Rosa-Costa et al. (2012) |
| | Granulites | 2.065 ±5 Ma[a] | | Rosa-Costa et al. (2012) |
| | Granulitic gneiss | 2.580 ±5 Ma[a] | | Avelar et al. (2003) |
| **Araguari Complex** | Tonalite | 2.103 ±3 Ma[a] | 2.64-2.52 Ga | Barreto et al. (2013) |
| | Tonalite | 2.096 ±4 Ma[a] | 2.97-2.47 | Barreto et al. (2013) |
| | Tonalite/granodiorite | | 2.64-2.52 Ga | Rosa-Costa et al. (2012) |
| | Tonalite/granodiorite | | 2.97-2.47 Ga | Rosa-Costa et al. (2012) |
| **Undifferentiated granitoids of French Guiana (TTG Complex)** | Monzogranite | 2.060 ±4 Ma[e] | | Delor et al. (2003a) |
| | Migmatite | 2.094 ±7 Ma[e] | | |
| | Granite | 2.112 ±2 Ma[e] | | |
| | Granite | 2.089 ±4 Ma[e] | | |
| | Monzogranite | 2.092 ±4 Ma[e] | | |
| **(D2 thermotectonic event)** | Granite | 2.100 ±1 Ma[e] | | |
| | Granite | 2.104 ±2 Ma[e] | | |
| | Granodiorite | 2.104 ±2 Ma[e] | | |
| | Granite | 2.069 ±4 Ma[e] | | |
| **PALEOPROTEROZOIC ARC RELATED GRANITES (2.26-2.13 Ga)** | | | | |
| **Ananaí Complex (Paru Domain)** | Throndjemitic gneiss | 2.150 ±2 Ma[a] | 2.32 Ga | Rosa-Costa et al. (2006) |
| **Flexal Suite (Cupixi Domain)** | Tonalite | 2.197 ±3 Ma[a] | | Rosa-Costa et al. (2012) |
| | Granodiorite | 2.184 ±13 Ma[b] | | Rosa-Costa et al. (2012) |
| | Monzogranite | 2.181 ±2 Ma[a] | | Avelar (2002) |
| | Monzogranite | | 2.61 Ga | Avelar (2002) |
| | Monzogranite | | 2.75-2.39 Ga | Avelar (2002) |
| | Monzogranite | | 2.73-2.37 Ga | Rosa-Costa et al. (2012) |
| **Undifferentiated granitoids of French Guiana (TTG Complex)** | Gabbro | 2.208 ±12 Ma[e] | | Delor et al. (2003a) |
| | Granodiorite | 2.155 ±3 Ma[e] | | |
| | Tonalite | 2.173 ±9 Ma[e] | | |
| | Granodiorite | 2.183 ±3 Ma[a] | | |
| | Diorite | 2.161 ±3 Ma[a] | | |
| **(D1 thermotectonic event)** | Tonalite | 2.160 ±6 Ma[a] | | |
| | Granite | 2.163 ±3 Ma[a] | | |
| | Tonalite | 2.172 ±2 Ma[a] | | |
| | Granite | 2.165 ±6 Ma[a] | | |
| | Tonalite | 2.141 ±8 Ma[a] | | |
| | Meta-andesite | 2.137 ±6 Ma[a] | | |
| | Granite | 2.132 ±3 Ma[a] | | |
| **Rio Santo Antônio Diorite** | Tonalite | 2.262 ±2 Ma[a] | | Barreto et al. (2013) |
| | Hb qz-diorite | | 2.68 Ga | Barreto et al. (2013) |
| **Undifferentiated granitoids of Jari Domain** | Syenogranite | 2.098 ±2 Ma[a] | | Rosa-Costa et al. (2006) |
| | Monzogranite | 2.177 ±3 Ma[a] | | Rosa-Costa et al. (2006) |
| | Alkali-feldspar granite | 2.146 ±3 Ma[a] | | Rosa-Costa et al. (2003) |
| | TTG gneiss | 2.150 ±1 Ma[a] | | Rosa-Costa et al. (2003) |
| | Diorite | 2.140 ±1 Ma[a] | | Rosa-Costa et al. (2003) |
| | Monzogranite | 2.185 ±4 Ma[b] | | Rosa-Costa et al. (2006) |
| | Monzogranite | 2.218 ±3 Ma[b] | | Rosa-Costa et al. (2006) |

| STRATIGRAPHIC UNITS | ROCK TYPE | Pb-Pb or U-Pb (Zircon) | $T_{DM}$ (Sm-Nd WR) | References |
|---|---|---|---|---|
| **Carecuru Suite** | Diorite | 2.139 ±2 Ma[a] | | Rosa-Costa et al. (2006) |
| **Paru-Maratiá Complex** | Granodioritic gneiss | 2.191 ±2 Ma[a] | | Rosa-Costa et al. (2006) |
| **Granitoids intrusive in the Vila Nova Complex (Cupixi Domain)** | Granodiorite | 2.23 Ga[a] | | Tavares (2009) |
| | Monzogranite | 2.23 Ga[a] | | Tavares (2009) |
| | Monzogranite | 2.25 Ga[a] | | Tavares (2009) |
| | Granodior./monzogranite | | 2.83-2.24 Ga | Tavares (2009) |
| **Bacuri Mafic-ultramafic Complex** | Mafic and ultramafic rocks | | 2.218 ±120 Ma[c] | Pimentel et al. (2002) |
| **PALEOPROTEROZOIC GREENSTONE BELTS (2.26-2.08 Ga)** | | | | |
| **Ipitinga Group (Jari Domain)** | Amphibol./actinol. schist | | 2.267 ±66 Ma[c] | Mc Reath and Faraco (2006) |
| **Vila Nova Complex (Cupixi Domain)** | Metapelite | | 2.087 ±22 Ma[d] | Pimentel et al. (2002) |
| | Amphibolite/actin. schist | | 3.03-2.85 Ga | Rosa-Costa et al. (2006) |
| | Metandesite | 2.154 ±6 Ma[b] | | Hoffmann et al. (2018) |
| | Metandesite | 2.170 ±9 Ma[b] | | Borghetti et al. (2018a) |
| | Metaconglomerate | 3.6-2.4 Ga[b] | | Borghetti et al. (2018a) |
| | Quarzite | 3.6-2.7 Ga[b] | | Borghetti et al. (2018a) |
| **ARCHEAN BASEMENT ROCKS (2.85-2.58 Ga)** | | | | |
| **Riozinho Granite (Jari Domain)** | Monzogranite | 2.626 ±5 Ma[b] | 3.03 Ga[c] | Rosa-Costa et al. (2006) |
| **Noucouru Intrusive Suite (Jari Domain)** | Mesopertite granite | 2.656 ±4 Ma[a] | | Rosa-Costa et al. (2006) |
| | Mesopertite granite | 2.649 ±2 Ma[a] | | Rosa-Costa et al. (2006) |
| **Anauerapucu Granite (Jari Domain)** | Monzogranite | 2.791 ±23 Ma[a] | | Rosa-Costa et al. (2012) |
| **Paru Granulitic Nucleus** | Enderbitic gneiss | 2.597 ±4 Ma[a] | | Rosa-Costa et al. (2003) |
| **Guianense Complex (Jari Domain)** | Granulite | 2.580 ±5 Ma[a] | | Avelar et al. (2003) |
| | Granodioritic gneiss | 2.652 ±4 Ma[a] | | Rosa-Costa et al. (2003) |
| | Charnockite | 2.605 ±6 Ma[a] | | Ricci et al. (2002) |
| | Monzogranitic gneiss | 2.628 ±2 Ma[a] | | Rosa-Costa et al. (2006) |
| | Tonalitic orthogneiss | | 2.96-2.94 Ga | Avelar et al. (2003) |
| | Orthogneiss | | 3.12-2.83 Ga | Rosa-Costa et al. (2006) |
| | Orthogneiss | 2.656 ±4 Ma[a] | 3.15- 3.01 Ga | Rosa-Costa et al. (2012) |
| | Orthogneiss | 2.605 ±3 Ma[a] | | Rosa-Costa et al. (2006) |
| **Jari-Guaribas Complex (Jari Domain)** | Orthogranulites | 2.797 ±3 Ma[a] | | Rosa-Costa et al. (2012) |
| | Enderbitic gneiss | 2.788 ±2 Ma[a] | 3.26-3.19 Ga | Rosa-Costa et al. (2006) |
| | Enderbitic gneiss | 2.790 ±8 Ma[a] | | Rosa-Costa et al. (2006) |
| | Enderbitic gneiss | 3.238 ±6 Ma[a] | | Rosa-Costa et al. (2006) |
| **Mungubas Granite (Cupixi Domain)** | Monzogranite | 2.661 ±9 Ma[a] | | Barreto et al. (2013) |
| **Tumucumaque Complex (Cupixi Domain)** | Gneisses | | 3.36-3.07 Ga[d] | Pimentel et al. (2002) |
| | Tonalitic gneiss | 2.849 ±6 Ma[a] | | Avelar et al. (2003) |
| | Tonalitic gneiss | 2.844 ±2 Ma[a] | | Avelar et al. (2003) |
| | Tonalitic gneiss | 2.851 ±37 Ma[b] | | This work |
| | Granodioritic gneiss | 2.852 ±32 Ma[b] | | This work |
| | Metagranodiorite | 2.822 ±33 Ma[b] | | This work |
| | Metagranodiorite | 2.812 ±17 Ma[b] | | This work |
| | Gabbro | 2.671 ±46 Ma[b] | | This work |

**Table 1.** Summary of the isotopic data of the basement units and of greenstone belts of Vila Nova and Serra do Navio regions. Key to abbreviations: WR - whole rock, [a] $^{207}Pb/^{206}Pb$ zircon evaporation, [b] U-Pb zircon LA-MC-ICPMS, [c] Sm-Nd whole rock isochron, [d] Sm-Nd whole rock garnet isochron and [e] U-Pb zircon SHRIMP.

## 2.2 Paleoproterozoic orogenic belts

The study area is marked by the NW-SE elongated metavolcano-sedimentary sequences of the Vila Nova (VNGB) and Serra do Navio (SNGB) greenstone belts and by the basement rocks of TC. Intrusive orogenic granites present Pb-Pb zircon

ages between 2.25 and 2.06 Ga (Avelar et al. 2003; Rosa-Costa et al. 2003, 2006; Tavares, 2009; Barreto et al. 2013; Barbosa et al. 2013) **(Table 1)**.

The VNGB consists of metabasalts, meta-andesites and rare metadacites at the base, and metasedimentary rocks intercalated with mafic metavolcanic and exhalative chemical rocks at the top (Borghetti et al. 2018; Hoffmann et al. 2018). These rocks are metamorphosed from greenschist to intermediate amphibolite facies and intermediate pressure. U-Pb zircon ages between 2.17 and 2.15 Ga obtained from meta-andesite defines the period of volcanic activity in the basin (Borghetti et al. 2018, Hoffmann et al. 2018). The Hf values, from +1.17 to +6.5, and between -2.44 and -11.79, indicate that two sources (MORB and sub-lithospheric continental mantle) were important in the genesis of meta-andesites. The Hf $T_{DM}$ ages show Siderian values, between 2.26 and 2.43 Ga, with a small participation of zircons of Neo- and Paleo-archean, between 2.52 and 3.43 Ga and $\varepsilon_{Hf(t)}$ positive, between +3.64 and +7.98. Detrital zircon grains from metasediments yielded ages between 3.6 and 2.4 Ga suggesting that the rocks derived mainly from the Archean basement **(Table 1)**. The available data suggest an evolution model based on the opening and closure of an ocean, with development of magmatic arc system and arc-related basin rocks during the Rhyacian (Hoffmann et al. 2018).

The basement complexes and the Paleoproterozoic greenstone belts are cut by three groups of Paleoproterozoic intrusive granites. The oldest plutons have NW-SE direction elongate shapes, consistent with regional foliation and are considered orogenic granites by Rosa-Costa et al. (2003, 2006, 2012), Avelar et al. (2003), Tavares (2009), Barbosa et al. (2013) and Barreto et al. (2013). They have Pb-Pb zircon ages between 2.26 and 2.1 Ga and were described as syenogranites and biotite monzogranites with massive structure and medium equigranular texture, with local mylonitic shear zones. Barreto et al. (2013) characterize in the southeastern of

Guyana Shield, the occurrence of metaluminous low-K tholeiitic tonalites and quartz-diorites, with geochemical affinity with tholeiitic to komatiitic volcanic arc association suggesting a back-arc basin-island arc system. The second group of granites present Pb-Pb zircon ages between 2.11 and 2.03 Ga and are related to collisional orogenic metamorphism. This granites are represented by syeno- to monzogranites (Tartarugal Grande Complex, Igarapé Careta Suite, Carrapatinho Granite and Sucuriju Metagranite) and by charnockitic to enderbitic granulites (Avelar et al. 2003; Rosa-Costa et al. 2003, 2006; Barbosa et al. 2013; Barreto et al. 2013). The last group is represented by late-orogenic to anorogenic granites. The Amapari Granite is intrusive in the VNGB and constitutes two elongated bodies in the NW-SE direction. They have composition between alkali-feldspar granites to monzogranites, massive structure and equigranular to porphyritic textures. It have Pb-Pb zircon age of 1.99 Ga and Nd $T_{DM}$ model age of 2.6 Ga (Avelar et al. 2003; Rosa-Costa et al., 2003, 2006; Barreto et al. 2013). The Porto Grande Granite constitutes a circular pluton composed of syeno- to monzogranites with equigranular to porphyritic textures and magmatic foliation. It present Pb-Pb zircon age of 1.84 Ga and Nd $T_{DM}$ model age of 2.87 Ga **(Table 1)**.

The ages obtained in monazites of high-grade paragneisses from the southwest of the Amapá Terrane revealed two orogenic metamorphism events (Rosa-Costa et al. 2006). The first event of 2.09 Ga characterizes the granulitic metamorphism and the collisional stage, associated with the formation of the thrusting systems represented by the regional oblique ductile shear zones. The second event occurred between 2.06 and 2.04 Ga and define the late to post-collisional stage, with extensive migmatization of the Archean basement and emplacement of granitic suites along transcurrent ductile shear zones (Rosa-Costa et al. 2003, 2006).

The VNGB and the orogenic granites of the Cupixi Domain are correlated with French Guyana Paleoproterozoic units (Delor et al. 2003a) and West-African Craton units (Ledru et al. 1994; Zhao et al. 2002).

.

**3. Material and Methods**

Five samples of the TC were selected for LA-MC-ICPMS U-Pb zircon geochronology studies, and include a tonalitic (CB-28) and granodioritic (VGN-28) gneisses, two metagranodiorites (CB-14 and CB-17A) and an intrusive gabbro (CB-09). The zircon grains of the metagranodiorite CB-17A was selected for Lu-Hf isotopic studies. The samples were crushed and milled using a mandible crusher and then pulverized. Zircon grains were concentrated by conventional magnetic and heavy liquid techniques, and the final concentration was made by hand panning. The samples were prepared in the Geoscience Institute at Rio Grande do Sul Federal University (UFRGS).

The grains used for zircon dating were mounted in epoxy resin, polished until half of the grain thickness was reached so as to expose internal oscillatory zoning for further imaging. Backscattered electron (BSE) and cathodoluminescence (CL) imaging were performed to identify internal structures, crystallization phases and other complexities. Cathodoluminescence (CL) images of zircons were obtained using a Quanta 250 FEG electron microscope equipped with a Mono CL3+ cathodoluminescence spectroscope (Centaurus) at the Geochronological Research Center (CEPEGEO) at Geosciences Institute of São Paulo University (USP).

U-Pb zircon analyses were performed at the LA-MC-ICPMS Laboratory of the CEPEGEO at São Paulo University by a Neptune Inductively Coupled Plasma-Mass Spectrometer (ICPMS) coupled with an Excimer laser ablation system (LA). The routine of the U-Pb method consists of the analysis of 2 blanks, 2 NIST standards, 3

external GJ1 standards, 13 unknown samples, 2 external standards and 2 blanks. The $^{204}Hg$ interference on $^{204}Pb$ measurements was corrected using $^{202}Hg$ and adopting $^{204}Hg/^{202}Hg$ ratio of 4.2. $^{207}Pb/^{206}Pb$ ratio normalization was achieved by combined NIST and external standards. $^{206}Pb/^{238}U$ ratio normalization was achieved by external standards. The GJ1 standard (602 ±4.4 Ma, Elholou et al. 2006) was used for mass bias correction. The residual common Pb was corrected according to the measured $^{204}Pb$ concentration using the known terrestrial composition (Stacey and Kramers 1975).

The uncertainty introduced by laser-induced element fractionation and mass instrumental discrimination was corrected and evaluated using the GJ-1 zircon standard. External errors were calculated using error propagation of the individual standard GJ-1 measurements and measurements of the individual zircon samples (spots). Age calculations were made using the Isoplot version 4 software, and mainly $^{206}Pb/^{238}U$ measurements (Ludwig, 2008). Chemale et al. (2011) describe in detail the analytical method and data treatment.

The Lu-Hf isotopic composition was analyzed whenever possible in the same spot previously analyzed for U-Pb isotopes. Zircon data were reduced using SQUID (Ludwig, 2002). Data were plotted on weighted average and Concordia diagrams using Isoplot software (Ludwig, 2008); error ellipses on Concordia plots are shown at the 95% confidence level (2σ). The analytical uncertainty in all grouped age data is quoted at the 95% confidence level (2σ).

Hf isotopic measurements were carried out using a Thermo-Finnigan Neptune multicollector ICP-MS coupled to a Photon-Machines 193 nm laser system, at Departament of Geology, at Ouro Preto Federal University. Data were collected in static mode during 60 s of ablation with a spot size of 60 μm. Nitrogen (~0.080 l/min) was introduced into the Ar sample carrier gas. Typical signal intensity was ca. 10 V

for $^{180}$Hf. The isotopes $^{172}$Yb, $^{173}$Yb and $^{175}$Lu were simultaneously monitored during each analysis step to allow for correction of isobaric interferences of Lu and Yb isotopes on mass 176. The $^{176}$Yb and $^{176}$Lu were calculated using a $^{176}$Yb/$^{173}$Yb of 0.796218 (Chu et al., 2002) and $^{176}$Lu/$^{175}$Lu of 0.02658 (JWG in-house value). The correction for instrumental mass bias utilized an exponential law and a $^{179}$Hf/$^{177}$Hf value of 0.7325 (Patchett and Tatsumoto, 1980) for correction of Hf isotopic ratios. The mass bias of Yb isotopes generally differs slightly from that of the Hf isotopes with a typical offset of the βHf/βYb of ca. 1.04 to 1.06 when using the $^{172}$Yb/$^{173}$Yb value of 1.35274 from Chu et al. (2002). This offset was determined for each analytical session by averaging the βHf/βYb of multiple analyses of the JMC 475 solution doped with variable Yb amounts and all the laser ablation analyses (typically n> 50) of zircon that have a $^{173}$Yb signal intensity of >60 mV. The mass bias behavior of Lu was assumed to follow that of Yb. The Yb and Lu isotopic ratios were corrected using the βHf of the individual integration steps (n=60) of each analysis divided by the average offset factor of the complete analytical session.

## 4. Results

### 4.1 Geology of the Vila Nova area

Vila Nova and Cupixi regions are located in the eastern portion of the Amapá Block and are composed by Archean TTG basement complexes, by the Rhyacian metavolcano-sedimentary sequences of VNGB and SNGB and by the arc-related granitoids and late- to post-collisional granitic associations **(Fig. 2)**. This area is characterized by a conspicuous NW-SE ductile structuring, constituted of medium-grade orthogneisses and metagranites of the Tumucumaque and Guianense complexes, by the Bacuri Mafic-Ultramafic Complex (BMUC), by linear belts of metavolcano-sedimentary sequences and intrusive granites **(Fig. 3).** The Vila Nova

Complex was used generally to refer to all the metavolcano-sedimentary units occurring as several greenstone belts regionally named Serra do Navio, Vila Nova, Ipitinga, Tumucumaque, Tartarugalzinho, Lombarda and Oiapoque (Mc Reath and Faraco 2006).

The TC is the main basement rocks of Cupixi Domain and in Vila Nova region it is represented by orthogneisses, metagranites and amphibolites with subordinate occurrence intrusive gabbros characterized by stocks with 300 to 1500 meters in diameter. The gneisses are metamorphosed under conditions of middle to upper Amphibolite-facies. Overlapping the TC are the intrusive mafic-ultramafic rocks of Bacuri Complex. These complex constitute an EW-trending elongated body located in the southern part of the study area.

The Guianense Complex (GC) is composed by grey tonalitic to granodioritic gneisses and is the main basement unit of the Jari Domain (Rosa-Costa et al. 2006). The Pb-Pb zircon data around 2.6 Ga indicate that these gneisses are Neo-archean. The contact with the TC is tectonic, defined by the mylonites of the Cupixi Shear Zone. A detailed vertical view of the relationships of the geological units can be inferred from the geological cross-section given in figure 4, highlighting the tectonic contact between the TC and GC. In the northwest portion of the studied area the TC is cut by the Mungubas Granite (Barbosa et al., 2013). This granite has an elongated shape in NW-SE direction and yielded a Pb-Pb zircon age of 2.66 Ga. It is composed of monzogranites to syenogranites with massive structure and inequigranular texture.

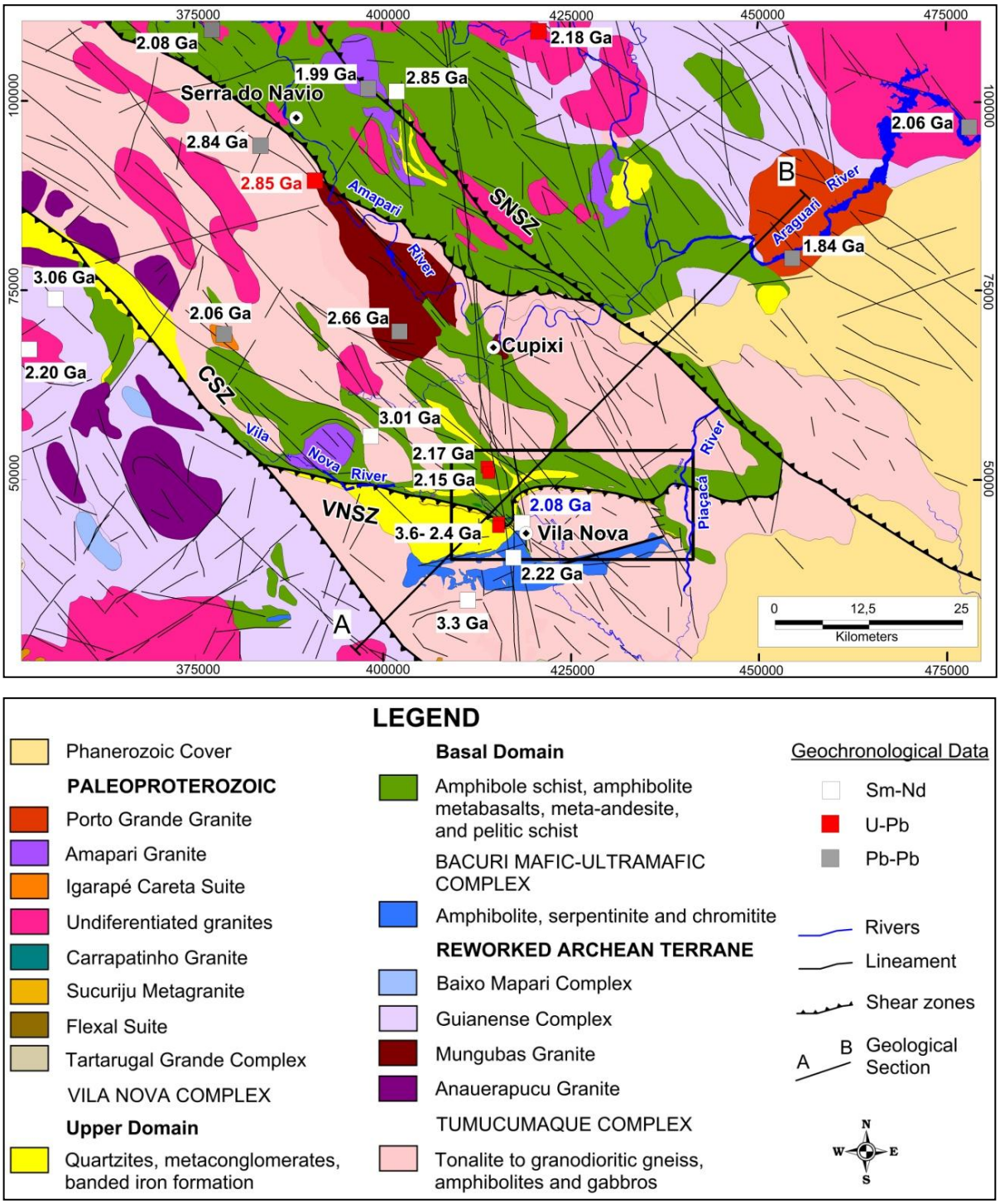


**Figure 3.** Geological map of the Vila Nova and Cupixi region, highlighting the study area bounded by the rectangle in black. Radiometric data compilation is presented with black numbers for crystalization ages and blue numbers for metamorphic ages. The numbers in red color is related to the sample (CB-28) from this work. Interpretation and structural data by authors, modified from Faraco et al. (2004), Magalhães et al. (2007) and Barbosa et al. (2013). Main Shear Zones: Cupixi (CSZ), Serra do Navio (SNSZ) and Vila Nova (VNSZ).

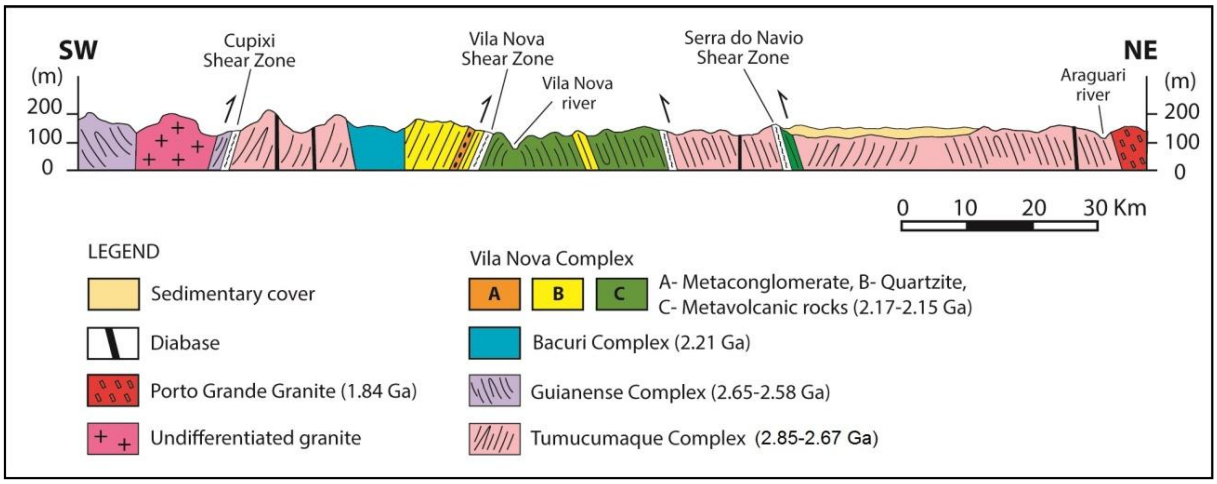


**Figure 4.** Schematic geological section shows the main structures and contact relationships between metavolcano-sedimentary rocks of the VNGB and the basement orthogneisses.

The Vila Nova greenstone belt (VNGB) is metavolcano-sedimentary sequence that overlie the TC and the BMUC rocks, and is intruded by orogenic granitoids **(Fig. 5).** The VNGB is divided into a basal metavolcanic domain and an upper metasedimentary domain (Borghetti et al. 2018; Hoffmann et al. 2018). The basal domain is composed of amphibolite and amphibole schist with associated metadacites, metabasalts and metandesites and locally mica schist, marble and graphite schist lenses. The upper domain consists mainly of quartzites, metaconglomerates and banded iron formation, subordinated by felsic to mafic metavolcanic rocks and chemical exhalative rocks. The rocks of the VNGB was metamorphosed in conditions of the Upper Greenschist to Middle Amphibolite facies and intermediate pressure (Borghetti et al. 2018; Hoffman et al. 2018).

### 4.2 The Geology of the Tumucumaque Complex (TC)

The TC occurs as NW-trending elongated domes, separated by the metavolcano-sedimentary rocks of the VNGB and intruded by elongated bodies of Rhyacian orogenic granites in the western portion of the study area. The contact between the infra- and supracrustal rocks is defined by E-W trending ductile Vila

Nova Shear Zone (VNSZ), which dip at high angles to south. The Serra do Navio and Cupixi shear zones present N45°-55°W trending and are connected with the VNSZ (**Fig. 5**).

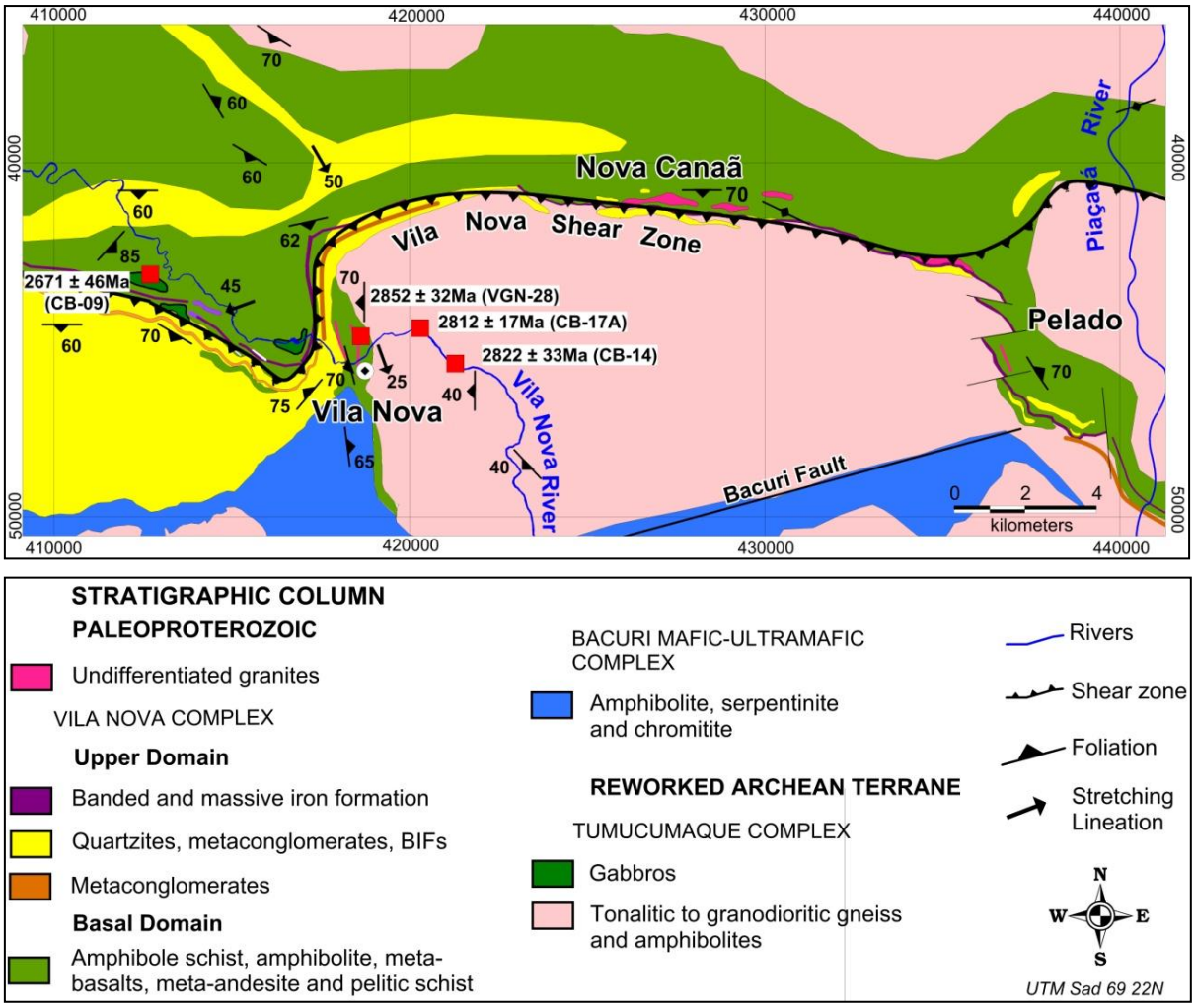


**Figure 5**. Geological map of the study area. Interpretation and structural data by the authors. The red points indicate the new crystallization U-Pb zircon ages presented in this work.

The complex consists of tonalitic to granodioritic gneisses, metagranodiorites and amphibolites, which are cut by undeformed gabbros plutons. The light grey orthogneisses are the dominant unit and shows a irregular and discontinuous fine banding ~~is~~ defined by quartz-feldspar felsic bands and biotite-rich mafic bands **(Figs. 6A and 6B)**. The main texture is equigranular granoblastic with polygonal to interlobate contacts. A medium to coarse-grained lepidoblastic and nematoblastic textures occurs subordinately.

Light grey metagranodiorites occur as elongated NW-SE trending bodies, according to the regional foliation. Their incipient foliation is defined by millimeter-thick discontinuous biotite-rich levels and locally hornblende. The main texture is blastoequigranular with euhedral to sub-euhedral prismatic plagioclase, amoeboid to elongated quartz, and aggregates of euhedral biotite. Metamorphic textures are restricted and have irregular distribution within the rock fabric. These include the granoblastic equigranular texture with polygonal to interlobate contacts, characterized by partial recrystallization of quartz and feldspar.

Amphibolite bodies present elongated shapes along the regional banding with thicknesses from 50 to 150 meters. The amphibolite have black color and are foliated according to the orientation of hornblende aggregates (**Fig. 6C, D**). The texture is nematoblastic, with medium-grained (0.2 to 1.0 mm), defined by elongated hornblende, with interstitial spaces occupied by plagioclase aggregates in a polygonal to interlobate granoblastic arrangement.

EW to NW-SE-trending elongated gabbro bodies have 1 to 2 km long and 0.2 to 0.5 km wide, and are parallel to the regional foliation ($S_2$). The gabbro is dark grey and locally records a igneous foliation defined by the orientation of prismatic plagioclase at the border of the body **(Fig. 6E, F)**. The texture is coarse-grained equigranular, defined by Ca-plagioclase and interstitial spaces occupied by clinopyroxene (Augite) aggregates with rare magnetite.

Structural data obtained for the rocks of TC and VNGB aid the recognition of three main ductile deformation events (Borghetti et al., 2018; Hoffmann et al. 2018). The first two events caused regional foliations $S_1$ and $S_2$, and pronounced stretching and mineral lineation according to the S-SW direction **(Fig. 7)**. A third deformation event is responsible for regional antiformal $F_3$ folds with axes parallel to the regional foliation.

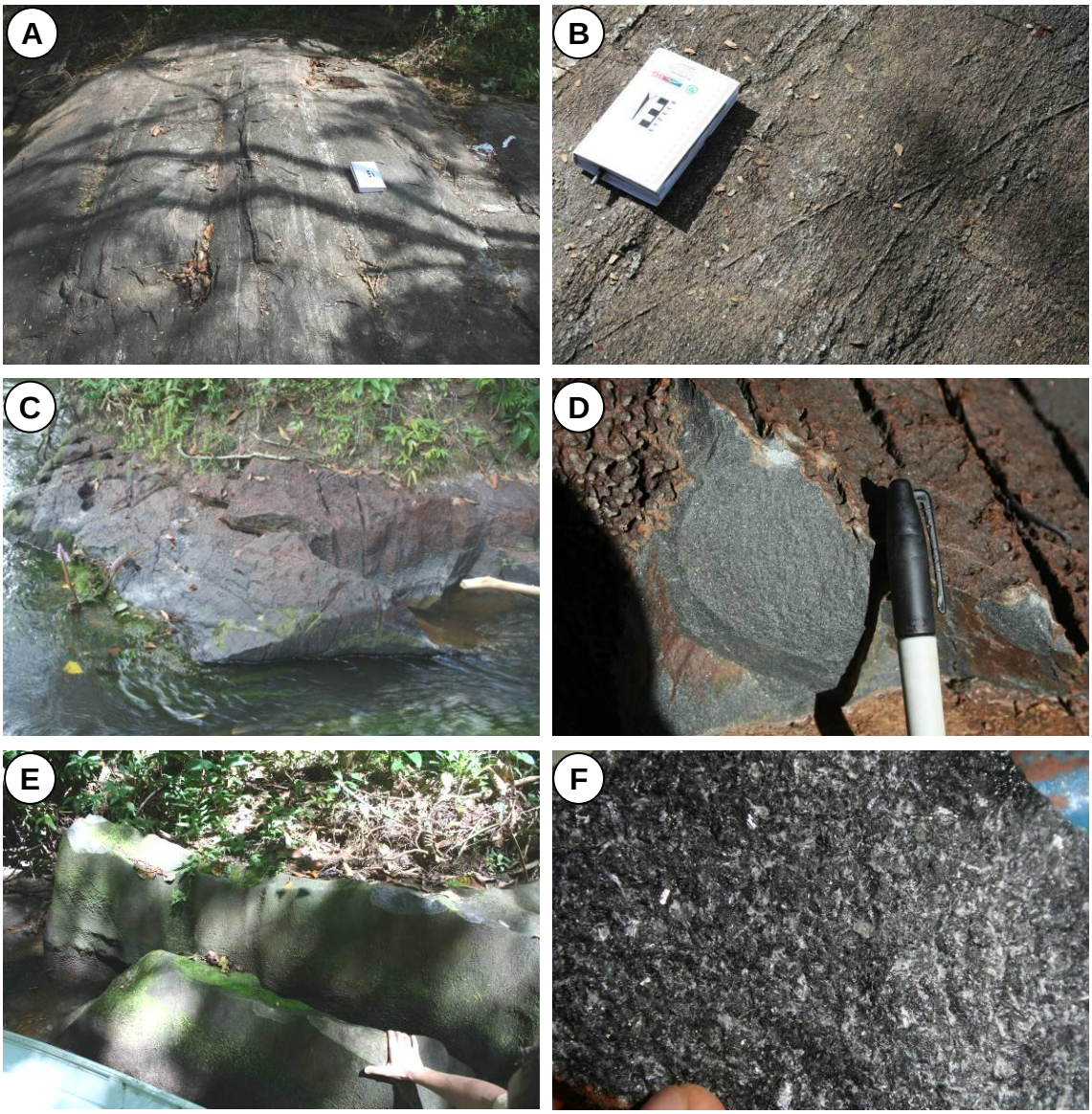


**Figure 6.** Macroscopic and structural aspects of the Tumucumaque Complex rocks. **A)** Tonalitic gneiss (Outcrop CB-28) with irregular and discontinuous 1 to 5 cm-thick banding; **B)** Granodioritic gneiss (Outcrop CB-14) highlighting a pronounced mylonitic foliation defined by feldspar and quartz stretching; **C)** Amphibolite cropping out in the Vila Nova River; **D)** Detail of the amphibolite (Outcrop CB-12) showing the fine nematoblastic texture with incipient foliation formed by the orientation of hornblende and biotite. **E)** Gabbro (CB-09) outcrop along of the Igarapé 21 creek; **F)** Gabbro sample, showing the massive structure and the coarse equigranular texture with euhedral prismatic plagioclase (white) and interstitial clinopyroxene aggregates.

The banding of the orthogneisses has a NW-SE regional orientation and is defined by a $S_2$ crenulation cleavage. Deformed $S_1$ foliation is preserved as isoclinal folds ($F_2$). Such structures are affected by open to closed $F_3$ fold, with axial surface and axes plugging N40-60$^o$W. SC planes observed in fuchsite quartzite and deformed metaconglomerate of the Vila Nova region, indicate that the Vila Nova Shear Zone represents a north-verging thrust zone and is responsible by the tectonic

intercalation of supra- and infracrustal rocks (Borghetti et al. 2018). The main phase of regional folding ($F_3$) is characterized by shortening in the EW to NE-SW direction, which probably resulted in the generation of the NW-SE-trending Serra do Navio and Cupixi shear zones.

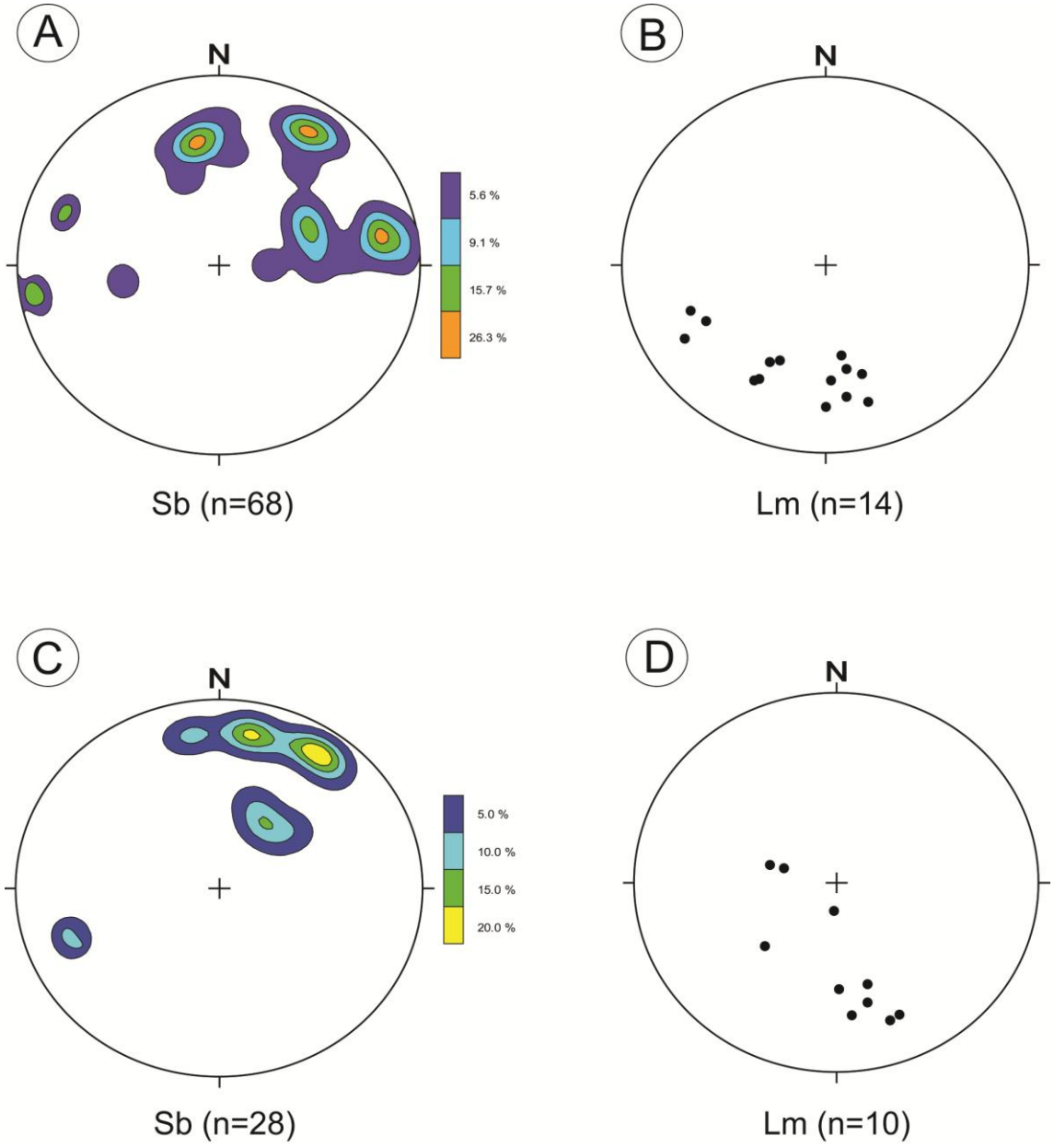


**Figure 7.** Lower hemisphere stereoplots representing the main structures of the tonalitic to granodioritic gneisses and metagranites of Tumucumaque Complex, equal area. **A)** Pole density diagram of the gneiss banding, **B)** Mineral lineation, **C)** Mylonitic foliation of the Vila Nova Shear Zone, **D)** Pole density diagram of the mylonitic foliation of the VNSZ.

### 4.3 U-Pb zircon geochronology

The samples locations are shown in Figures 3 and 5. We performed analyses of magmatic zircons according to their internal structure, which was revealed through cathodoluminescence (CL) images **(Fig.8)**. Generally, the isotopic data showed some scatter in the concordia diagrams **(e.g. Fig. 9)** because of the heterogeneous lead loss that affected the isotopic systems. Sample results are in the Table 2 and 3.

#### 4.3.1 Tonalitic gneiss (CB-28)

This sample was collected near the Amapari river, south of the city of Serra do Navio at UTM zone 22N, coordinates 390986E and 89533N **(Fig. 5).** The tonalitic gneiss present an irregular and discontinuous fine banding (grey), defined by felsic bands of quartz-feldspar composition and mafic bands rich in biotite and hornblende. The main texture in thin section is equigranular granoblastic, with polygonal to interlobate limits, and subordinate lepidoblastic and nematoblastic texture. Plagioclase, quartz, biotite and hornblende were the main mineral constituents, whereas zircon, apatite and opaque minerals were the accessory phases.

A total of 26 zircons were selected for LA-MC-ICPMS analysis, but 09 of them yielded unacceptable total common Pb values (not shown) and were discarded. The zircon crystals are prismatic and elongate, euhedral with pyramidal terminations and show well-defined oscillatory zoning. The grain size vary from 100 to 250 μm and the length: width ratios from 2:1 to 6:1. In CL images, most of the crystals reveal internal igneous textures and well-defined oscillatory zoning. Some grains show homogeneous to slightly oscillating zoning (grains 9.1 and 10.1, **Fig. 8A**), or partially preserved zoning (grains 13.1 and 21.1, **Fig. 8A).** Larger crystals show corroded edges, whereas small grains are prismatic, elongate and often fractured. Some grains are slightly fractured and may present overgrowth rims.

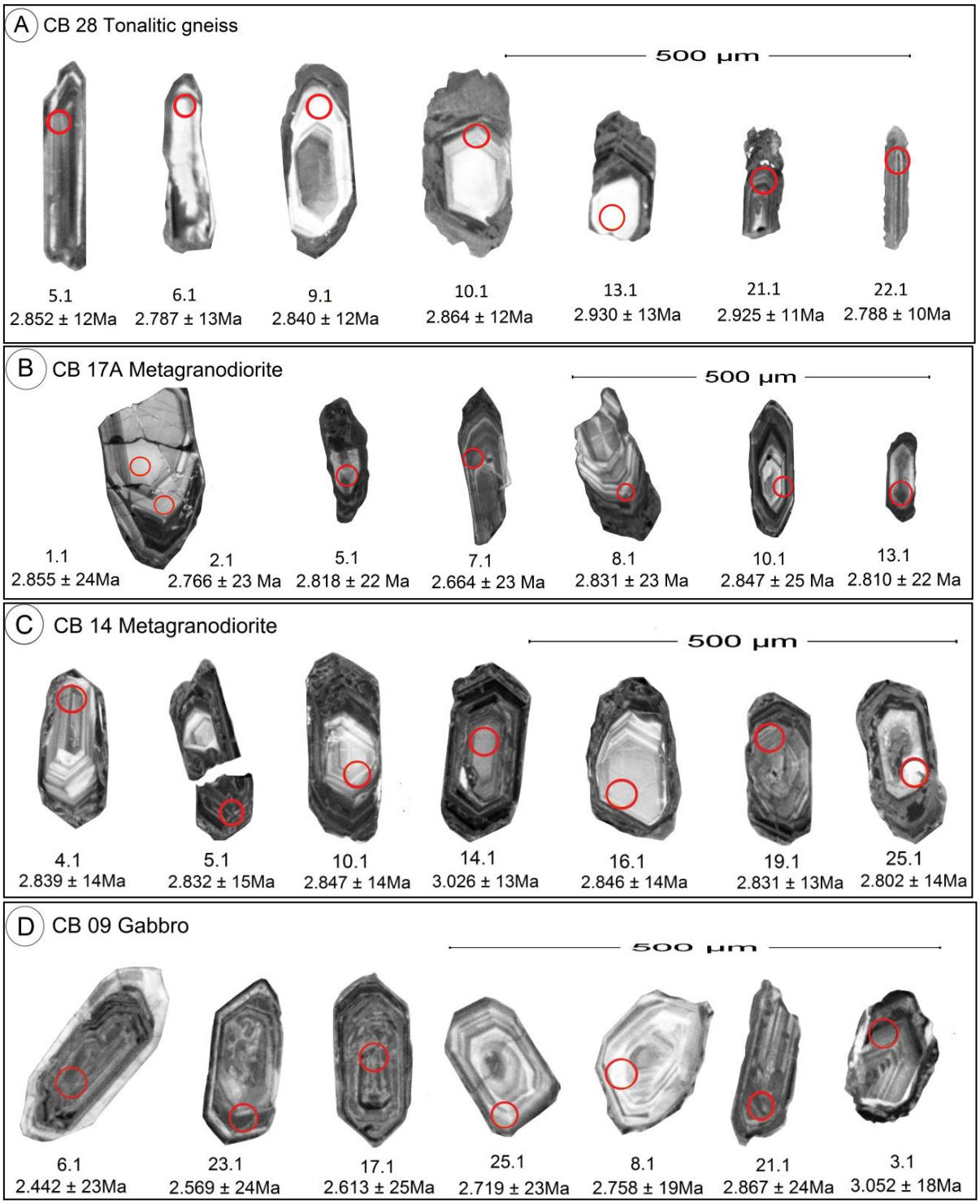


**Figure 8.** Cathodoluminescence (CL) images of analyzed zircon grains showing the location of the laser spot and the calculated $^{207}Pb/^{206}Pb$ ages. **A)** Tonalitic gneiss (CB-28), **B)** Metagranodiorite (CB-17A), **C)** Metagranodiorite (CB-14), **D)** Gabbro (CB-09).

Th/U ratios of seven concordant zircon analyses range between 0.389 and 0.979, consistent with a magmatic origin (Belousova et al. 2002). Corresponding $^{207}Pb/^{206}Pb$ ages range between 2.930 Ma and 2.794 Ma, yielding a mean age of

2.851 ±37 Ma (MSWD= 4.5) and represents the crystallization age of the tonalitic gneiss. **(Fig. 9A, Table 2)**. Younger zircon ages falling in the 2.564 to 2.385 Ma interval yielded a concordia age of 2.446 ±51 Ma (MSWD= 2.0). This age is interpreted as related to a rejuvenating younger event, probably metamorphic.

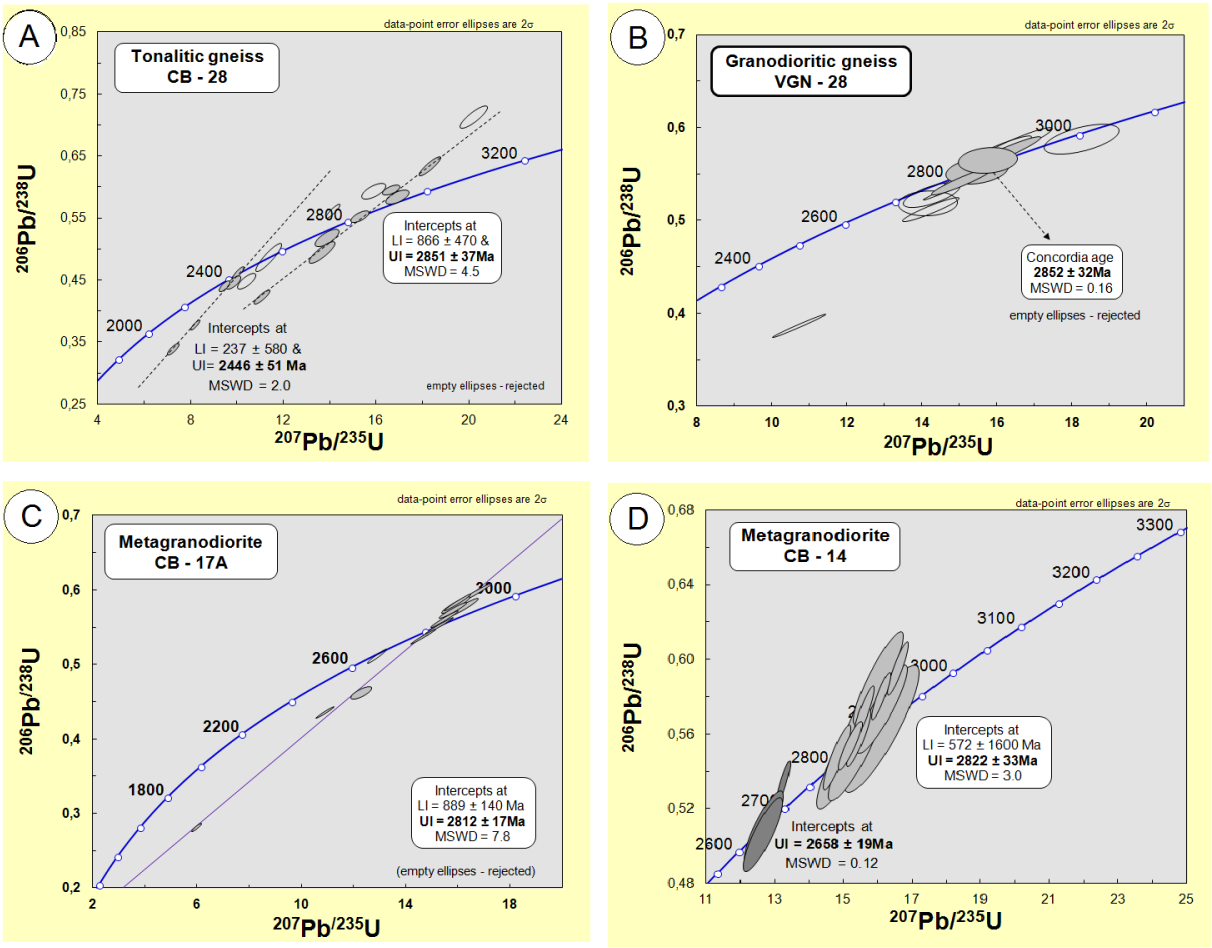


**Figure 9.** U-Pb zircon concordia diagram with the age determination for the samples of Tumucumaque Complex. **A)** Tonalitic gneiss CB-28, **B)** Granodioritic gneiss VGN-28, **C)** Metagranodiorite CB-17A, **D)** Metagranodiorite CB-14.

### 4.3.2 Granodioritic gneiss (VGN-28)

Granodioritic gneiss sample was selected in a drilling hole located near the city of Vila Nova, at UTM zone 22N, coordinates 418606E and 44999N **(Fig. 5)**. The gneiss shows discontinuous mafic and felsic bands of biotite and plagioclase, microcline and quartz, respectively. Apatite, zircon and opaques minerals are the accessory phases, and chlorite and muscovite are secondary phases. The main

texture is equigranular granoblastic and polygonal, with subordinate lepidoblastic texture.

| Spot | Isotopic ratios | | | | | | | | Pb[c] | Th | U | Th/U | Calculated Ages (Ma) | | | | | |
|---|---|---|---|---|---|---|---|---|---|---|---|---|---|---|---|---|---|---|
| | $^{207}Pb/^{235}U$ | ±(1σ) | $^{206}Pb/^{238}Pb$ | ±(1σ) | CC | $^{207}Pb/^{206}Pb$ | ±(1σ) | Pb[b] | Estimated values (ppm) | | | | $T_{206/238}$ | ±(1σ) | $T_{207/235}$ | ±(1σ) | $T_{207/206}$ | ± (1σ) |
| **Tonalitic gneiss CB-28** | | | | | | | | | | | | | | | | | | |
| 1.1 | 8.232 | 0.13 | 0.3982 | 0.004 | 0.72 | 0.1539 | 0.0015 | 9.61 | 159,9 | 46,4 | 398,3 | 0.117 | 2.161 | 0.022 | 2.257 | 0.015 | 2.385 | 0.01 |
| 2.1 | 11.362 | 0.22 | 0.4865 | 0.009 | 0.90 | 0.1708 | 0.0013 | 0.78 | 165,0 | 82,0 | 311,6 | 0.263 | 2.556 | 0.040 | 2.553 | 0.019 | 2.564 | 0.01 |
| 3.1 | 12.924 | 0.19 | 0.5363 | 0.006 | 0.78 | 0.1771 | 0.0014 | 23.5 | 115,7 | 81,2 | 191,2 | 0.425 | 2.768 | 0.027 | 2.674 | 0.014 | 2.627 | 0.01 |
| 4.1 | 16.633 | 0.28 | 0.5778 | 0.008 | 0.86 | 0.2016 | 0.0017 | 33.0 | 123,6 | 340,0 | 153,7 | 2.211 | 2.940 | 0.035 | 2.914 | 0.016 | 2.845 | 0.01 |
| 5.1 | 13.661 | 0.22 | 0.4944 | 0.007 | 0.86 | 0.2024 | 0.0014 | 6.00 | 185,3 | 181,1 | 278,9 | 0.649 | 2.590 | 0.031 | 2.727 | 0.016 | 2.852 | 0.01 |
| 6.1 | 13.886 | 0.21 | 0.5178 | 0.005 | 0.72 | 0.1947 | 0.0015 | 0.63 | 94,1 | 60,3 | 155,1 | 0.389 | 2.690 | 0.024 | 2.742 | 0.014 | 2.787 | 0.01 |
| 8.1 | 10.419 | 0.15 | 0.4481 | 0.005 | 0.75 | 0.1696 | 0.0013 | 2.38 | 142,8 | 73,6 | 278,8 | 0.264 | 2.387 | 0.022 | 2.473 | 0.014 | 2.552 | 0.01 |
| 9.1 | 15.289 | 0.16 | 0.5528 | 0.004 | 0.69 | 0.2010 | 0.0014 | 3.35 | 59,5 | 47,5 | 88,0 | 0.540 | 2.837 | 0.017 | 2.833 | 0.010 | 2.840 | 0.01 |
| 10.1 | 16.651 | 0.15 | 0.5956 | 0.003 | 0.62 | 0.2039 | 0.0014 | 4.32 | 88,7 | 81,5 | 117,8 | 0.692 | 3.012 | 0.014 | 2.915 | 0.009 | 2.864 | 0.01 |
| 12.1 | 9.855 | 0.12 | 0.4463 | 0.004 | 0.72 | 0.1635 | 0.0013 | 2.15 | 264,6 | 283,2 | 516,1 | 0.549 | 2.379 | 0.019 | 2.421 | 0.012 | 2.489 | 0.01 |
| 13.1 | 16.929 | 0.20 | 0.5845 | 0.004 | 0.64 | 0.2123 | 0.0018 | <0.0 | 29,7 | 23,8 | 41,2 | 0.577 | 2.967 | 0.019 | 2.931 | 0.012 | 2.930 | 0.01 |
| 14.1 | 14.151 | 0.12 | 0.5603 | 0.004 | 0.90 | 0.1816 | 0.0010 | 0.78 | 314,4 | 315,9 | 445,0 | 0.710 | 2.868 | 0.019 | 2.760 | 0.008 | 2.670 | 0.01 |
| 17.1 | 15.893 | 0.21 | 0.5932 | 0.005 | 0.66 | 0.1955 | 0.0014 | 4.11 | 283,6 | 137,8 | 387,7 | 0.355 | 3.003 | 0.022 | 2.870 | 0.013 | 2.794 | 0.01 |
| 18.1 | 10.420 | 0.20 | 0.4779 | 0.005 | 0.62 | 0.1699 | 0.0014 | 48.3 | 188,9 | 314,7 | 359,1 | 0.877 | 2.518 | 0.025 | 2.473 | 0.018 | 2.555 | 0.01 |
| 19.1 | 9.443 | 0.09 | 0.4409 | 0.003 | 0.74 | 0.1565 | 0.0012 | 5.41 | 236,5 | 120,0 | 495,2 | 0.242 | 2.355 | 0.015 | 2.382 | 0.010 | 2.414 | 0.01 |
| 21.1 | 18.334 | 0.19 | 0.6338 | 0.006 | 0.90 | 0.2117 | 0.0014 | 1.02 | 265,9 | 252,1 | 304,7 | 0.828 | 3.165 | 0.025 | 3.007 | 0.010 | 2.925 | 0.01 |
| **Granodioritic gneiss VGN-28** | | | | | | | | | | | | | | | | | | |
| 4.1 | 15.491 | 0.37 | 0.5534 | 0.006 | 0.96 | 0.2030 | 0.0046 | 0.08 | 87 | 81 | 94 | 0.86 | 2.839 | 0.027 | 2.846 | 0.022 | 2.851 | 0.03 |
| 5.1 | 15.448 | 0.34 | 0.5531 | 0.005 | 0.29 | 0.2026 | 0.0044 | 0.06 | 108 | 134 | 110 | 1.22 | 2.838 | 0.024 | 2.843 | 0.021 | 2.847 | 0.03 |
| 8.1 | 16.119 | 0.41 | 0.5721 | 0.007 | 0.95 | 0.2044 | 0.0051 | 0.17 | 53 | 48 | 56 | 0.87 | 2.916 | 0.031 | 2.884 | 0.024 | 2.861 | 0.04 |
| 12.1 | 15.737 | 0.32 | 0.5647 | 0.005 | 0.15 | 0.2021 | 0.0042 | 0.28 | 132 | 121 | 137 | 0.88 | 2.886 | 0.023 | 2.861 | 0.020 | 2.844 | 0.03 |
| 13.1 | 15.061 | 0.33 | 0.5420 | 0.006 | 0.94 | 0.2015 | 0.0044 | 0.56 | 78 | 103 | 88 | 1.17 | 2.792 | 0.025 | 2.819 | 0.021 | 2.839 | 0.03 |
| **Metagranodiorite CB-17A** | | | | | | | | | | | | | | | | | | |
| 1.1 | 16.177 | 0.23 | 0.5765 | 0.005 | 0.95 | 0.2035 | 0.003 | 1.03 | 128,3 | 119,6 | 179,8 | 0.665 | 2.935 | 0.02 | | | 2.855 | 0.02 |
| 2.1 | 12.276 | 0.16 | 0.4619 | 0.003 | 0.76 | 0.1928 | 0.0027 | 4.84 | 425,7 | 315 | 785 | 0.401 | 2.448 | 0.016 | | | 2.766 | 0.02 |
| 3.1 | 5.982 | 0.08 | 0.2815 | 0.002 | 0.94 | 0.1541 | 0.0018 | 2.06 | 558,6 | 316,5 | 1338,8 | 0.236 | 1.599 | 0.011 | | | 2.392 | 0.02 |
| 5.1 | 15.914 | 0.22 | 0.5798 | 0.004 | 0.93 | 0.1991 | 0.0027 | 1.85 | 293,8 | 181,8 | 420,7 | 0.432 | 2.948 | 0.019 | | | 2.818 | 0.02 |
| 6.1 | 15.467 | 0.21 | 0.5612 | 0.004 | 0.98 | 0.1999 | 0.0028 | 1.63 | 246,5 | 147,7 | 363,9 | 0.406 | 2.872 | 0.019 | | | 2.825 | 0.02 |
| 7.1 | 10.89 | 0.15 | 0.4359 | 0.003 | 0.98 | 0.1812 | 0.0025 | 2.25 | 299,8 | 229,7 | 511,2 | 0.449 | 2.332 | 0.015 | | | 2.664 | 0.02 |
| 8.1 | 15.27 | 0.22 | 0.552 | 0.004 | 0.99 | 0.2006 | 0.0029 | 0.58 | 236,5 | 304,1 | 322,6 | 0.943 | 2.833 | 0.019 | | | 2.831 | 0.02 |
| 10.1 | 16.667 | 0.25 | 0.5967 | 0.005 | 0.98 | 0.2026 | 0.0031 | 0.39 | 205,5 | 280,4 | 265,2 | 1.057 | 3.017 | 0.022 | | | 2.847 | 0.02 |
| 11.1 | 15.780 | 0.21 | 0.573 | 0.004 | 0.96 | 0.1997 | 0.0026 | 0.25 | 573,4 | 470,1 | 802,2 | 0.586 | 2.92 | 0.018 | | | 2.824 | 0.02 |
| 13.1 | 14.666 | 0.19 | 0.5372 | 0.004 | 0.99 | 0.198 | 0.0026 | 0.41 | 268,4 | 147,2 | 419,3 | 0.351 | 2.772 | 0.017 | | | 2.81 | 0.02 |

**Table 2.** Summary of LA-ICPMS U-Pb zircon isotopic data for CB-28 - Tonalitic Gneiss, VGN-28 - Granodioritic Gneiss and CB-17A - Metagranodiorite. C.C = Correlation coefficient, $Pb^b$ = Common Pb (%), $Pb^C$ = Radiometric values (ppm).

We selected 13 zircon grains from VGN-28 sample for LA-MC-ICPMS analysis, but 8 showed highly discordance. The crystals are prismatic with elongate shapes and pyramidal terminations, with size between 250 to 80 μm. The five concordant analyzed zircon grains present Th/U ratios that range between 0.855 and 1.215, consistent with a magmatic origin (Belousova et al. 2002). The selected zircon grains yielded a $^{207}Pb/^{206}Pb$ ages between 2.861 Ma and 2.844 Ma. The Concordia

mean age of 2.852 ±32 Ma (MSWD= 0.16) represents the crystallization time of the granodioritic gneiss (**Fig. 9B, Table 2**).

### 4.3.3 Metagranodiorite (CB-17A)

The metagranodiorite sample was collected in a outcrop located at the Vila Nova river, in the ~~at~~ UTM zone 22N, coordinates 420302E and 45329N **(Fig. 5)**. The metagranodiorite showing incipient foliation defined by discontinuous, millimeter-thick levels rich in biotite and sometimes hornblende intercalated with dominant quartz and feldspar levels. The granite have a medium-grained equigranular texture with prismatic plagioclase and K-feldspar, amoeboid to elongate quartz and biotite aggregates. Allanite, zircon, apatite and opaque minerals are the accessory minerals.

We selected 12 zircon crystals for U-Pb analyses, however, 2 grains presented high total common Pb values and were discarded. The zircons have prismatic shape with pyramidal terminations, sub-euhedral. The grain size vary from 70 to 280 μm. CL images reveal internal igneous textures with oscillatory zoning and fractured grains (1.1, 4.1), and subordinate homogeneous to slightly oscillatory zoning (5.1, 13.1, **Fig. 8B**).

The concordant analyzed zircon grains present Th/U ratios range between 0.236 and 1.057, which is consistent with a magmatic origin (Belousova et al. 2002). $^{207}Pb/^{206}Pb$ ages range between 2.855 and 2.766 Ma Ma, with a mean igneous crystallization age of 2.812 ±17 Ma (MSWD= 7.8) **(Fig. 9C, Table 2)**.

### 4.3.4 Metagranodiorite (CB-14)

This sample was collected in a outcrop located in the Vila Nova river, at UTM zone 22N, coordinates 421291E and 44328N **(Fig. 5)**. The metagranodiorite exhibit an irregular fabric and a medium equigranular interlobate granoblastic texture, characterized by partial recrystallization of quartz and locally K-feldspar. The oriented

recrystallized biotite define a medium lepidoblastic texture characterized by fine aggregates of biotite, titanite and magnetite. Zircon, apatite and opaque minerals are the accessory minerals.

A total of 26 zircons crystals were selected for isotopic analyses. Eight zircon crystals yielded high total common Pb values (not shown) and were discarded. The euhedral zircon present a short prismatic shape with pyramidal terminations. The grain size vary from 285 to 70 μm. The CL images reveal well-defined oscillatory zoning. The grains are slightly fractured and may present overgrowth rims (**Fig. 8C**).

The selected zircon grains have Th/U ratios range between 0.104 and 0.773 for the main concordant analyses, which is consistent with a magmatic origin (Belousova et al. 2002). The concordant $^{207}Pb/^{206}Pb$ ages range between 3.026 and 2.831 Ma, yielding a mean concordia age of 2.822 ±33 Ma (MSWD= 3.0) interpreted as crystallization time **(Fig. 9D, Table 3)**. Five concordant $^{207}Pb/^{206}Pb$ ages range between 2.799 Ma and 2.640 Ma, from which three define a mean age of 2.658 ±19 Ma (MSWD= 0.12). This age is interpreted as a disturbance of the original U-Pb system, probably by the contact metamorphism associated to emplacement of intrusive gabbro bodies.

### 4.3.5 Gabbro (CB-09)

The selected gabbro present a massive structure and a medium- to coarse-grained equigranular (4-8 mm) texture. The sample was collected in a outcrop located at NW of the Vila Nova city, at UTM zone 22N, coordinates 412708E and 46842N **(Fig. 5)**. The sample have black color and a magmatic foliation defined by the orientation of prismatic plagioclase and by clinopyroxene and magnetite aggregates.

| Spot | Isotopic ratios | | | | | | | | Pb[c] | Th | U | Th/U | Calculated Ages (Ma) | | | | | |
|---|---|---|---|---|---|---|---|---|---|---|---|---|---|---|---|---|---|---|
| | $^{207}Pb/^{235}U$ | ±(1σ) | $^{206}Pb/^{238}Pb$ | ±(1σ) | CC | $^{207}Pb/^{206}Pb$ | ±(1σ) | Pb[b] | Estimated values (ppm) | | | | $T_{206/238}$ | ±(1σ) | $T_{207/235}$ | ±(1σ) | $T_{207/206}$ | ± (1σ) |
| **Metagranodiorite CB-14** | | | | | | | | | | | | | | | | | | |
| 1.1 | 16.101 | 0.45 | 0.5628 | 0.013 | 0.87 | 0.2074 | 0.0019 | 0.30 | 171,8 | 120,8 | 274,1 | 0.441 | 2.878 | 0.057 | 2.883 | 0.027 | 2.892 | 0.01 |
| 2.1 | 16.128 | 0.30 | 0.5734 | 0.009 | 0.90 | 0.2039 | 0.0020 | 0.25 | 35,7 | 26,9 | 50,6 | 0.532 | 2.922 | 0.040 | 2.884 | 0.018 | 2.864 | 0.01 |
| 4.1 | 15.163 | 0.39 | 0.5515 | 0.012 | 0.90 | 0.2008 | 0.0017 | <0.0 | 37,8 | 41,2 | 53,3 | 0.773 | 2.831 | 0.053 | 2.826 | 0.025 | 2.839 | 0.01 |
| 5.1 | 15.315 | 0.31 | 0.5486 | 0.009 | 0.88 | 0.2000 | 0.0018 | 0.60 | 100,2 | 82,1 | 140,3 | 0.585 | 2.819 | 0.041 | 2.835 | 0.019 | 2.832 | 0.01 |
| 6.1 | 14.233 | 0.27 | 0.5272 | 0.009 | 0.88 | 0.1961 | 0.0016 | 0.24 | 167,4 | 95,8 | 291,8 | 0.328 | 2.730 | 0.038 | 2.765 | 0.018 | 2.799 | 0.01 |
| 7.1 | 12.671 | 0.23 | 0.5102 | 0.008 | 0.85 | 0.1803 | 0.0016 | 0.18 | 235,5 | 62,7 | 419,0 | 0.150 | 2.657 | 0.034 | 2.656 | 0.017 | 2.657 | 0.01 |
| 9.1 | 14.119 | 0.29 | 0.5383 | 0.010 | 0.90 | 0.1937 | 0.0018 | 0.18 | 275,7 | 25,4 | 469,8 | 0.054 | 2.776 | 0.044 | 2.758 | 0.020 | 2.778 | 0.01 |
| 10.1 | 15.653 | 0.30 | 0.5727 | 0.010 | 0.90 | 0.2019 | 0.0017 | <0.0 | 27,5 | 18,9 | 38,4 | 0.492 | 2.919 | 0.041 | 2.856 | 0.018 | 2.847 | 0.01 |
| 11.1 | 15.998 | 0.29 | 0.5899 | 0.010 | 0.90 | 0.2093 | 0.0019 | <0.0 | 104,9 | 16,2 | 155,4 | 0.104 | 2.989 | 0.041 | 2.877 | 0.018 | 2.907 | 0.01 |
| 14.1 | 20.379 | 0.31 | 0.6503 | 0.009 | 0.89 | 0.2256 | 0.0019 | 0.95 | 58,5 | 24,6 | 72,6 | 0.339 | 3.230 | 0.035 | 3.110 | 0.015 | 3.026 | 0.01 |
| 15.1 | 12.642 | 0.23 | 0.5062 | 0.008 | 0.86 | 0.1806 | 0.0017 | 0.26 | 229,1 | 30,6 | 420,9 | 0.073 | 2.640 | 0.035 | 2.653 | 0.017 | 2.660 | 0.01 |
| 16.1 | 15.189 | 0.14 | 0.5541 | 0.005 | 0.90 | 0.2018 | 0.0017 | 1.19 | 56,5 | 53,4 | 83,2 | 0.642 | 2.842 | 0.022 | 2.827 | 0.009 | 2.846 | 0.01 |
| 19.1 | 16.094 | 0.11 | 0.5805 | 0.005 | 0.90 | 0.2000 | 0.0015 | <0.0 | 183,5 | 137,3 | 254,3 | 0.540 | 2.951 | 0.021 | 2.882 | 0.007 | 2.831 | 0.01 |
| 20.1 | 16.581 | 0.12 | 0.5952 | 0.005 | 0.90 | 0.2028 | 0.0016 | <0.0 | 116,3 | 94,4 | 156,2 | 0.604 | 3.010 | 0.023 | 2.911 | 0.007 | 2.855 | 0.01 |
| 22.1 | 13.239 | 0.08 | 0.5337 | 0.004 | 0.90 | 0.1785 | 0.0014 | <0.0 | 101,9 | 134,6 | 144,9 | 0.929 | 2.757 | 0.021 | 2.697 | 0.006 | 2.640 | 0.01 |
| 23.1 | 15.576 | 0.12 | 0.5719 | 0.005 | 0.90 | 0.2020 | 0.0017 | 0.16 | 103,2 | 80,9 | 149,4 | 0.542 | 2.916 | 0.023 | 2.851 | 0.007 | 2.848 | 0.01 |
| 25.1 | 14.809 | 0.16 | 0.5476 | 0.007 | 0.90 | 0.1964 | 0.0017 | 0.74 | 209,9 | 98,2 | 340,7 | 0.288 | 2.815 | 0.029 | 2.803 | 0.011 | 2.802 | 0.01 |
| 26.1 | 15.446 | 0.14 | 0.5579 | 0.006 | 0.90 | 0.2024 | 0.0016 | 0.57 | 82,9 | 55,7 | 121,3 | 0.459 | 2.858 | 0.026 | 2.843 | 0.009 | 2.851 | 0.01 |
| **Gabro CB-09** | | | | | | | | | | | | | | | | | | |
| 8.1 | 14.504 | 0.17 | 0.5500 | 0.003 | 0.56 | 0.1914 | 0.0022 | <0.0 | 130,5 | 119,8 | 206,0 | 0.581 | 2.825 | 0.016 | 2.783 | 0.012 | 2.758 | 0.01 |
| 25.1 | 14.113 | 0.33 | 0.5448 | 0.008 | 0.62 | 0.1870 | 0.0025 | 0.35 | 153,8 | 129,2 | 217,0 | 0.595 | 2.803 | 0.033 | 2.757 | 0.022 | 2.719 | 0.02 |
| 26.1 | 12.530 | 0.29 | 0.5015 | 0.007 | 0.62 | 0.1805 | 0.0024 | <0.0 | 235,9 | 139,4 | 378,0 | 0.369 | 2.620 | 0.031 | 2.645 | 0.022 | 2.659 | 0.02 |
| 17.1 | 12.027 | 0.31 | 0.4968 | 0.008 | 0.68 | 0.1757 | 0.0026 | 0.56 | 319,3 | 45,3 | 459,4 | 0.099 | 2.600 | 0.037 | 2.607 | 0.024 | 2.613 | 0.02 |
| 23.1 | 10.137 | 0.25 | 0.4311 | 0.007 | 0.68 | 0.1712 | 0.0024 | 3.89 | 294,9 | 387,7 | 553,2 | 0.701 | 2.311 | 0.033 | 2.447 | 0.023 | 2.569 | 0.02 |
| 9.1 | 9.265 | 0.14 | 0.4259 | 0.004 | 0.65 | 0.1591 | 0.0019 | 0.37 | 169,9 | 216,5 | 353,9 | 0.612 | 2.287 | 0.019 | 2.365 | 0.014 | 2.443 | 0.02 |
| 6.1 | 8.230 | 0.16 | 0.3827 | 0.005 | 0.71 | 0.1590 | 0.0021 | 0.96 | 229,3 | 375,3 | 551,4 | 0.681 | 2.089 | 0.025 | 2.257 | 0.018 | 2.442 | 0.02 |
| 11.1 | 7.068 | 0.15 | 0.3367 | 0.006 | 0.86 | 0.1535 | 0.0019 | 2.51 | 184,1 | 200,8 | 479,3 | 0.419 | 1.871 | 0.031 | 2.120 | 0.020 | 2.381 | 0.02 |
| 1.1 | 7.373 | 0.10 | 0.3602 | 0.002 | 0.54 | 0.1502 | 0.0018 | 0.19 | 145,4 | 414,7 | 358,4 | 1.157 | 1.983 | 0.013 | 2.158 | 0.012 | 2.344 | 0.02 |
| 20.1 | 5.165 | 0.13 | 0.2924 | 0.004 | 0.64 | 0.1278 | 0.0018 | 4.85 | 312,0 | 376,9 | 901,3 | 0.418 | 1.653 | 0.023 | 1.847 | 0.021 | 2.066 | 0.02 |
| **Inherited crystals** | | | | | | | | | | | | | | | | | | |
| 7.1 | 31.779 | 0.38 | 0.7316 | 0.003 | 0.40 | 0.3128 | 0.0036 | 0.06 | 104,9 | 63,2 | 113,8 | 0.555 | 3.539 | 0.013 | 3.543 | 0.012 | 3.538 | 0.01 |
| 18.1 | 26.793 | 0.63 | 0.6946 | 0.010 | 0.64 | 0.2791 | 0.0038 | 0.15 | 217,8 | 250,1 | 227,2 | 1.101 | 3.400 | 0.040 | 3.376 | 0.023 | 3.353 | 0.02 |
| 19.1 | 24.937 | 0.64 | 0.6755 | 0.012 | 0.69 | 0.2725 | 0.0037 | <0.0 | 187,2 | 139,3 | 197,8 | 0.704 | 3.327 | 0.046 | 3.306 | 0.025 | 3.316 | 0.02 |
| 14.1 | 23.041 | 0.55 | 0.6396 | 0.009 | 0.62 | 0.2627 | 0.0035 | 0.16 | 212,0 | 81,3 | 254,1 | 0.320 | 3.187 | 0.038 | 3.229 | 0.023 | 3.260 | 0.02 |
| 15.1 | 20.740 | 0.50 | 0.6210 | 0.009 | 0.63 | 0.2402 | 0.0032 | 0.12 | 65,9 | 47,4 | 77,8 | 0.610 | 3.114 | 0.038 | 3.127 | 0.023 | 3.124 | 0.02 |
| 3.1 | 18.993 | 0.30 | 0.6022 | 0.007 | 0.71 | 0.2293 | 0.0027 | <0.0 | 249,3 | 72,8 | 374,3 | 0.195 | 3.039 | 0.028 | 3.041 | 0.016 | 3.052 | 0.01 |
| 24.1 | 18.793 | 0.46 | 0.6129 | 0.009 | 0.63 | 0.2237 | 0.0035 | <0.0 | 302,9 | 104,8 | 396,1 | 0.264 | 3.082 | 0.038 | 3.031 | 0.024 | 3.013 | 0.02 |
| 12.1 | 17.510 | 0.21 | 0.5893 | 0.003 | 0.46 | 0.2145 | 0.0025 | 0.15 | 205,9 | 77,0 | 316,5 | 0.243 | 2.986 | 0.013 | 2.963 | 0.012 | 2.946 | 0.01 |
| 4.1 | 16.368 | 0.19 | 0.5545 | 0.002 | 0.40 | 0.2140 | 0.0024 | <0.0 | 235,5 | 291,9 | 325,8 | 0.896 | 2.844 | 0.011 | 2.899 | 0.011 | 2.943 | 0.01 |
| 21.1 | 14.266 | 0.58 | 0.5574 | 0.012 | 0.55 | 0.2044 | 0.0031 | 0.71 | 228,4 | 673,1 | 371,3 | 1.813 | 2.856 | 0.052 | 2.768 | 0.038 | 2.867 | 0.02 |
| 16.1 | 16.513 | 0.40 | 0.5910 | 0.009 | 0.65 | 0.2011 | 0.0028 | 0.15 | 103,8 | 130,7 | 122,8 | 1.064 | 2.993 | 0.038 | 2.907 | 0.023 | 2.840 | 0.02 |
| 5.1 | 16.179 | 0.20 | 0.5823 | 0.004 | 0.54 | 0.1999 | 0.0023 | 0.06 | 139,3 | 84,4 | 217,2 | 0.389 | 2.958 | 0.017 | 2.887 | 0.012 | 2.831 | 0.01 |
| 13.1 | 14.724 | 0.19 | 0.5419 | 0.004 | 0.58 | 0.1962 | 0.0023 | 0.41 | 85,8 | 160,8 | 132,8 | 1.211 | 2.791 | 0.017 | 2.798 | 0.012 | 2.799 | 0.01 |

**Table 3.** Summary of LA-ICPMS U-Pb zircon isotopic data for CB-14 - Metagranodiorite and CB-09 - Gabbro. C.C = Correlation coefficient, $Pb^b$ = Common Pb (%), $Pb^C$ = Radiometric values (ppm).

We selected a total of 26 zircon crystals for analyses. The magmatic zircons are euhedral to sub-euhedral, prismatic in shape with pyramidal to straight terminations. The grain size range from 300 to 70 μm. The CL images reveal well-defined oscillatory zoning, with some grains showing overgrowth rims (grain 6.1, **Fig. 8D**). Three zircon crystals have high total common Pb values and were discarded.

The eleven igneous zircon crystals selected yielded an upper intercept of 2.671 ±46 Ma (MSWD= 1.3), interpreted as the gabbro crystallization age **(Fig. 10, Table 3)**. The selected zircon grains have Th/U ratios ranges between 0.369 and 1.81, which is consistent with a magmatic origin (Belousova et al. 2002).

The remaining 12 isotopic analyses zircon crystals yielded older ages, between 3.538 Ma and 2.799 Ma. These crystals were considered inherited zircon from surrounding units of basement. The inherited zircon usually have short prismatic inherited nuclei with pyramidal terminations and typically magmatic oscillatory zoning. These crystals usually exhibit broken and corroded edges (grains 3.1 and 21.1, **Fig. 8D**).

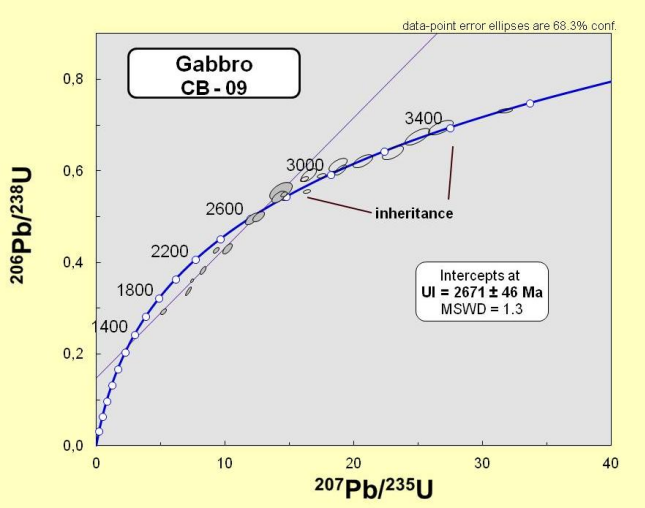


**Figure 10.** U-Pb concordia diagram and age determination for gabbro sample (CB-09).

### 4.4 Lu-Hf data

The metagranodiorite CB-17 shows variable negative initial $^{176}Hf/^{177}Hf$ values (0.280955 to 0.281588) which correspond to $\varepsilon Hf_{(2.81\ Ga)}$ values from mostly negative (from -0.01 to -12.93) to positive (+0.71) (only one value). The respective Hf $T_{DM}$ ages range from 3.63 to 3.08 Ga **(Table 4)**. The Hf $T_{DM}$ model ages show Meso- and Paleo-archean values, between 4.69 and 2.9 Ga with epsilon Hf positive, between +2.9 and +4.95. All data fall below CHUR and indicating two distinct signatures: (i)

the negative values (>-5) suggest an enriched mantle source and (ii) the strong negative values (<-5) suggest some sort of partial melts of Archean crustal rocks (i.e. reworked zircons). This is also consistent with the Hf $T_{DM}$ ages in the range 4.6 to 2.9 Ga **(Fig. 11)**.

| spot | $^{176}Hf/^{177}Hf$ | ± 2 se | $^{176}Lu/^{177}Hf$ | ± 2 se | U-Pb Age (T1) Ma | e Hf(0) | $^{176}Hf/^{177}Hf$ (T1) | e Hf (T1) | $^{176}Hf/^{177}Hf$ DM(T) | T DM (Ga) | $^{176}Hf/^{177}Hf$ DM(T) | e Hf (TDM) |
|---|---|---|---|---|---|---|---|---|---|---|---|---|
| 1.1 | 0.280940 | 0.000069 | 0.001180 | 0.0000164 | 2980 | -64.79 | 0.280872 | -0.01 | 0.281022 | 3321 | 0.280763 | 4.06 |
| 2.1 | 0.280877 | 0.000072 | 0.000903 | 0.0000057 | 2677 | -67.02 | 0.280831 | -8.53 | 0.281251 | 3631 | 0.280524 | 2.90 |
| 6.1 | 0.280961 | 0.000058 | 0.001467 | 0.0000165 | 2918 | -64.04 | 0.280879 | -1.22 | 0.281069 | 3351 | 0.280740 | 3.95 |
| 7.1 | 0.281145 | 0.000055 | 0.001250 | 0.0000138 | 2650 | -57.54 | 0.281081 | -0.24 | 0.281272 | 3084 | 0.280943 | 4.95 |
| 8.1 | 0.281024 | 0.000068 | 0.001729 | 0.0000238 | 2928 | -61.83 | 0.280926 | 0.71 | 0.281061 | 3235 | 0.280828 | 4.38 |
| 9.1 | 0.281090 | 0.000064 | 0.001522 | 0.0000230 | 2566 | -59.48 | 0.281015 | -4.53 | 0.281335 | 3293 | 0.280784 | 4.17 |
| 13.1 | 0.280911 | 0.000056 | 0.000905 | 0.0000272 | 2804 | -65.81 | 0.280862 | -4.45 | 0.281155 | 3470 | 0.280648 | 3.50 |
| 3.1 | 0.281024 | 0.000035 | 0.000651 | 0.0000052 | 2230 | -61.80 | 0.280997 | -12.93 | 0.281588 | 3566 | 0.280574 | 3.14 |
| 4.1 | 0.281036 | 0.000036 | 0.001336 | 0.0000057 | 2837 | -61.40 | 0.280963 | -0.11 | 0.281130 | 3218 | 0.280841 | 4.45 |
| 5.1 | 0.280835 | 0.000057 | 0.001294 | 0.0000172 | 2998 | -68.50 | 0.280760 | -3.57 | 0.281008 | 3561 | 0.280578 | 3.16 |
| 10.1 | 0.280991 | 0.000055 | 0.001235 | 0.0000105 | 3068 | -62.99 | 0.280918 | 3.67 | 0.280955 | 3152 | 0.280891 | 4.69 |

**Table 4.** Summary of LA-ICP-MS Lu-Hf zircon isotopic data for metagranodiorite sample (CB-17).

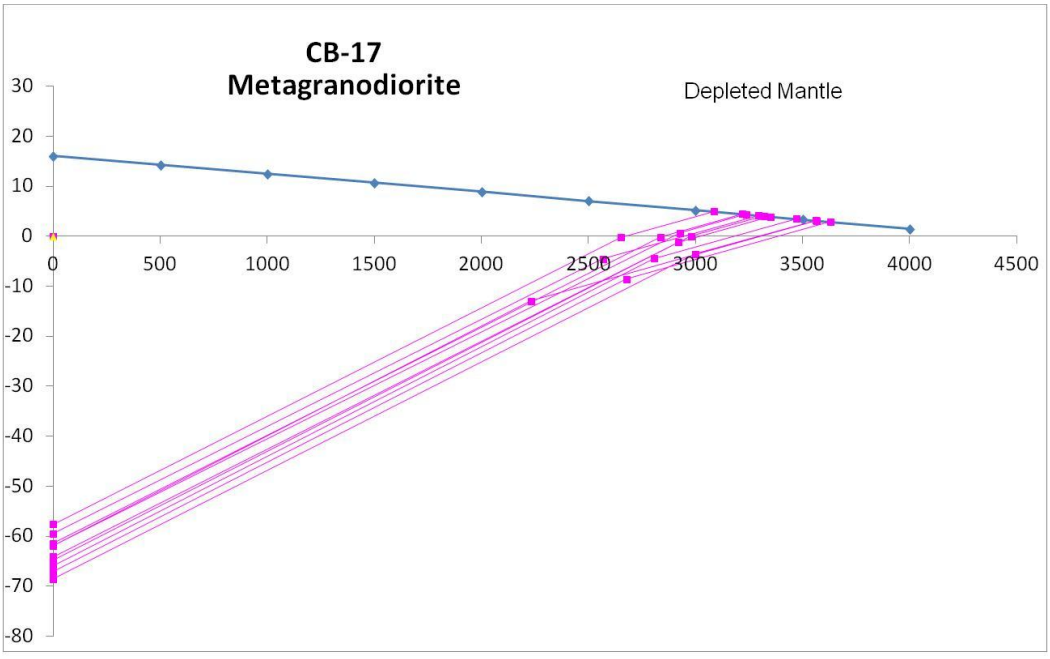


**Figure 11.** Lu-Hf data for Metagranodiorite sample (CB-17).

## 5. Discussion

### *5.1 Zircon ages and significance*

The central region of Amapá was considered by Tassinari and Macambira (1999, 2004), based on U-Pb zircon data, to be constituted by Archean protoliths

reworked during the Rhyacian orogenic events and which were preserved as inliers. In this same area, based on regional geologic mapping and isotopic data (Pb-Pb zircon, whole-rock Sm-Nd and Nd $T_{DM}$ data), Avelar et al. (2003) and Rosa-Costa et al. (2003, 2006) suggests that the Archean rocks of this segment of the Amazonian Craton constitute an extensive crustal segment. Based on this data the authors define the Amapá Block as an ancient domain situated in Amapá and northern Pará States. This block represents a large Archean continental landmass involved and strongly reworked by the Rhyacian belt of the Maroni-Itacaiúnas Province. These block consists of Meso- to Neo-archean medium- to high-grade metamorphic rocks, including tonalitic to granodioritic gneisses, metasedimentary granulites and charnockite plutons. Rhyacian granitic plutons and metavolcano-sedimentary sequences constitute the main Paleoproterozoic units (Rosa-Costa et al. 2003, 2006; Avelar et al. 2003; Barbosa et al. 2013; Barreto et al. 2013; Borghetti et al. 2018; Hoffmann et al. 2018).

Avelar (2002) and Avelar et al. (2003) identified by Pb-Pb zircon ages two magmatic pulses in the central-northern portion of Amapá. The first pulse is defined by ages between 2.85 to 2.84 Ga, in the orthogneisses of the TC located in Archean Cupixi Domain. The second pulse affected the igneous precursors of the Tartarugal Grande Complex, and is characterized by ages in the 2.65 to 2.58 Ga interval (Avelar, 2002; Rosa-Costa et al. 2003, 2006). The Sm-Nd data presented by Pimentel et al. (2002), Avelar et al. (2003) and Rosa-Costa et al. (2003, 2006) stand out the a main Paleo- to Meso-archean episode of crustal growth while the Neo-archean is dominated by crustal reworking of the pre-existing Meso-archean crust. Rosa-Costa et al. (2006) and Barreto et al. (2013) report from the Sm-Nd data that the sources of the Rhyacian orogenic granites are of Meso- to Neo-archean age. The oldest U-Pb zircon ages of our study are Meso-archean (2.85 to 2.81 Ga), and were

obtained for the tonalitic to granodioritic gneiss and metagranodiorite samples of the TC. They represent very well the first Archean magmatic pulse referred by Avelar (2002) and Avelar et al. (2003).

The Neo-archean (2.67 Ga) U-Pb zircon ages obtained for the intrusive gabbro may be related to the referred second magmatic pulse. The identification of Neo-archean ages is the main tectonic implication associated with the geochronological data presented in this paper. The Meso- and Paleo-archean zircon crystals that have been found in the gabbro indicates the presence of heritage crystals of the surrounding basement rocks and confirm the stratigraphic relationships observed in the field geology. Inherited crystals have more elongated prismatic forms, usually anhedral, with irregular borders and with edges suggesting magmatic corrosion.

The Archean U-Pb zircon ages obtained by LA-MC-ICPMS confirm that the basement rocks which crops out in the Cupixi, Vila Nova and Serra do Navio regions are part of an extensive Archean nucleus (Amapá Block) surrounded by the Maroni-Itacaiúnas Province, as proposed previously by Avelar et al. (2003), Rosa-Costa et al. (2003, 2006) and Barbosa et al. (2013). The continuity of this Archean unit was also confirmed by crustal thickness seismological studies performed by Rosa et al. (2016), which verified that this area presents a lower thickness (~ 50 Km), in relation to the values obtained on the areas occupied by the Rhyacian belt (> 60 Km), located to the north of this terrane. These belts with crustal thickening correspond to magmatic arcs of the Paleoproterozoic.

The northeast portion of the AC and east of the Guiana Shield presents tectonic records of intense magmatic activity between the Meso- and Neo-archean, with Pb-Pb and U-Pb zircon ages between 3.3 (3.48) and 2.58 Ga. After this interval occurs an extensive tectonic activity related to the development of orogenic belts

related to the Rhyacian orogeny (2.26 and 2.0 Ga). It was not recognized magmatism and metamorphism activities during the Siderian in the eastern (Brazil) and north portion (French Guiana and Suriname) of the Guiana Shield (Rosa-Costa et al. 2003, 2006; Avelar et al. 2003; Delor et al. 2003a,b; Roever et al. 2003) and the West African Craton (Gasquet et al., 2003; Peucat et al., 2005). Even on a global scale, the Siderian period shows very little evidence of crustal growth, reworking, and orogenic activities (Griffin et al., 2014). In the Guiana Shield, the Neo-archean magmatism is well constrained from 2.85 Ga to 2.58 Ga, without record of younger ages (Avelar et al. 2003; Rosa-Costa et al. 2003, 2006).

Most of the Archean ages obtained for the Amapá Block result from Pb-Pb zircon analyzes obtained mainly in the Jari Domain, with two results in the Cupixi Domain (Avelar et al. 2003; Rosa-Costa et al. 2003, 2006). Despite the quality of the Pb-Pb analyzes, the ages obtained in each sample result from the investigation of 3 to 5 zircon crystals, and most of them have no image of the internal structure. In this way the U-Pb ages presented in this paper were obtained in a larger number of crystals and also have the location of the analyzed spot in catodoluminescence images.

The continental crust of the Cupixi Domain has a long-lived evolution, which started at the end of Meso-archean and continued for all Rhyacian period. U-Pb and Pb-Pb zircon geochronology and Nd $T_{DM}$ and Hf $T_{DM}$ model ages data of the TC rocks reveals three phases of magmatic activity during Paleo-archean, i.e. at about 3.36 to 3.07 Ga, at the Meso- to Neo-archean transition, ca. 2.85 to 2.81 Ga, and during the Neo-archean, between 2.67 to 2.66 Ga. The Nd $T_{DM}$ model ages reveal that the main period of crust generation is related to the end of Paleo-archean an during the Meso-archean (Pimentel et al. 2002). These same characteristics were

described in the Jari Domain, which is located west of the Cupixi Domain (Rosa-Costa et al., 2003, 2006).

The new U-Pb and Lu-Hf zircon data presented in this paper confirm the continuity of the Amapá Block and consolidate the occurrence of a wide exposure of the Archean crust in the southeast portion of the Guiana Shield. The combination of the Pb-Pb and U-Pb zircon geochronology with Lu-Hf and Sm-Nd isotopic data define the Neo-archean as a period of crustal reworking, without significant generation of juvenile crust and accretion processes.

The recognition of an extended Archean landmass as suggested by Rosa-Costa et al. (2003, 2006) and Avelar et al. (2003) precludes previous statements that the Archean in the southeast of the Guiana Shield, was restricted to isolate remnants or basement inliers within Paleoproterozoic terranes (Tassinari, 1996; Tassinari and Macambira, 1999; Santos et al. 2000; Tassinari et al. 2000; Tassinari and Macambira, 2004). In addition, these Archean remnants were previously interpreted by Avelar et al. (2003) as a possible northward prolongation of the Archean Carajás associations strongly affected by the Rhyacian orogeny. This possibility was questioned by Rosa-Costa et al. (2006) that admit that Amapá Block represents an independent continental landmass, on base in available geochronological data that indicate a distinct geodynamic evolution for these Archean segment. The authors highlighting the remarkable period of plutonic magmatic activity in Amapá Block during the Neo-archean, between 2.85 and 2.58 Ga, while in the Carajás Province this phase correspond to rift-related volcanism and sedimentary deposition (Vasquez and Rosa-Costa, 2008; Feio & Dall'Agnol, 2012; Feio et al., 2013). The authors stand out the occurrence of Rhyacian arc-granite magmatism in the north portion of Carajás Province and the relation of this activities with the Paleoproterozoic rocks of the Carecuru Domain located in the southern border of the Amapá Block, suggesting

a substantial development of a magmatic arc system associated to Rhyacian orogeny.

### *5.2 Metamorphism and Deformation*

The orogenic metamorphism are recorded in the orthogneisses and metagranites of the Tumucumaque Complex and in the metavolcano-sedimentary rocks of the Vila Nova Greenstone Belt (VNGB), which are affected by the same deformational events (Borghetti et al. 2018; Hoffmann et al. 2018). The medium-grade conditions defined by Amphibolite facies and by medium lithospheric pressure are associated with continental collision metamorphism event, resulting in the development of the $S_1$ and $S_2$ regional foliations and by a late regional $F_3$ folding phase and associated high-angle ductile transcurrent shear zones. **(Table 5)**.

The reconstruction of ancient orogens within cratonic areas can be complex and face challenges and limitations, when it comes to sampling. Petrographic analysis helped the identification of two main metamorphic events recorded by the TC. The older event corresponds to orogenic collisional metamorphism, which generated metamorphic banding, folding and the formation of oblique ductile shear zones. The second event corresponds to a later contact metamorphism associated with the emplacement of Paleoproterozoic intrusive granites.

As the orogenic metamorphism evolved, three metamorphic foliations ($S_1$, $S_2$ and $S_3$) were generated. Compositional banding $S_1$ corresponds to the regional foliation and the metamorphic mineral assemblages indicates Lower to Upper Amphibolite facies metamorphic conditions. This foliation has a general NW-SE trend, with a penetrative SW down-dip lineation. In highly deformed areas, $S_1$ foliation is preserved as isoclinal folds ($F_2$) and by the $S_2$ crenulation cleavage. The transposition zones are marked by ductile shear zones and in these conditions the

gneisses show a more developed and regular banding. These zones are also accompanied by stretching and intense recrystallization of plagioclase, K-feldspar and quartz. A third foliation $S_3$ is recognized locally in the metavolcano-sedimentary rocks of the VNGB as fracture cleavage, which is associated with a Upper Greenschist facies retrograde metamorphic event (Borghetti et al. 2018; Hoffmann et al. 2018). This deformational event is responsible for the regional open $F_3$ folds and by the changes in attitudes of $S_1$ and $S_2$ foliations and of the stretching lineation. A later contact metamorphism event associated with Orosirian intrusive granites is recognized by superposition of decussate and bow-tie textures, with crystal growing in the absence of deformation.

The new U-Pb zircon ages available for the meta-andesites of the Vila Nova Complex presented values between 2.154 ±6 Ma and 2.170 ±9 Ma, which were interpreted as the crystallization age of the metavolcanic rocks and as the maximum deposition age of the basin of the VNGB (Borghetti et al 2018; Hoffmann et al. 2018). This ages was corroborated by the U-Pb ages of detrital zircons of the metasediments of VNGB (*ca.* 3.6 and 2.4 Ga). Garnet-whole rock Sm-Nd isochron of the basal amphibolite of the Vila Nova Complex provided age of 2.080 ±20 Ma, indicating a metamorphism that coincides with late-orogenic magmatism in the Maroni-Itacaiúnas Province (Pimentel et al. 2002). Furthermore, U-Th-Pb monazite dating performed on samples of high-grade gneisses indicates that the Granulite-facies metamorphism took place between 2.100 and 2.080 Ma, during the collisional stage of the Rhyacian orogeny (Rosa-Costa et al. 2006). Monazite ages also reveal post-collisional migmatization events between 2.060 Ma and 2.040 Ma that occurred under Amphibolite-facies conditions and were coeval with some episodes of granite emplacement (Rosa-Costa et al. 2006). A Osirian age also has been proposed for the Granulite-facies metamorphism, constrained by garnet-whole rock Sm-Nd

isochron, yielding ages between 2.020 Ma and 1.980 Ma (Oliveira et al. 2008) and by a Pb-Pb zircon age of 2.050 Ma of a coeval charnockitic magmatism (Avelar et al. 2003).

| Complex | Rock | Mineral Assemblage | | Temporal Relationships | Metamorphic facies | Microstructural features | |
|---|---|---|---|---|---|---|---|
| Vila Nova | Amphibolite | Hb + Pl + Grt (Di) | **OM** | Syn-tectonic | Upper Amphibolite | Intrafolial folds and crenulation cleavage | **$S_1$ and $S_2$** |
| | | Chl + Ser + Ep | **OM** | Tardi-tectonic | Ab-Ep hornfels/ Greenschist | Fractures with retro-metamorphism | **$S_3$** |
| | Amphibole schist | Bio + Tr | **OM** | Syn-tectonic | Amphibolite | Mineral orientation | **$S_1/S_2$** |
| | | Hb + Clo + Cln | **OM** | | Upper Greenschist | | |
| | Mafic cornubianites | Hb + tr | **OM** | | Amphibolite | | |
| | | Di + Hb | **CM** | Post-tectonic | Px Hornfels | ---------- | |
| | | Hb + Pl | **CM** | | Hbl Hornfels | ---------- | |
| | Meta-ultramafites | Tr | **OM** | Syn-tectonic | Amphibolite | Intrafolial folds and crenulation cleavage | **$S_1$ and $S_2$** |
| | Metapelites | Grt + Crd + Bio | **OM** | Syn-tectonic | Amphibolite | Intrafolial folds and crenulation cleavage | **$S_1/S_2$** |
| | Mylonitic quartzites | Qtz + Mgt | **OM** | Syn-tectonic | Upper Greenschist/ Amphibolite | Mineral stretching | **$S_1/S_2$** |
| | Mylonitic meta-conglomerates | Qtz + Ep (Fct) | **OM** | Syn-tectonic | Upper Greenschist/ Amphibolite | Mineral stretching | |
| Tumucumaque | Orthogneisses | Pl + Hb + Bt | **OM** | Syn-tectonic | Amphibolite | Mineral stretching and lineation | **$S_1/S_2$** |
| | Metagranites | Pl + Kf +Bt | **OM** | Syn-tectonic | Amphibolite | Mineral stretching and lineation | **$S_1/S_2$** |

**Table 5.** Relationships between the main microstructures observed under the microscope and the metamorphic events. Legend - Metamorphic events: OM = orogenic metamorphism, CM = contact metamorphism; - Foliation: $S_1$ = schistosity, $S_2$ = crenulation cleavage, $S_3$ = fracture cleavage; - Minerals: Hb = hornblende, Pl = plagioclase, Grt = garnet, Di = diopside, Chl = chlorite, Ser = sericite, Ep = Epidote, Tr = tremolite, Bio = biotite, Crd = cordierite, Qtz = quartz, Mgt = magnetite, Fct = fuchsite, Px = pyroxene, Cln = clinochlore, Kf = K-feldspar(microcline).

The spatial relationship between the $S_1$ and $S_2$ low-angle metamorphic foliation, the mineral stretching lineation and the kinematic indicators, suggest a deformational process associated with an oblique continental collision event. The sinistral sense registered in SC planes of the foliation in quartzites and the asymmetry of deformed pebbles of the metaconglomerates of the VNGB indicate that

the Vila Nova Shear Zone is an thrust zone with northwards hanging wall movement (Borghetti et al. 2018). These considerations suggest that regional deformation that affected the Tumucumaque and Vila Nova complexes occurred through the installation of a low-angle to oblique shear zones system (Borghetti et al. 2018; Hoffmann et al. 2018).

## 6. Conclusions

According to geochronological results, supported by additional geological mapping, petrographic and structural data, the following conclusions are proposed:

1) A combination of new and compiled geologic, geochronologic and isotopic information of the orthogneisses and metagranodiorites of the TC suggest the presence of the broad Archean area in the Vila Nova, Cupixi and Serra do Navio regions corroborant the existence of the Amapá Block.

2) Two magmatic episodes, an older Meso-archean (2.85 to 2.81 Ga) and a later Neo-archean (2.67 Ga), are identified by U-Pb zircon geochronology in tonalitic to granodioritic gneisses, metagranodiorites and intrusive gabbro of the TC at the Vila Nova region. The Meso-archean rocks were generated in an environment of crustal reworking of the older Archean crust, while the Neo-archean gabbro, were probably emplaced under the late-orogenic or anorogenic extensional regime.

3) The Vila Nova and Tumucumaque complexes record the same deformation features characterized by the development of two main metamorphic foliations (schistosity and metamorphic banding) and by the same mineral and stretching lineations, developed under Upper Greenschist to Medium Amphibolite facies metamorphism in the Vila Nova Complex and in Medium to Upper Amphibolite facies in the Tumucumaque Complex.

4) The stratigraphic relationship between VNGB and TC are tectonic and defined by low-angle ductile Vila Nova Shear Zone. The compilation of the structural and isotopic data suggest that the development of the complexes are related to the same Late-rhyacian event of orogenic metamorphism.

5) The geometric relationship between the metamorphic foliations ($S_1$ and $S_2$) and the mineral and stretching lineations suggest an evolution under contractional tectonic stresses probably related to an oblique collisional tectonic process associated to Archean nucleus and the Rhyacian orogenic belts of the Maroni-Itacaiúnas Province.

**Acknowledgments**

The authors thanks to the National Council for Scientific and Technological Development of Brazil (CNPq) for the research grants. To Geoscience Institute at Rio Grande do Sul Federal University (UFRGS) and PETROBRÁS S.A. company for financial support. We acknowledge the Amapari Mining Company for making data and field logistics available. To geologists Persio Mandetta (in memorian), João Batista Guimarães Teixeira, and Carlos Alexandre Leite de Souza for the fruitful discussions; geologists Heiny Paim Kloss and Gustavo Zvirtes for their cooperation in acquiring LA-ICPMS data; geologists Elaine Cunha and Jordão Isaac Ramos for the valuable support given to this study. We thank the technicians of Geochoronological Research Center of the Geosciences Institute at São Paulo University, Walter Maurício Sproesser and Solange Lucena de Souza for their cooperation in obtaining the geochronological data. We thank the reviewers for the critical suggestions presented.

**References**

Almeida, F.F.M., Brito Neves, B.B., Carneiro, C.D.R. 2000. The origin and evolution of the South American Platform. Earth-Science Review, 50(1-2), 77-111.

Avelar, V.G. 2002. Geocronologia Pb-Pb em zircão e Sm-Nd em rocha total da porção centro norte do Estado do Amapá, Brasil: Implicações para a evolução geodinâmica do setor oriental do Escudo das Guianas. Ph Thesis. Universidade Federal do Pará.

Avelar, V.G.; Lafon, J.M.; Delor, C.; Guerrot, C.; Lahondère, D. 2003. Archean crustal remnants in the easternmost part of the Guiana Shield: Pb-Pb and Sm-Nd geochronological evidence for Mesoarchean versus Neoarchean signatures. Geologie de la France, 2-3-4, 83-100.

Barbosa, J.P.O., Costa Neto, M.C., Rosa-Costa, L.T., Anjos, G.C., Chaves, C.L., 2013. Mapa Geológico Folha Macapá (NA.22-Y-D), CPRM, escala 1:250.000.

Barreto, C.J.S., Lafon, J.M., Rosa-Costa, L.T., Dantas, E.L. 2013. Paleoproterozoic granitoids from the northern limit of the Archean Amapá block (Brazil), southeastern Guyana Shield: Pb-Pb evaporation in zircons and Sm-Nd geochronology. Journal of South American Earth Sciences. 45, 97-116.

Belousova, E.A.; Griffin, W.L.; O'reilly, S.Y., Fisher, N.I. 2002. Igneous zircon: Trace element composition as an indicator of source rock type. Contributions to Mineralogy and Petrology, 143, 602-622.

Borghetti, C.; Philipp, R.P.; Basei, M.A.S.; Mandetta, P. 2014. New ages from Vila Nova and Tumucumaque Complex in the Cupixi region, Porto Grande, Amapá, Brazil. 9$^{th}$ South American Symposium on Isotope Geology. Boletim de Resumos Expandidos, São Paulo, Brasil.

Borghetti, C.; Philipp, R.P. 2017. Geologia e geofísica do *greenstone belt* Vila Nova, porção nordeste do Cráton Amazônico, estado do Amapá, Brasil. Geologia USP, 17, 109-127.

Borghetti, C.; Philipp, R.P.; Hoffmann, I.B.; Basei, M.A.S.; Mandetta, P. 2018. Geology, U-Pb zircon geochronology and Lu-Hf isotopes of the Vila Nova Greenstone Belt, Amapá, Brazil: arc-related basins associated to a Rhyacian orogeny in the northern Amazonian Craton. Precambrian Research, Submitted.

Chemale Jr. F., Dussin I.A., Alkmim F.F., Martins M., Queiroga G.N., Armstrong R., Santos M. 2011. Unravelling a Proterozoic basin history through detrital zircon

geochronology: The case of the Espinhaço Supergroup, Minas Gerais, Brazil. *Gondwana Research:* doi 10.1016/j.gr.2011.08.016.

Chu, N.C., Taylor, R.N., Chavagnac, V., Nesbitt, R.W., Boella, R.M., Milton, J.A., German, C.R., Bayon, G., Burton, K., 2002. Hf isotope ratio analysis using multi collector inductively coupled plasma mass spectrometry: an evaluation of isobaric interference corrections. J. Anal. At. Spectrom. 17, 1567-1574.

Cordani, U.G., Sato, K. 1999. Crustal evolution of the South American Platform based on Nd isotopic systematics on granitoid rocks. Episodes, 22, 167-173.

Delor, C.; Lahondère, D.; Egal, E.; Lafon, J.M.; Cocherie, A.; Guerrot, C.; Rossi, Ph.; Trufert, C.; Theveniaut, H.; Phillips, D.; Avelar, V.G. 2003a. Transamazonian crustal growth and reworking as revealed by the 1:500.000-scale geological map of French Guiana (2nd edition). Géologie de la France, 2-3-4, 5-57.

Delor, C.; Roever, E.W.F.; Lafon, J.M.; Lahondère, D.; Rossi, P.; Cocherie, A.; Guerrot, C.; Potrel, A. 2003b. The Bakhuis ultrahigh-temperature granulite belt (Suriname): II. Implications for late Transamazonian crustal stretching in a revised Guiana Shield framework. Géologie de la France, 2-3-4, 207-230.

De Wit M, Stankiewicz J, Reeves C (2008) Restoring Pan-African-Brasiliano connections: more Gondwana control, less Transatlantic corruption. Geological Society of London, Special Publications, 294, 399-412.

Elholou, S., Belousova, E., Griffin, W. L., Peasom, N. J., O'Reilly, S. Y. 2006. Trace element and isotopic composition of GJ red zircon standard by laser ablation. Geochimica and Cosmochimica Acta, 70(18), 158.

Faraco, M. T. L., Marinho, P. A. C., Costa, E. J. S., Vale, A. G., Camozzato, E. 2004. Carta Geológica do Brasil ao Milionésimo: Sistema de Informações Geográficas-SIG. Folha Macapá (NA.22), CPRM, escala 1:1.000.000.

Feio, G.R.L., Dall'Agnol, R., 2012. Geochemistry and petrogenesis of the Mesoarchean granites from the Canaã dos Carajás area, Carajás Province, Brazil: Implications for the origin of Archean granites, Lithos 154, 33-52.

Feio, G.R.L., Dall'Agnol, R., Dantas, E.L., Macambira, M.J.B., Santos, J.O.S., Althoff, F.J., Soares, J.E.B., 2013. Archean granitoid magmatism in the Canaã dos Carajás area: Implications for crustal evolution of the Carajás province, Amazonian craton, Brazil. Precambrian Research 227, 157-185.

Gasquet, D.; Barbey, P.; Adou, M.; Paquette, J.L. 2003. Structure, Sr-Nd isotope geochemistry and zircon U-Pb geochronology of the granitoids of the

Dabakala area (Côte d'Ivoire): evidence for a 2.3 Ga crustal growth event in the Paleoproterozoic of West Africa? *Precambrian Res.*, 127, 329-354.

Griffin, W.L., Belousova, E.A., O'Neill, C., O'Reilly, S.Y., Malkovets, V., Pearson, N.J., Spetsius, S., Wilde, S.A. 2014. The world turns over: Hadean-Archean crust-mantle evolution. Lithos, 189, 2-15.

Hoffmann, I., Philipp, R.P., Borghetti, C., 2018. Geochemistry and origin of the tholeiitic metabasalts from the 2.15 Ga Vila Nova greenstone belt, Amapá, Brazil. Journal of South American Earth Sciences. In press.

Lafon J.M., Avelar V.G., Rossi PH., Delor C., Guerrot C., Pidgeon, R.T. 2000. Geochronological evidence for reworked Neoarchean crust during Transamazonian orogeny (2.1 Ga) in the southeastern Guiana Shield. *In*: International Geological Congress, 31, Rio de Janeiro, *Abstracts*.

Ledru, P.; Johan, V.; Milési, J.P.; Tegyey, M. 1994. Markers of the last stages of the Paleoproterozoic collision: evidence for a 2,0 Ga continent involving circun-South Atlantic provinces. Precambrian Res., 69, 169-191.

Ludwig, K.R., 2002. SQUID. User's manual (Version 1.02). Berkeley Geochronology Center. Special Publication. 2, pp. 17.

Ludwig, K.R., 2008, Manual for Isoplot 3.7: Berkeley Geochronology Center, Special Publication, 4, 77 pp.

Machado, N.; Lyndenmayer, Z.; Krogh, T.E.; Lindenmayer, D. 1991. U-Pb geochronology of Archean magmatism and basement reactivation in the Carajás area, Amazonian shield, Brazil. Precambrian Res., 49, 329-354.

Magalhães, L.A., Souza Filho, C.R., Silva, A.M. 2007. Caracterização geológica-geofísica da porção central do Amapá com base em processamento e interpretação de dados aerogeofísicos. Revista Brasileira de Geociências. 37(3), 464-477.

Mc Reath I., Faraco M.T.L. 2006. Paleoproterozoic greenstone-granite belts in northern Brazil and the former Guyana Shield-West African craton province. Geol. USP Sér. Cient., 5(2), 49-63.

Oliveira, E.C.; Lafon, J.M.; Gioia, S.M.C.L., Pimentel, M.M. 2008. Datação Sm-Nd em rocha total e granada do metamorfismo granulítico da região de Tartarugal Grande, Amapá Central. Rev. Bras. Geoc., 38(1), 114-127.

Patchett, P.J. and Tatsumoto, M. (1980). A routine high-precision method for Lu-Hf isotope geochemistry and chronology. Contributions to Mineralogy and Petrology 75, 263-267.

Peucat, J.J., Capdevila, R., Drareni, A., Mahdjoub, Y., Kahoui, M., 2005. The Eglab massif in the West African Craton (Algeria), an original segment of the Eburnean orogenic belt: petrology, geochemistry and geochronology. Precambrian Research, 136, 309-352.

Pimentel, M.M.; Ferreira Filho, C.F.; Spier, C.A. 2002. Estudo Sm-Nd do Complexo Máfico-Ultramáfico Bacuri, Amapá: idade da intrusão, metamorfismo e natureza do magma original. Rev. Bras. Geoc., 32, 371-376.

Ricci, P.S.F., Carvalho, J.M.A., Rosa-Costa, L.T., Klein, E.L., Vasquez, M.L., Vale, A.G., Macambira, E.M.B., Araújo, O.J.B., 2001. Geologia e Recursos Minerais do Projeto RENCA (Fase I). CPRM, Belém.

Roever, E.W.F., Lafon, J.M., Delor, C., Cocherie, A., Rossi, P., Guerrot, C., Potrel, A., 2003. The Bakhuis ultrahigh-temperature granulite belt (Suriname): petrological and geochronological evidence for a counterclockwise *P–T* path at 2.07–2.05 Ga. Géologie de la France 2–3–4, 175-206.

Rosa, J.W.C., Rosa, J.W.C; Fuck, R.A. 2016. The structure of the Amazonian craton: Available geophysical evidence. Journal of South American Earth Sciences. 70, 162-173.

Rosa-Costa, L.T; Ricci, P.S.F.; Lafon, J.M.; Vasquez, M.L.; Carvalho, J.M.A.; Klein, E.L.; Macambira, E.M.B. 2003. Geology and geochronology of Archean and Paleoproterozoic domains of the southeastern Amapá and northwestern Pará, Brazil, southeastern Guyana Shield. Géologie de la France, 2-3-4, 101-120.

Rosa-Costa, L.T. 2006. Geocronologia $^{207}Pb/^{206}Pb$, Sm-Nd, U-Th-Pb e $^{40}Ar$-$^{39}Ar$ do Segmento Sudeste do Escudo das Guianas: Evolução Crustal e Termocronologia do Evento Transamazônico. 226p. Tese de Doutorado, Universidade Federal do Pará, Belém.

Rosa-Costa, L.T., Silva, C.M.G., Barbosa, J.P.O., Costa Neto, M.C., 2012. Mapa Geológico da Folha Rio Araguari (NA.22-Y-B), CPRM, escala 1:250.000.

Santos, J.O.S.; Hartmann, L.A.; Gaudette, H.E.; Groves, D.I.; Mcnaughton, N.J.; Fletcher, I.R. 2000. A new understanding of the provinces of the Amazon Craton based on integration of field mapping and U-Pb and Sm-Nd geochronology. Gondwana Research, 3(4), 453-488.

Stacey, J.S., Kramers, J.D., 1975. Approximation of terrestrial lead isotopic evolution by a two stage model. Earth Plan. Sci. Letters 26, 207-221.

Tassinari, C.C.G., Macambira, M.J.B. 1999. Geochronological provinces of the Amazonian Craton. Episodes, 22(3), 174-182.

Tassinari, C.C.G.; Bettencourt, J.S.; Geraldes, M.C.; Macambira, M.J.B.; Lafon, J.M. 2000. The Amazonian Craton. In: Cordani, U.G.; Milani, E.J.; Filho, A.T.; Campos, D.A. (eds.) Tectonic Evolution of South America. Rio de Janeiro, 31º International Geological Congress, SBG, 41-95.

Tassinari, C.C.G., Macambira, M.J.B., 2004. A evolução tectônica do Cráton Amazônico. In: Mantesso-Neto, V. (Ed.), Geologia do continente Sul-americano: evolução da obra de Fernando Flávio Marques de Almeida. São Paulo, 471-485.

Tavares, R.P.S. 2009. Granitóides e anfibolitos da Serra do Navio, borda norte do bloco arqueano Amapá: caracterização petrográfica e geoquímica, geocronologia Pb-Pb em zircão e isótopos de Nd. Dissertação de Mestrado, Universidade Federal do Pará, Belém, pp. 114.

Teixeira, W.; Tassinari, C.C.G.; Cordani, U.G.; Kawashita, K. 1989. A review of the geochronology of the Amazonian Craton: Tectonic implications. Precambrian Res., 42, 213-227.

Trendall, A.F., Basei, M.A.S., Laeter, J.R., Nelson, D.R., 1998. SHRIMP zircon U–Pb constraints on the age of the Carajás formation, Grão Pará group, Amazon Craton. Journal of South American Earth Sciences 11, 265–277.

Zhao, G., Cawood, P.A., Simon, A.W., Sun, M., 2002. Review of global 2.1-1.8 Ga orogens: implications for a pre-Rodinia supercontinent. Earth-Science Reviews 59, 125–162.

Vasquez, M.L., Rosa-Costa, L.T., 2008. Geologia e recursos minerais do Estado do Pará: texto explicativo do mapa geológico e de recursos minerais do Estado do Pará, CPRM, 328 pp.

**2.3** Geology, U-Pb zircon geochronology and Lu-Hf isotopes of the Vila Nova greenstone belt: arc-related associations of the Rhyacian orogeny in the northern Amazonian Craton, Brazil. Artigo submetido a revista *Precambrian Research.*

**Successfully received: submission Geology, U-Pb zircon geochronology and Lu-Hf isotopes of the Vila Nova greenstone belt: arc-related associations of the Rhyacian orogeny in the northern Amazonian Craton, Brazil for Precambrian Research**
**Ter 17/04/18 16:23**
Precambrian Research

**para:** cborghetti@terra.com.br
*This message was sent automatically. Please do not reply.*

Ref: PRECAM_2018_169
Title: Geology, U-Pb zircon geochronology and Lu-Hf isotopes of the Vila Nova greenstone belt: arc-related associations of the Rhyacian orogeny in the northern Amazonian Craton, Brazil
Journal: Precambrian Research

Dear Mr. Borghetti,

Thank you for submitting your manuscript for consideration for publication in Precambrian Research. Your submission was received in good order.

To track the status of your manuscript, please log into EVISE® at: http://www.evise.com/evise/faces/pages/navigation/NavController.jspx?JRNL_ACR=PRECAM and locate your submission under the header 'My Submissions with Journal' on your 'My Author Tasks' view.

Thank you for submitting your work to this journal.

Kind regards,

Precambrian Research

**Have questions or need assistance?**

For further assistance, please visit our Customer Support site. Here you can search for solutions on a range of topics, find answers to frequently asked questions, and learn more about EVISE® via interactive tutorials. You can also talk 24/5 to our customer support team by phone and 24/7 by live chat and email.

---

# Geology, U-Pb zircon geochronology and Lu-Hf isotopes of the Vila Nova greenstone belt: arc-related associations of the Rhyacian orogeny in the northern Amazonian Craton, Brazil

Cristiano Borghetti[1], Ruy Paulo Philipp[2], Itiana Borges Hoffmann[1], Persio Mandetta[3]

[1]Programa de Pós Graduação em Geociências (PPGGEO), Instituto de Geociências, Universidade Federal do Rio Grande do Sul, UFRGS. Av. Bento Gonçalves 9.500, CEP 91501-970, Porto Alegre, RS, BR, e-mail: cborghetti@terra.com.br
[2]Centro de Estudos em Petrologia e Geoquímica (CPGq), Instituto de Geociências, Universidade Federal do Rio Grande do Sul, UFRGS, Porto Alegre, RS, e-mail: ruy.philipp@ufrgs.br
[3]Amapari Mineração Ltda.

## Abstract

The north portion of the Guiana Shield, northeastern Amazonian Craton, in South America, represents a large orogenic belt generated during the Transamazonian orogenic cycle (2.26-1.95 Ga), which consists of extensive areas of Paleoproterozoic crust bordering the Archean Amapá Terrane. Geologic-structural mapping and airborne geophysical data (magnetometric and gammaspectrometric) supported by drilling holes and U-Pb zircon data coupled with zircon Hf isotopic constrains on metavolcano-sedimentary rocks unravel the nature and tectonic significance of Rhyacian Vila Nova greenstone belt (VNGB). U-Pb isotopic data reveal a long-lived tectonic evolution characterized by several stages of crustal accretion and reworking. The VNGB is an elongated belt in the E-W direction, in tectonic contact with Archean orthogneisses and metagranites from the Tumucumaque Complex. The sequence consists of metabasalts, meta-andesites and rare metadacites at the base, and metasedimentary rocks intercalated with mafic metavolcanic and exhalative chemical rocks at the top. The metasediments are characterized by a thick package of quartzite, hematite quartzite and pelitic schists, with subordinate metaconglomerate lenses and hematite schists. The Vila Nova units are metamorphosed from greenschist to intermediate amphibolite facies and intermediate lithostatic pressure. U-Pb age of 2.17 Ga obtained from meta-andesite defines the period of volcanic activity in the basin. The Hf values, from +1.17 to +6.5, and between -2.44 and -11.79, indicate that two sources (MORB and sublithospheric continental mantle) were

important in the genesis of meta-andesites. The Hf $T_{DM}$ model ages show Siderian values, between 2.26 and 2.43 Ga, with a small participation of zircons of Neo and Paleo-archean, between 3.43 and 2.51 Ga and $\varepsilon_{Hf(t)}$ positive, between +3.6 and +7.9. Detrital zircons from quartzites and metaconglomerates yielded ages between 3.6 and 2.4 Ga suggesting that the rocks were dominantly derived from the Archean basement. The available data suggest an evolution model based on the opening and closure of an ocean, with development of magmatic arc system and arc-related basin rocks during the Transamazonian orogenic cycle.

**Keywords:**
Amazonian Craton, Archean, Paleoproterozoic, Transamazonian orogenesis, Crustal evolution, U-Pb geochronology.

## 1. Introduction

The Precambrian shields form the cores of the present continents and represent geologically stable areas composed of small Archean cratons welded by ancient orogenic areas of the Paleoproterozoic (Ernst, 2009; Sleep and Windley, 1982; Van Kranendonk, 2010). These older cores consist of granite-gneiss terranes, which represent the primitive continents, and the older or younger greenstone belts, representing arc associations and fragments of the primitive oceans (Prothero and Dott, 2009).

The study area is located in the eastern part of the Guiana Shield, northeastern portion of the Amazonian Craton, Amapá state, Brazil **(Fig. 1A)**. Geochronological data are scarce for this area, especially because of difficult access, deep weathering and the lack of outcrops. The Amazonian Craton is composed to the north by the Guyana Shield and to the south by the Central Brazil Shield, covered by the sediments of the Solimões and Amazonas basins. The central portion of the craton consisting of an Archean core, composed by metamorphic medium- to high-grade gneiss complexes surrounded by Paleo- and Mesoproterozoic NW-SE-

trending mobile belts (Teixeira et al., 1989; Tassinari and Macambira 1999, 2004; Tassinari et al., 2000; Santos et al., 2000; Avelar et al., 2003; Rosa-Costa et al., 2006) **(Fig. 1B)**. The Paleoproterozoic mobile belts are formed by extensive arc-related basins and remnants of small oceans, made of discontinuous tracks of greenstone belts and TTG-type granitic associations (Avelar et al., 2003; McReath and Faraco, 2006; Rosa-Costa et al., 2006). The Vila Nova Complex is composed of several metavolcano-sedimentary associations occurring as regional greenstone belts (Mc Reath and Faraco, 2006) **(Fig. 2)**.

To investigate the stratigraphy and to increase the geological knowledge structural mapping was carried out, integrated with airborne geophysical data (magnetometric and gammaspectrometric) and with geological profiles obtained by data integration from drilling holes. The results allowed the detailed depiction of the lithological units and their internal relationships in the Vila Nova greenstone belt.

The U-Pb geochronologic analysis of detrital zircon populations is a well known technique that helps tracing the tectonic histories and the reconstruction of the paleogeography of deformed Precambrian terranes. Interpretation of detrital zircon signatures are based on the comparison of detrital zircon population age peaks with the age of the exposed rocks found in the same region (Condie et al., 2009). Nevertheless, preservation of the source rocks must be taken into account (Hawkesworth et al., 2009). Regardless of interpretation problems, the technique is an effective method to determine the maximum age for sedimentary systems, and it also indicates whether a particular sedimentary basin evolved in an active or a passive margin setting, or within an intracontinental environment (Cawood and Nemchin, 2001; De Graaff-Surpless et al., 2002; Chew et al., 2008; Cawwod et al., 2012).

The Amapá State is located in a strategic position at the eastern portion of the Guiana Shield to help understand and reconstruct the evolution of the West Gondwana. The provenance of the supracrustal rocks within these metasedimentary domains and their role in the tectonic context is crucial to reconstruct part of the Gondwanaland paleogeography and pre-drift correlations between South America and West Africa. Furthermore, we establish paleogeographic reconstructions by comparing detrital zircon ages with the ages of the surrounding rocks, including those from stable Archaean cratonic areas and those involved in crust-forming events (exposed or not).

This paper aims to characterize the magmatic and sedimentary evolution of the Vila Nova greenstone belt (VNGB). We provide LA-MC-ICPMS U-Pb ages on detrital zircon grains from two samples of metasedimentary and U-Pb and Lu-Hf data from magmatic zircon crystals of metavolcanic rock. The provenance of the metasediments was investigated in order to obtain further information on the depositional ages of the metavolcanic rocks. The choice of samples was supported by geologic mapping (1:50.000 scale) and geophysical data and took into account previously published geochronology of the region. We evaluate the involvement of the basement rocks, considering both the new U-Pb zircon ages and compiled information to provide petrogenetic fingerprints for volcanic and sedimentary episodes of the VNGB. The integration of geological and structural mapping with airborne geophysical data and U-Pb zircon analysis of the rocks of the VNGB produced results that contribute to the better understanding of the crustal evolution of the northeastern portion of the Amazonian Craton.

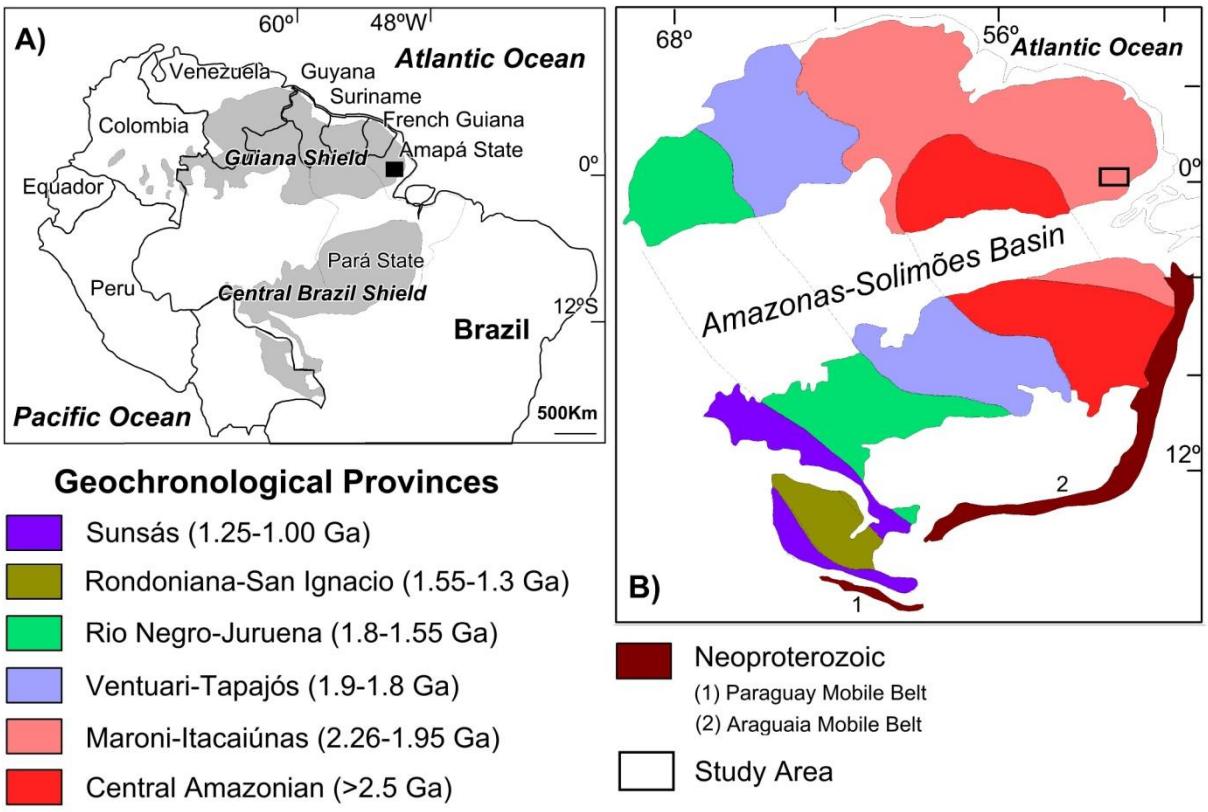


**Figure 1. A)** Map of the Amazonian Craton in South America and location of the Guiana and Central Brazil shields, **B)** Geochronological Provinces of the Amazonian Craton proposed by Tassinari and Macambira (2004) and location of the study area (Black rectangle).

## 2. Geologic-tectonic framework

The Amazonian Craton (AC) is one of the largest and least known Precambrian areas of the world and the major tectonic unit of the South America. In Brazil, the AC comprises an area of around 4.4 million km$^2$, bordered by to the east by the Araguaia belt, and to the south and southeast by Paraguai belt, both related to Neoproterozoic Brasiliano Orogeny (900-540 Ma) (Almeida et al., 2000) (**Fig. 1B**).

The southeast region of the Guiana Shield is contained in one of the largest orogenic Paleoproterozoic belts in Earth's crust, with a tectonic evolution related to the so-called Transamazonian Orogenic Cycle (2.26-1.95 Ga). The southeastern portion of the Guiana Shield is enclosed in the Maroni-Itacaiúnas Province, within the AC evolutionary model that involves an extensive Archean continental crust core surrounded by mobile belts of Paleo- and Mesoproterozoic ages (Tassinari and Macambira, 1999, 2004; Tassinari et al., 2000; Avelar et al., 2003) **(Fig. 1B)**. The

Maroni-Itacaiúnas Province surrounds the Central Amazonian Province as a wide strip at the north-northeast edge of the AC, having evolved during the Transamazonian Orogeny (2.26-1.95 Ga) (Tassinari et al., 2000; Avelar et al., 2003; Delor et al., 2003a; Rosa-Costa et al., 2003, 2006; Tavares, 2009; Barreto et al., 2013).

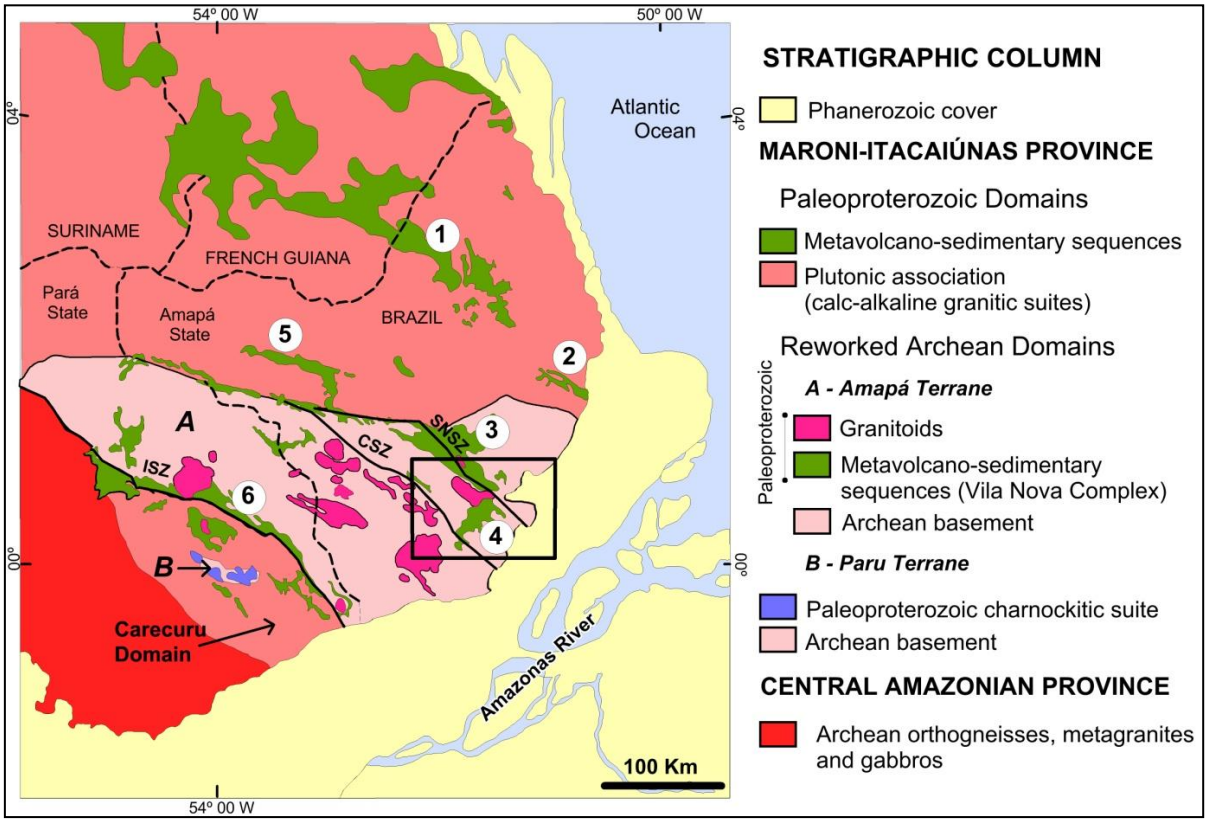


**Figure 2.** Archean and Paleoproterozoic tectonic-geochronological domains of the southeastern portion of the Guiana Shield, modified after Rosa-Costa et al. (2006). The geochronological provinces are according to Tassinari and Macambira (2004). The area of Vila Nova and Serra do Navio greenstone belts and the geological map of the Figure 3 is highlighted on the black square. Main greenstone belts: 1- Lombarda, 2- Tartarugalzinho, 3- Serra do Navio, 4- Vila Nova, 5- Tumucumaque and 6- Ipitinga. Shear zones: SNSZ: Serra do Navio, CSZ: Cupixi, ISZ: Ipitinga.

The polycyclic basement in northern portion of the AC contains two major crustal segments, characterized by Archean and Paleoproterozoic units, respectively. The integration shows the wide Archean core domain made of orthogneisses, metagranites and gabbros, which are separated by thin belts of metavolcano-sedimentary rocks. Large intrusive granitic bodies cross-cut all former units. For a more accurate geologic evaluation of the Vila Nova area, regional maps were

recompiled and integrated to the interpretation of magnetometric data (total count and analytical signal) and gammaspectrometric data, associated to structural, petrographic and geochronological data.

The geology of the Amapá state can be divided into two areas: the northern one, dominated by Paleoproterozoic orthogneisses, metavolcano-sedimentary complexes and intrusive granites, and the southern-central portion, dominated by Archean rocks reworked during the Transamazonian Orogeny (Avelar et al., 2003; Rosa Costa et al., 2003, 2006) **(Fig. 2)**. The orthogneisses and granitoids of the northern Amapá area and the border with French Guiana are primarily related to the Neo-rhyacian evolution of the Transamazonian Orogeny, as demonstrated by U-Pb data in titanite and zircon, and by Pb-Pb zircon geochronology (Avelar et al., 2002, 2003; Delor et al., 2003a) **(Table 1)**. Remnants of Archean crust were first recorded by Pb-Pb evaporation (3.2-2.7 Ga) in detrital zircons from metasedimentary rocks, in inherited zircons (2.6-2.9 Ga) and also by Sm-Nd $T_{DM}$ model ages (2.75 to 2.39 Ga) of the Ryacian orthogneisses and granitoids (Lafon et al., 2000; Avelar et al., 2002, 2003). For the Amapá southern-central portion, Rosa Costa et al. (2003, 2006) obtained Pb-Pb zircon ages of 3.48 Ga for the tonalitic gneiss of the Tartarugalzinho region. Pimentel et al. (2002) obtained whole-rock Sm-Nd $T_{DM}$ model ages of 3.3 Ga for the orthogneisses of the Tumucumaque Complex in Vila Nova area. In addition, a tonalitic gneiss yielded a Paleo-archean Pb-Pb zircon age of 3.3 Ga (Klein et al., 2003) **(Table 1)**.

| STRATIGRAPHIC UNITS | ROCK TYPE | Pb-Pb or U-Pb (Zircon) | $T_{DM}$ (Sm-Nd WR) | References |
|---|---|---|---|---|
| **PALEOPROTEROZOIC LATE-OROGENIC TO ANOROGENIC GRANITES (1.99-1.84 Ga)** | | | | |
| **Porto Grande Granite** | Syenogran./monzogran. | 1.842 ±23 Ma[a] | | Barbosa et al. (2013) |
| **Amapari Granite** | Alkali-feldspar granite | 1.993 ±13 Ma[a] | | Faraco et al. (2004) |
| **Late-orogenic volcanic French Guiana (Uatumã)** | Acid volcanic rock | 1.96 Ga | | Delor et al. (2003a) |
| **Late orogenic granite French Guiana** | Biotite granite | 2.01 Ga | | Delor et al. (2003a) |
| **PALEOPROTEROZOIC COLLISIONAL GRANITES (2.11-2.03 Ga)** | | | | |
| **Undifferentiated granitoids** | Biotite monzogranite | | 2.9 Ga | Rosa-Costa et al. (2012) |
| | Biotite monzogranite | | 2.2 Ga | Barreto et al. (2013) |
| | Tonalite | 2.184 ±13 Ma[b] | | Barreto et al. (2013) |
| | Charnockitic granulites | 2.065 ±5 Ma[a] | | Barreto et al. (2013) |
| | Biotite monzogranite | 2.124 ±21 Ma[a] | | Barreto et al. (2013) |
| | Tonalite | 2.160 ±130 Ma[b] | 2.34-2.24 Ga | Nogueira et al. (2000) |
| **Peraluminous granite** | Two mica granite | 2.030 ±2 Ma[a] | | Rosa-Costa et al. (2006) |
| **Parintins Suite** | Monzogranite | 2.053 ±4 Ma[a] | | Rosa-Costa et al. (2006) |
| **Igarapé Careta Suite (Cupixi Domain)** | Syenogranite | 2.065 ±35 Ma[a] | | Barbosa et al. (2013) |
| **Carrapatinho Granite** | Monzogran./syenogranite | 2.025 ±17 Ma[a] | | Barbosa et al. (2013) |
| | Monzogran./syenogranite | 2.08-2.02 | 2.66 Ga | Barreto et al. (2013) |
| | Monzogran./syenogranite | | 3.68 Ga | Rosa-Costa et al. (2012) |
| **Sucuriju Metagranite (Cupixi Domain)** | Monzogranite | 2.08-2.02 Ga[a] | | Barreto et al. (2013) |
| | Monzogran./syenogranite | | 3.0-2.88 Ga | Barreto et al. (2013) |
| | Monzogran./syenogranite | | 2.59 Ga | Rosa-Costa et al. (2012) |
| **Igarapé Urucu Suite (Cupixi Domain)** | Charnockite | 2.074 ±5 Ma[a] | | Rosa-Costa et al. (2006) |
| **Tartarugal Grande Complex** | Enderbitic to charnockitic | 2.125.±4 Ma[a] | 3.29-2.25 Ga[c] | Rosa-Costa et al. (2012) |
| | Granulites | 2.065 ±5 Ma[a] | | Rosa-Costa et al. (2012) |
| | Granulitic gneiss | 2.580 ±5 Ma[a] | | Avelar et al. (2003) |
| **Araguari Complex** | Tonalite | 2.103 ±3 Ma[a] | 2.64-2.52 Ga | Barreto et al. (2013) |
| | Tonalite | 2.096 ±4 Ma[a] | 2.97-2.47 Ga | Barreto et al. (2013) |
| | Tonalite/granodiorite | | 2.64-2.52 Ga | Rosa-Costa et al. (2012) |
| | Tonalite/granodiorite | | 2.97-2.47 Ga | Rosa-Costa et al. (2012) |
| **Undifferentiated granitoids of French Guiana (TTG Complex) (D2 thermotectonic event)** | Monzogranite | 2.060 ±4 Ma[e] | | Delor et al. (2003a) |
| | Migmatite | 2.094 ±7 Ma[e] | | |
| | Granite | 2.112 ±2 Ma[e] | | |
| | Granite | 2.089 ±4 Ma[e] | | |
| | Monzogranite | 2.092 ±4 Ma[e] | | |
| | Granite | 2.100 ±1 Ma[e] | | |
| | Granite | 2.104 ±2 Ma[e] | | |
| | Granodiorite | 2.104 ±2 Ma[e] | | |
| | Granite | 2.069 ±4 Ma[e] | | |
| **PALEOPROTEROZOIC ARC RELATED GRANITES (2.26-2.13 Ga)** | | | | |
| **Ananaí Complex (Paru Domain)** | Throndjemitic gneiss | 2.150 ±2 Ma[a] | 2,32 Ga | Rosa-Costa et al. (2006) |
| **Flexal Suite (Cupixi Domain)** | Tonalite | 2.197 ±3 Ma[a] | | Rosa-Costa et al. (2012) |
| | Granodiorite | 2.184 ±13 Ma[b] | | Rosa-Costa et al. (2012) |
| | Monzogranite | 2.181 ±2 Ma[a] | | Avelar (2002) |
| | Monzogranite | | 2.61 Ga | Avelar (2002) |
| | Monzogranite | | 2.75-2.39 Ga | Avelar (2002) |
| | Monzogranite | | 2.73-2.37 Ga | Rosa-Costa et al. (2012) |
| **Undifferentiated granitoids of French Guiana (TTG Complex) (D1 thermotectonic event)** | Gabbro | 2.208 ±12 Ma[e] | | Delor et al. (2003a) |
| | Granodiorite | 2.155 ±3 Ma[e] | | |
| | Tonalite | 2.173 ±9 Ma[e] | | |
| | Granodiorite | 2.183 ±3 Ma[a] | | |
| | Diorite | 2.161 ±3 Ma[a] | | |
| | Tonalite | 2.160 ±6 Ma[a] | | |
| | Granite | 2.163 ±3 Ma[a] | | |
| | Tonalite | 2.172 ±2 Ma[a] | | |
| | Granite | 2.165 ±6 Ma[a] | | |
| | Tonalite | 2.141 ±8 Ma[a] | | |
| | Meta-andesite | 2.137 ±6 Ma[a] | | |
| | Granite | 2.132 ±3 Ma[a] | | |

| STRATIGRAPHIC UNITS | ROCK TYPE | Pb-Pb or U-Pb (Zircon) | $T_{DM}$ (Sm-Nd WR) | References |
|---|---|---|---|---|
| **Rio Santo Antônio** | Tonalite | 2.262 ±2 Ma[a] | | Barreto et al. (2013) |
| **Diorite** | Hb qz-diorite | | 2.68 Ga | Barreto et al. (2013) |
| **Undifferentiated granitoids of Jari Domain** | Syenogranite | 2.098 ±2 Ma[a] | | Rosa-Costa et al. (2006) |
| | Monzogranite | 2.177 ±3 Ma[a] | | Rosa-Costa et al. (2006) |
| | Alkali-feldspar granite | 2.146 ±3 Ma[a] | | Rosa-Costa et al. (2003) |
| | TTG gneiss | 2.150 ±1 Ma[a] | | Rosa-Costa et al. (2003) |
| | Diorite | 2.140 ±1 Ma[a] | | Rosa-Costa et al. (2003) |
| | Monzogranite | 2.185 ±4 Ma[b] | | Rosa-Costa et al. (2006) |
| | Monzogranite | 2.218 ±3 Ma[b] | | Rosa-Costa et al. (2006) |
| **Carecuru Suite** | Diorite | 2.139 ±2 Ma[a] | | Rosa-Costa et al. (2006) |
| **Paru-Maratiá Complex** | Granodioritic gneiss | 2.191 ±2 Ma[a] | | Rosa-Costa et al. (2006) |
| **Granitoids intrusive in the Vila Nova Complex (Cupixi Domain)** | Granodiorite | 2.23 Ga[a] | | Tavares (2009) |
| | Monzogranite | 2.23 Ga[a] | | Tavares (2009) |
| | Monzogranite | 2.25 Ga[a] | | Tavares (2009) |
| | Granodior./monzogranite | | 2.83-2.24 Ga | Tavares (2009) |
| **Bacuri Mafic-ultramafic Complex** | Mafic and ultramafic rocks | | 2.218 ±120 Ma[c] | Pimentel et al. (2002) |
| **PALEOPROTEROZOIC GREENSTONE BELTS (2.26-2.08 Ga)** | | | | |
| **Ipitinga Group (Jari Domain)** | Amphibol./actinol. schist | | 2.267 ±66 Ma[c] | Mc Reath and Faraco (2006) |
| **Vila Nova Complex (Cupixi Domain)** | Metapelite | | 2.087 ±22 Ma[d] | Pimentel et al. (2002) |
| | Amphibolite/actin. schist | | 3.03-2.85 Ga | Rosa-Costa et al. (2006) |
| | Metandesite | 2.154 ±6 Ma[b] | | Hoffmann et al. (2018) |
| | Metandesite | 2.170 ±9 Ma[b] | | This work |
| | Metaconglomerate | 3.6-2.4 Ga[b] | | This work |
| | Quarzite | 3.6-2.7 Ga[b] | | This work |
| **ARCHEAN BASEMENT ROCKS (2.85-2.58 Ga)** | | | | |
| **Riozinho Granite (Jari Domain)** | Monzogranite | 2.626 ±5 Ma[b] | 3.03 Ga[c] | Rosa-Costa et al. (2006) |
| **Noucouru Intrusive Suite (Jari Domain)** | Mesopertite granite | 2.656 ±4 Ma[a] | | Rosa-Costa et al. (2006) |
| | Mesopertite granite | 2.649 ±2 Ma[a] | | Rosa-Costa et al. (2006) |
| **Anauerapucu Granite (Jari Domain)** | Monzogranite | 2.791 ±23 Ma[a] | | Rosa-Costa et al. (2012) |
| **Paru Granulitic Nucleus** | Enderbitic gneiss | 2.597 ±4 Ma[a] | | Rosa-Costa et al. (2003) |
| **Guianense Complex (Jari Domain)** | Granulite | 2.580 ±5 Ma[a] | | Avelar et al. (2003) |
| | Granodioritic gneiss | 2.652 ±4 Ma[a] | | Rosa-Costa et al. (2003) |
| | Charnockite | 2.605 ±6 Ma[a] | | Ricci et al. (2002) |
| | Monzogranitic gneiss | 2.628 ±2 Ma[a] | | Rosa-Costa et al. (2006) |
| | Tonalitic orthogneiss | | 2.96-2.94 Ga | Avelar et al. (2003) |
| | Orthogneiss | | 3.12-2.83 Ga | Rosa-Costa et al. (2006) |
| | Orthogneiss | 2.656 ±4 Ma[a] | 3.15- 3.01 Ga | Rosa-Costa et al. (2012) |
| | Orthogneiss | 2.605 ±3 Ma[a] | | Rosa-Costa et al. (2006) |
| **Jari-Guaribas Complex (Jari Domain)** | Orthogranulites | 2.797 ±3 Ma[a] | | Rosa-Costa et al. (2012) |
| | Enderbitic gneiss | 2.788 ±2 Ma[a] | 3.26-3.19 Ga | Rosa-Costa et al. (2006) |
| | Enderbitic gneiss | 2.790 ±8 Ma[a] | | Rosa-Costa et al. (2006) |
| | Enderbitic gneiss | 3.238 ±6 Ma[a] | | Rosa-Costa et al. (2006) |
| **Mungubas Granite (Cupixi Domain)** | Monzogranite | 2.661 ±9 Ma[a] | | Barreto et al. (2013) |
| **Tumucumaque Complex (Cupixi Domain)** | Gneisses | | 3.36-3.07 Ga[d] | Pimentel et al. (2002) |
| | Tonalitic gneiss | 2.849 ±6 Ma[a] | | Avelar et al. (2003) |
| | Tonalitic gneiss | 2.844 ±2 Ma[a] | | Avelar et al. (2003) |
| | Tonalitic gneiss | 2.851 ±37 Ma[b] | | Borghetti et al. (2018) |
| | Granodioritic gneiss | 2.852 ±32 Ma[b] | | Borghetti et al. (2018) |
| | Metagranodiorite | 2.822 ±33 Ma[b] | | Borghetti et al. (2018) |
| | Metagranodiorite | 2.812 ±17 Ma[b] | | Borghetti et al. (2018) |
| | Gabbro | 2.671 ±46 Ma[b] | | Borghetti et al. (2018) |

**Table 1.** Summary of the isotopic data of the basement units and greenstone belts of Vila Nova and Serra do Navio regions. Key to abbreviations: WR - whole rock, [a] $^{207}Pb/^{206}Pb$ zircon evaporation, [b] U-Pb zircon LA-MC-ICPMS, [c] Sm-Nd whole rock isochron, [d] Sm-Nd whole rock garnet isochron and [e] U-Pb zircon SHRIMP.

In the southwestern region of the Amapá, the U-Pb and Pb-Pb zircon ages of the orthogneisses and metagranites of the Tumucumaque, Jari-Guaribas and Guianense complexes presented ages between the 2.85 and 2.64 Ga, confirming the existence of a wide area of Archean basement in this region (Rosa Costa et al., 2006; Borghetti et al., 2018). This old continental fragment was named Amapá Block by Rosa-Costa et al. (2006), bounded to the south by a Paleoproterozoic magmatic arc that takes place in the Carecuru Domain **(Fig. 2)**. The northern boundary of this block is marked by elongated metavolcano-sedimentary sequences of the Serra do Navio and Vila Nova greenstone belts and by granitic rocks associated. Table 1 shows a summary of the published isotopic data of the basement and of the two greenstone belts.

The basement of the Vila Nova greenstone belt (VNGB) is made up of orthogneisses, metagranodiorites and undeformed gabbros from the Tumucumaque Complex (TC) and by the stratiform metamafic to ultramafic rocks of the Bacuri Complex. The TC is the oldest and predominant unit and occurs as elongated domes in NW-SE and E-W directions. This basement is surrounded by deformed belts of metavolcano-sedimentary rocks of the VNGB. **(Fig. 3).**

The complex is represented by tonalitic, granodioritic and dioritic gneisses with subordinate occurrence of elongate amphibolite bodies, concordant with the regional gneissic banding. The gneisses shows foliated to banded structure, defined by millimeter thick, irregular and discontinuous biotite and/or hornblende levels. Tonalitic to granodioritic gneiss is clear gray in color and has medium to coarse blastoequigranular texture (2 to 8 mm), permeated by a medium (0.2 to 0.5 mm) inequigranular granoblastic texture. Amphibolites have black color, are composed by hornblende and plagioclase and present a foliated structure defined by a medium nematoblastic texture. These rocks register intermediate amphibolite facies

metamorphic conditions. The intrusive gabbros constitute elongate bodies of 100 to 1.500 meters long, concordant with the regional structure and particularly occur along of the Vila Nova Shear Zone **(Fig. 4)**. It is massive; with equigranular medium- to coarse-grained texture (2-6 mm) characterized by plagioclase and augite crystals, with magnetite as the main accessory mineral.

The Bacuri Mafic-Ultramafic Complex (BMUC) is an elongate body in the N80°E direction, located south of the Vila Nova village. The rocks of this complex intrude the Tumucumaque gneisses and have a tectonic contact with the metasediments of the VNGB. The BMUC is composed of amphibolites, serpentinites, tremolitites and chromitites, which are metamorphosed and complexly deformed as a result of refolding and faulting. Primary structures and textures are occasionally preserved in low-strain zones. The mineral assemblage that characterizes the mafic rocks is made up of diopside, hornblende, plagioclase and biotite and defines conditions of intermediate to upper amphibolite facies metamorphism. The stratiform nature of BMUC is defined by the magmatic banding and cumulate textures, associated to the chemical and textural characteristics of the chromitite (Spier and Ferreira Filho, 1999).

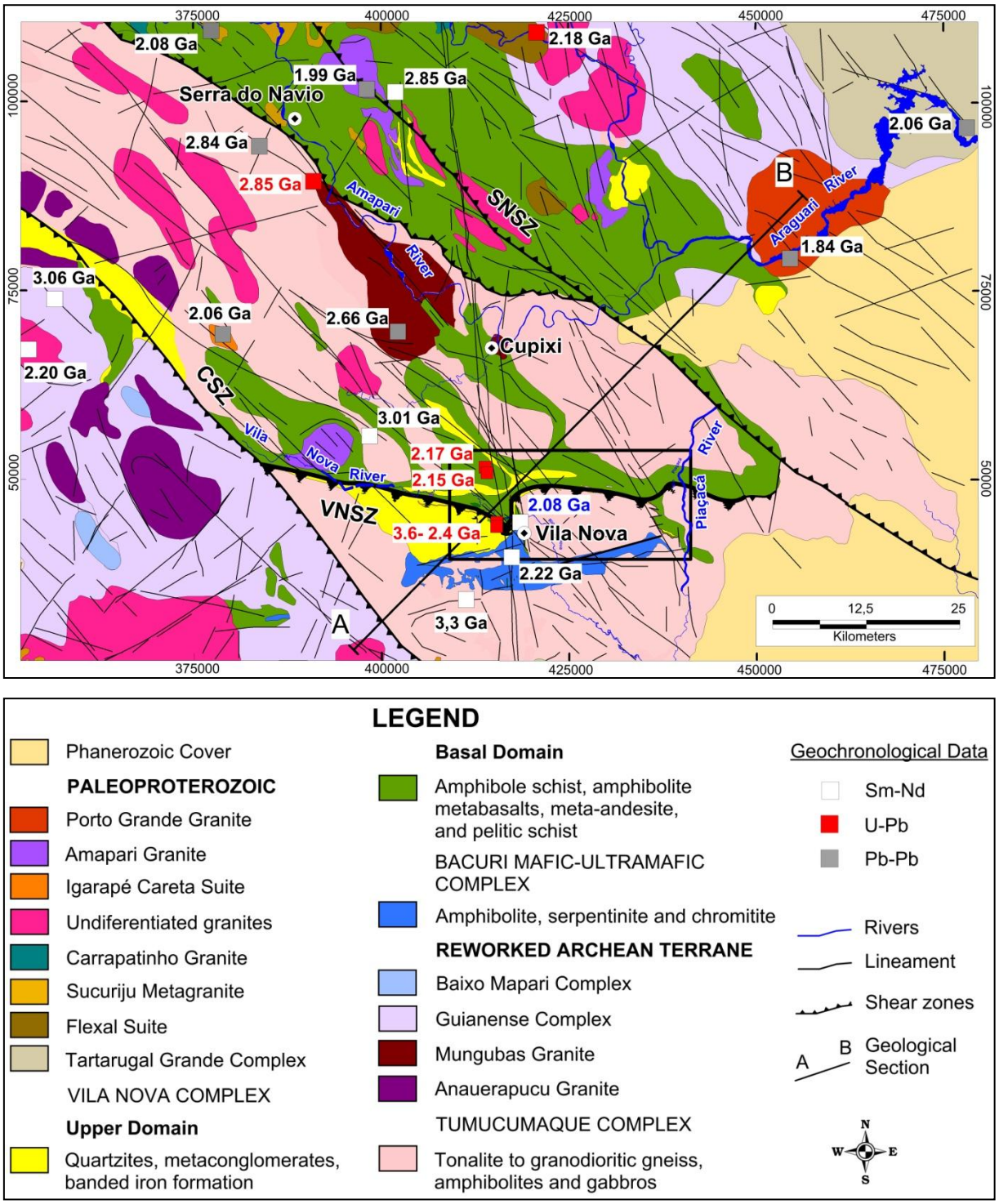


**Figure 3.** Geological map of the Vila Nova and Cupixi region, showing the Serra do Navio and Vila Nova greenstone belts. The study area is marked by the black rectangle. Geochronological compilation highligths the crystallization ages in black and the metamorphic ages in blue. The new radiometric data from this study is labeled in red. Interpretation and structural data modified from Faraco et al. (2004), Magalhães (2007) and Barbosa et al. (2013). Shear zones: SNSZ: Serra do Navio, CSZ: Cupixi, ISZ: Ipitinga.

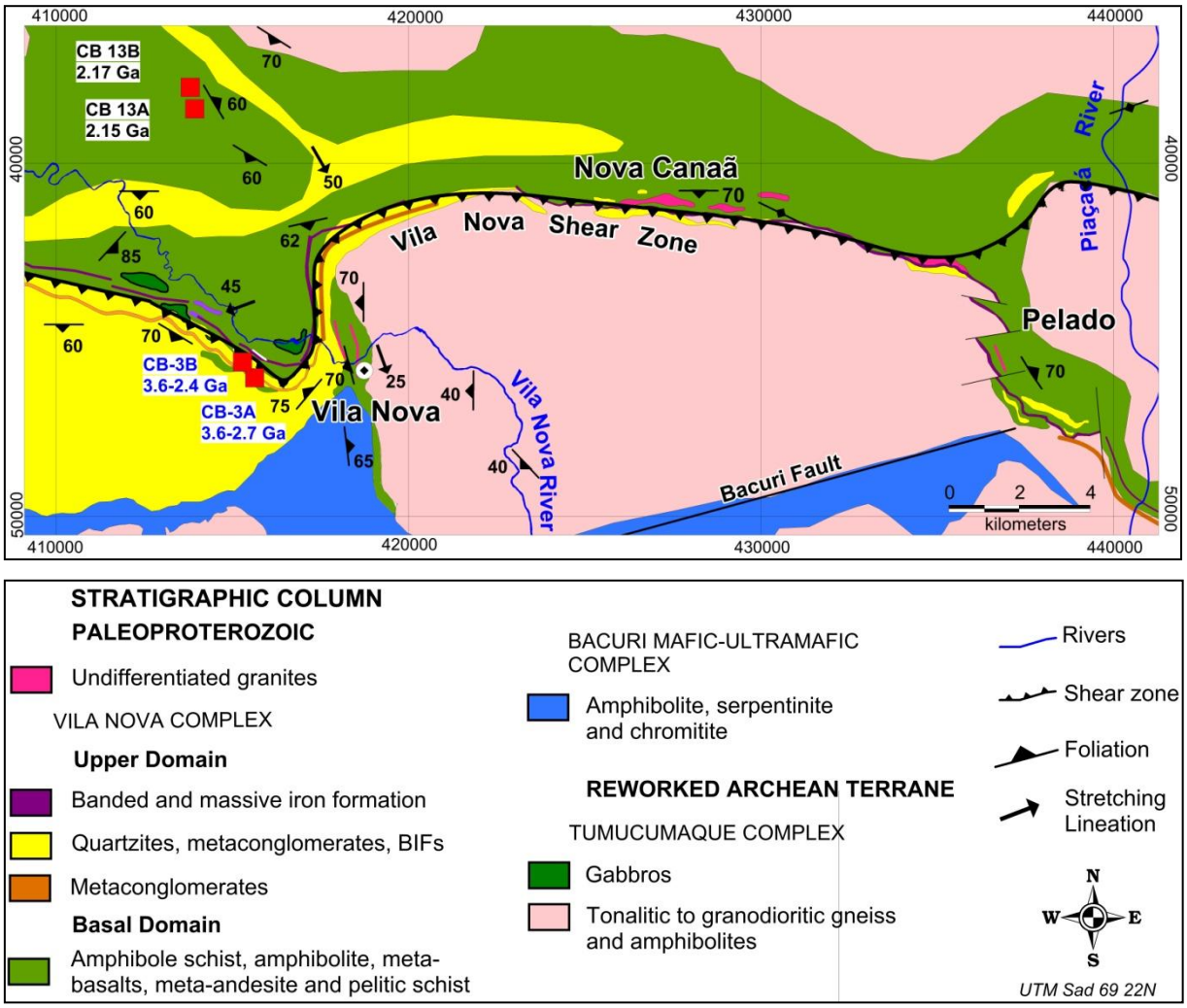


**Figure 4.** Geological map of the study area including Vila Nova, Nova Canaã and Pelado subareas. Red dots show the location of the sampled points for U-Pb crystallization age determinations in zircon (black labels) and U-Pb age determinations in detrital zircons (blue labels). CB-13A U-Pb zircon age obtained by Hoffmann et al. (2018).

The VNGB is a metavolcano-sedimentary complex overlaying the Tumucumaque and the Bacuri complexes, and is intruded by Paleoproterozoic granitoids **(Fig. 3)**. The VNGB consists of basic to intermediate metavolcanic rocks, clastic metasediments and chemical-exhalative rocks. These units were metamorphosed at greenschist to intermediate amphibolite facies conditions, and under intermediate pressure (Rosa-Costa et al., 2003, 2006; Mc Reath and Faraco, 2006; Hoffmann et al., 2018). The geochemical data presented by Hoffmann et al. (2018) indicate that the metabasites of the VNGB comprise Fe-tholeiites and Mg-tholeiites with komatiitic affinity, with compositions enriched in LILE and REE and

depleted in HFSE (with negative Nb, Ti and P anomalies) and MORB-like REE patterns. The authors obtained the U-Pb age of 2.15 Ga for a meta-andesite of the Vila Nova region, establishing the Rhyacian period as the maximum deposition age of the basin. The observed features indicate magmatism related to back-arc basins and island arcs.

The intrusive granites occur as elongate bodies, oriented according to regional metamorphic foliation of E-W direction. It can be well delineated in gammaspectrometric images. They include biotite monzogranites and syenogranites and foliated leucomonzogranites. The granites are white to light pink in color and have equigranular hypidiomorphic texture, and are locally mylonitized.

This dominantly metavolcano-sedimentary sequence and the associated granites comprise belts that form part of a Maroni-Itacaiúnas Province, predominantly of Rhyacian age. This province extends from the Guyana Shield of to the West Africa Craton and his evolution occurred in stages, with an activity peak around 2.26 to 2.2 Ga, decreasing after 2.11 Ga (Delor et al., 2003a; Avelar et al., 2003; Velasquez et al., 2011). The last authors proposed a crustal evolution model characterized by two main events. The first one is related to the development of young arcs, and the second one is related to the formation of more mature arcs involving the reworking of an ancient continental crust. These units are characterized by metavolcano-sedimentary complexes and TTG-type granitic associations, and register an orogenic metamorphism of intermediate pressure and low to medium grade, between greenschist and amphibolite facies (Avelar et al., 2003; Delor et al., 2003a; Rosa-Costa et al., 2003, 2006; Velasquez et al., 2011; Hoffmann et al., 2018). Most authors suggest that subsequent deformation of transcurrent nature was responsible for the current structure of the belts (Avelar et al., 2003; Delor et al., 2003a,b; Mc Reath and Faraco, 2006). Due to the strong structural control, most metasedimentary

rocks display a steep foliation, whereas banded iron formations present a complex pattern of folds, due to the more plastic behavior during the deformation.

The Phanerozoic cover includes pelitic, ferruginous sandstones and conglomeratic sandstones deposited in a fluvial and estuarine environment, and sandy-clay to sandy-conglomeratic friable sediments associated with fluvial systems.

### *2.1 Geology of the Vila Nova greenstone belt (VNGB)*

The VNGB occurs as a deformed belt in the E-W direction, with several subordinate bodies elongated in the N40-50$^{o}$W direction, interconnected on its southern portion by the Vila Nova Shear Zone (VNSZ) **(Fig. 3)**. The VNSZ is an E-W trending ductile shear zone and represents a thrust fault with top movement in the north direction. This shear zone defines the contact of the VNGB with the basement rocks of the TC to the south. The geologic features were partially observed in the field and also inferred from the interpretation of airborne geophysical data (magnetometric and gammaspectrometric). On the western portion of the area, this shear zone defines the contact between the main mafic metavolcanic and metasedimentary rock packages **(Fig. 4)**.

The VNGB has been divided into two lithological domains. The Basal Domain is defined by the predominance of metavolcanic rocks, which are interlayered with mica schists, lenses of marble, calc-silicate and graphite schists. The Upper Domain is composed of clastic metasediments, interspersed with the mafic and felsic metavolcanics and subordinate exhalative chemical rocks. A schematic stratigraphic section of the VNGB based on field and drill core data is shown in **figure 5**. In comparison to other units of the greenstone belt occurring in Pelado and Nova Canaã localities, there is great similarity and continuity of the outcrops of the Vila Nova units to the east of the study area **(Fig. 6)**.

The *Basal Domain* extending in the E-W direction for about 50 km from Vila Nova, crossing the localities of Nova Canaã and Pelado, between the Vila Nova and Piaçacá rivers **(Figs. 4 and 5)**. Metamafic rocks are represented mainly by biotite-amphibole schists and amphibolites. Metabasalts, meta-andesites and metadacites are subordinate. Associated with the mafic rocks there are small metaultramafite and marble lenses. Mafic cornubianites are also recognized as products of thermal metamorphism associated with intrusive Paleoproterozoic granites.

Amphibole schists are dark green, containing mainly tremolite and hornblende, and their structure is defined by the orientation of amphibole, biotite and chlorite. Accessory minerals are biotite, clinochlore, chlorite, titanite and magnetite. The amphibolites present a dark-gray to greenish color and foliated structure defined by the orientation of hornblende. The mineral composition is mainly hornblende and plagioclase, with biotite, titanite, magnetite, epidote, quartz and chlorite as accessory minerals. Metabasalts were recognized from the observation of plagioclase phenocryst relicts in blastoporphyritic arrangement, and from the common occurrence of a blastoamygdaloidal texture defined by circular to elliptical quartz aggregates.

Mafic cornubianites correspond to a small fraction of the analyzed metavolcanics. Their composition varies from hornblende hornfels to tremolite-diopside-hornblende hornfels. Acicular texture predominates in both compositions. Epidote and carbonates occur in millimeter-thick veins as a product of alteration of amphibole and biotite.

Metaultramafic rocks are represented by tremolite schist and actinolite-tremolite schist of light grey to green color and fine-grained schistosity. They consist of tremolite, actinolite and clinochlore, with rare plagioclase and magnetite as accessory minerals.

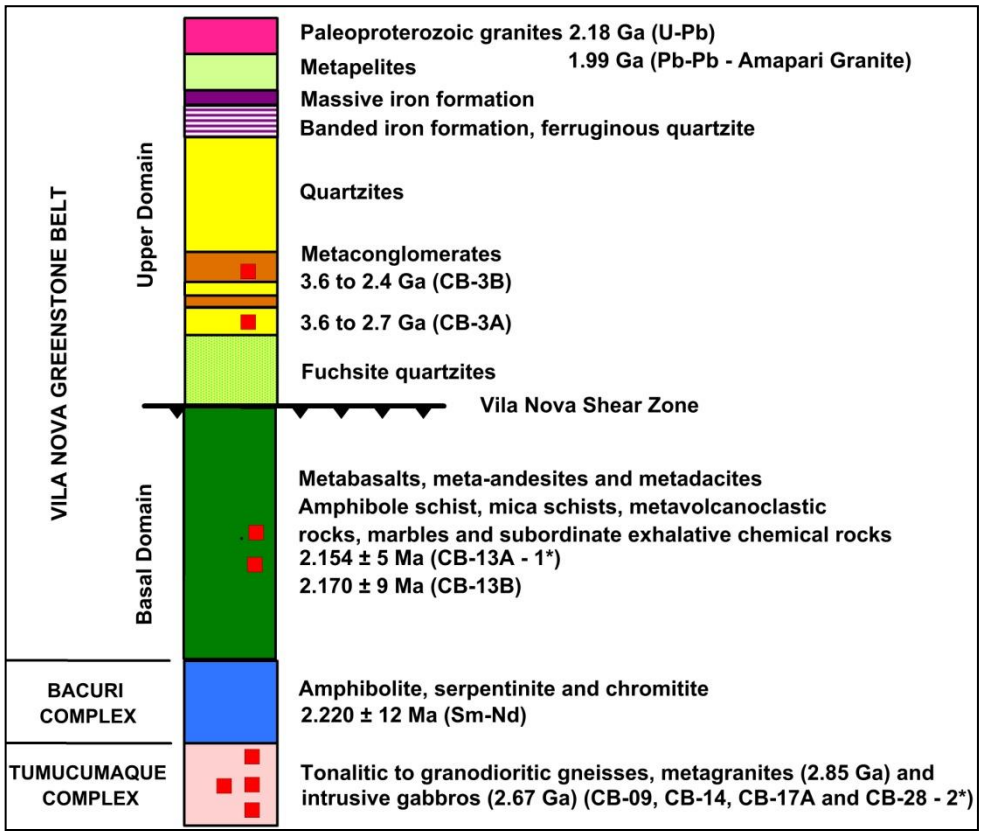


**Figure 5.** Schematic stratigraphic profile of the Vila Nova greenstone belt and basement rocks based on field and drilling holes data with the location of the analyzed samples (red symbols). 1* Result of CB-13A from Hoffmann et al. (2018), 2* Results of CB-09, CB-14, CB-17A and CB-28 from Borghetti et al. (2018).

Lenses of marble and calc-silicate schist occur intercalated between the basal and upper units mainly along the E-W structure of the VNSZ. They present light gray to white color and are composed of carbonates and in a smaller proportion, tremolite and biotite.

The *Upper Domain*, composed of clastic metasedimentary rocks, is restricted to the western portion of the area, occurring as three elongate bodies interspersed with the metavolcanic rocks, and are deformed and folded along major regional structures **(Figs. 4 and 5)**. The metasedimentary rocks include quartzite, ferruginous quartzite, metaconglomerates, fuchsite-quartz schist and mica schists, while the chemical rocks include calc-silicate schist and banded iron formations (BIF), such as hematite phyllites and hematite schists.

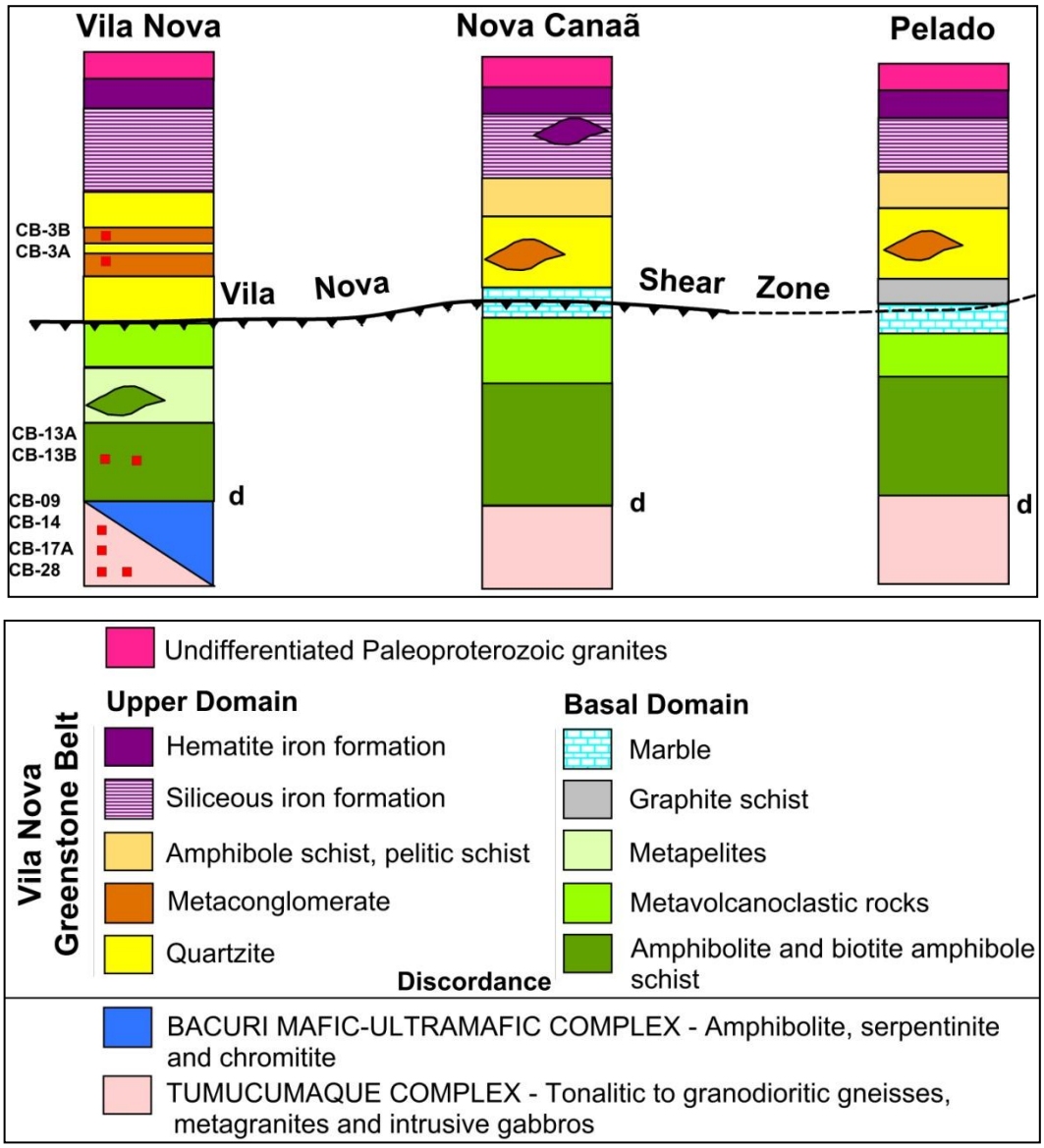


**Figure 6.** Comparative stratigraphic profiles between the VNGB units occurring in the Vila Nova, Pelado and Nova Canaã areas (see map of Fig.4). The stratigraphic sections were made based on the integration of field data with drilling holes.

Metaconglomerates occur as continuous 2- to 20-meter lenses, associated with quartzites. Two types of metaconglomerates were identified. The basal, unconformably overlying layer of metaconglomeratic schistose quartzite is 6- to 12-meter thick. It is an immature, poorly selected, matrix-supported and polymictic rock, displaying a light gray to white color, composed of rounded pebbles of quartz veins and quartzite with an average diameter of 5 to 10 cm **(Fig. 7A)**. Pebbles of mica schist and mafic-ultramafic rocks are frequent at the base. The matrix constitutes 40 to 45% of the rock volume and is formed by quartz, with subordinate contents of

feldspar and white mica. The common accessories are fuchsite and black tourmaline (schorlite) with rare chromite. The upper metaconglomerate is a centimeter to meter-sized continuous layer, interlayered with a sequence of medium- to coarse-grained quartzite. It is predominantly composed of well selected pebbles of quartz and quartzite, with an average diameter of 5 cm, supported by a sandy matrix composed of 0.05 mm- to 0.1 mm quartz and magnetite. The accessory minerals are muscovite, fuchsite, biotite, chlorite, epidote and titanite.

The bedding ($S_0$) is marked by continuous layers showing grain-size and compositional variations, which may possibly define an erosive surface, that grades to discontinuous and irregular 0.03 mm- to 0.06 mm-thick, fuchsite-rich layers. When close to the VNSZ the metaconglomerates are deformed and present a mylonitic structure with stretched quartz pebbles involved by a matrix rich in fuchsite and tourmaline **(Figs. 7B and 7C)**.

The quartzites are distributed throughout the area, the most representative one occurring in the western region of Vila Nova, and consisting of a basal and an upper unit. The basal unit comprises a thick, monotonous sequence of “clean”, mature, well sorted, coarse-grained quartz-arenites showing cross-bedding. Thin oligomictic basal layers of quartz veins pebbles are occasionally found. These quartzites have foresets marked by green aggregates of fuchsite (chromium-rich white mica), possibly related to chromite derived from the Bacuri Complex ultramafic rocks **(Fig. 7D)**. The upper quartzite unit is white to light grey in color and shows a massive to foliated structure. It grades from a fine- to medium-grained equigranular meta-arenite to a very coarse-grained lithic meta-arenite. The latter comprises a thick, monotonous sequence of submature, moderately sorted, cross-bedded meta-arenites. Lower concentrations of magnetite, zircon and fuchsite occur in the foresets.

The pelitic schists are dark brown and their well-defined schistosity is defined by the orientation of muscovite and biotite. The schists are composed of muscovite, biotite, quartz and garnet, and locally contain cordierite porphyroblasts. $S_0$ is defined by compositional banding characterized by continuous, interlaying mica-rich and quartz-rich levels.

Metamorphosed chemical sedimentary rocks are composed by ferruginous quartzite (metachert), hematite schists and hematite phyllites. The ferruginous quartzite is foliated, and shows a fine- to medium-grained granoblastic equigranular texture and discontinuous, muscovite-rich lenses, interlayered with centimeter-thick bands composed of mica, magnetite and amphibole (grunerite). These bands may represent an exhalative chert.

The banded iron formation consists of hematite and specularite-type schist forming elongate crests and defining an E-W oriented macrostructure **(Figs. 7E and 7F)**. In the Vila Nova region, the banded iron formation was divided into two types: (i) Massive Iron Formation (MIF), composed predominantly of hematite and magnetite, and fine- to medium-grained, foliated, showing strong magnetism in less weathered areas; (ii) Siliceous Iron Formation (SIF), with banded structure defined by gray beds composed of hematite and magnetite, interspersed with white-colored layers composed of quartz, showing moderate magnetism in the least weathered zones. Along the ferriferous formations, continuous lenses of foliated metapelites occur. They are composed of amphibole, biotite, chlorite and magnetite, showing moderate to weak magnetism. These rocks grade to gray to red quartz-chlorite-sericite schist, amphibole-quartz-muscovite schist containing oblique ferruginous laminae or bands, and muscovite-chlorite schist.

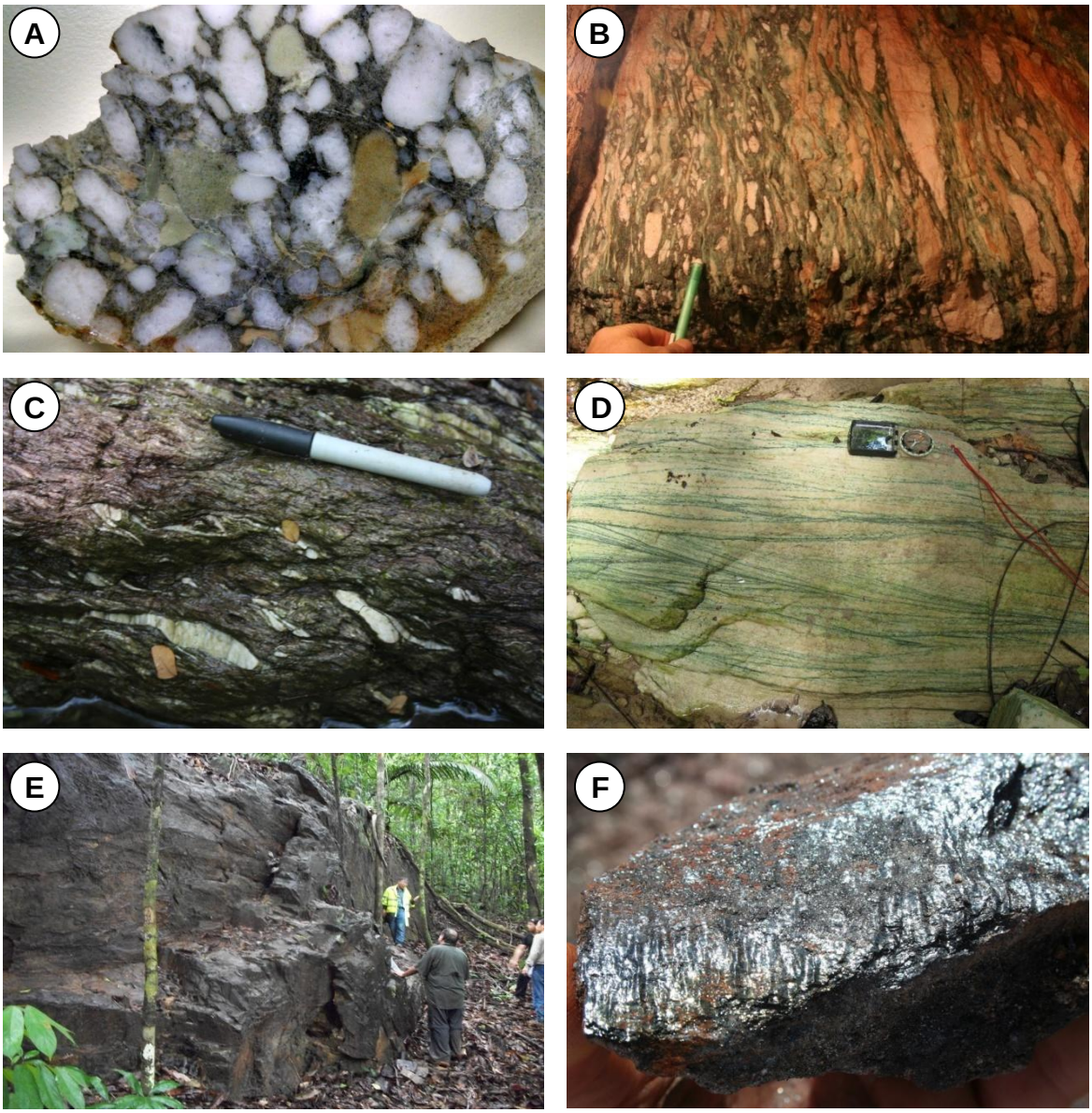


**Figure 7.** Structural aspects of the rocks of Vila Nova greenstone belt. **A)** Metaconglomerate with rounded pebble of quartz veins (white) and quartzite (grey and orange), **B)** Mylonitic metaconglomerate within Vila Nova Shear Zone with stretched pebbles involved by matrix rich in fuchsite and tourmaline (schorlite), **C)** Mylonitic metaconglomerate with stretched quartz vein peebles (white), **D)** Fuchsite quartzite showing tangential and low angle cross-bedding, **E)** Outcrop of massive iron formation and **F)** Hematite schist.

## 3. Analytical Methods

Sampling was based on an integrated analysis of satellite images and airborne geophysical data, which clearly defined the metasedimentary and metavolcanic domains. In addition to the sampling for petrography and geochronological analysis, structural and stratigraphic data were collected to validate satellite and geophysical

interpretation. To investigate the stratigraphy and to improve the geology, a total of 5.000 meters of drilling holes data was described.

Airborne geophysical data (magnetometry and gammaspectrometry) were obtained and processed by the Brazilian Geological Survey (CPRM) through the Rio Araguari (CPRM, 2004) and Amapá (CPRM, 2006) projects. Data collection was established based on parallel flight lines spaced 500 meter apart, and a measurement recorded every 70 meters and 7 meters, respectively. The direction of the acquisition lines of the Rio Araguari project was N45ºW and N-S for the Amapá project. Topographic data were taken from the Shuttle Radar Topography Mission (SRTM) survey, with a spatial resolution of approximately 90 meters in the study region.

The basic processing of the airborne geophysical data used was carried out by CPRM (leveling and micro-leveling), and they were then processed to obtain the products needed for regional interpretation and evaluation. In the execution of this project the following geophysical products were used: (1) Total Magnetic Field (CMT); (2) Analytical Signal Amplitude (ASA), (3) Total Horizontal Gradient (GHT) and (4) First Magnetic Vertical Derivative (1DZ); (5) Anomalous Potassium (Kd), (6) Factor F (F) and (7) Map of the Terrestrial Radiometric Distribution (TER) of the radio elements K, U and Th.

Two samples of metasedimentary rocks from the Upper Domain of the VNGB (CB-03A and CB-03B) were selected to determine the U-Pb zircon ages of detritic provenance. One sample of meta-andesite (CB-13B) from the Basal Domain was selected to determine the U-Pb zircon ages and Lu-Hf composition of the volcanism associated with the basin. The LA-MC-ICPMS method was used for U-Pb and Lu-Hf zircon analysis at the Geochronologic Research Center (CPGEO) of the Geosciences Institute of São Paulo University (USP).

Sample preparation was carried out in the laboratories of the Rio Grande do Sul Federal University (UFRGS). Rock samples were crushed and milled using a mandible crusher and then pulverized. Zircon grains were concentrated by conventional magnetic and heavy liquid techniques. The final concentrate was obtained by handpicking. To avoid any bias, no visual morphological or color differentiation was made. The zircon grains were mounted in epoxy and polished using diamond pastes until half of the grain thickness was exposed, to ensure that all internal oscillatory zoning was visible for further imaging. Backscattered-electron (BSE) and cathodoluminescence (CL) imaging was performed to record internal structures and crystallization phases. Only zircon grains free of imperfections, fractures, and mineral inclusions were selected for isotopic analysis. Cathodoluminescence (CL) images of zircons were obtained using a Quanta 250 FEG electron microscope equipped with Mono CL3+ cathodoluminescence spectroscope (Centaurus) at CPGEO of São Paulo University.

Isotopic data were obtained using a NEPTUNE inductively coupled plasma-mass spectrometer (ICP-MS) coupled with an Excimer laser ablation system (LA). The diameter of laser spots for the zircon U-Pb analyses was 35 to 50 µm. The routine of the U-Pb method consists of the analysis of 2 blanks, 2 NIST standards, 3 external (GJ1) standards, 13 unknown samples, 2 external standards and 2 blanks. The $^{204}$Hg interference on $^{204}$Pb measurements was corrected by $^{202}$Hg, adopting a $^{204}$Hg/$^{202}$Hg ratio of 4.2. The $^{207}$Pb/$^{206}$Pb ratio normalization was achieved by combining NIST and external standards. The $^{206}$Pb/$^{238}$U ratio normalization was achieved by external standards. The GJ1 standard (602 ±4.4 Ma, Elholou et al., 2006) was utilized for mass bias correction. The residual common Pb was corrected according to the measured $^{204}$Pb concentration using the known terrestrial composition (Stacey & Kramers 1975).

The uncertainty introduced by laser-induced fractionation of elements and mass instrumental discrimination was corrected using the zircon reference standard GJ-1 (Jackson et al., 2004). External errors were calculated using error propagation of the individual GJ-1 measurements and measurements of the individual zircon samples (spots). Age calculations were made using Isoplot version 4 and $^{238}U/^{206}Pb$ data (Ludwig, 2008). Chemale et al. (2011) described in detail the analytical methods and data treatment used here. Zircon data were reduced using SQUID (Ludwig, 2002). Data were plotted on weighted average and Concordia diagrams using ISOPLOT/Ex software (Ludwig, 1999); error ellipses on Concordia plots are shown at the 95% confidence level (2σ). The analytical uncertainty in all grouped age data is quoted at the 95% confidence level (2σ).

Hf isotopic measurements were carried out using a Thermo-Finnigan Neptune multicollector ICP-MS coupled to a Photon-Machines 193 nm laser system, at Departament of Geology, at Ouro Preto Federal University. The Lu-Hf isotopic composition was analyzed whenever possible in the same spot previously analyzed for U-Pb isotopes. Data were collected in static mode during 60 s of ablation with a spot size of 60 μm. Nitrogen (~0.080 l/min) was introduced into the Ar sample carrier gas. Typical signal intensity was ca. 10 V for $^{180}Hf$. The isotopes $^{172}Yb$, $^{173}Yb$ and $^{175}Lu$ were simultaneously monitored during each analysis step to allow for correction of isobaric interferences of Lu and Yb isotopes on mass 176. The $^{176}Yb$ and $^{176}Lu$ were calculated using a $^{176}Yb/^{173}Yb$ of 0.796218 (Chu et al., 2002) and $^{176}Lu/^{175}Lu$ of 0.02658 (JWG in-house value). The correction for instrumental mass bias utilized an exponential law and a $^{179}Hf/^{177}Hf$ value of 0.7325 (Patchett and Tatsumoto, 1980) for correction of Hf isotopic ratios. The mass bias of Yb isotopes generally differs slightly from that of the Hf isotopes with a typical offset of the βHf/βYb of ca. 1.04 to 1.06 when using the $^{172}Yb/^{173}Yb$ value of 1.35274 from Chu et al. (2002). This offset was

determined for each analytical session by averaging the βHf/βYb of multiple analyses of the JMC 475 solution doped with variable Yb amounts and all the laser ablation analyses (typically n> 50) of zircon that have a $^{173}$Yb signal intensity of > 60 mV. The mass bias behavior of Lu was assumed to follow that of Yb. The Yb and Lu isotopic ratios were corrected using the βHf of the individual integration steps (n=60) of each analysis divided by the average offset factor of the complete analytical session.

Rare earth elements and Y, Nb, Ta, Th, U and Th/U data from zircon grains were obtained via LA-ICP-MS (a New Wave 213 laser ablation coupled to a Agillent 7700) at the Departamento de Geologia, Universidade Federal de Ouro Preto. The laser was set to produce spot sizes of 20 um in diameter, during a period of 30 seconds at 10 Hz frequency. The data acquisition was done in bracketing mode and consisted of 3 to 4 analyses of standards (NIST 612 and NIST 210) bracketing 10-15 unknowns. The data reduction was done via the Glitter software (GEMOC Laser ICP-MS Total Trace Element Reduction), which provides an interactive environment for analytic selection of background and sample signals (Van Achterbergh et al., 2001; Jackson et al., 2004). Instrumental mass bias and ablation depth-dependent elemental fractionation were corrected by tying the time-resolved signal for the unknown zircon to the identical integration window of the primary standard NIST612. NIST 610 that was used as a secondary control standard.

## 4. Results

### *4.1. Structure of the Vila Nova greenstone belt*

The analysis of satellite images and airborne geophysical maps indicates that the main regional structures, including the Tumucumaque basement rocks and Vila Nova and Serra do Navio greenstone belts, strike NW to E-W. These structures are characterized as the metamorphic foliations and the main ductile shear zones were

generated in intermediate to deep crustal levels, and controlled the main disposition of the units in both complexes. Despite the intense rain-forest coverage, satellite images (SRTM, JERS-1/SAR and LANDSAT) and magnetometric data can highlight the N40-70$^{o}$E-trending brittle to brittle-ductile structures, which affect the entire Vila Nova region **(Fig. 8)**. The brittle structures are younger, probably Phanerozoic, and are associated with the development of the Amazonas-Solimões basin.

The total magnetic field data present a pattern of magnetic anomalies that show the regional structuring of the area, with strong control of NW-SE direction structures **(Fig. 8)**. The VNGB shows an elongated shape along the E-W direction marked by continuous and elongate low-amplitude magnetic anomalies. The high-magnetic amplitude areas are occupied by gneisses and metagranitoids of the Tumucumaque and Guianense complexes. The main magnetic lineaments have NW-SE and E-W directions, and, subordinately, N-S and NE-SW directions. The low-amplitude magnetic anomalies correspond to the greenstone belt sequences, and the boundaries of the Amapari, Anauerapucu and others Paleoproterozoic granites can also be traced. In addition, the Bacuri Mafic-Ultramafic Complex also presents a defined magnetic response, characterizing a main body with N80$^{o}$E direction. The dominant structural pattern is marked by a NW-SE direction, more expressive in the central area, extending NW and SE. These structures are characterized in the field by the Cupixi (CSZ) and Serra do Navio (SNSZ) shear zones that cut through the entire area and present a large E-W steering structure, represented by the Vila Nova Shear Zone.

The VNGB presents a main structure of E-W direction, characterized by the metamorphic foliations $S_1$ and $S_2$ that are affected by later events of ductile deformation resulting in the formation of phase three ($F_3$) regional folds. In the central-northeast sector of the area, N-S direction lineaments predominate,

expressed by rectilinear, continuous and well-defined structures that cut the greenstone belts units in the gold mines areas of the Vila Nova region. The NE-SW and N-S direction lineaments occur preferentially southwest and northeast of the area and represent ruptile tectonics that displaces all previous lineaments **(Fig. 8)**.

The gammaspectometric data are affected by the strong influence of drainage. The K and Th maps show the enrichment of potassium in the central region of the area, coincident with the magnetic anomaly attributed to the VNGB **(Fig. 9)**. In greenstone belts, the expected radiometric response is characterized by low radiometric counts. Generally, the K enrichment detected is caused by zones of hydrothermal alteration.

The characteristics of gold mineralization, associated with low temperature quartz veins, suggest that they may be related to this type of alteration. In the Th distribution map, the main positive anomalies are related mainly to the Amapari Granite, undifferentiated Paleoproterozoic granites and the Archean Anauerapucu granite **(Fig. 9)**. The quartzites of the Upper Domain of the VNGB also show a positive anomaly in the central part of the map, as well as the Phanerozoic cover sediments.

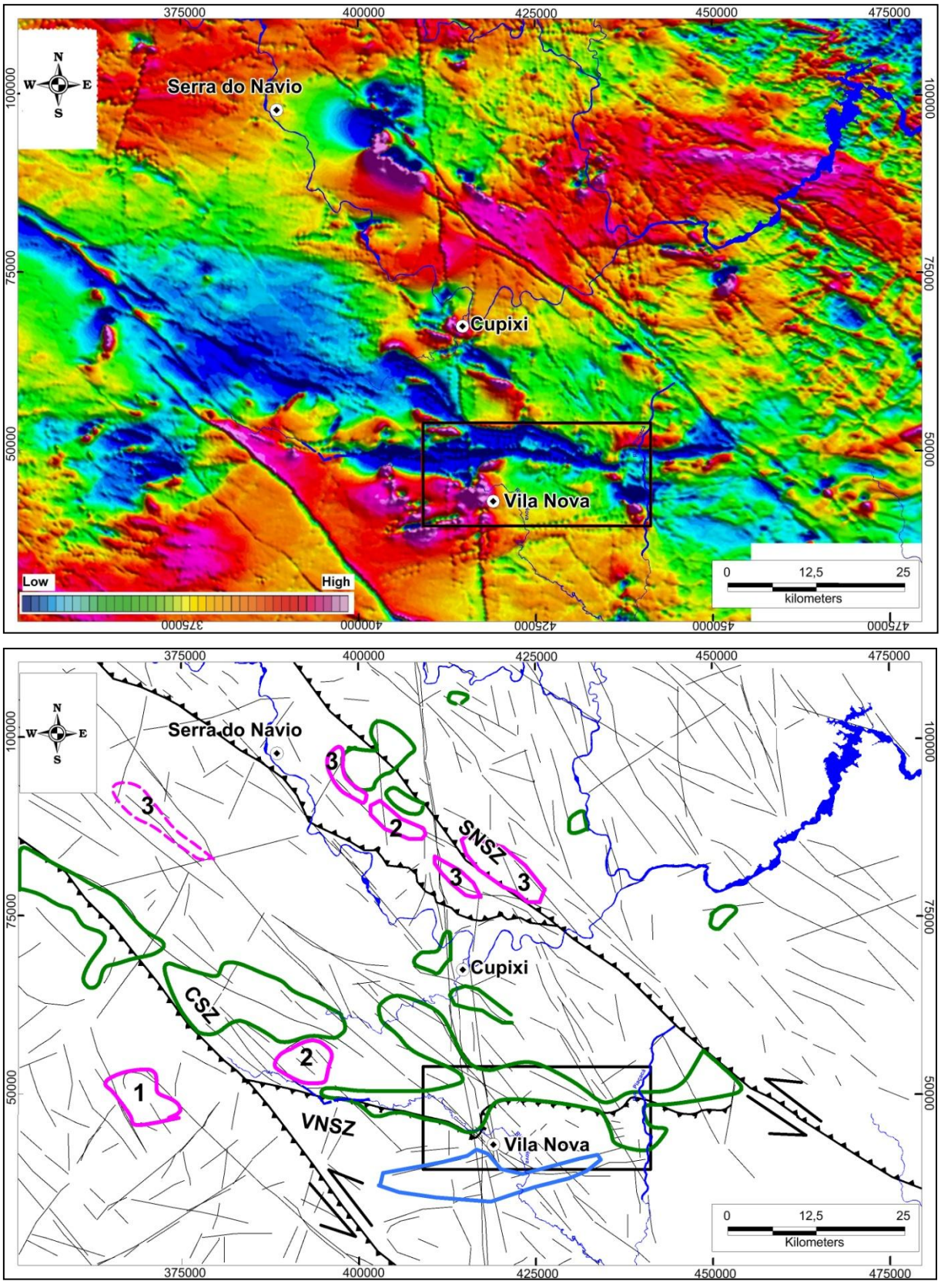


**Figure 8.** Total magnetic field with delimitation of large magnetic amplitude anomalies corresponding to the metavolcano-sedimentary rocks of the VNGB (green line), the Anauerapuru Granite (1), Amapari Granite (2) and paleoproterozoic intrusive granites (3) (pink line), the Bacuri Mafic-Ultramafic Complex (blue line) and the main structural guidelines. Shear Zones: Cupixi (CSZ), Serra do Navio (SNSZ) and Vila Nova (VNSZ).

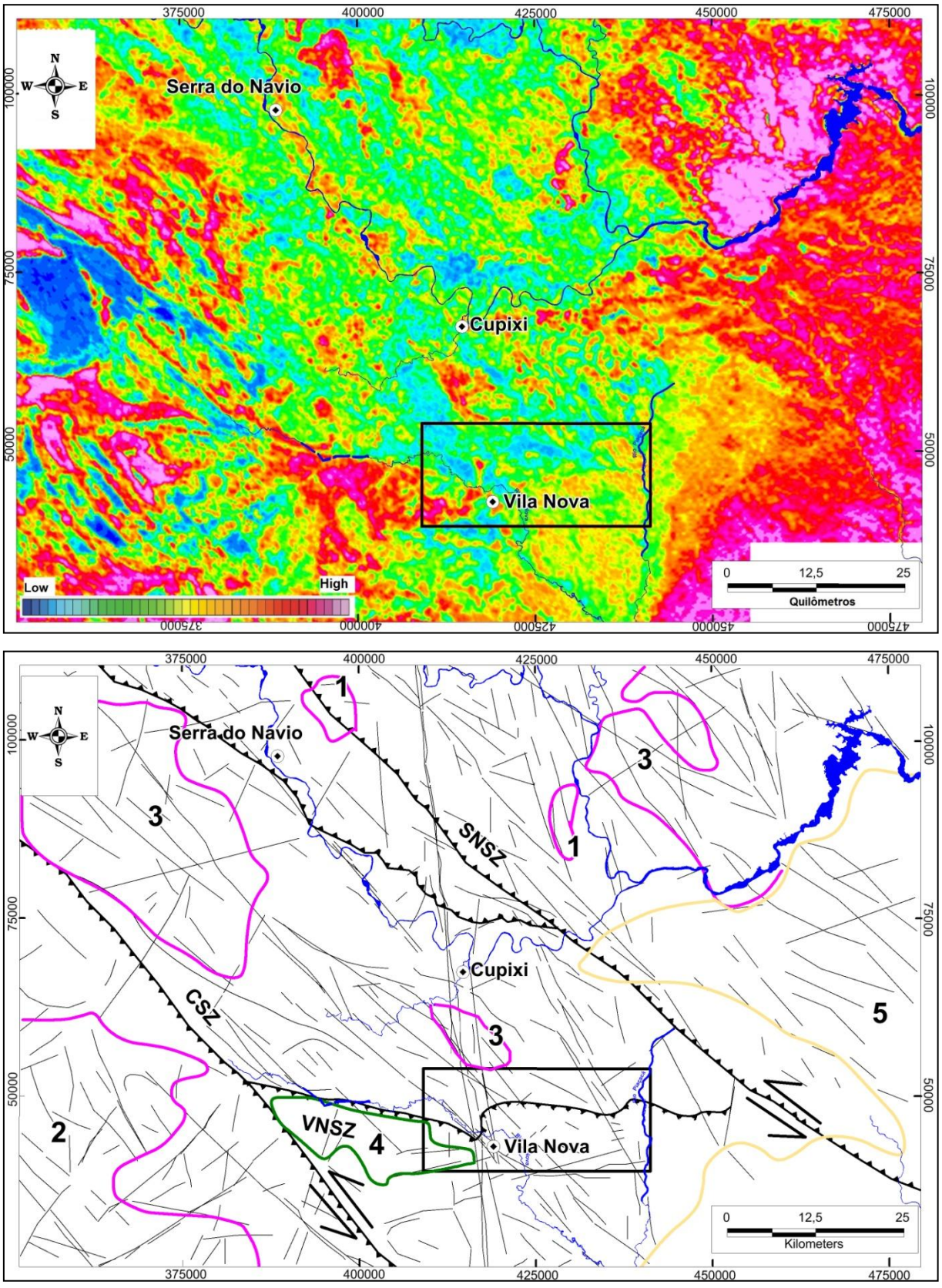


**Figure 9.** Thorium distribution map highlighting the paleoproterozoic granite intrusions such as the Amapari (1) and the Archean Anauerapucu (2) granites, the undifferentiated paleoproterozoic granites (3), the quartzites of VNGB (4) and the Phanerozoic cover (5).

Structural data collected in geologic mapping indicate that four deformational events affected the rocks of VNGB generated ductile ($D_1$ and $D_2$) to ductile-brittle structures ($D_3$ and $D_4$) (Hoffmann et al., 2018). The rocks of VNGB show a regional schistosity trending NW to E-W, with a pronounced lineation stretching in the SE to SW direction. The schematic geological section shown in figure 10A shows the main structures and contact relationships between metavolcano-sedimentary rocks of the VNGB and the basement orthogneisses, represented by the Tumucumaque and Guianense complexes. Structural surveys indicate that the main deformation and metamorphism events that affected the VNGB resulted in a regional N70°-85°W-trending foliation, dipping mainly SW at high angles **(Fig. 11A)**.

Four phases of regional deformation were recognized. The $S_1$ schistosity was preserved in isoclinal $F_2$ folds, and the transposition resulted in crenulation cleavage $S_2$, which is the main foliation **(Fig. 11B)**. These relationships can be observed in outcropping **(Fig. 10B)** and also in the geological section generated from integration of the drilling holes **(Fig. 10C)**. The formation of the $S_1$ and $S_2$ was accompanied by development of mineral and stretching lineations. The disposition of the lineations can be observed in figures 11C to 11F. These stereoplots show the varying lineation attitudes, creating relatively well-defined garlands associated with the development of the $F_3$ and $F_4$ folding. In both cases, a broad similarity between both lineations is observed.

The refolding of $S_1$ and $S_2$ foliations and lineations is associated with the generation of $F_3$ and $F_4$ folds. The $F_3$ folds show an axis with low dip in the NW direction and were accompanied by the formation of an axial surface cleavage trending N60°-30°W in quartzites and metaconglomerates. The $F_3$ folds control the regional relief, as can be observed in the geological map **(Fig. 4)** and in the geologic

section **(Fig.10A)**. The last deformation phase is responsible for the $F_4$ open- to close-type folds with N50°-70°E trending axial surfaces.

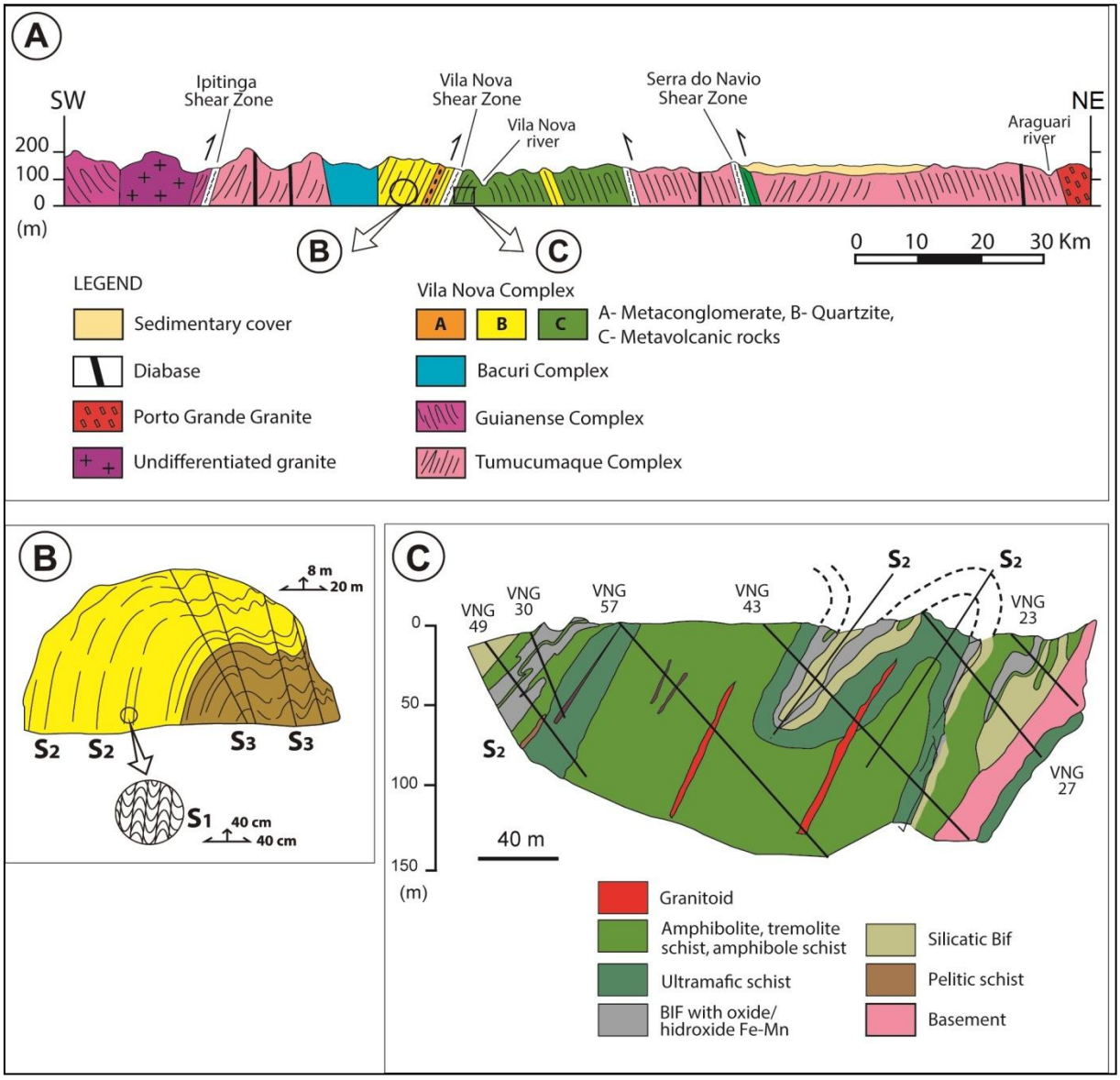


**Figure 10. A)** Schematic geological section shows the main structures and contact relationships between metavolcano-sedimentary rocks of the VNGB and the basement orthogneisses, **B)** Contact between quartzites (yellow) and pelitic schist (brown) highlighting the F3 and F2 folds, **C)** geological section generated from integration of the drilling holes. Location in the figure 4.

The main foliation ($S_1$-$S_2$) and lineation dip at relatively high angles, which is suggestive of deformation associated with a collisional context generated by oblique shear zones systems. The installation of the first deformational phases of ductile nature is responsible for tectonic interleaving and slicing of the metavolcanic and metasedimentary units.

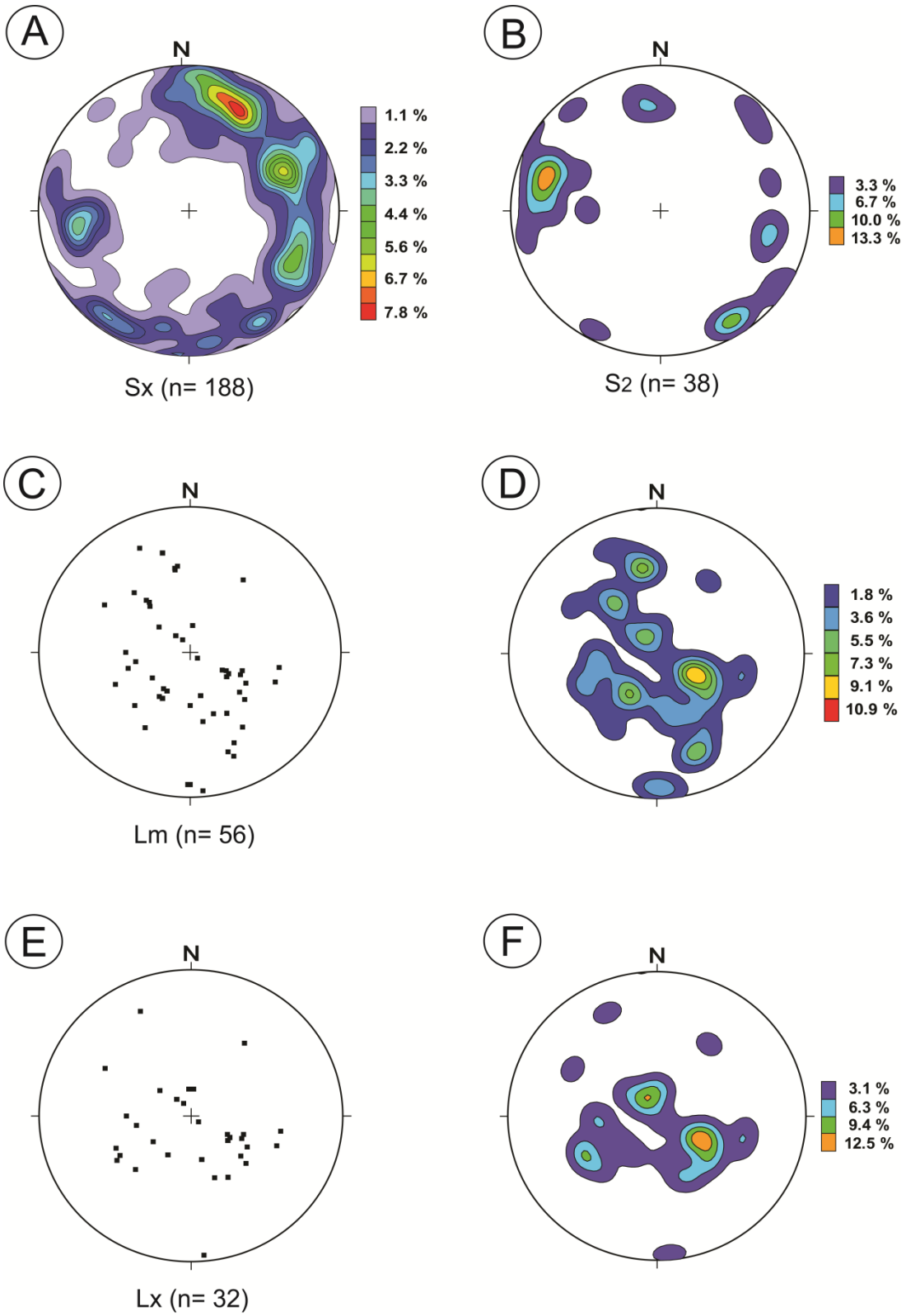


**Figure 11.** Stereographic projection representing the main structures of the Vila Nova Complex, equal area and lower hemisphere projection. **A)** Regional foliation (Sx) pole density (data points= 188); **B)** Crenulation cleavage, main foliation (S2) pole density (data points= 38); **C)** Mineral lineation (data points= 56); **D)** pole density diagram; **E)** Stretching lineation density, (data points= 32); **F)** pole density diagram.

### *4.2. In situ zircon U-Pb geochronology*

#### *4.2.1. Metasedimentary rocks*

Two hundred and sixty-two detrital zircon grains were separated from the Upper Domain metasedimentary rocks of the VNGB for U-Pb analysis by LA-MC-ICPMS. Ninety-six analyses were performed in zircon grains from quartzite sample CB-03A and metaconglomerate sample CB-03B. The CL images of representative zircon grains from both samples are shown in **figure 12**. Confidence ages with less than 5% discrepancy ($^{238}U/^{206}Pb$ to $^{235}U/^{207}Pb$) and 10% discrepancy ($^{238}U/^{206}Pb$ to $^{207}Pb/^{206}Pb$) were obtained for 96 zircon grains. U-Pb ages are shown in the histograms in terms of $^{207}Pb/^{206}Pb$ ratios for ages older than 1.3 Ga and of $^{206}Pb/^{238}U$ ratios for ages younger than 1.3 Ga **(Fig. 13)**.

*Quartzite (CB-03A)*

Quartzite sample CB-03A (UTM zone 22N, coordinates 415612 and 43999) represents the Upper Domain of the VNGB and was taken from the top of the basal quartzite unit, near the contact with the overlying metaconglomerate **(Figs. 4 and 5)**. Mineral separation yielded 13 zircon grains suitable for U-Pb analysis, resulting in $^{207}Pb/^{206}Pb$ ages ranging between 3.609 ±27 Ma and 2.747 ±29 Ma (Paleoarchean to Neoarchean) **(Fig. 13 and Table 2)**.

The analyzed zircon grains are predominantly translucent to transparent, with slightly rounded and subrounded terminations, typical of transport for long distances, from the source area to the sedimentary basin. Few grains are prismatic and euhedral, with lengths between 120 to 260 μm and 1:1 to 2:1, respectively. In general, the zircons are metamict (that could not be dated), but some show oscillatory zoning (see **Fig. 12**). Th/U ratios between 0.39 and 1.01 are typical of igneous rocks **(Table 2)**.

| Isotopic Ratios | | | | | | | | | | | | | | Calculated Ages (Ma) | | | | | | |
|---|---|---|---|---|---|---|---|---|---|---|---|---|---|---|---|---|---|---|---|---|
| Spot | $^{207}Pb/^{235}U$ | ±(1σ) | $^{206}Pb/^{238}Pb$ | ±(1σ) | CC | $^{238}U/^{206}Pb$ | ±(1σ) | $^{207}Pb/^{206}Pb$ | ±(1σ) | $^{208}Pb/^{206}Pb$ | ±(1σ) | $Pb^{3}$ | Th/U | $^{206}Pb/^{238}U$ | ±(1σ) | $^{207}Pb/^{235}U$ | ±(1σ) | $^{207}Pb/^{206}Pb$ | ±(1σ) |
| 1.1 | 20.0911 | 0.8301 | 0.6106 | 0.0132 | 0.52 | 1.6377 | 0.0354 | 0.2388 | 0.0041 | 0.5757 | 0.6406 | <0.001 | 0.742 | 3.072 | 0.053 | 3.096 | 0.039 | 3.115 | 0.026 |
| 2.1 | 13.6084 | 0.5775 | 0.5228 | 0.0120 | 0.54 | 1.9128 | 0.0439 | 0.1903 | 0.0033 | 0.3013 | 0.3353 | 0.26 | 0.466 | 2.711 | 0.051 | 2.723 | 0.039 | 2.748 | 0.029 |
| 1.2 | 19.8569 | 0.8222 | 0.6027 | 0.0131 | 0.52 | 1.6591 | 0.0360 | 0.2392 | 0.0041 | 0.6757 | 0.7519 | 0.13 | 0.852 | 3.041 | 0.052 | 3.084 | 0.039 | 3.117 | 0.026 |
| 3.1 | 17.3118 | 0.7190 | 0.5700 | 0.0124 | 0.52 | 1.7544 | 0.0381 | 0.2208 | 0.0038 | 0.3823 | 0.4254 | 0.08 | 0.477 | 2.908 | 0.051 | 2.952 | 0.039 | 2.993 | 0.027 |
| 4.1 | 24.2741 | 1.0033 | 0.6649 | 0.0144 | 0.52 | 1.5040 | 0.0325 | 0.2667 | 0.0046 | 0.7453 | 0.8294 | <0.001 | 0.954 | 3.286 | 0.055 | 3.279 | 0.040 | 3.283 | 0.026 |
| 5.1 | 14.4223 | 0.5965 | 0.5406 | 0.0118 | 0.53 | 1.8497 | 0.0402 | 0.1940 | 0.0033 | 0.5240 | 0.5831 | 0.08 | 0.643 | 2.786 | 0.049 | 2.778 | 0.039 | 2.781 | 0.028 |
| 6.1 | 14.7791 | 0.6267 | 0.5435 | 0.0124 | 0.54 | 1.8401 | 0.0421 | 0.1973 | 0.0034 | 0.3935 | 0.4379 | 0.13 | 0.492 | 2.798 | 0.052 | 2.801 | 0.040 | 2.809 | 0.028 |
| 7.1 | 17.2155 | 0.7766 | 0.5900 | 0.0165 | 0.62 | 1.6949 | 0.0473 | 0.2196 | 0.0039 | 0.5197 | 0.5791 | <0.001 | -3.54 | 2.990 | 0.066 | 2.947 | 0.042 | 2.984 | 0.028 |
| 8.1 | 32.9545 | 1.3687 | 0.7195 | 0.0156 | 0.52 | 1.3898 | 0.0301 | 0.3264 | 0.0056 | 0.6177 | 0.6873 | 0.08 | 0.831 | 3.494 | 0.058 | 3.579 | 0.040 | 3.609 | 0.027 |
| 9.1 | 13.5964 | 0.5623 | 0.5170 | 0.0112 | 0.52 | 1.9342 | 0.0419 | 0.1908 | 0.0033 | 0.8043 | 0.8950 | 0.13 | 1.012 | 2.687 | 0.047 | 2.722 | 0.038 | 2.753 | 0.029 |
| 10.1 | 13.3790 | 0.5519 | 0.5158 | 0.0112 | 0.52 | 1.9388 | 0.0419 | 0.1901 | 0.0033 | 0.3147 | 0.3501 | <0.001 | 0.391 | 2.681 | 0.047 | 2.707 | 0.038 | 2.747 | 0.029 |
| 11.1 | 28.6269 | 1.2081 | 0.7078 | 0.0163 | 0.55 | 1.4128 | 0.0326 | 0.2944 | 0.0051 | 0.5960 | 0.6632 | 0.05 | 0.918 | 3.450 | 0.061 | 3.441 | 0.041 | 3.438 | 0.028 |
| 12.1 | 13.9989 | 0.5786 | 0.5225 | 0.0113 | 0.52 | 1.9139 | 0.0413 | 0.1948 | 0.0033 | 0.3940 | 0.4385 | 0.01 | 0.503 | 2.710 | 0.048 | 2.750 | 0.038 | 2.788 | 0.028 |

**Table 2.** Summary of LA-ICPMS U-Pb zircon isotopic data for quartzite CB-3A. C.C = Correlation coefficient. $Pb^{C}$ = Common Pb (%).

*Metaconglomerate (CB-03B)*

Metaconglomerate sample CB-03B was collected from the base of the Upper Domain of the VNGB (UTM zone 22N, coordinates 415575 and 44020), which lies stratigraphically above quartzite CB-03A. The contact between both units is defined by an erosive unconformity **(Fig. 5)**. The grain size of the analyzed zircons ranged from 100 to 550 μm. The shape surfaces of the zircon grains are mainly rounded (65%), characteristic of sedimentary transport. However, a significant population of more preserved grains (35%) with prismatic and sub-euhedral shapes, probably indicates minor transport from its source. Because different sources contributed to this sedimentary rock, it is difficult to relate family ages with similar characteristics. This would be possible with larger (300-550 μm) and more preserved grains showing prismatic (CB-03B 35.1 and 65.1), pyramidal to straight termination and well-defined oscillatory zoning (spots 4.1, 63.1). Some crystals show features typical of sedimentary transport, such as eroded edges, and are partly fractured. Smaller grains (100-250 μm) were intensely corroded and fractured; resulting in angular and rounded grains (spots 61.1, 69.1, 71.1). Cathodoluminescence images show that

many of the grains have inherited cores and edges with oscillatory zoning (spots 27.1, 40.2) **(see Fig. 12)**.

| Isotopic Ratios | | | | | | | | | | | | | | Calculated Ages (Ma) | | | | | | |
|---|---|---|---|---|---|---|---|---|---|---|---|---|---|---|---|---|---|---|---|---|
| Spot | $^{07}Pb/^{235}U$ | ±(1σ) | $^{206}Pb/^{238}Pb$ | ±(1σ) | CC | $^{238}U/^{206}Pb$ | ±(1σ) | $^{207}Pb/^{206}Pb$ | ±(1σ) | $^{208}Pb/^{206}Pb$ | ±(1σ) | $Pb^3$ | Th/U | $^{206}Pb/^{238}U$ | ±(1σ) | $^{207}Pb/^{235}U$ | ±(1σ) | $^{207}Pb/^{206}Pb$ | ±(1σ) |
| 1.1 | 23.9419 | 0.6271 | 0.6517 | 0.0118 | 0.69 | 1.5345 | 0.0279 | 0.2660 | 0.0030 | 0.0344 | 0.0215 | <0.00 | 0.068 | 3.235 | 0.046 | 3.266 | 0.025 | 3.279 | 0.017 |
| 2.1 | 14.1717 | 0.3752 | 0.5341 | 0.0098 | 0.69 | 1.8725 | 0.0343 | 0.1923 | 0.0022 | 0.2157 | 0.1346 | <0.00 | 0.406 | 2.759 | 0.041 | 2.761 | 0.025 | 2.766 | 0.019 |
| 3.1 | 29.6243 | 0.7707 | 0.7166 | 0.0131 | 0.70 | 1.3955 | 0.0255 | 0.2999 | 0.0035 | 0.2167 | 0.1353 | <0.00 | 0.414 | 3.483 | 0.049 | 3.474 | 0.025 | 3.468 | 0.019 |
| 4.1 | 16.8466 | 0.4400 | 0.5595 | 0.0102 | 0.70 | 1.7873 | 0.0325 | 0.2174 | 0.0025 | 0.2409 | 0.1504 | 0.02 | 0.447 | 2.865 | 0.042 | 2.926 | 0.025 | 2.968 | 0.018 |
| 5.1 | 14.4729 | 0.3929 | 0.5390 | 0.0104 | 0.71 | 1.8553 | 0.0357 | 0.2020 | 0.0026 | 0.0539 | 0.0337 | 1.07 | 0.122 | 2.779 | 0.043 | 2.781 | 0.025 | 2.848 | 0.021 |
| 6.1 | 17.0380 | 0.4428 | 0.5707 | 0.0104 | 0.70 | 1.7521 | 0.0318 | 0.2156 | 0.0024 | 0.1919 | 0.1198 | 0.04 | 0.358 | 2.911 | 0.042 | 2.937 | 0.025 | 2.954 | 0.018 |
| 7.1 | 16.5435 | 0.4289 | 0.5569 | 0.0101 | 0.70 | 1.7956 | 0.0325 | 0.2146 | 0.0024 | 0.4092 | 0.2554 | 0.00 | 0.810 | 2.854 | 0.042 | 2.909 | 0.025 | 2.947 | 0.018 |
| 8.1 | 17.0075 | 0.4474 | 0.5664 | 0.0104 | 0.70 | 1.7656 | 0.0324 | 0.2162 | 0.0024 | 0.4230 | 0.2640 | 0.05 | 0.796 | 2.893 | 0.043 | 2.935 | 0.025 | 2.959 | 0.018 |
| 9.1 | 16.5916 | 0.5357 | 0.6044 | 0.0129 | 0.66 | 1.6546 | 0.0354 | 0.2303 | 0.0034 | 0.0752 | 0.0470 | 0.28 | 0.185 | 3.047 | 0.052 | 2.912 | 0.030 | 3.059 | 0.023 |
| 10.1 | 16.1197 | 0.4335 | 0.5610 | 0.0107 | 0.71 | 1.7825 | 0.0341 | 0.2063 | 0.0024 | 0.2859 | 0.1784 | <0.00 | 0.275 | 2.871 | 0.044 | 2.884 | 0.025 | 2.883 | 0.019 |
| 11.1 | 19.3441 | 0.5013 | 0.6062 | 0.0111 | 0.70 | 1.6496 | 0.0301 | 0.2319 | 0.0026 | 0.4031 | 0.2516 | 0.39 | 0.799 | 3.055 | 0.044 | 3.059 | 0.025 | 3.070 | 0.018 |
| 12.1 | 17.9303 | 0.7985 | 0.6071 | 0.0218 | 0.81 | 1.6472 | 0.0593 | 0.2168 | 0.0041 | 0.2488 | 0.1553 | <0.00 | 0.359 | 3.058 | 0.087 | 2.986 | 0.042 | 2.963 | 0.030 |
| 13.1 | 21.8803 | 0.6105 | 0.6570 | 0.0136 | 0.74 | 1.5220 | 0.0314 | 0.2462 | 0.0030 | 0.2499 | 0.1560 | <0.00 | 0.406 | 3.256 | 0.053 | 3.178 | 0.027 | 3.162 | 0.019 |
| 14.1 | 32.9634 | 0.6284 | 0.7424 | 0.0045 | 0.32 | 1.3469 | 0.0082 | 0.3224 | 0.0050 | 0.1692 | 0.0452 | <0.00 | 0.516 | 3.580 | 0.017 | 3.580 | 0.019 | 3.589 | 0.025 |
| 15.1 | 20.9613 | 0.4037 | 0.6326 | 0.0040 | 0.33 | 1.5807 | 0.0101 | 0.2402 | 0.0037 | 0.0371 | 0.0100 | 0.16 | 0.144 | 3.160 | 0.016 | 3.137 | 0.018 | 3.124 | 0.024 |
| 16.1 | 17.4186 | 0.3352 | 0.5839 | 0.0037 | 0.32 | 1.7126 | 0.0107 | 0.2161 | 0.0034 | 0.1898 | 0.0507 | 0.12 | 0.582 | 2.965 | 0.015 | 2.958 | 0.018 | 2.958 | 0.025 |
| 17.1 | 17.8539 | 0.3420 | 0.5900 | 0.0037 | 0.33 | 1.6950 | 0.0107 | 0.2187 | 0.0034 | 0.2286 | 0.0611 | 0.12 | 0.640 | 2.989 | 0.015 | 2.982 | 0.018 | 2.977 | 0.025 |
| 18.1 | 23.0445 | 0.4392 | 0.6421 | 0.0041 | 0.33 | 1.5575 | 0.0099 | 0.2603 | 0.0040 | 0.1658 | 0.0443 | 0.02 | 0.510 | 3.197 | 0.016 | 3.229 | 0.018 | 3.246 | 0.023 |
| 19.1 | 17.5854 | 0.3457 | 0.5773 | 0.0037 | 0.32 | 1.7323 | 0.0110 | 0.2186 | 0.0034 | 0.4091 | 0.1093 | 0.04 | 1.270 | 2.938 | 0.015 | 2.967 | 0.019 | 2.977 | 0.025 |
| 20.1 | 32.3992 | 0.6214 | 0.7348 | 0.0046 | 0.33 | 1.3608 | 0.0086 | 0.3217 | 0.0050 | 0.1763 | 0.0471 | 0.03 | 0.552 | 3.551 | 0.017 | 3.563 | 0.019 | 3.585 | 0.025 |
| 21.1 | 9.6478 | 0.2635 | 0.4558 | 0.0083 | 0.67 | 2.1937 | 0.0401 | 0.1566 | 0.0028 | 0.1191 | 0.0318 | 0.78 | 0.568 | 2.421 | 0.037 | 2.402 | 0.025 | 2.415 | 0.030 |
| 22.1 | 32.4496 | 0.6570 | 0.7421 | 0.0067 | 0.44 | 1.3474 | 0.0121 | 0.3179 | 0.0050 | 0.1710 | 0.0457 | 0.07 | 0.599 | 3.579 | 0.025 | 3.564 | 0.020 | 3.566 | 0.026 |
| 23.1 | 27.5724 | 0.6107 | 0.6985 | 0.0113 | 0.73 | 1.4316 | 0.0232 | 0.2878 | 0.0046 | 0.2021 | 0.0541 | 3.26 | 0.900 | 3.415 | 0.043 | 3.404 | 0.021 | 3.401 | 0.026 |
| 24.1 | 16.9197 | 0.3264 | 0.5782 | 0.0038 | 0.34 | 1.7296 | 0.0114 | 0.2112 | 0.0033 | 0.1099 | 0.0294 | 0.36 | 0.331 | 2.941 | 0.016 | 2.930 | 0.018 | 2.921 | 0.025 |
| 25.1 | 20.7680 | 0.3986 | 0.6172 | 0.0039 | 0.33 | 1.6203 | 0.0103 | 0.2427 | 0.0038 | 0.0019 | 0.0006 | <0.00 | 0.001 | 3.099 | 0.016 | 3.128 | 0.018 | 3.140 | 0.024 |
| 26.1 | 29.4330 | 0.6040 | 0.7127 | 0.0062 | 0.43 | 1.4032 | 0.0122 | 0.3004 | 0.0047 | 0.2586 | 0.0691 | 0.10 | 0.789 | 3.469 | 0.023 | 3.468 | 0.020 | 3.471 | 0.026 |
| 27.1 | 10.1215 | 0.3644 | 0.4534 | 0.0080 | 0.49 | 2.2053 | 0.0389 | 0.1617 | 0.0033 | 0.2573 | 0.1147 | 1.17 | 0.702 | 2.411 | 0.035 | 2.446 | 0.033 | 2.471 | 0.035 |
| 28.1 | 26.9054 | 1.0374 | 0.6857 | 0.0096 | 0.36 | 1.4584 | 0.0205 | 0.2841 | 0.0074 | 0.3061 | 0.1364 | <0.00 | 1.419 | 3.366 | 0.037 | 3.380 | 0.037 | 3.380 | 0.041 |
| 29.1 | 17.5493 | 0.5498 | 0.5822 | 0.0044 | 0.24 | 1.7176 | 0.0129 | 0.2175 | 0.0043 | 0.2186 | 0.0974 | 0.02 | 0.512 | 2.958 | 0.018 | 2.965 | 0.030 | 2.969 | 0.031 |
| 30.1 | 8.2809 | 0.3146 | 0.4036 | 0.0098 | 0.64 | 2.4779 | 0.0599 | 0.1530 | 0.0032 | 0.2209 | 0.0986 | 2.03 | 2.208 | 2.185 | 0.045 | 2.262 | 0.034 | 2.376 | 0.036 |
| 31.1 | 27.9176 | 0.8780 | 0.6708 | 0.0050 | 0.24 | 1.4908 | 0.0111 | 0.2990 | 0.0059 | 0.3631 | 0.1632 | 0.07 | 0.840 | 3.309 | 0.019 | 3.416 | 0.030 | 3.463 | 0.032 |
| 32.1 | 16.9292 | 0.5392 | 0.6007 | 0.0053 | 0.28 | 1.6647 | 0.0147 | 0.2056 | 0.0041 | 0.3589 | 0.1599 | 0.12 | 0.800 | 3.033 | 0.021 | 2.931 | 0.030 | 2.877 | 0.032 |
| 33.1 | 26.1144 | 0.8205 | 0.6859 | 0.0053 | 0.24 | 1.4579 | 0.0112 | 0.2764 | 0.0054 | 0.1251 | 0.0558 | 0.11 | 0.287 | 3.367 | 0.020 | 3.351 | 0.030 | 3.337 | 0.030 |
| 34.1 | 23.1491 | 0.7385 | 0.6414 | 0.0058 | 0.28 | 1.5591 | 0.0142 | 0.2598 | 0.0051 | 0.0099 | 0.0045 | 0.05 | 0.027 | 3.195 | 0.023 | 3.233 | 0.031 | 3.243 | 0.030 |
| 35.1 | 16.6619 | 0.5431 | 0.5709 | 0.0068 | 0.37 | 1.7515 | 0.0209 | 0.2157 | 0.0042 | 0.2505 | 0.1116 | 0.25 | 0.574 | 2.912 | 0.028 | 2.916 | 0.031 | 2.955 | 0.031 |
| 36.1 | 13.4623 | 0.4214 | 0.5147 | 0.0035 | 0.22 | 1.9430 | 0.0132 | 0.1891 | 0.0037 | 0.2583 | 0.1151 | <0.00 | 0.584 | 2.676 | 0.015 | 2.713 | 0.029 | 2.738 | 0.033 |
| 37.1 | 25.8016 | 0.8081 | 0.6752 | 0.0048 | 0.22 | 1.4811 | 0.0104 | 0.2765 | 0.0054 | 0.1663 | 0.0741 | 0.03 | 0.393 | 3.326 | 0.018 | 3.339 | 0.030 | 3.338 | 0.030 |
| 39.1 | 23.1625 | 0.7247 | 0.6397 | 0.0045 | 0.22 | 1.5633 | 0.0109 | 0.2626 | 0.0052 | 0.3144 | 0.1401 | 0.12 | 0.759 | 3.188 | 0.018 | 3.234 | 0.030 | 3.259 | 0.030 |
| 40.1 | 15.5014 | 0.2188 | 0.5578 | 0.0017 | 0.21 | 1.7926 | 0.0054 | 0.2021 | 0.0025 | 0.2833 | 0.0665 | <0.00 | 0.645 | 2.858 | 0.007 | 2.847 | 0.013 | 2.849 | 0.021 |
| 41.1 | 13.2839 | 0.2296 | 0.5132 | 0.0044 | 0.50 | 1.9485 | 0.0167 | 0.1888 | 0.0027 | 0.1698 | 0.0399 | 5.06 | 0.639 | 2.670 | 0.019 | 2.700 | 0.016 | 2.735 | 0.024 |
| 42.1 | 20.6804 | 0.3198 | 0.6711 | 0.0043 | 0.41 | 1.4900 | 0.0095 | 0.2256 | 0.0028 | 0.1229 | 0.0289 | 0.27 | 0.338 | 3.310 | 0.016 | 3.124 | 0.015 | 3.026 | 0.019 |
| 43.1 | 14.4660 | 0.2172 | 0.5400 | 0.0035 | 0.43 | 1.8518 | 0.0119 | 0.1932 | 0.0024 | 0.2081 | 0.0489 | 0.12 | 0.514 | 2.783 | 0.015 | 2.781 | 0.014 | 2.774 | 0.020 |
| 44.1 | 16.8884 | 0.2345 | 0.5740 | 0.0020 | 0.25 | 1.7421 | 0.0059 | 0.2117 | 0.0025 | 0.2113 | 0.0496 | 0.03 | 0.501 | 2.924 | 0.008 | 2.929 | 0.013 | 2.925 | 0.019 |
| 45.1 | 23.8369 | 0.3372 | 0.6513 | 0.0020 | 0.22 | 1.5355 | 0.0048 | 0.2649 | 0.0032 | 0.0828 | 0.0195 | 0.10 | 0.210 | 3.233 | 0.008 | 3.262 | 0.014 | 3.272 | 0.018 |
| 46.1 | 17.3792 | 0.2447 | 0.5918 | 0.0022 | 0.26 | 1.6898 | 0.0062 | 0.2120 | 0.0025 | 0.3001 | 0.0706 | 0.14 | 0.666 | 2.997 | 0.009 | 2.956 | 0.013 | 2.927 | 0.019 |
| 47.1 | 19.4809 | 0.2722 | 0.6095 | 0.0023 | 0.27 | 1.6406 | 0.0061 | 0.2304 | 0.0028 | 0.0523 | 0.0123 | <0.00 | 0.132 | 3.068 | 0.009 | 3.066 | 0.013 | 3.060 | 0.019 |
| 48.1 | 25.5683 | 0.3544 | 0.6833 | 0.0021 | 0.22 | 1.4636 | 0.0044 | 0.2700 | 0.0033 | 0.2051 | 0.0482 | 0.16 | 0.502 | 3.357 | 0.008 | 3.330 | 0.013 | 3.301 | 0.018 |
| 50.1 | 13.7162 | 0.1916 | 0.5248 | 0.0022 | 0.29 | 1.9055 | 0.0078 | 0.1900 | 0.0023 | 0.1597 | 0.0375 | 0.10 | 0.400 | 2.719 | 0.009 | 2.730 | 0.013 | 2.746 | 0.020 |
| 51.1 | 16.7982 | 0.2338 | 0.5840 | 0.0021 | 0.26 | 1.7124 | 0.0063 | 0.2087 | 0.0026 | 0.1263 | 0.0297 | 0.19 | 0.308 | 2.965 | 0.009 | 2.923 | 0.013 | 2.902 | 0.020 |
| 52.1 | 17.1551 | 0.2922 | 0.5803 | 0.0044 | 0.44 | 1.7231 | 0.0130 | 0.2131 | 0.0026 | 0.2657 | 0.0654 | 0.21 | 0.770 | 2.950 | 0.018 | 2.944 | 0.016 | 2.936 | 0.020 |
| 53.1 | 25.3064 | 0.4330 | 0.6713 | 0.0050 | 0.43 | 1.4895 | 0.0111 | 0.2722 | 0.0033 | 0.0428 | 0.0106 | 0.12 | 0.125 | 3.311 | 0.019 | 3.320 | 0.017 | 3.314 | 0.019 |
| 54.1 | 16.3185 | 0.2798 | 0.5578 | 0.0041 | 0.43 | 1.7927 | 0.0132 | 0.2107 | 0.0026 | 0.2384 | 0.0587 | 0.02 | 0.644 | 2.858 | 0.017 | 2.896 | 0.016 | 2.918 | 0.020 |
| 55.1 | 11.4764 | 0.2219 | 0.4507 | 0.0051 | 0.59 | 2.2190 | 0.0252 | 0.1859 | 0.0023 | 0.1742 | 0.0429 | 0.13 | 0.523 | 2.398 | 0.023 | 2.563 | 0.018 | 2.709 | 0.021 |

| | | | | | | | | | | | | | | | | | | | |
|---|---|---|---|---|---|---|---|---|---|---|---|---|---|---|---|---|---|---|---|
| 56.1 | 22.5032 | 0.9368 | 0.6468 | 0.0189 | 0.70 | 1.5460 | 0.0452 | 0.2536 | 0.0058 | 0.2506 | 0.0617 | 0.59 | 1.043 | 3.216 | 0.074 | 3.206 | 0.040 | 3.206 | 0.034 |
| 57.1 | 33.5776 | 0.6451 | 0.7407 | 0.0067 | 0.47 | 1.3501 | 0.0122 | 0.3283 | 0.0041 | 0.0861 | 0.0214 | 0.01 | 0.295 | 3.573 | 0.025 | 3.598 | 0.019 | 3.618 | 0.019 |
| 58.1 | 17.0894 | 0.2926 | 0.5788 | 0.0043 | 0.44 | 1.7276 | 0.0130 | 0.2130 | 0.0026 | 0.1316 | 0.0324 | 0.46 | 0.365 | 2.944 | 0.018 | 2.940 | 0.016 | 2.935 | 0.020 |
| 59.1 | 14.1875 | 0.2451 | 0.5399 | 0.0043 | 0.46 | 1.8520 | 0.0148 | 0.1898 | 0.0023 | 0.2142 | 0.0527 | <0.00 | 0.545 | 2.783 | 0.018 | 2.762 | 0.016 | 2.744 | 0.020 |
| 60.1 | 25.5235 | 0.4330 | 0.6692 | 0.0049 | 0.43 | 1.4943 | 0.0109 | 0.2755 | 0.0033 | 0.1088 | 0.0268 | <0.00 | 0.284 | 3.303 | 0.019 | 3.328 | 0.016 | 3.333 | 0.019 |
| 61.1 | 12.4853 | 0.2457 | 0.5049 | 0.0066 | 0.66 | 1.9806 | 0.0258 | 0.1769 | 0.0022 | 0.1978 | 0.0487 | 0.64 | 0.768 | 2.635 | 0.028 | 2.642 | 0.018 | 2.624 | 0.021 |
| 62.1 | 16.6562 | 0.2838 | 0.5684 | 0.0042 | 0.43 | 1.7594 | 0.0129 | 0.2118 | 0.0025 | 0.2030 | 0.0499 | <0.00 | 0.511 | 2.901 | 0.017 | 2.915 | 0.016 | 2.925 | 0.019 |
| 63.1 | 23.1749 | 0.4196 | 0.6723 | 0.0060 | 0.50 | 1.4874 | 0.0134 | 0.2531 | 0.0032 | 0.1951 | 0.0480 | 0.08 | 0.920 | 3.315 | 0.023 | 3.234 | 0.017 | 3.203 | 0.019 |
| 64.1 | 17.0926 | 0.2951 | 0.5996 | 0.0053 | 0.51 | 1.6679 | 0.0148 | 0.2049 | 0.0025 | 0.1435 | 0.0353 | 0.07 | 0.486 | 3.028 | 0.021 | 2.940 | 0.016 | 2.871 | 0.020 |
| 65.1 | 17.2454 | 0.1909 | 0.5740 | 0.0025 | 0.39 | 1.7423 | 0.0075 | 0.2171 | 0.0023 | 0.3035 | 0.1274 | <0.00 | 0.671 | 2.924 | 0.010 | 2.949 | 0.011 | 2.966 | 0.017 |
| 66.1 | 16.3316 | 0.1835 | 0.5598 | 0.0029 | 0.47 | 1.7863 | 0.0094 | 0.2132 | 0.0022 | 0.2509 | 0.1053 | <0.00 | 0.533 | 2.866 | 0.012 | 2.896 | 0.011 | 2.937 | 0.017 |
| 67.1 | 17.5482 | 0.2170 | 0.6000 | 0.0040 | 0.54 | 1.6666 | 0.0112 | 0.2086 | 0.0022 | 0.1685 | 0.0707 | 0.24 | 0.481 | 3.030 | 0.016 | 2.965 | 0.012 | 2.901 | 0.017 |
| 68.1 | 13.0543 | 0.1454 | 0.5089 | 0.0026 | 0.47 | 1.9651 | 0.0102 | 0.1863 | 0.0019 | 0.2707 | 0.1136 | <0.00 | 0.643 | 2.652 | 0.011 | 2.684 | 0.010 | 2.713 | 0.017 |
| 69.1 | 16.1471 | 0.1894 | 0.5553 | 0.0030 | 0.46 | 1.8009 | 0.0096 | 0.2097 | 0.0022 | 0.2816 | 0.1182 | <0.00 | 0.648 | 2.847 | 0.012 | 2.886 | 0.011 | 2.910 | 0.017 |
| 70.1 | 11.9499 | 0.1639 | 0.4503 | 0.0048 | 0.78 | 2.2208 | 0.0236 | 0.1922 | 0.0022 | 0.7783 | 0.3268 | 0.01 | 2.147 | 2.397 | 0.021 | 2.600 | 0.013 | 2.765 | 0.019 |
| 71.1 | 17.0438 | 0.1898 | 0.5677 | 0.0025 | 0.39 | 1.7614 | 0.0077 | 0.2162 | 0.0022 | 0.2110 | 0.0885 | <0.00 | 0.496 | 2.899 | 0.010 | 2.937 | 0.011 | 2.959 | 0.016 |
| 74.1 | 18.1369 | 0.2155 | 0.5997 | 0.0038 | 0.53 | 1.6675 | 0.0106 | 0.2199 | 0.0023 | 0.2436 | 0.1022 | <0.00 | 0.592 | 3.029 | 0.015 | 2.997 | 0.011 | 2.986 | 0.017 |
| 75.1 | 19.6751 | 0.2166 | 0.6096 | 0.0028 | 0.41 | 1.6405 | 0.0074 | 0.2328 | 0.0024 | 0.1826 | 0.0766 | <0.00 | 0.452 | 3.068 | 0.011 | 3.076 | 0.011 | 3.076 | 0.016 |
| 76.1 | 15.2275 | 0.2102 | 0.5319 | 0.0047 | 0.65 | 1.8802 | 0.0168 | 0.2095 | 0.0024 | 0.1492 | 0.0626 | 0.09 | 0.382 | 2.749 | 0.020 | 2.830 | 0.013 | 2.908 | 0.018 |
| 77.1 | 24.9717 | 0.3235 | 0.6682 | 0.0040 | 0.46 | 1.4966 | 0.0089 | 0.2681 | 0.0029 | 0.2763 | 0.1159 | <0.00 | 0.727 | 3.299 | 0.015 | 3.307 | 0.013 | 3.291 | 0.016 |
| 78.1 | 17.0570 | 0.1865 | 0.5778 | 0.0031 | 0.48 | 1.7306 | 0.0092 | 0.2151 | 0.0030 | 0.2083 | 0.0866 | <0.00 | 0.531 | 2.940 | 0.012 | 2.938 | 0.010 | 2.950 | 0.023 |
| 79.1 | 32.6695 | 0.5215 | 0.7448 | 0.0084 | 0.71 | 1.3427 | 0.0151 | 0.3226 | 0.0047 | 0.3407 | 0.1417 | <0.00 | 1.303 | 3.588 | 0.031 | 3.571 | 0.016 | 3.590 | 0.023 |
| 80.1 | 27.2496 | 0.2895 | 0.6960 | 0.0023 | 0.32 | 1.4368 | 0.0048 | 0.2826 | 0.0040 | 0.4509 | 0.1875 | <0.00 | 1.053 | 3.405 | 0.009 | 3.392 | 0.010 | 3.373 | 0.022 |
| 82.1 | 32.5330 | 0.3401 | 0.7297 | 0.0025 | 0.33 | 1.3705 | 0.0047 | 0.3217 | 0.0045 | 0.3963 | 0.1648 | 0.06 | 0.953 | 3.532 | 0.009 | 3.567 | 0.010 | 3.586 | 0.023 |
| 84.1 | 25.9640 | 0.3219 | 0.6702 | 0.0043 | 0.52 | 1.4920 | 0.0096 | 0.2790 | 0.0040 | 0.1580 | 0.0657 | 0.09 | 0.429 | 3.307 | 0.017 | 3.345 | 0.012 | 3.352 | 0.022 |
| 85.1 | 25.3353 | 0.4957 | 0.6858 | 0.0083 | 0.62 | 1.4581 | 0.0177 | 0.2811 | 0.0040 | 0.3163 | 0.1315 | 0.27 | 0.656 | 3.367 | 0.032 | 3.321 | 0.019 | 3.364 | 0.022 |
| 86.1 | 17.0401 | 0.1796 | 0.5770 | 0.0019 | 0.31 | 1.7332 | 0.0056 | 0.2130 | 0.0030 | 0.2679 | 0.1114 | 0.12 | 0.659 | 2.936 | 0.008 | 2.937 | 0.010 | 2.935 | 0.023 |
| 87.1 | 33.1141 | 0.3447 | 0.7398 | 0.0023 | 0.30 | 1.3516 | 0.0043 | 0.3220 | 0.0045 | 0.2203 | 0.0916 | 0.02 | 0.571 | 3.570 | 0.009 | 3.584 | 0.010 | 3.587 | 0.023 |
| 88.1 | 18.2831 | 0.2189 | 0.5957 | 0.0034 | 0.47 | 1.6787 | 0.0095 | 0.2243 | 0.0032 | 0.0459 | 0.0192 | 0.09 | 0.137 | 3.012 | 0.014 | 3.005 | 0.011 | 3.018 | 0.022 |
| 89.1 | 17.4495 | 0.1953 | 0.5758 | 0.0023 | 0.35 | 1.7367 | 0.0069 | 0.2166 | 0.0031 | 0.2971 | 0.1235 | 0.08 | 0.724 | 2.932 | 0.009 | 2.960 | 0.011 | 2.962 | 0.023 |
| 90.1 | 13.0195 | 0.1409 | 0.5223 | 0.0023 | 0.40 | 1.9148 | 0.0083 | 0.1796 | 0.0026 | 0.1659 | 0.0690 | 0.09 | 0.355 | 2.709 | 0.010 | 2.681 | 0.010 | 2.650 | 0.024 |

**Table 3.** Summary of LA-ICPMS U-Pb zircon isotopic data for metaconglomerate CB-3B. C.C = Correlation coefficient. $Pb^C$ = Common Pb (%).

Eighty-three U-Pb zircon concordant analyzes were obtained for metaconglomerate sample CB-03B, yielding $^{207}Pb/^{206}Pb$ ages in the 3.618 ±19 Ma to 2.376 ±36 Ma range (from the Paleoarchean, Mesoarchean, Neoarchean to the Paleoproterozoic-Siderian). Th/U ratios ranging between 0.275 and 2.208 are typical of igneous rocks (Belousova et al., 2002) **(Table 3)**. The zircon populations of Archaean ages range between 3.61 and 2.7 Ga. A very small zircon population yielded a Paleoproterozoic age **(Fig. 13 and Table 3)**.

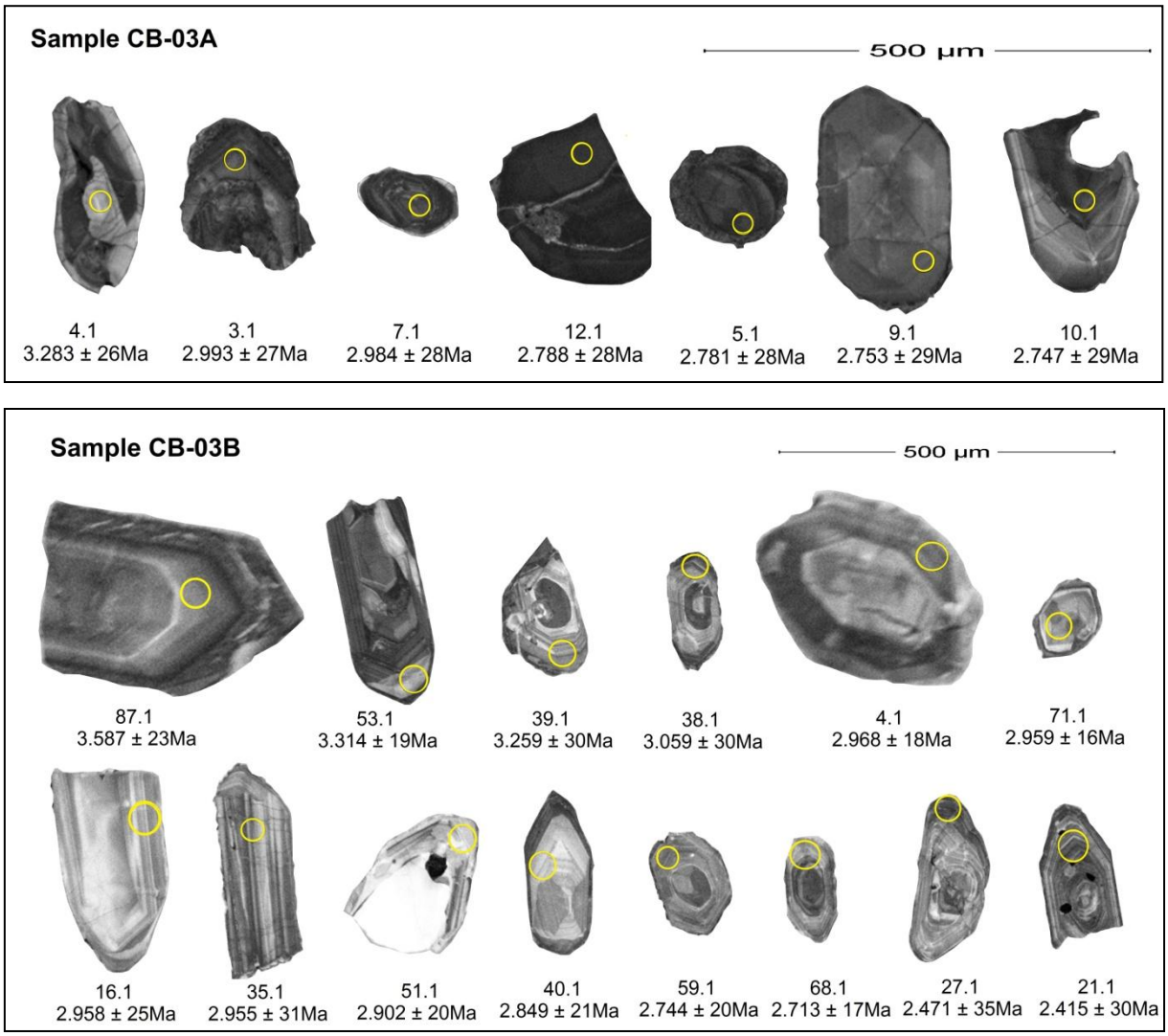


**Figure 12.** Cathodoluminescence images of analyzed zircons groups of samples CB-03A (Quartzite) and CB-03B (Metaconglomerate). The circle locates the spot analyzed and the corresponding $^{207}U/^{206}Pb$ age.

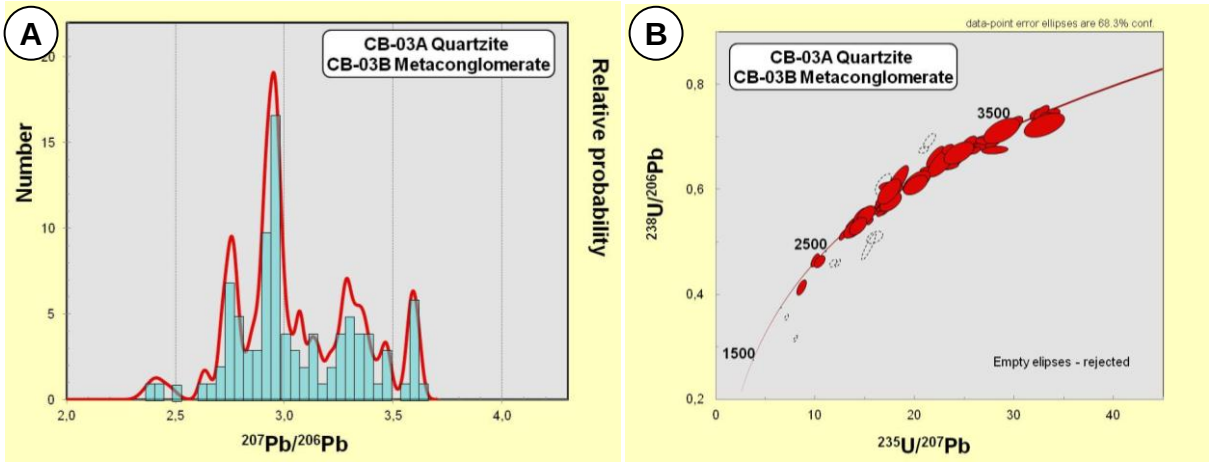


**Figure 13. A)** Relative $^{207}U/^{206}Pb$ ages probability and **B)** Concordia diagram for selected zircons from quartzite (CB-03A) and metaconglomerate (CB-03B) samples of the Upper Domain of the Vila Nova greenstone belt (n=96). Ages in Ga.

*4.2.2. Igneous zircon*

*Meta-andesite (CB-13B)*

The sample of meta-andesite (CB-13B) was collected near the Vila Nova gold-digging site (UTM zone 22N, coordinates 413825 and 51693). Sample CB-13B is from the tabular andesite body, with gray color and a blastoporphyritic texture characterized by plagioclase porphyroclasts of 1 to 2 mm in size, immersed in an actinolite-chlorite-muscovite-rich matrix. It shows prominent mylonitic foliation and stretching lineation.

The zircons crystals are euhedral, brown in color, and translucent to opaque. They have prismatic habit and almost always straight terminations, and range in size from 120 to 300 μm. Cores display oscillatory zoning in CL images with small dark rims **(Fig. 14A)**. Metamictic zircons are also present (e.g., 3.1). Some cores of xenocrysts display engulfment of overgrowth material, apparently due to magmatic corrosion (e.g., 17.1; 23.1) and/or resorption. Twenty-six LA-MC-ICPMS isotopic analyses were performed and most are nearly collinear in the U-Pb diagram. An attempt using all these data for estimating the crystallization age yields unacceptable high MSWD value (not shown). The calculated concordant $^{207}Pb/^{206}Pb$ ages range between 2.200 and 2.137 Ma, but the best collinear analyses (five spots) regress to yield an upper intercept of 2.170 ±9 Ma (MSWD = 0.085) **(Fig. 14B, Table 4)**. This age is interpreted as the meta-andesite zircon crystallization age. The two oldest zircons chosen for U-Pb analysis showed ages between 2.747 and 2.699 Ma and were considered to be inherited from basement host rocks.

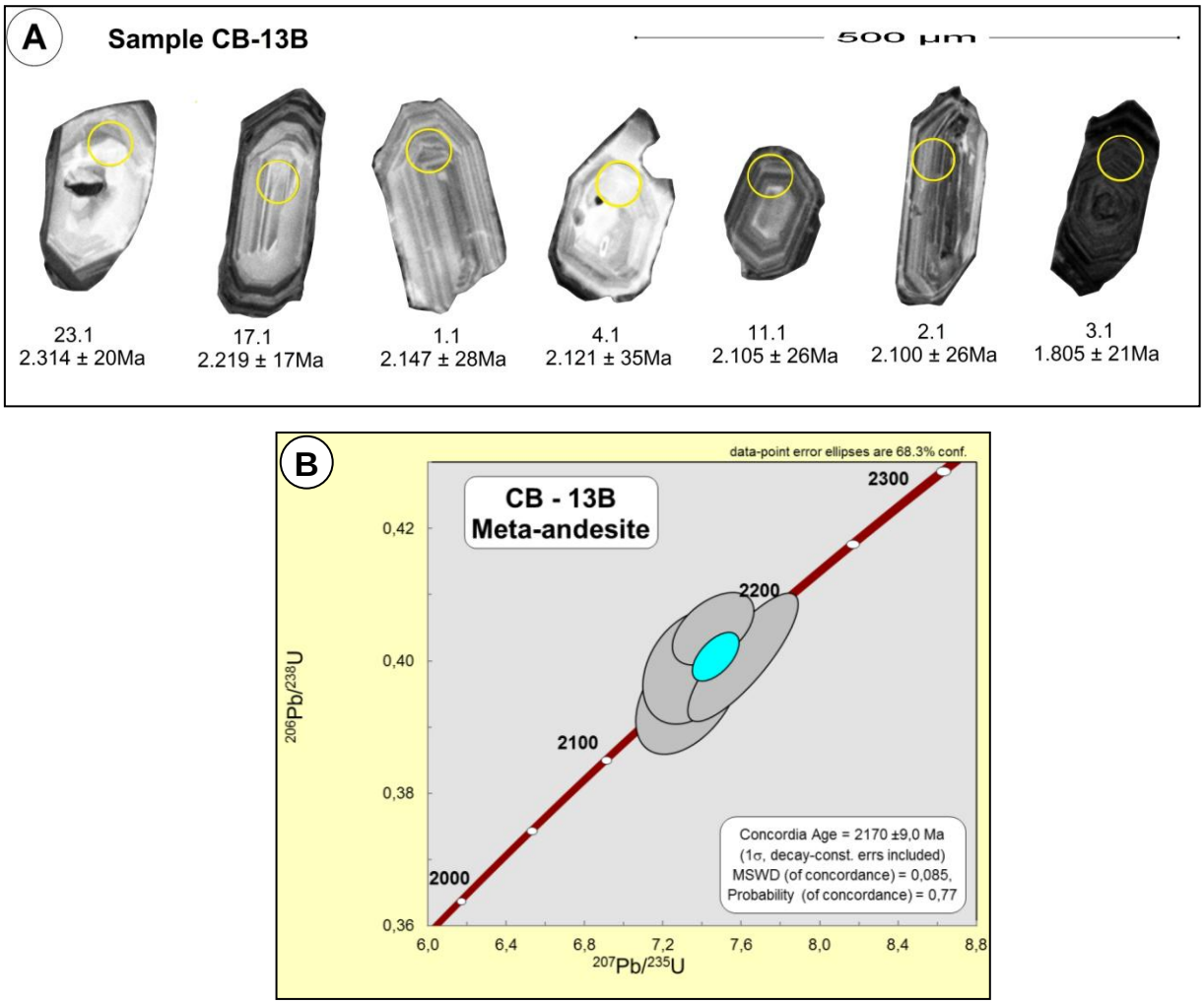


**Figure 14. A)** Cathodoluminescence images of selected zircons from sample CB- 13B. The circle locates the spot of the analysis in the zircons and the corresponding age. **B)** Concordia diagram for analyzed zircons from meta-andesite sample CB-13B (n=5).

### *4.3 Hf isotopes*

Hf zircon isotope compositions (mean ratios and the individual values for the spots) determined for selected zircon grains of meta-andesite (CB-13B) are presented in Table 5. Fig. 15 show the individual $\varepsilon_{Hf(t)}$ values versus Time based on the concordant $^{207}Pb/^{206}Pb$ crystallization age.

| Isotopic Ratios | | | | | | | | | | | | | Calculated Ages (Ma) | | | | |
|---|---|---|---|---|---|---|---|---|---|---|---|---|---|---|---|---|---|
| Spot | $^{207}Pb/^{235}U$ | ±(1σ) | $^{206}Pb/^{238}Pb$ | ±(1σ) | CC | $^{238}U/^{206}Pb$ | ±(1σ) | $^{207}Pb/^{206}Pb$ | ±(1σ) | $^{208}Pb/^{206}Pb$ | ±(1σ) | $Pb^{3}$ | Th/U | $^{206}Pb/^{238}U$ | ±(1σ) | $^{207}Pb/^{235}U$ | ±(1σ) |
| 1.1 | 7.3311 | 0.1780 | 0.3952 | 0.0061 | 0.46 | 2.5304 | 0.0388 | 0.1345 | 0.0027 | 0.1017 | 0.0043 | 0.26 | 0.76 | 2.147 | 0.028 | 2.158 | 0.035 |
| 9.1 | 7.3507 | 0.1665 | 0.3991 | 0.0057 | 0.33 | 2.5059 | 0.0360 | 0.1336 | 0.0025 | 0.2969 | 0.0184 | 0.00 | 1.02 | 2.165 | 0.026 | 2.146 | 0.032 |
| 13.1 | 7.6106 | 0.1862 | 0.4006 | 0.0064 | 0.83 | 2.4962 | 0.0396 | 0.1378 | 0.0029 | 0.1316 | 0.0069 | 0.76 | 1.47 | 2.172 | 0.029 | 2.200 | 0.037 |
| 22.1 | 7.4561 | 0.1374 | 0.4049 | 0.0036 | 0.49 | 2.4697 | 0.0217 | 0.1336 | 0.0025 | 0.0875 | 0.0033 | 0.10 | 0.36 | 2.192 | 0.016 | 2.145 | 0.033 |
| 16.1 | 7.4278 | 0.1371 | 0.4052 | 0.0035 | 0.91 | 2.4678 | 0.0213 | 0.1329 | 0.0024 | 0.1843 | 0.0086 | 0.13 | 0.61 | 2.193 | 0.016 | 2.137 | 0.031 |
| 8.1 | 7.5790 | 0.1737 | 0.4079 | 0.0060 | 0.98 | 2.4513 | 0.0358 | 0.1347 | 0.0026 | 0.1028 | 0.0044 | 0.34 | 0.65 | 2.206 | 0.027 | 2.161 | 0.033 |
| 26.1 | 7.3631 | 0.1294 | 0.3911 | 0.0032 | 0.99 | 2.5568 | 0.0209 | 0.1365 | 0.0023 | 0.1704 | 0.0041 | 0.62 | 1.35 | 2.128 | 0.015 | 2.184 | 0.029 |
| 4.1 | 7.2842 | 0.2188 | 0.3896 | 0.0075 | 0.62 | 2.5667 | 0.0496 | 0.1356 | 0.0036 | 0.1662 | 0.0108 | 0.47 | 0.60 | 2.121 | 0.035 | 2.172 | 0.047 |
| 15.1 | 7.6326 | 0.1430 | 0.4171 | 0.0037 | 0.97 | 2.3975 | 0.0213 | 0.1327 | 0.0025 | 0.1502 | 0.0035 | 0.12 | 0.52 | 2.247 | 0.017 | 2.134 | 0.033 |
| 18.1 | 7.6257 | 0.1451 | 0.4163 | 0.0038 | 0.83 | 2.4020 | 0.0218 | 0.1328 | 0.0026 | 0.1099 | 0.0133 | 0.02 | 0.50 | 2.244 | 0.017 | 2.136 | 0.034 |
| 19.1 | 7.6506 | 0.1469 | 0.4149 | 0.0038 | 0.90 | 2.4101 | 0.0222 | 0.1337 | 0.0026 | 0.0856 | 0.0047 | 0.20 | 0.33 | 2.237 | 0.017 | 2.148 | 0.034 |
| 21.1 | 7.5255 | 0.1367 | 0.4149 | 0.0035 | 0.96 | 2.4104 | 0.0205 | 0.1316 | 0.0024 | 0.1607 | 0.0067 | 0.04 | 0.61 | 2.237 | 0.016 | 2.119 | 0.032 |
| 24.1 | 7.6470 | 0.1412 | 0.4157 | 0.0036 | 0.79 | 2.4057 | 0.0211 | 0.1334 | 0.0024 | 0.1722 | 0.0044 | 0.06 | 0.61 | 2.241 | 0.017 | 2.144 | 0.032 |
| 25.1 | 7.5446 | 0.1298 | 0.4108 | 0.0033 | 0.92 | 2.4340 | 0.0194 | 0.1332 | 0.0023 | 0.1915 | 0.0183 | 0.14 | 0.52 | 2.219 | 0.015 | 2.140 | 0.031 |
| 2.1 | 6.9572 | 0.1582 | 0.3850 | 0.0055 | 0.94 | 2.5972 | 0.0373 | 0.1311 | 0.0025 | 0.2654 | 0.0339 | 0.56 | 0.70 | 2.100 | 0.026 | 2.112 | 0.033 |
| 6.1 | 6.9448 | 0.2176 | 0.3764 | 0.0074 | 0.62 | 2.6568 | 0.0522 | 0.1338 | 0.0039 | 0.1536 | 0.0153 | 0.77 | 0.90 | 2.059 | 0.035 | 2.149 | 0.051 |
| 7.1 | 6.8667 | 0.1623 | 0.3752 | 0.0057 | 0.92 | 2.6654 | 0.0403 | 0.1327 | 0.0026 | 0.2276 | 0.0108 | 2.16 | 4.04 | 2.054 | 0.027 | 2.135 | 0.035 |
| 11.1 | 7.1547 | 0.1606 | 0.3861 | 0.0055 | 0.97 | 2.5901 | 0.0370 | 0.1344 | 0.0025 | 0.1995 | 0.0045 | 0.27 | 0.73 | 2.105 | 0.026 | 2.156 | 0.032 |
| 5.1 | 13.9742 | 0.2922 | 0.5476 | 0.0073 | 0.97 | 1.8261 | 0.0244 | 0.1851 | 0.0031 | 0.1092 | 0.0038 | 0.20 | 0.51 | 2.815 | 0.031 | 2.699 | 0.028 |
| 10.1 | 5.6107 | 0.1462 | 0.3193 | 0.0050 | 0.99 | 3.1322 | 0.0495 | 0.1275 | 0.0023 | 0.1814 | 0.0855 | 1.64 | 3.76 | 1.786 | 0.024 | 2.063 | 0.031 |
| 12.1 | 8.4369 | 0.2467 | 0.4543 | 0.0085 | 0.97 | 2.2013 | 0.0411 | 0.1347 | 0.0036 | 0.1482 | 0.0200 | 0.56 | 0.62 | 2.414 | 0.038 | 2.160 | 0.046 |
| 14.1 | 8.0078 | 0.1512 | 0.4312 | 0.0039 | 0.69 | 2.3192 | 0.0210 | 0.1347 | 0.0026 | 0.1458 | 0.0056 | 0.28 | 0.48 | 2.311 | 0.018 | 2.160 | 0.034 |
| 20.1 | 11.4524 | 0.1853 | 0.4359 | 0.0032 | 0.98 | 2.2943 | 0.0171 | 0.1906 | 0.0030 | 0.1560 | 0.0375 | 1.06 | 0.79 | 2.332 | 0.015 | 2.747 | 0.026 |
| 23.1 | 7.9733 | 0.1692 | 0.4318 | 0.0045 | 0.73 | 2.3161 | 0.0240 | 0.1339 | 0.0029 | 0.1088 | 0.0056 | 0.20 | 0.44 | 2.314 | 0.020 | 2.150 | 0.038 |

**Table 4.** Summary of LA-ICPMS U-Pb zircon isotopic data for meta-andesite CB-13B. C.C = Correlation coefficient. $Pb^{C}$ = Common Pb (%).

The average of $^{176}Lu/^{177}Hf$ ratios ranges from 0.0004-0.001288 suggesting a strong partitioning between Lu and Hf isotopes (< 0.08) which is usually acquired during the partial melting (Berad and Johnson, 1997). Vervoort and Blichert-Toft (1999) suggesting that the behavior of the Lu-Hf system in igneous rocks results in a positive correlation of the isotopic composition of Hf in mantle-derived rocks, as indicated in Fig. 15. The wide variations in the Lu-Hf ratios are indicative of heterogeneous mantle sources which were subjected to crustal assimilation and/or partial melting of the continental crust. The analyses exhibit variable Hf $T_{DM}$ average ages, between 3.4 to 2.2 Ga **(Table 5)**, in agreement with this hypothesis. The variation of the Hf $T_{DM}$ model ages suggests the influence of some type of assimilation of different crustal sources.

| Grain /spot | 176Hf/177Hf | ± 2 se | 176Lu/177Hf | ± 2 se | U-Pb Age (T1) Ma | e Hf(0) | 176Hf/177Hf (T1) | e Hf (T1) | 176Hf/177Hf DM(T) | T DM (Ga) | 176Hf/177Hf DM(T) | e Hf (TDM) |
|---|---|---|---|---|---|---|---|---|---|---|---|---|
| 1,1 | 0,281507 | 0,000046 | 0,000489 | 0,0000035 | 2145 | -44,72 | 0,281487 | 2,56 | 0,281651 | 2519 | 0,281371 | 7,03 |
| 4,1 | 0,281628 | 0,000042 | 0,000641 | 0,0000045 | 2139 | -40,44 | 0,281602 | 6,50 | 0,281656 | 2262 | 0,281565 | 7,98 |
| 8,1 | 0,281583 | 0,000042 | 0,000734 | 0,0000048 | 2153 | -42,04 | 0,281553 | 5,07 | 0,281645 | 2364 | 0,281488 | 7,60 |
| 9,1 | 0,281582 | 0,000034 | 0,001288 | 0,0000156 | 2138 | -42,09 | 0,281529 | 3,89 | 0,281657 | 2428 | 0,281439 | 7,37 |
| 13,1 | 0,281098 | 0,000049 | 0,000433 | 0,0000043 | 2151 | -59,21 | 0,281080 | -11,79 | 0,281647 | 3434 | 0,280676 | 3,64 |
| 15,1 | 0,281560 | 0,000037 | 0,000738 | 0,0000072 | 2142 | -42,86 | 0,281530 | 4,00 | 0,281654 | 2424 | 0,281442 | 7,38 |
| 26,1 | 0,281343 | 0,000041 | 0,000706 | 0,0000131 | 2196 | -50,52 | 0,281314 | -2,44 | 0,281613 | 2877 | 0,281101 | 5,71 |
| 16.1 | 0,281486 | 0,000053 | 0,000544 | 0,0000052 | 2149 | -45,48 | 0,281464 | 1,81 | 0,281648 | 2570 | 0,281333 | 6,85 |
| 18.1 | 0,281529 | 0,000054 | 0,001021 | 0,0000447 | 2152 | -43,96 | 0,281487 | 2,71 | 0,281646 | 2515 | 0,281374 | 7,05 |
| 19.1 | 0,281541 | 0,000026 | 0,000465 | 0,0000090 | 2169 | -43,52 | 0,281522 | 4,34 | 0,281633 | 2423 | 0,281443 | 7,39 |
| 21.1 | 0,281470 | 0,000035 | 0,000591 | 0,0000103 | 2149 | -46,04 | 0,281446 | 1,17 | 0,281648 | 2611 | 0,281302 | 6,70 |

**Table 5.** Summary of LA-MC-ICPMS Lu-Hf zircon isotopic data for meta-andesite CB-13B.

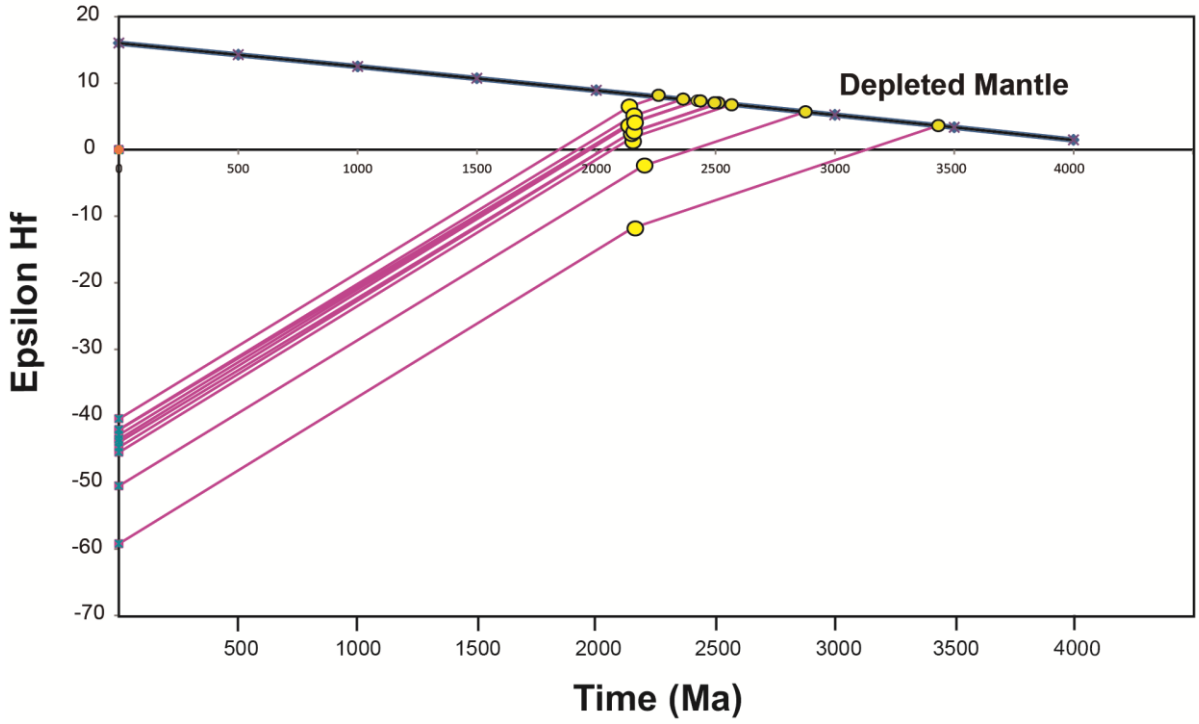


**Figure 15.** $\varepsilon_{Hf(t)}$ evolution vs. Time diagram based on concordant $^{207}Pb/^{206}Pb$ zircon (for the given spot analyses).

## 5. Discussion

### *5.1 Sources of the sedimentary rocks of the VNGB basin and age of volcanism*

From a tectonic perspective, the new and compiled U-Pb and Pb-Pb igneous zircon data demonstrate that recurrent volcanism in the 2.17 and 2.15 Ga. These time interval represent the orogenic phase of the VNGB and maximum depositional age for the basin (see section 2 and Table 1). Nine analyzed zircon crystals

presented Hf values between +1.17 and +6.5, and two zircons, between -2.44 and -11.79, suggesting a combination of sources (MORB and minor sublithospheric continental mantle) in the genesis of meta-andesites. The Hf $T_{DM}$ model ages show Paleoproterozoic (Siderian) values, between 2.26 and 2.42 Ga. Two zircon crystal shows Paleo- and Neo-archean, between 2.52 and 3.43 Ga and εHf(t) positive, between +3.64 and +7.98. The bulk feature of meta-andesite sample suggests a broad juvenile episode that was subjected to some kind of crustal contribution. This data are in agreed with the geochemical signature of these rocks presented by McReath and Faraco (2006) and with the geochemical and isotopic data from Hoffmann et al. (2018).

The geologic data and U-Pb age patterns of detrital zircon grains from the metasediments of the VNGB demonstrate that the original sediments are derived from the erosion of the older basement crustal rocks. The source rocks that generated the sedimentary package are predominantly Archean, in the interval between 3.6 and 2.7 Ga, as partially previously reported by Sm-Nd, Pb-Pb and U-Pb available data (see Section 2). U-Pb zircon data obtained in a quartzite and in the metaconglomerate of the Upper Domain of the VNGB characterize four groups of sedimentary sources with specific patterns: 3.6 Ga, 3.4-3.2 Ga, 2.9-2.8 and 2.7-2.6 Ga. Three groups are distinguished by Paleo- to Meso-archean and the fourth by transitional ages from Neo-archean to Paleoproterozoic (Siderian). The Archean groups are represented by 31% Paleo-archean, 46% Meso-archean and 18% Neo-archean zircon ages. The fourth group with 5% of zircon ages represents the Neo-archean to Paleoproterozoic transition. The zircon grains yielding these ages have in common overgrowth around inherited cores that provides these younger ages. These ages may indicate an event of Siderian age (2.4 Ga).

Assigning source areas for detrital zircons is not a simple task, and it can be highly speculative. The success of these correlations depends mainly on the recognition of the basement unit within the basin and on the availability of good geochronological information. The basement on the VNGB region is composed of orthogneisses, metagranitoids and gabbros of the Tumucumaque Complex (TC) and by the metamafic-ultramafic rocks of the Bacuri Complex. The TC rocks yielded ages between 2.9 and 2.6 Ga, corroborating the existence of a wide Archean basement in this region (Rosa-Costa et al., 2006). This hypothesis corroborates with the ages obtained recently by Borghetti et al. (2018) for the units of TC occurring in the Vila Nova region. The oldest U-Pb zircon ages were obtained for a tonalitic gneiss (2.85 Ga), two metagranodiorites (2.82 and 2.81 Ga), and a gabbro (2.67 Ga).

As mentioned above, the Paleo- and Meso-archean U-Pb zircon ages between 3.6 and 3.0 Ga obtained in our study, are similar to those of crustal relics found in the Vila Nova, Serra do Navio and Tartarugalzinho regions (Pimentel et al., 2002; Klein et al., 2003, Rosa-Costa et al., 2003, 2006, 2012) and probably related to some Archean undifferentiated granitoids of the study area (*cf*. whole-rock Sm-Nd $T_{DM}$ ages by Barbosa et al., 2013). Teixeira et al. (2015) obtained Sm-Nd model ages between 3.56 and 2.94Ga for the mafic and ultramafic rocks of the Carajás Mineral Province, located 800 km southeast of the study area.

The Archean to Paleoproterozoic transition, characterized by ages around 2.4 Ga, allow us to indicate 2.37 Ga as the minimum depositional age for the sediments of the Vila Nova greenstone belt.

### *5.2 Metamorphism and deformation*

Successive deformation stages and metamorphism are commonly recorded by metamorphic rocks and the correct recognition and interpretation of the original

processes is essential to the understanding of their evolution. Deformation phases are related to specific periods during which a rock is deformed under the influence of differential stress, leaving visible records, such as folds, cleavage and lineation (Passchier and Trouw, 2005). During a metamorphism stage, a specific mineral assemblage will be present under certain P-T conditions. The metamorphism stage can also be replaced by other metamorphic events, leaving a recognizable record only if equilibrium is not reached, enabling the recognition of previous assemblages (Passchier and Trouw, 2005).

The VNGB rocks were subjected to upper greenschist and intermediate amphibolite metamorphic facies, similar to those reported by Avelar et al. (2003), Delor et al. (2003a,b), Mc Reath and Faraco (2006), Rosa-Costa et al. (2003, 2006) and Spier and Ferreira Filho (1999). The metamorphic assemblage observed in metamafites include, in increasing temperature order: (i) Act + Ab + Ep + Chl**,** (ii) Ca Plag + Hb, (iii) Ca Plag + Hb + Gt + Bt, (iv) Hb + Trem and (v) Ca Plag + Hb + Diop. The metapelites present the following assemblages: (i) Musc + Bt, (ii) Musc + Bt + Gt, and (iii) Musc + Bt + Cord + Gt. Pressure conditions are intermediate, as indicated by the metamorphic assemblage Ca Plag + Hb + Gt observed in metamafites and by Cord + Gt in metapelites **(Table 6)**.

Integration of structural and micro-structural data allowed the recognition of four main metamorphic events in the VNGB. $M_1$ and $M_2$ events correspond to orogenic collisional-type metamorphism, and $M_3$ corresponds to a cataclastic metamorphism related to development of the transcurrent ductile shear zones. The last $M_4$ event is younger and related to thermal contact metamorphism associated with emplacement of the Late-rhyacian to Orosirian intrusive granites. The collisional metamorphism is responsible for the generation of $S_1$ and $S_2$ metamorphic foliations which resulted in a regional N70°W to N85°W trend, associated with $F_2$ folding

phase. The development of the regional structures such as the Serra do Navio, Cupixi and Vila Nova ductile shear zones is related to $S_2$ and probably evolved from thrust kinematics to oblique shear zones. During the late- to post-collisional period occur the developments of the $F_3$ folding phase and of the transcurrent shear zones. These structures control the emplacement of the intrusive Paleoproterozoic granites. Ab-ep hornfels and Hb hornfels metamorphism has also been identified in the metavolcano-sedimentary rocks of the VNGB and are related to intrusions of the Late-rhyacian to Orosirian intrusive granites. The last deformational phase is characterized by the formation of brittle-ductile shear zones of NE-SW direction associated to open folding.

| **Rock** | **Mineral Assemblage** | | **Temporal Relationships** | **Metamorphic facies** | **Microstructural features** | |
|---|---|---|---|---|---|---|
| Amphibolite | Hb + Pl + Grt (Di) | **OM** | Syn-tectonic | Upper Amphibolite | Intrafolial folds and crenulation cleavage | **$S_1$ and $S_2$** |
| | Chl + Ser + Ep | **OM** | Tardi-tectonic | Ab-Ep hornfels/ Greenschist | Fractures with retrometamorphism | **$S_3$** |
| Amphibole schist | Bio + Tr | **OM** | Syn-tectonic | Amphibolite | Mineral orientation | **$S_1/S_2$** |
| | Hb + Clo + Cln | **OM** | | Upper Greenschist | | |
| Mafic cornubianites | Hb + Tr | **OM** | | Amphibolite | | |
| | Di + Hb | **CM** | Post-tectonic | Px Hornfels | ---------- | |
| | Hb + Pl | **CM** | | Hb Hornfels | ---------- | |
| Metaultramafites | Tr | **OM** | Syn-tectonic | Amphibolite | Intrafolial folds and crenulation cleavage | **$S_1$ and $S_2$** |
| Metapelites | Grt + Crd + Bio | **OM** | Syn-tectonic | Amphibolite | Intrafolial folds and crenulation cleavage | **$S_1/S_2$** |
| Mylonitic quartzites | Qtz + Mgt | **CM** | Syn-tectonic | Upper Greenschist/ Amphibolite | Mineral stretching | **$S_1/S_2$** |
| Mylonitic metaconglomerates | Qtz + Ep (Fct) | **OM** | Syn-tectonic | Upper Greenschist/ Amphibolite | Mineral stretching | |

**Table 6.** Relationships between the main microstructures observed under the microscope and the metamorphic events. Legend - OM = orogenic metamorphism, CM = cataclastic metamorphism; - Foliation: $S_1$= schistosity, $S_2$= crenulation cleavage, $S_3$= fracture cleavage; Minerals: Hb = hornblende, Pl = plagioclase, Grt = garnet, Di = diopside, Chl = chlorite, Ser =sericite, Ep = Epidote, Tr = tremolite, Bio = biotite, Crd = cordierite, Qtz = quartz, Mgt = magnetite, Fct = fuchsite, Px = pyroxene, Cln = clinochlore.

The metasedimentary rocks investigated presented U-Pb detrital zircons ages between 3.6 and 2.4 Ga, confirming the erosion of the Archean basement in the

formation of the VNGB. The obtained ages of 2.15 Ga (Hoffmann et al., 2018) and 2.17 Ga (this work) for two meta-andesites of the VNGB establishing the Rhyacian period as the maximum deposition age of the basin. The units of the VNGB are cut by the Amapari, Porto Grande and Igarapé Careta Suite granites and by other undifferentiated granitic plutons of Paleoproterozoic age. The emplacement of these granites causes textural transformations in the metavolcano-sedimentary rocks related to thermal metamorphism. The Pb-Pb evaporation zircon ages obtained by Barbosa et al. (2013) and Faraco et al. (2004) in the intrusive granites, such as the Igarapé Careta Suite (2.06 Ga), Amapari Granite (1.99 Ga) and the Porto Grande Granite (1.84 Ga) suggest that the orogenic metamorphism that affected the rocks of the VNGB occurred between 2.15 and 2.06 Ga.

### *5.3 Tectonic Environment*

A suggestion of evolutionary model based on the available information and modified from Delor et al. (2003a) is presented in **Figure 16**. In this model, we can observe that the basin that generated the VNGB was originated from a rift in the basement represented by the Amapá Terrane. This rift evolves into a small ocean and the erosion of the basement areas generates the sedimentary package as passive margin sequence **(Fig. 16A)**. The closure of the ocean generates an intra-oceanic magmatic arc characterized by the generation of a high-Al tholeiitic to low-K calc-alkaline volcanism, chemical sediments and related TTG granites (Hoffmann et al., 2018) **(Figs. 16B** and **16C)**. The final evolution of the ocean closure occurs with the collision between the southwestern and northeast portion of the Amapá Terrane and the formation of oblique shear zones of continental scale. These structures evolve during the late- to post-collisional period to transcurrent shear zones and

control the generation and the positioning of Paleoproterozoic intrusive granites **(Fig. 16D)**.

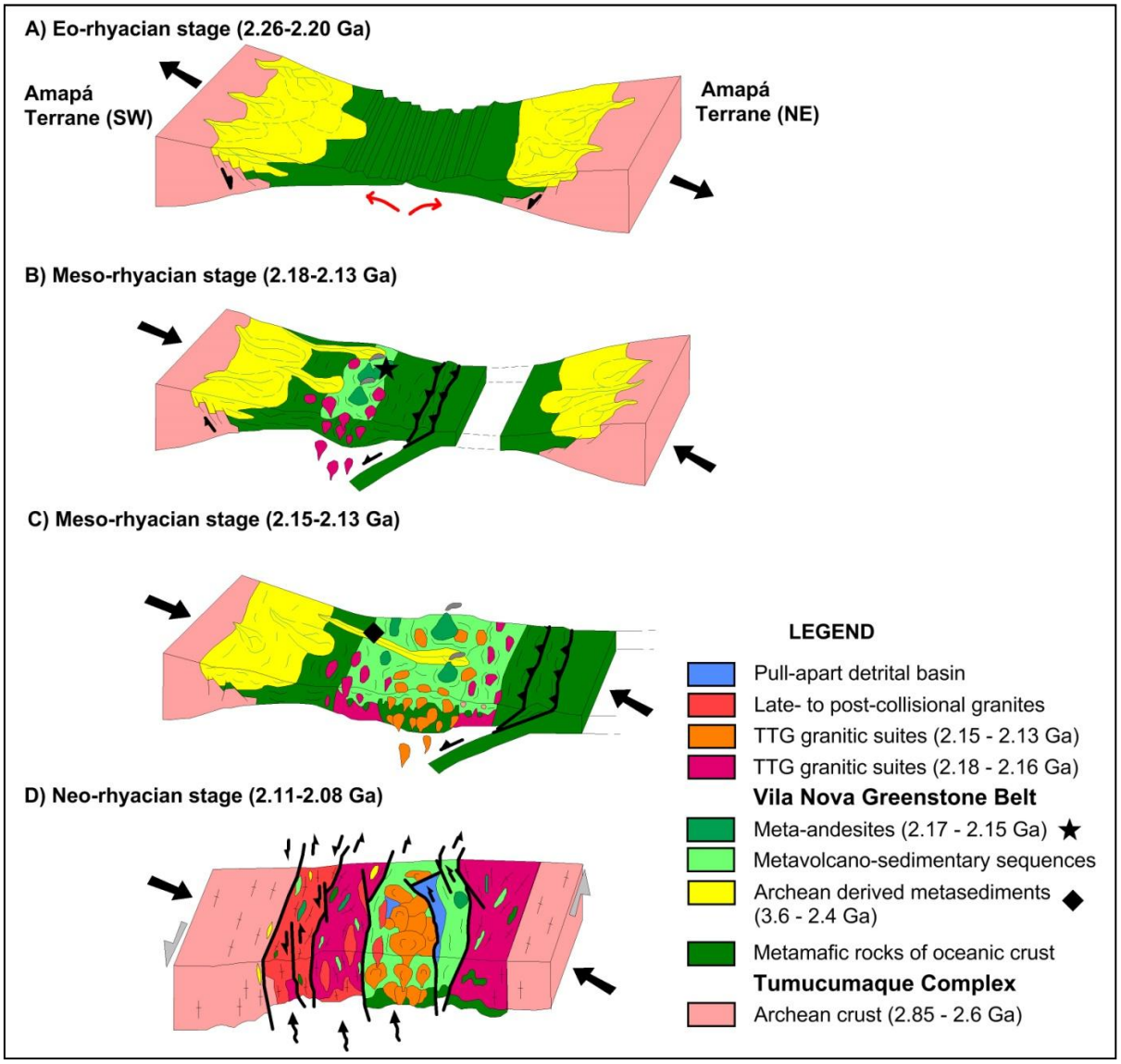


**Figure 16.** Proposed model of geodynamic evolution adapted from Delor et al. (2003a) for the study area.

## 6. Conclusions

The Vila Nova greenstone belt is composed by a metavolcanic domain at the base, and of metasedimentary upper domain, intercalated with mafic metavolcanic rocks and exhalative chemical rocks. The metasediments were probably generated in a passive margin environment.

The U-Pb detrital zircons ages obtained for the metasedimentary rocks of the VNGB are related to erosion of the basement rocks of the Tumucumaque and Guianense complexes. Paleo-archean ages (3.6 to 3.0 Ga) were reported for an orthogneiss of the Serra do Navio (3.3 Ga), Tartarugalzinho (3.48 Ga) and Vila Nova (3.3 Ga) regions. Ages around 3.6 Ga are abundant and represent Archean source rocks that not outcrop in the Vila Nova region. These new detrital zircon provenance data corroborate the existing hypothesis of an Archean core in the southeastern portion of the Guiana Shield.

U-Pb ages obtained for the zircon crystals of the meta-andesites (2.17 and 2.15 Ga) suggest that the Vila Nova basin evolved during the Meso-rhyacian period. Orogenic metamorphism is younger than the basin deposition and, therefore, younger than 2.15 Ga. Contact metamorphism is suggested by Pb-Pb zircon ages obtained for intrusive granites, such as the Igarapé Careta Suite (2.06 Ga) and the Amapari Granite (1.99 Ga). Thus, the orogenic metamorphism may have occurred between 2.15 and 2.07 Ga.

The Vila Nova basin probably represents the evolution of a continental rift of Neo-rhyacian age, which evolved into a small ocean under tectonic extension conditions. Subsequently, the inversion of the tectonic conditions to contractional tectonics is responsible for the closure of the ocean and the generation of islands arcs and back-arc to fore-arc basins with generation of intense tholeiitic to low-K calc-alkaline mafic volcanism (Hoffmann et al., 2018). The deformation of the VNGB was associated with the collisional metamorphism and accompanied by the intrusion of syn- to late-collisional granitic plutons at the end of the Rhyacian period. The generation of the VNGB is related to the construction of the Maroni-Itacaiúnas Province around of the old Archean nucleus represented by the Amapá Terrane.

**Acknowledgments**

We would like to acknowledge the Brazilian National Council for Scientific and Technological Development (CNPq) for the research grants to the first and second authors, the Geoscience Institute of Rio Grande do Sul Federal University (UFRGS) and PETROBRAS S.A. oil company for field work support and laboratories; the Amapari Mining Company for field logistics and making geologic and drilling hores data available, and specially geologists João B.G. Teixeira and Carlos A.L. Souza for fruitful discussions. We thank geologists Heiny P. Kloss and Gustavo Zvirtes for their cooperation in collecting LA-MC-ICPMS data. Special thanks to geologists Tarso L. Rosenhain, Elaine Cunha, and Jordão I. Ramos and to Eng. Vitor Rosenhain for the valuable support given to this work. We thank Walter M. Sproesser and Solange L. Souza from the Geochronologic Research Center (CEPEGEO) of the Geosciences Institute from the São Paulo University (USP) for their cooperation in obtaining the geochronological data. We are grateful to reviewers for the helpful comments and suggestions and to the editors for comments and editorial handling of the manuscript.

## References

Almeida, F.F.M., Brito Neves, B.B., Carneiro, C.D.R. 2000. The origin and evolution of the South American Platform. Earth-Science Review, 50(1-2): 77-111.

Avelar, V.G., 2002. Geocronologia Pb-Pb em zircão e Sm-Nd em rocha total da porção centro-norte do Estado do Amapá – Brasil: Implicações para a evolução geodinâmica do setor oriental do Escudo das Guianas. Tese de Doutorado, Universidade Federal do Pará.

Avelar, V.G., Lafon, J.M., Delor, C., Guerrot, C., Lahondère, D., 2003. Archean crustal remnants in the easternmost part of the Guiana Shield: Pb-Pb and Sm-Nd geochronological evidence for Mesoarchean versus Neoarchean signatures. Geologie de la France. 2-3-4, 83-100.

Barbosa, J.P.O., Costa Neto, M.C., Rosa-Costa, L.T., Anjos, G.C., Chaves, C.L., 2013. Projeto Folha Macapá (NA-22-Y-D). Mapa Geológico (1:250.000). CPRM, Belém.

Barreto, C.J.S., Lafon, J.M., Rosa-Costa, L.T., Dantas, E.L., 2013. Paleoproterozoic granitoids from the northern limit of the Archean Amapá block (Brazil), southeastern Guyana Shield: Pb-Pb evaporation in zircons and Sm-Nd geochronology. Journal of South American Earth Sciences. 45, 97-116.

Belousova, E.A., Griffin, W.L., O'reilly, S.Y., Fisher, N.I., 2002. Igneous zircon: Trace element composition as an indicator of source rock type. Contributions to Mineralogy and Petrology. 143, 602-622.

Beard, B.L., Johnson, C.M., 1997. Hafnium isotope evidence for the origin of Cenozoic basaltic lavas from the south-western United States. Journal of Geophysical Research, 102, 20149-20178.

Borghetti, C., Philipp, R.P., Basei, M.A.S., Mandetta, P., Hoffman, I.B., 2018. Geochronology of the Archean Tumucumaque Complex in the Vila Nova and Serra do Navio regions, northeast portion of the Amazon Craton, Amapá State, Brazil. Journal of South American Earth Sciences. Submitted.

Cawood, P. A., Nemchin, A.A., 2001. Paleogeographic development of the east Laurentian margin: Constraints from U-Pb dating of detrital zircons in the Newfoundland Appalachians In: Geological Society of America Bulletin. 113(9), 1234-1246.

Cawood, P.A., Hawkesworth, C.J., Dhuime, B., 2012. Detrital zircon record and tectonic setting. Geology. 40(10), 875–878.

Chemale Jr. F., Dussin I.A., Alkmim F.F., Martins M., Queiroga G.N., Armstrong R., Santos M., 2011. Unravelling a Proterozoic basin history through detrital zircon geochronology: The case of the Espinhaço Supergroup, Minas Gerais, Brazil. Gondwana Research. 22(1), 200-206.

Chew, D.M., Flowerdew, M.J., Page, L.M., Crowley, Q.G. Daly, J.S., Cooper, M., Whitehouse, M.J., 2008. The tectonothermal evolution and provenance of Tyrone Central Inlier, Ireland: Grampian imbrication of an outboard Laurentian microcontinent. Journal of the Geological Society. 165, 675-685.

Chu, N.C., Taylor, R.N., Chavagnac, V., Nesbitt, R.W., Boella, R.M., Milton, J.A., German, C.R., Bayon, G., Burton, K., 2002. Hf isotope ratio analysis using multi collector inductively coupled plasma mass spectrometry: an evaluation of isobaric interference corrections. J. Anal. At. Spectrom. 17, 1567-1574.

Condie, K.C., O´Neill, C., Aster, R., 2009. Evidence and implications for a widespread magmatic shutdown for 250 My on Earth. Earth and Planetary Science Letters. 282, 294-298.

CPRM – Serviço Geológico do Brasil. (2004). Programa Geologia do Brasil, Projeto Aerogeofísico Rio Araguari, Relatório Final do Levantamento e Processamento dos Dados Magnetométricos e Gamaespectrométricos.Texto Técnico, Volume I, 136p. Rio de Janeiro: Lasa Engenharia e Prospecções S/A.

CPRM – Serviço Geológico do Brasil. (2006). Programa Geologia do Brasil, Projeto Aerogeofísico Amapá, Relatório Final do Levantamento e Processamento dos Dados Magnetométricos e Gamaespectrométricos. Texto Técnico, Volume I, 272p. Rio de Janeiro: Lasa Engenharia e Prospecções S/A.

De Graaff-Surpless, K., Graham, S.A., Wooden, J.L., McWilliams, M.O., 2002. Detrital zircon provenance analysis of the Great Valley Group, California: Evolution of an arc-forearc system. Geological Society of America Bulletin. 114, 1564–1580.

Delor, C., Lahondère, D., Egal, E., Lafon, J.M., Cocherie, A., Guerrot, C., Rossi, Ph., Trufert, C., Theveniaut, H., Phillips, D., Avelar, V.G., 2003a. Transamazonian crustal growth and reworking as revealed by the 1:500.000-scale geological map of French Guiana (2nd edition). Géologie de la France. 2-3-4, 5-57.

Delor, C., Roever, E.W.F., Lafon, J.M., Lahondère, D., Rossi, P., Cocherie, A., Guerrot, C., Potrel, A., 2003b. The Bakhuis ultrahigh-temperature granulite

belt (Suriname): II. Implications for late Transamazonian crustal stretching in a revised Guiana Shield framework. Géologie de la France. 2-3-4, 207-230.

Elholou, S., Belousova, E., Griffin, W.L., Peasom, N.J., O'Reilly, S.Y., 2006. Trace element and isotopic composition of GJ red zircon standard by laser ablation. Geochimica and Cosmochimica Acta. 70(18), 158-164.

Ernst, W.G., 2009. Archean plate tectonics, rise of proterozoic supercontinentality and onset of regional episodic stagnant-lid behavior. Gondwana Research. 15 (3/4), 243-253.

Faraco, M. T. L., Marinho, P. A. C., Costa, E. J. S., Vale, A. G., Camozzato, E., 2004. Carta Geológica do Brasil ao Milionésimo: Sistema de Informações Geográficas-SIG. Folha NA.22 – Macapá. Escala 1:1.000.000. *(CDROM) Programa Geologia do Brasil*. Brasília: CPRM.

Hawkesworth, C., Cawood, P., Kemp, T., Storey, C., Dhuime, B., 2009. A Matter of Preservation: Science. 323,49–50.

Hoffmann, I., Philipp, R.P., Borghetti, C., 2018. Geochemistry and origin of the tholeiitic metabasalts from the 2.15 Ga Vila Nova greenstone belt, Amapá, Brazil. Journal of South American Earth Sciences. Submitted.

Jackson, S.E., Pearson, N.J., Griffin, W.L., Belousova, E.A., 2004. The application of laser ablation inductively coupled plasma mass spectrometry to in situ U-Pb zircon geochronology. Chemical Geology. 211, 47-69.

Klein, E.L., Rosa-Costa, L.T. da, Lafon, J.M., 2003. Magmatismo Paleoarqueano (3,32Ga) na região do Rio Cupixi, SE do Amapá, SE do Escudo das Guianas. In: VII Simpósio de Geologia da Amazônia 8, Manaus. Resumos Expandidos, Manaus, SBG-NO. CD ROM.

Lafon, J.M., Avelar, V.G., Rossi, P.H., Delor, C., Guerrot, C., Pidgeon, R.T., 2000. Geochronological evidence for reworked Neoarchean crust during Transamazonian orogeny (2,1 Ga) in the southeastern Guiana Shield. In: International Geological Congress, 31, Rio de Janeiro, Abstracts, CD Rom.

Ludwig, K.R., 1999. User's manual for ISOPLOT/EX: a geochronological toolkit for Microsoft Excel (version 2.05). Berkeley Geochronology Center. Special Publication. 1a, pp. 1-48.

Ludwig, K.R., 2002. SQUID. User's manual (Version 1.02). Berkeley Geochronology Center. Special Publication. 2, 17p.

Ludwig, K.R., 2008, Manual for Isoplot 3.7: Berkeley Geochronology Center, Special Publication No. 4. rev. August 26, 2008, 77 pp.

Magalhães, L.A., Souza Filho, C.R., Silva, A.M. (2007). Caracterização geológica – geofísica da porção central do Amapá com base em processamento e interpretação de dados aerogeofísicos. Revista Brasileira de Geociências. 37(3): 464-477.

McReath I., Faraco M.T.L., 2006. Paleoproterozoic greenstone-granite belts in northern Brazil and the former Guyana Shield-West African craton province. Revista do Instituto de Geociências-USP. Sér. Cient. 5(2), 49-63.

Passchier, C.W., Trouw, R.A.J., 2005. Microtectonics. Springer-Verlag, Berlim, pp. 1-366.

Patchett, P.J. and Tatsumoto, M. (1980). A routine high-precision method for Lu-Hf isotope geochemistry and chronolgy. Contributions to Mineralogy and Petrology 75, 263-267.

Pimentel, M.M., Ferreira Filho, C.F., Spier, C.A., 2002. Estudo Sm-Nd do Complexo Máfico-Ultramáfico Bacuri, Amapá: idade da intrusão, metamorfismo e natureza do magma original. Rev. Bras. Geoc. 32, 371-376.

Prothero, D.R., Dott Jr., R.H., 2009. Evolution of the Earth, Eighth ed. McGraw-Hill Science and Engineering, pp. 1-576.

Ricci, P.S.F.; Carvalho, J.M.A.; Rosa-Costa, L.T.; Lafon, J.M. 2002. Plúton charnoenderbítico arqueano intrusivo nos ortognaisses granulíticos do Cinturão Jari–Terreno Arqueano expressivo do sudeste do Escudo das Guianas. In: Congresso Brasileiro de Geologia, 41, João Pessoa. Anais, SBG-NE, p.524.

Rosa-Costa, L.T., Ricci, P.S.F., Lafon, J.M., Vasquez, M.L., Carvalho, J.M.A., Klein, E.L., Macambira, E.M.B., 2003. Geology and geochronology of archean and paleoproterozoic domains of the southeastern Amapá and northwestern Pará, Brazil – southeastern Guyana Shield. Géologie de la France. 2-3-4,101-120.

Rosa-Costa, L.T., (Ph Thesis) 2006. Geocronologia $^{207}Pb/^{206}Pb$, Sm-Nd, U-Th-Pb e $^{40}Ar$-$^{39}Ar$ do Segmento Sudeste do Escudo das Guianas: Evolução Crustal e Termocronologia do Evento Transamazônico. Universidade Federal do Pará, CG, Curso de Pós-Graduação em Geologia e Geoquímica, Belém, pp. 226.

Rosa-Costa, L.T., Silva, C.M.G., Barbosa, J.P.O., Costa Neto, M.C., 2012. Projeto Folha Rio Araguari (NA-22-Y-B). Mapa Geológico (1:250.000). CPRM, Belém.

Santos, J.O.S., Hartmann, L.A., Gaudette, H.E., Groves, D.I., Mc Naughton, N.J., Fletcher, I.R., 2000. A new understanding of the provinces of the Amazon

Craton based on integration of field mapping and U-Pb and Sm-Nd geochronology. Gondwana Research. 3(4), 453-488.

Sleep, N.H., Windley, B.F., 1982. Archean plate tectonics: constraints and inferences. Journal of Geology. 90(4), 363-397.

Spier, C.A., Ferreira Filho, C.F., 1999. Geologia, estratigrafia e depósitos minerais do Projeto Vila Nova, Escudo das Guianas, Amapá, Brasil. Rev. Bras. Geoc. 29, 173-178.

Stacey, J.S., Kramers, J.D., 1975. Approximation of terrestrial lead isotopic evolution by a two stage model. Earth Planetary Sciences Letters. 26, 207-221.

Tassinari, C.C.G., Macambira, M.J.B., 1999. Geochronological provinces of the Amazonian Craton. Episodes. 22(3), 174-182.

Tassinari, C.C.G., Bettencourt, J.S., Geraldes, M.C., Macambira, M.J.B., Lafon, J.M., 2000. The Amazonian Craton. In: Cordani, U.G., Milani, E.J., Filho, A.T., Campos, D.A. (Eds.). Tectonic Evolution of South America. Rio de Janeiro, 31º International Geological Congress, SBG. pp. 41-95.

Tassinari, C.C.G., Macambira, M.J.B., 2004. A evolução tectônica do Cráton Amazônico. In: Mantesso-Neto, V. (Ed.), Geologia do continente Sul-americano: evolução da obra de Fernando Flávio Marques de Almeida. São Paulo. pp. 471-485.

Tavares, R.P.S. (MSc thesis) 2009. Granitóides e anfibolitos da Serra do Navio, borda norte do bloco arqueano Amapá: caracterização petrográfica e geoquímica, geocronologia Pb-Pb em zircão e isótopos de Nd. Universidade Federal do Pará, Centro de Geociências, Pós-Graduação em Geologia e Geoquímica, Belém, pp. 114.

Teixeira, W., Tassinari, C.C.G., Cordani, U.G., Kawashita, K., 1989. A review of the geochronology of the Amazonian Craton: Tectonic implications. Precambrian Research., 42, 213-227.

Teixeira, A.S., Ferreira Filho, C.F., Giustina, M.E.S.D., Araújo, S.M., Silva, H.H.A.B., 2015. Geology, petrology and geochronology of Lago Grande Layered Complex: evidence for a PGE-mineralized magmatic suite in Carajás Mineral Province, Brazil. J. S. Am. Earth Sci. 64, 116-138.

Van Achterbergh, E., Ryan, C. G., Jackson, S. E., Griffin, W. L. (2001). Data reduction software for LA-ICP-MS: appendix. In: P. J. Sylvester (Ed.), Laser Ablation-ICP Mass Spectrometry in the Earth Sciences: Principles and

Applications. Ottawa: Mineralogical Association of Canada (MAC) Short Course Series. 29, 239-243.

Van Kranendonk, M.J., 2010. Two types of Archean continental crust: plume and plate tectonics on early Earth. Am. J. Sci. 310(10), 1187-1209.

Velásquez, G., Béziat, D., Salvi, S., Tosiani, T., Debat., P. 2011. First occurrence of Paleoproterozoic oceanic plateau in the Guiana Shield: The gold-bearing El Callao Formation, Venezuela. Precambrian Research. 186, 181-192.

Vervoort, J.D. and Blichert-Toft, J. (1999). Evolution of the depleted mantle: Hf isotope evidence from juvenile rocks through time. Geochimica et Cosmochimica Acta 63(3-4): 533-556. doi: 10.1016/S0016-7037(98)00274-9.

## 3. ANEXOS

**3.1.** Geochemistry and origin of the Rhyacian tholeiitic metabasalts and meta-andesites from the Vila Nova Greenstone Belt, Guiana Shield, Amapá, Brazil. Artigo aceito para publicação no *Journal of South American Earth Sciences*.

From: **Reinhardt Fuck (Journal of South American Earth Sciences)** <EviseSupport@elsevier.com>

Date: 2018-06-28 16:01 GMT-03:00

Subject: Invitation to revise manuscript SAMES_2017_244_R3

To: itianahoffmann@gmail.com

Ref: SAMES_2017_244_R3

Title: Geochemistry and origin of the Rhyacian tholeiitic metabasalts and meta-andesites from the Vila Nova Greenstone Belt, Guiana Shield, Amapá, Brazil

Journal: Journal of South American Earth Sciences

Dear Ms. Hoffmann,

Thank you for submitting your manuscript to Journal of South American Earth Sciences. I have been through your revised manuscript and came up with quite a few corrections and suggestions to improve it. I have made the file available toy through dropbox, the message of which is probably in your mailbox by now. While revising the paper please consider the comments carefully. We look forward to receiving your detailed response and your revised manuscript.

To submit your revised manuscript:

- Log into EVISE® at: http://www.evise.com/evise/faces/pages/navigation/NavController.jspx?JRNL_ACR=SAMES
- Locate your manuscript under the header 'My Submissions that need Revisions' on your 'My Author Tasks' view
- Click on 'Agree to Revise'
- Make the required edits
- Click on 'Complete Submission' to approve

**What happens next?**

After approving your submission you will receive a notification that the submission is complete. To track the status of your paper throughout the editorial process, log into EVISE® at: http://www.evise.com/evise/faces/pages/navigation/NavController.jspx?JRNL_ACR=SAMES

**Enrich your article to present your research with maximum impact.** This journal supports the following Content Innovations:

- Explain your research in your own words and attract interest in your work using AudioSlides : 5-minute webcast-style presentations that are displayed next to your published article and can be posted on other websites. You will receive an invitation email to create an AudioSlides presentation within three weeks after your paper has been accepted.

- Interactive Map Viewer: Interactive viewer displaying geospatial data on a Google Map
- . Please use the online KML/KMZ Editor or your own geographic information system (GIS) to create the file required for uploading. GIS users can preview how files will display here.

- Interactive Plots: Interactive plot viewer providing easy access to the data behind plots. Please prepare a .CSV file with your plot data and test it online here before submitting as supplementary material.

Data in Brief (optional)

We invite you to convert your supplementary data (or a part of it) into a Data in Brief article. Data in Brief articles are descriptions of the data and associated metadata which are normally buried in supplementary material. They are actively reviewed, curated, formatted, indexed, given a DOI and freely available to all upon publication. Data in Brief should be uploaded with your revised manuscript directly to Journal of South American Earth Sciences. If your Journal of South American Earth Sciences research article is accepted, your Data in Brief article will automatically be transferred over to our new, fully Open Access journal, Data in Brief, where it will be editorially reviewed and published as a separate data article upon acceptance. The Open Access fee for Data in Brief is $500.

Please just fill in the template found here: http://www.elsevier.com/inca/publications/misc/dib_data%20article%20template_for%20other%20journals.docx. Then, place all Data in Brief files (whichever supplementary files you would like to include as well as your completed Data in Brief template) into a .zip file and upload this as a Data in Brief item alongside your Journal of South American Earth Sciences revised manuscript. Note that only this Data in Brief item will be transferred over to Data in Brief, so ensure all of your relevant Data in Brief documents are zipped into a single file. Also, make sure you change references to supplementary material in your Journal of South American Earth Sciences manuscript to reference the Data in Brief article where appropriate.

Questions? Please send your inquiries to dib@elsevier.com. Example Data in Brief can be found here: http://www.sciencedirect.com/science/journal/23523409

I look forward to receiving your revised manuscript as soon as possible.

Kind regards,

Reinhardt Fuck
Regional Editor
Journal of South American Earth Sciences

**Comments from the editors and reviewers:**

**Have questions or need assistance?**
For further assistance, please visit our Customer Support site. Here you can search for solutions on a range of topics, find answers to frequently asked questions, and learn more about EVISE® via

interactive tutorials. You can also talk 24/5 to our customer support team by phone and 24/7 by live chat and email.

---

# Geochemistry and origin of the tholeiitic metabasalts from the 2.15 Ga Vila Nova greenstone belt, Guiana Shield, Brazil

Itiana Hoffmann[1], Ruy Paulo Philipp[2] & Cristiano Borghetti[1]

[1]Programa de Pós-Graduação em Geociências, Instituto de Geociências, UFRGS, Av. Bento Gonçalves, 9500, Bairro Agronomia, Porto Alegre, RS, Brasil, CEP: 91509-900, e-mail:itianahoffmann@gmail.com
[2]Centro de Estudos em Petrologia e Geoquímica, Instituto de Geociências, UFRGS, Av. Bento Gonçalves, 9500, Bairro Agronomia, Porto Alegre, RS, Brasil, CEP: 91509-900, e-mail: ruy.philipp@ufrgs.br

## Abstract

The significance of the age of magmatism, magma series and tectonic settings that controls the origin of metavolcanic rocks of Vila Nova Greenstone Belt, is an important issue in order to understand the evolution of Guiana Shield in paleoproterozoic times. This work presents new U-Pb LA-ICP-MS geochronological and geochemical analyzes carried out on zircon grains and metavolcanic rocks of the Vila Nova greenstone belt (VNGB) which were supplemented by petrography, and stratigraphic and structural data acquired through description of boreholes and field work.In the Vila Nova region, the VNGB units rest on the Archaean basement composed of orthogneisses of the Tumucumaque Complex. The lower portion of the VNGB is composed of metabasalts and andesitic metabasalts, supported by an upper metasedimentary domain with exhalative chemical rocks and subordinate metavolcanic rocks. The metavolcanic rocks include amphibolites and amphibole schists, whose bodies are elongated according to the regional NW-SE schistosity. U-Pb zircon geochronology data showed an age of 2154±6 Ma for a meta-andesite of the lower portion of VNGB. Orogenic metamorphism event followed by three deformation events were recognized. The $D_1$ and $D_2$ events formed the schistosity ($S_1$), preserved as intrafolial folds ($F_2$) and the crenulation cleavage ($S_2$), derived from thrust movements. The garnet, hornblende and biotite, and hornblende, plagioclase and diopside assemblages define the metamorphic peak ($M_1$-$M_2$) with temperatures from 450-650 °C and lithostatic pressure between 4 and 6 kbars. The metabasites comprise Fe-tholeiites and Mg-tholeiites with komatiitic affinity, geochemical compositions enriched in LILE and REE and depleted in HFSE (with negative Nb, Ti

and P anomalies) and MORB-like REE patterns. The observed features indicate an expressive magmatism related to back-arc basins and island arcs at 2.15 Ga in Guiana Shield.

**Keywords**: Amazonian Craton, Guianas Shield, Vila Nova Greenstone Belt, Paleoproterozoic, metavolcanics, petrology.

## 1. Introduction

The major continental cores of Archean and Paleoproterozoic age in Amazonian Craton present limited knowledge regarding the evolution of their paleo-geographies and tectonic environments. In Brazil, most of the area contained by the Guiana Shield is inaccessible, covered by a thick mantle of weathering alteration and dense tropical forest.

The greenstone belts consist of a succession of ultramafic and mafic volcanic rocks, with subordinate occurrence of felsic rocks, interspersed with clastic and chemical sedimentary rocks. In the literature, tectonic generation environments of greenstones have been interpreted as back-arc basins associated with island arcs, mid-ocean ridges, oceanic plateaus, intracontinental rifts, or some combination of these environments (De Wit & Ashwal, 1986, Heubeck & Lowe, 1994, Lowe & Byerly, 1999, Kusky & Polat, 1999, Zeh *et al.,* 2009, 2013). These environments are related to submarine volcanism and are very common in the Archaean and Paleoproterozoic ages, being responsible for a large number of deposits of precious metals like gold, silver, copper, lead, nickel, chromium and zinc (Grant, 1984).

In Brazil, the occurrence of greenstone belts in the Amazonian and São Francisco cratons stands out, with emphasis on the mineralization of the greenstones of Rio das Velhas in Minas Gerais, Rio Itapicuru in Bahia, Crixás in Goiás (Jost *et al.,*

2014) and associated with the Carajás Province, in Pará (Lobato *et al.,* 2001; Noce *et al.,* 2007).

The Amazonian Craton is an extensive continental nucleus stabilized since the Archean (Central Amazonian Province > 2.5 Ga), surrounded by mobile belts of Paleo and Mesoproterozoic age (Cordani & Neves 1982; Teixeira *et al.*, 1989; Tassinari & Macambira, 1999, Santos *et al.*, 2000, Tassinari *et al.*, 2000; Tassinari & Macambira, 2004). These belts include granite-gneiss domes separated by elongated bodies of volcano-sedimentary associations of the greenstone-belt type, poorly investigated under the petrological aspect, with regional surveys with no integration of structural, petrographic and geochemical data.

The Vila Nova and Cupixi region is located in the northeast portion of the Amazonian Craton, in the Guiana Shield, and is part of the geological context of the Maroni-Itacaiúnas Province, a significant Paleoproterozoic mobile belt (2.2 - 1.9 Ga) bordering northeast of the Central Amazon Province. Metavolcano-sedimentary sequences of Paleoproterozoic age are recognized in several locations of the Guiana Shield, such as Brazil, Venezuela, Suriname, Guyana and French Guiana. These greenstone belts are elongated bodies in the NW-SE direction, separated by bands of basement rocks and have similar characteristics in terms of lithological units, chemical composition, and geochronology.

This study aims to discuss the origin of the Vila Nova greenstone belt (VNGB) metavolcanic rocks, based on the stratigraphic and structural relationships obtained in field work and boreholes, with petrographic, geochemical and geochronological analyses. The data integration allowed to investigate the magma series, to evaluate the differentiation processes, the magma sources and the tectonic discrimination of the units. The geological base was made by integrating aerogeophysical (magnetometric and gamma-spectrophotometric) data with the geological and

structural mapping in the 1:100,000 scale. The integration of these data with others available in the literature constitutes the basis for the investigation of the processes responsible for the generation of the metabasalts and andesitic basalts of the Vila Nova greenstone beltin order to understand the evolution of this island arc-back-arc system at 2.15 Ga and successive stages of metamorphism and deformational processes.

## 2. Tectonic context

### *2.1 Geology of the Vila Nova region*

The Vila Nova region is located in the northeast portion of the Amazonian Craton, located in the Maroni-Itacaiúnas Province, a Paleoproterozoic mobile belt with evolution related to Transamazonic Orogenesis (2.25 - 2.05 Ga) **(Figure 1A)**. The Paleoproterozoic mobile belts that surround the Archean nucleus of the Central Amazon Province are extensive basins represented by discontinuous paths of greenstone beltsassociated with magmatic arcs, interspersed with granite associations of the TTG type (Avelar et al., 2003; McReath and Faraco, 2006; Rosa-Costa et al., 2006) **(Figure 1B)**.

In the Vila Nova region, the basement rocks were initially included in the Maroni-Itacaiunas Province, of Paleoproterozoic age. Based on the contact relations, lithological types, geophysical and geochronological data, Rosa-Costa et al. (2003, 2006) identified within this province a vast segment of the Archean crust called Amapá Block. The Meso- and Neoarchean units of this block were intensely reworked in the Paleoproterozoic during the Transamazonic Orogenic Cycle.

The basement of the studied region is represented by the Tumucumaque Complex, by the Anauerapucu and Mungubas granites, and by the intrusive rocks of the Bacuri Complex (Spier & Ferreira Filho, 1999; Pimentel *et al.*, 2002; Barbosa *et*

*al.*, 2013; Borghetti & Philipp, 2017; Borghetti *et al.*, 2017b). On these units rest the Vila Nova greenstone belt rocks, affected by low to medium-grade orogenic metamorphism and intruded by Paleoproterozoic granites **(Figure 2).**

The Tumucumaque Complex is the oldest unit and is composed of tonalitic, granodioritic and dioritic gneisses of Archean age, with a subordinate occurrence of amphibolites (metagabbros) that are consistent with the regional gneissic banding (Rosa-Costa *et al.,* 2006; Borghetti *et al.* 2014, 2017a). The orthogneisses are light to dark gray in color and show incipient banding marked by discontinuous levels of biotite and/or hornblende, generated under metamorphic conditions of mid to upper amphibolite facies (Borghetti & Philipp, 2017). The orthogneisses are cut by stocks of Archean age gabbros, as well as by Paleoproterozoic granitoids with varying dimensions (Borghetti *et al.,* 2017a). In the Tartarugalzinho greenstone belt region, the orthogneisses were dated at 3.48 Ga by the Pb-Pb zircon method (TIMS). In the Vila Nova region, $T_{DM}$ model ages (total rock) were obtained in schist amphibole by the Sm-Nd method between 3.03 - 2.85 Ga (Rosa-Costa et al., 2012). More recently, Rosa-Costa et al. (2006) and Borghetti et al. (2014, 2017a) obtained the Pb-Pb (TIMS) and U-Pb (LA-MC-ICPMS) zircon ages of the Tumucumaque Complex in the range of 2.85 to 2.67 Ga.

The Mafic-Ultramafic Bacuri Complex (BMUC) corresponds to a stratiform body, elongated in the E-W direction, consisting of the intercalation of metagabbros, amphibolites, metaperidotites, chromitites, serpentinites, and tremolitites. These units show a record of intense ductile deformation and amphibolite facies metamorphism. The BMUC rocks occur in the southern part of the studied area, showing intrusive relationships with the basement gneisses and tectonic contact with the metasediments of the Vila Nova Group (Spier & Ferreira Filho, 1999). The stratiform nature is defined by the layered structure and the chemical and textural

characteristics of the chromitites and the mafic-ultramafic rocks (Spier & Ferreira Filho, 1999).

In Brazil, the metavolcano-sedimentary associations that constitute the Serra do Navio, Lombarda, Tartarugalzinho, Vila Nova, Tumucumaque, and Ipitinga greenstone belts were included from a lithostratigraphic perspective in the Vila Nova Complex (McReath & Faraco, 2006) **(Figure 2).** The VNGB is composed of basic to intermediate metavolcanic rocks, chemical-exhalative rocks, and classical metasedimentary rocks.

The geochronological relationships of the metasedimentary units were investigated by Borghetti et al. (2014, 2017a), which presented U-Pb ages in detrital zircons between 3.6 and 2.4 Ga, confirming the erosion of the Archean basement in the formation of the Vila Nova *greenstone belt.* The authors obtained the age of 2,170 ± 9 Ma for one meta-andesite of the Vila Nova region, establishing the Rhyacian period as the maximum deposition age of the VNGB basin.

The units of the Vila Nova greenstone belt are cut by the Amapari and Porto Grande granites and by other undisturbed granite bodies of Paleoproterozoic age. The first one is represented by sieno and monzogranites with massive structure and medium to coarse inequigranular texture. The Porto Grande Granite varies from sienogranite to monzogranite, showing a magmatic flow foliation and equigranular to porphyritic texture (Barbosa *et al.,* 2013). The intrusion of these granites causes textural transformations in the metavolcano-sedimentary rocks related to thermal metamorphism. The U-Pb zircon ages obtained in the intrusive granites, such as the Igarapé Careta Suite (2.06 Ga) and the Amapari Granite (1.99 Ga), suggest that the orogenic metamorphism occurred between 2.15 and 2.07 Ga.

The Phanerozoic cover that occurs to the east of the studied area includes fluvial and estuarine environment pelites, sandstones and ferruginous conglomeratic

sandstones, and sandy-clayey sediments to friable sandy-conglomeratic sediments associated with a fluvial system.

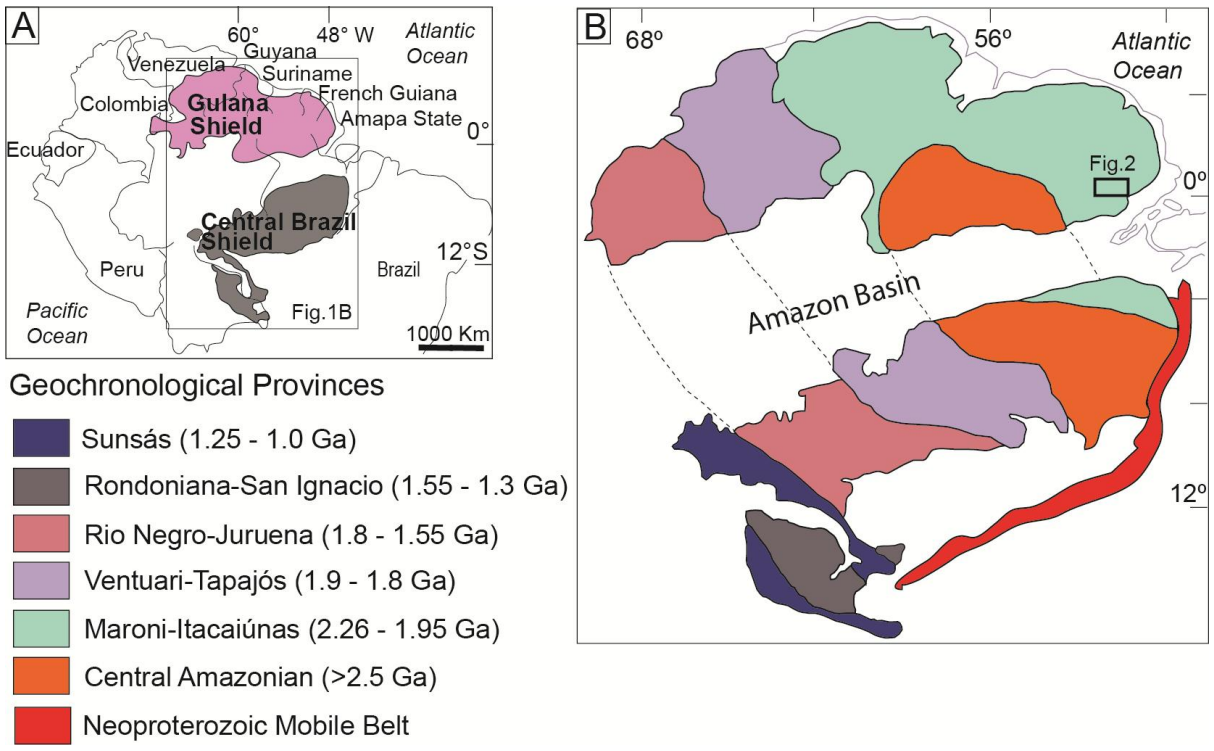


**Figure 1**. A) Map of the Amazonian Craton in South America and location of the Guiana and Central Brazil shields, B) Location of the study area and Geochronological Provinces proposed by Tassinari & Macambira (2004).

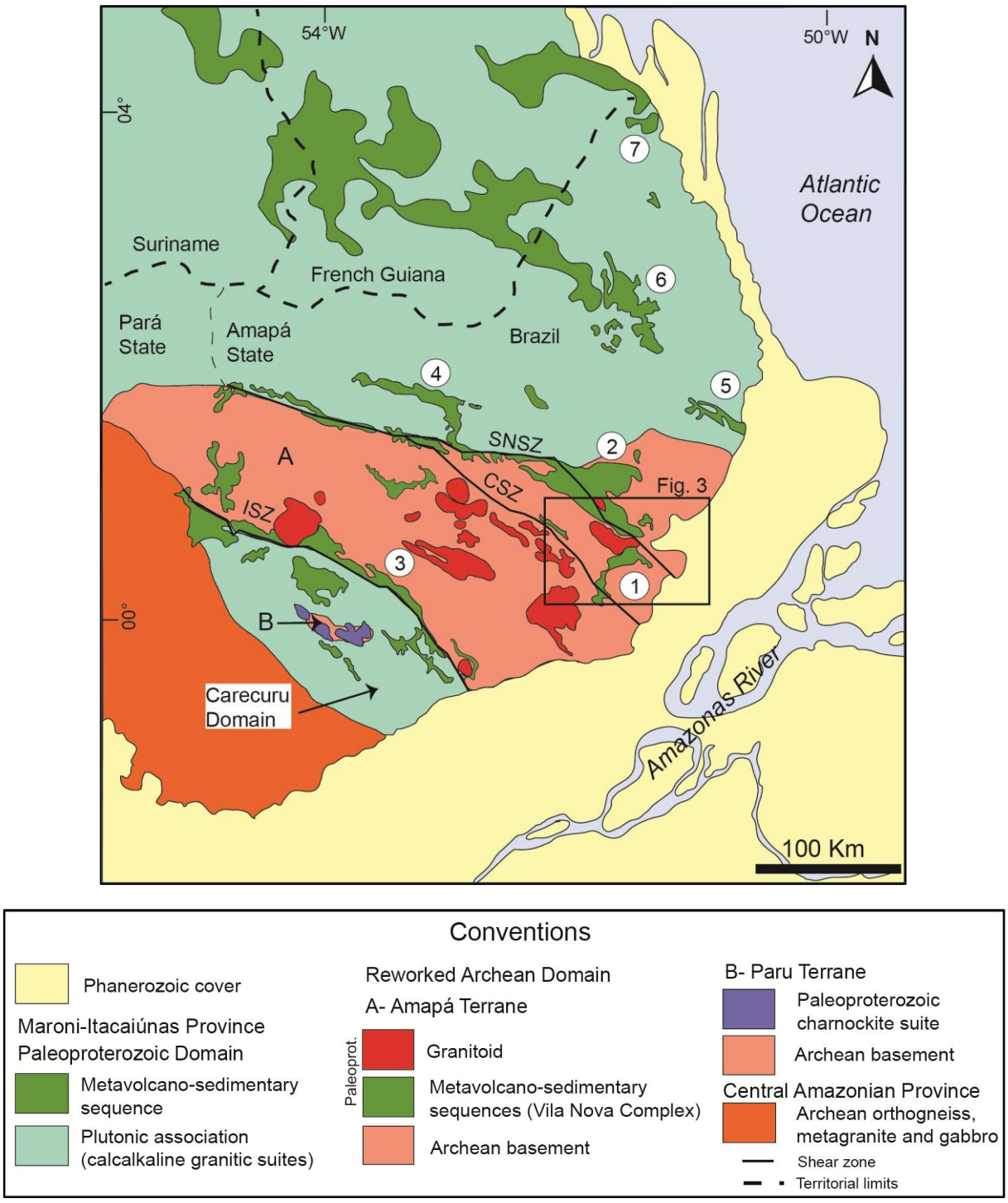


**Figure 2**. Archaean and Paleoproterozoic tectonic-geochronological domains of the eastern portion of the Guiana Shield, modified from Rosa-Costa et al. (2006). The geochronological provinces are in agreement with Tassinari & Macambira (2004). The area highlighted in the black rectangle corresponds to the greenstone belts of Vila Nova and Serra do Navio and to the geological map of Figure 3. Greenstone belts: 1-Serra do Navio, 2-Lombarda, 3-Tartarugalzinho, 4-Vila Nova, 5-Tumucumaque and 6-Ipitinga. Shear Zones: SNSZ: Serra do Navio, CSZ: Cupixi, ISZ: Ipitinga.

*2.2. The Vila Nova Greenstone Belt (VNGB)*

The Vila Nova Greenstone Belt(VNGB) occurs as a main body elongated along the E-W direction, with six subordinate belts in the N40-50$^{o}$W direction, interconnected in their southern portion by the Vila Nova Shear Zone (VNSZ) **(Figure 3).** This low-angle ductile shear zone with top-to-the-north thrust kinematics defines the contact of the greenstone with the basement rocks (Borghetti & Philipp, 2017).

Based on the geological map generated by the integration of field data, geophysical data, and borehole descriptions, the VNGB metavolcano-sedimentary rocks were subdivided into two petrotectonic associations or rocky domains **(Figure 3).** The Basal Domain presents the largest area of occurrence and is composed of mafic metavolcanic rocks, interspersed with subordinate lenses of mica schists. The Upper Domain occupies a restricted area, constituted by clastic metasediments, with subordinate intercalations of mafic metavolcanic rocks and chemical-exhalative rocks. The contact between both these domains is defined by the VNSZ and was partly inferred by the aerogeophysical data interpretation (Borghetti & Philipp, 2017).

Structural surveys indicate that the VNGB units were affected by an event of regional orogenic metamorphism followed by three major deformation events (Borghetti & Philipp, 2017). The action of these processes resulted in a regional foliation oriented in the N50-60ºW direction. The main schistosity is represented by an $S_2$ crenulation cleavage, which preserves partial remains of the $S_1$ foliation in the form of $F_2$ intrafolial isoclinal folds of metric to decametric scales. The previous structures are affected by $F_3$ folds, of normal type with plunge, with open to closed forms and axes with plunging between 10 and 25º in the N40-50ºW and S40-50ºE directions (Borghetti & Philipp, 2017). The metasediments present partial preservation of the primary structures, such as compositional bedding, plane-parallel and trough cross-bedding.

The Basal Domain is exposed as an elongated band along the E-W direction for about 30 km, from Vila Nova, extending eastward through the localities of Nova Canaã and Pelado, between the Vila Nova and Piaçacá rivers **(Figure 4)**. Amphibole schists and amphibolites are the predominant metamafic rocks. The metaultramafites are represented by tremolite schists and hornblende-tremolite schists and occur subordinately as lenses of 2 to 20 meters in thickness. Mafic cornubianites have also been recognized as products of thermal metamorphism associated with the positioning of the younger Paleoproterozoic granites, which constitute elongate bodies concordant with the VNSZ.

The Upper Domain is more restricted to the western portion of the area, occurring as three major elongated belts about 20 to 25 km long and 1 to 10 km wide (**Figure 4**). These belts are dominantly composed of quartzites, ferruginous quartzites, and fuchsite-quartz schist, with two continuous lenses of metaconglomerates, with subordinate lenses of pelitic schists, calc-silicate schists and BIF's (banded iron formations), with hematite phyllites, hematite schists and ferruginous quartzite. Based on the borehole descriptions made available by the company Amapari Mineração, a schematic geological section representative of the compositional variation occurring in the Vila Nova region was assembled, which illustrates well the presence of $F_2$ isoclinal folds **(Figure 5)**.

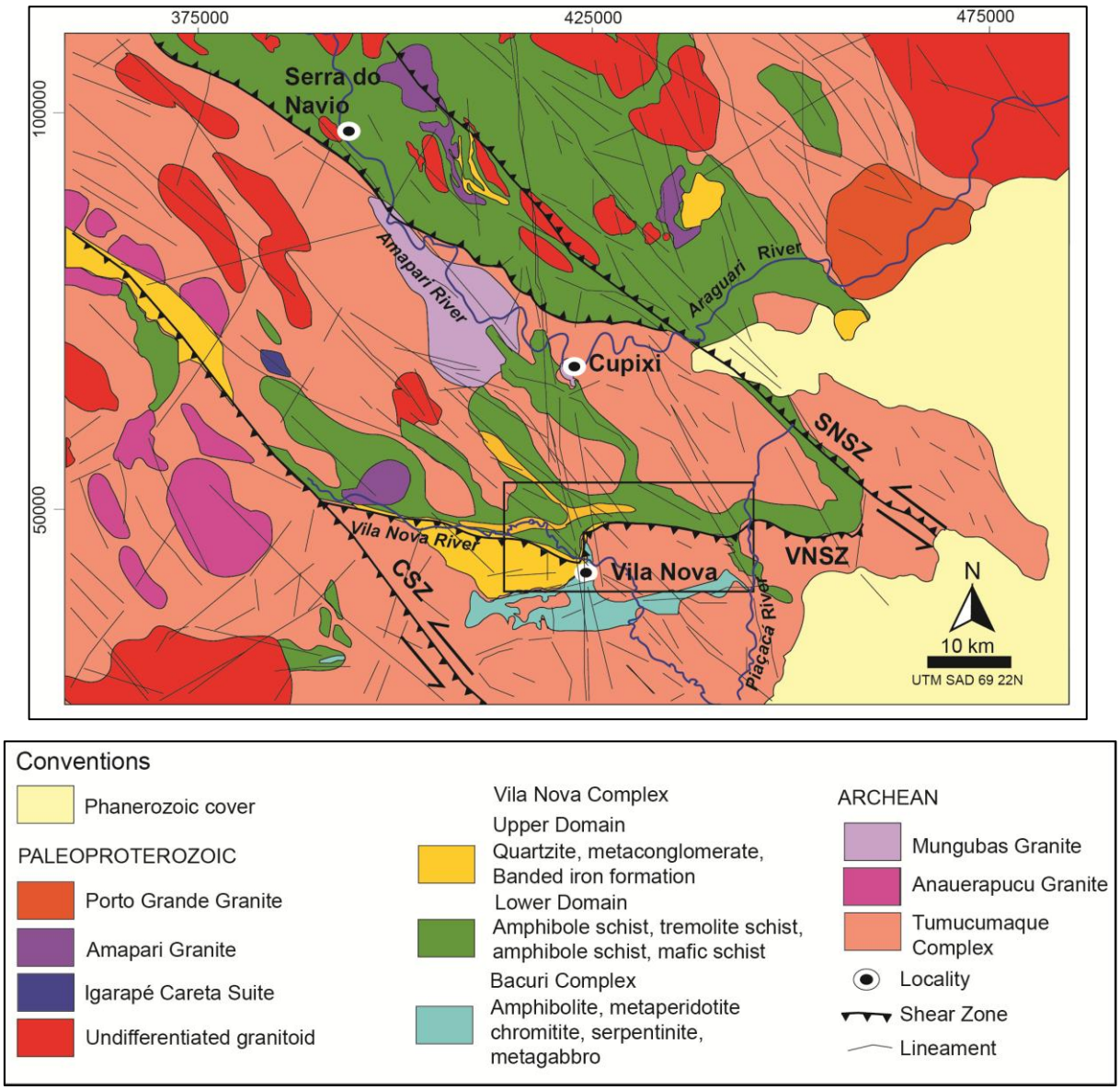


**Figure 3**. Geological map of Serra do Navio and Vila Nova regions generated from the integration of geophysical and field data, with emphasis on the area of study indicated by the black rectangle, representing the geological map of figure 4. Modified from CPRM (2004), Magalhães et al. (2007) and Barbosa et al. (2013). Shear Zones: SNSZ: Serra do Navio, CSZ: Cupixi, ISZ: Ipitinga.

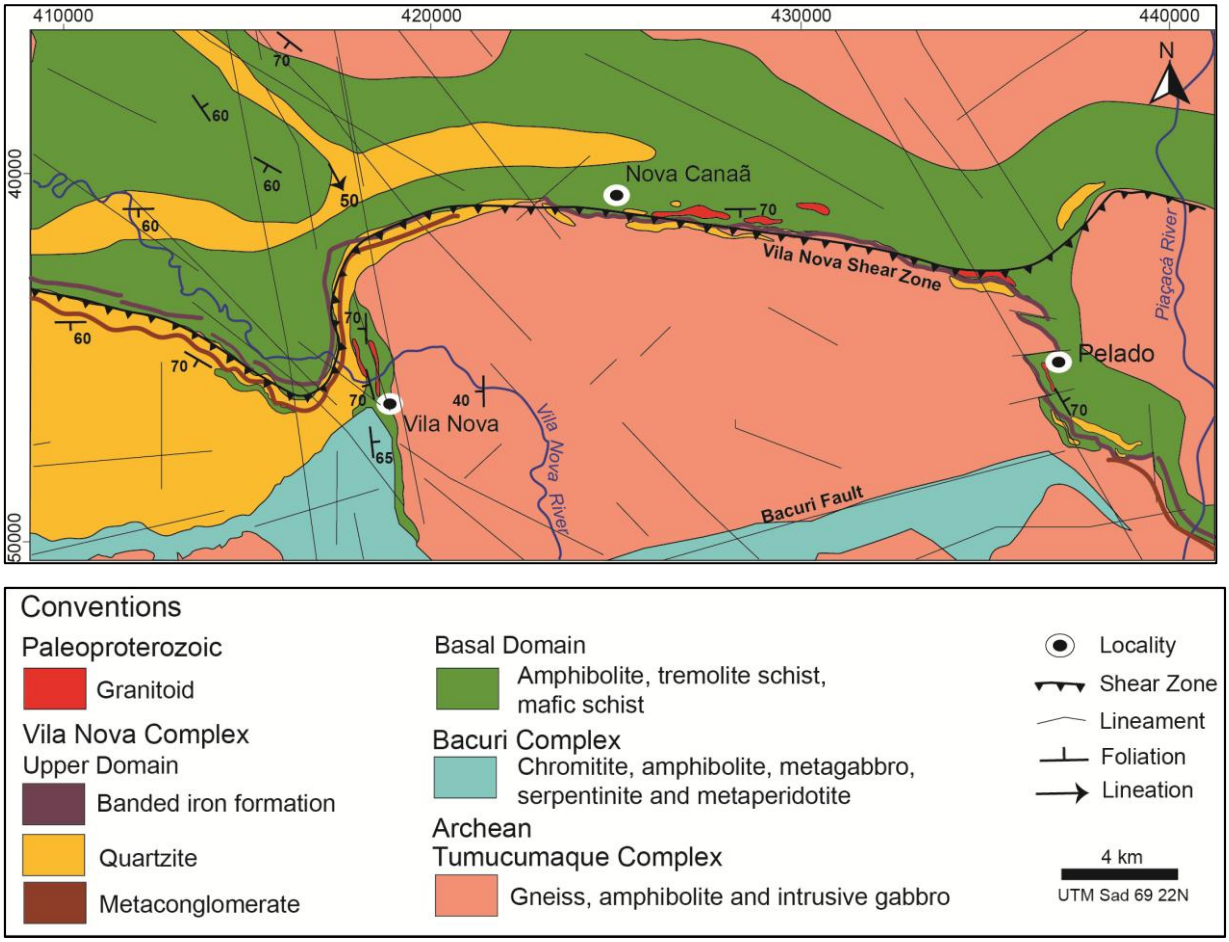


**Figure 4**. Geological map of the Vila Nova region.

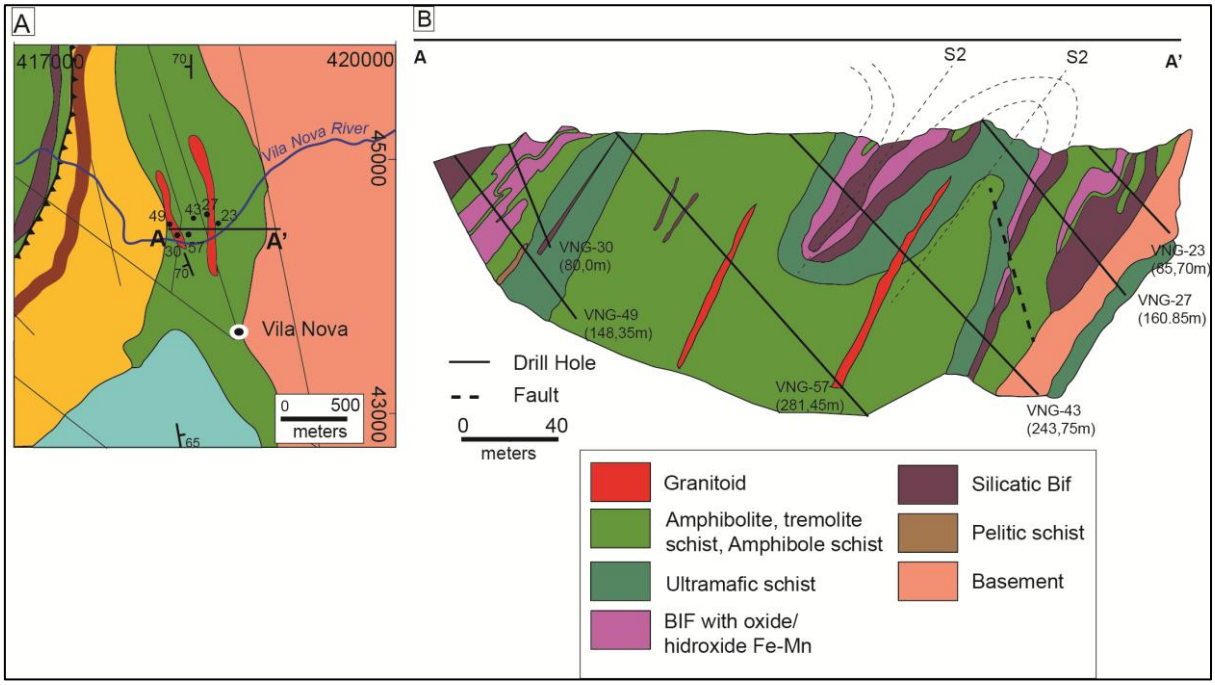


**Figure 5**. A) Geologic map of the Vila Nova with the location of the Pedra Pintada-Gaivotas (A-A') geological cross-section and the main drilling holes sampled for chemical analysis. B) Schematic geological cross-section representing the main structures and the compositional variation observed from the description of the drilling holes.

## 3. Material and Methods

Sampling was based on an integrated analysis of satellite images, aerogeophysical (aerogammaspectrometry and aeromagnetometry) survey data and geologic mapping, which clearly defined the metasedimentary and volcanic domains. In addition to the sampling for petrography and geochronological analysis, structural and stratigraphic data were collected to validate satellite and aerogeophysical interpretation. To investigate the stratigraphy and to improve the geology, a total of 5.000 meters of drill core data was described.

### *3.1 Whole-rock chemistry*

Thirty one samples were selected for geochemical analysis. They were collected from drilling holes along one transverse section of the Vila Nova greenstone belt and comprise metabasalts, meta-andesitic basalts, amphibole schists and

amphibolites. Sample preparation was conducted at the facilities of Geoscience Institute of the Rio Grande do Sul Federal University. The samples were comminuted in jaw crusher steel, processed in an agate mill, sieved and homogenized. Quartered rock powders were conducted for whole-rock chemical analysis at ACME Analytical Laboratories LTDA, Canada. Major and trace elements concentrations were determined using ICP-MS, while base metals, such as Ni, Cr, Co and Zn, were analyzed by Aqua Regia digestion (LF200 and AQ200 procedures, respectively), after metaborate/tetraborate fusion. Detecctions limits were 0,01 % wt. for major oxides and 0.01-0.1 ppm for trace elements. Geochemistry diagrams were made using GCD kit version 4.0 (Janousek et al., 2006).

*3.2 Geochronology*

One sample of meta-andesitic basalt (CB-13A) from the basal domain was selected to determine the U-Pb zircon age of volcanism from Vila Nova greenstone belt. The LA-MC-ICPMS method was used for U-Pb zircon analysis at the Geochronological Research Center of the Geosciences Institute of São Paulo University (CPGeo). Sample preparation was carried out in the laboratories of the Rio Grande do Sul Federal University (UFRGS). Rock samples were crushed and milled using a mandible crusher and then pulverized. Zircon grains were concentrated by conventional magnetic and heavy liquid techniques. The final concentrate was obtained by handpicking. To avoid any bias, no visual morphological or color differentiation was made.

The zircon grains were mounted in epoxy and polished using diamond pastes until half of the grain thickness was exposed, to ensure that all internal oscillatory zoning was visible for further imaging. Backscattered-electron (BSE) and cathodoluminescence (CL) imaging was performed to record internal structures and

crystallization phases. Only zircon grains free of imperfections, fractures, and mineral inclusions were selected for isotopic analysis. Cathodoluminescence (CL) images of zircons were obtained using a Quanta 250 FEG electron microscope equipped with Mono CL3+ cathodoluminescence spectroscope (Centaurus) at CPGeo-IGc-USP. Isotopic data were obtained using a NEPTUNE inductively coupled plasma-mass spectrometer (ICP-MS) coupled with an Excimer laser ablation system (LA). The diameter of laser spots for the zircon U-Pb analyses was 35 to 50 µm. The routine of the U-Pb method consists of the analysis of 2 blanks, 2 NIST standards, 3 external (GJ1) standards, 13 unknown samples, 2 external standards and 2 blanks. The $^{204}$Hg interference on $^{204}$Pb measurements was corrected by $^{202}$Hg, adopting a $^{204}$Hg/$^{202}$Hg ratio of 4.2. The $^{207}$Pb/$^{206}$Pb ratio normalization was achieved by combining NIST and external standards. The $^{206}$Pb/$^{238}$U ratio normalization was achieved by external standards. The GJ1 standard (602 ± 4.4 Ma, Elholou *et al*. 2006) was utilized for mass bias correction. The residual common Pb was corrected according to the measured $^{204}$Pb concentration using the known terrestrial composition (Stacey & Kramers, 1975). The uncertainty introduced by laser-induced fractionation of elements and mass instrumental discrimination was corrected using the zircon reference standard GJ-1 (Jackson *et al.* 2004). External errors were calculated using error propagation of the individual GJ-1 measurements and measurements of the individual zircon samples (spots). Age calculations were made using Isoplot version 4 and $^{238}$U/$^{206}$Pb data (Ludwig, 2008). Chemale *et al.* (2011) described in detail the analytical methods and data treatment used here.

## 4. Results

### *4.1 Petrography of metamafic and metaultramafic rocks*

*Amphibolites*

They are the rocks of greater representativeness among the metamafic rocks. The amphibolites have a dark gray color and schist structure defined by the amphibole and biotite orientation, constituting the nematoblastic and middle lepidoblastic textures **(Figure 6A).** The interlobate to polygonal granoblastic texture is subordinate and occurs at the discontinuous plagioclase levels. The blastoamygdaloidal texture is characterized by amygdala of round to elliptical shape and sizes from 2 to 4 mm, composed by fine mosaics of recrystallized quartz **(Figure 6B)**.

The mineral composition is dominated by hornblende (60-65% of modal volume) and plagioclase (25 to 45%), with low contents of biotite and diopside. Titanite, magnetite, epidote, quartz and chlorite are accessory minerals. Reliquary plagioclase crystals show prismatic shape and normal zonation, polysynthetic and Carlsbad-albite twinning, and sizes from 0.5-1 mm. Diopsidium crystals are rare and occur at the edges of the hornblende, indicating progressive metamorphism **(Figure 6C).** Titanite has granular and xenoblastic shape, with sizes smaller than 0.1 mm. The magnetite crystals have octahedral shape and are subhedral to anhedral.

The amphibolites show schistosity well defined by the orientation of hornblende and biotite. In banded amphibolites, this foliation is parallel to $S_0$, characterized by the intercalation of continuous levels rich in mafic minerals and discontinuous plagioclase levels. The transposition of the $S_1$ and $S_0$ schistosity results in crenulation cleavage ($S_2$) and closed to intrafolial isoclinal folds. The $S_2$ cleavage domains are discrete and sinuous. The main schistosity is cut by irregular

fractures filled by chlorite, sericite, and epidote, indicating a low-temperature retrometamorphic event **(Figure 6D)**.

*Amphibole Schists*

The tremolite and hornblende schists have a dark green color and schistosity characterized by the orientation of acicular crystals of amphibole, defining the thick nematoblastic texture. The lepidoblastic texture is subordinate and defined by the biotite orientation.

The main mineralogy is composed of tremolite (55%) and hornblende (40%), with biotite (4%), clinochlorite (0.3%), chlorite (0.3%), titanite and opaques (0.1%) as accessory minerals. Amphiboles are idioblastic to subdioblastic with sizes between 3 and 5 mm. The crystals show zoning, with a colorless tremolite core and a green-colored border composed of hornblende **(Figure 6E).** The biotite occurs interstitially, with reddish brown color, lamellar form and sizes from 1 to 1.5 mm.

*Mafic Cornubianites*

The metamafic rocks that show thermal effects superimposed to those of orogenic metamorphism correspond to a small fraction of the analyzed metavolcanics. They range from hornblende hornfels to tremolite-diopside-hornblende hornfels, with acicular texture defined by disoriented amphibole crystals **(Figure 6F)**. The decussate texture is marked by biotite crystals with no orientation. The polygonal granoblastic texture occurs interstitially, consisting of aggregates of plagioclase crystals with sizes between 0.06 and 0.1 mm.

The main mineralogy is composed of hornblende (40-50%), tremolite (15-20%), plagioclase (15-20%) and diopside (15-20%), with epidotes (2%), chlorites and opaque minerals (1%) as accessory minerals. Carbonate veins occur with millimetric

thickness. In the regions adjacent to the veins, an irregular formation of epidote and chlorite aggregates occurs on the mafic minerals.

*Metaultramafites*

Magnesium schists have a very subordinate occurrence, with usually less than 30 meters in thickness. They are represented by tremolite schists and hornblende-tremolite schists of gray to light green color, with schistosity defined by the amphibole orientation, characterizing the medium nematoblastic texture. The main mineralogy is composed of tremolite (75-80%) and hornblende (15-20%), with clinochlore (3-5%) and magnetite (1-2%) as accessories.

The $S_1$ schistosity is determined by tremolite microliths, constituting intrafolial isoclinal microcrystals, observed within the domains of the $S_2$ crenulation cleavage. The cleavage domains are sinuous, with spacing between 0.5 and 1 mm. The main schistosity is cut by quartz veins with thicknesses between 1 and 5 mm. The veins are deformed, discontinuous and irregular and are composed of quartz aggregates with fine granoblastic texture.

*4.2 Geochronology*

*Meta-andesite (CB-13A)*

Meta-andesite sample CB-13A was collected from a road cut located next to the Vila Nova gold-digging site (UTM zone 22N coordinates 413860 and 51672) at the top of the Basal Domain of the Vila Nova greenstone belt. The metavolcanic rock constitutes a lava flow with horizontal disposition, an approximately 20-35 m-thick tabular body, surrounded by muscovite schists, muscovite-biotite schists and magnetite-garnet-muscovite schist. Sample CB-13A is from a reddish, fine-grained meta-andesite showing prominent foliation and aphanitic texture with rare plagioclase

porphyroclasts of 0.2 to 1.0 mm in size. It contains some garnet porphyroblasts of 5 to 8 mm in size. The matrix has a lepidoblastic texture marked by muscovite and biotite, subordinately with plagioclase and quartz.

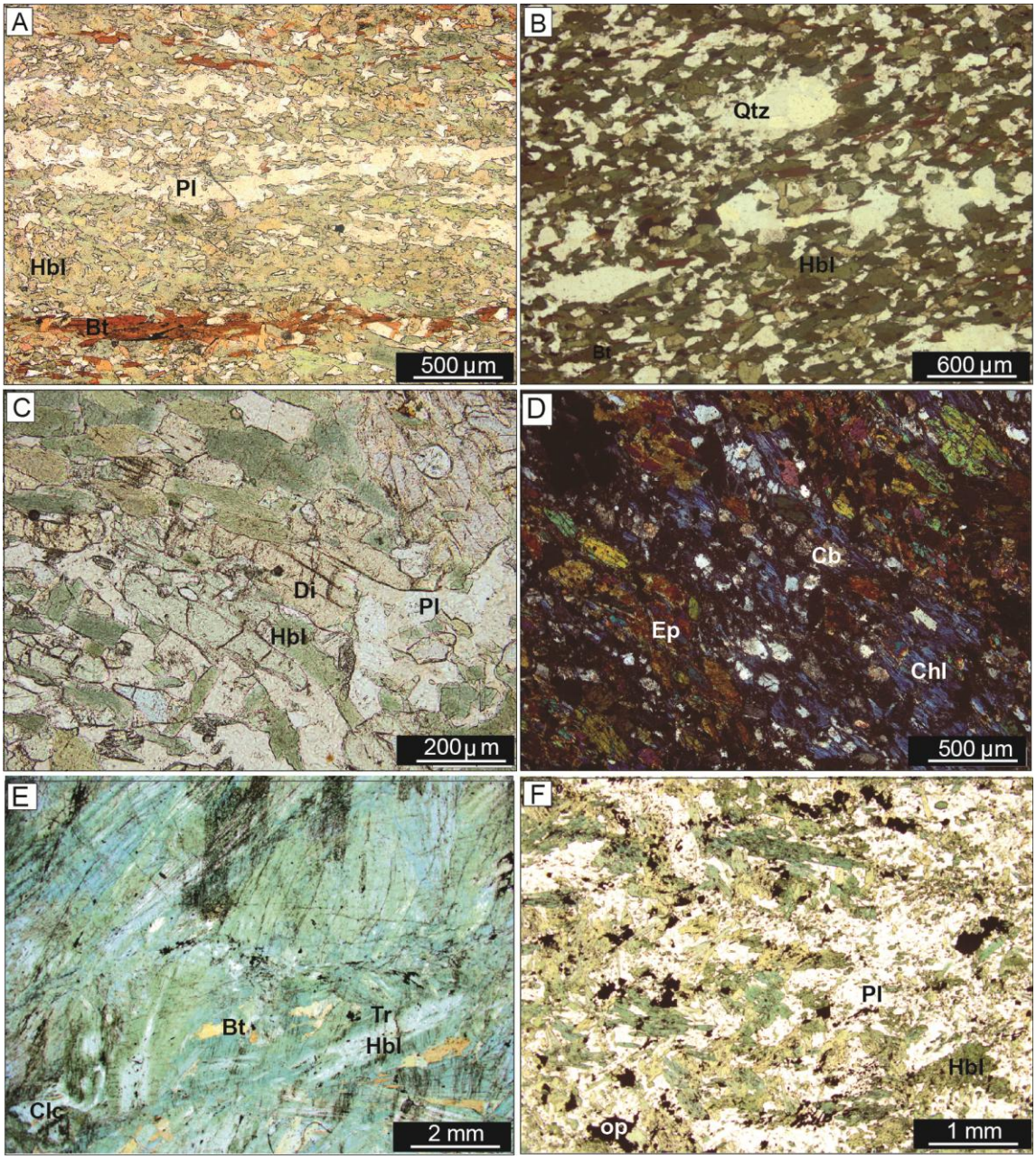


**Figure 6**. Microscopic aspects of VNGB metabasites. A) Composite banding in amphibolite evidenced by the alternation of hornblende levels and discontinuous levels of plagioclase and biotite, B) Blastoamigdaloidal texture in metabasalt consisting of deformed elliptic quartz aggregates, C) Diopside crystals growing on the edges of hornblende in amphibolite, D) Amphibolite presenting hornblende disequilibrium and transformation to chlorite, indicating greenschist facies retrometamorphism, E) Tremolite-hornblende schist with zoning amphiboles, with hornblende core wrapped by tremolite border, F) Mafic cornubianite with acicular and disoriented crystals of hornblende and decussed texture with biotite.

Eighteen out of 139 igneous zircons crystals were selected for U-Pb analysis by LA-MC-ICPMS. Sample CB-13A contains translucent to opaque zircons, ranging in color from brown to dark brown. The igneous zircon crystals are euhedral to sub-euhedral, showing prismatic shapes and almost always straight terminations and range in size from 70 to 380 µm. They are well preserved and show oscillatory zoning. The CL images show a few luminescent zircons with inherited nuclei, some of them with sector or faint oscillatory zoning **(Figure 7)**. Reabsorbed and metamict grains are also present (e.g., 6.1, 8.1). Concentric zoning resulting from metamorphic recrystallization was not observed. Xenocryst cores with magmatic overgrowths are also present. Eighteen analyses in cores and one metamict rim are nearly collinear in the Concordia diagram. The $^{207}Pb/^{206}Pb$ ages range from 2.110 Ma to 2.199 Ma and the data regress to yield an upper intercept age of 2.154 ± 5.5 Ma (MSWD = 0.022) **(Figure 8)**. This age is interpreted as the reddish metandesite zircon crystallization age. Th/U ratios obtained from 17 concordant analyses range between 0.15 and 0.88, which is consistent with a magmatic origin for these zircons (Belousova *et al.* 2002)**(Table 1)**.

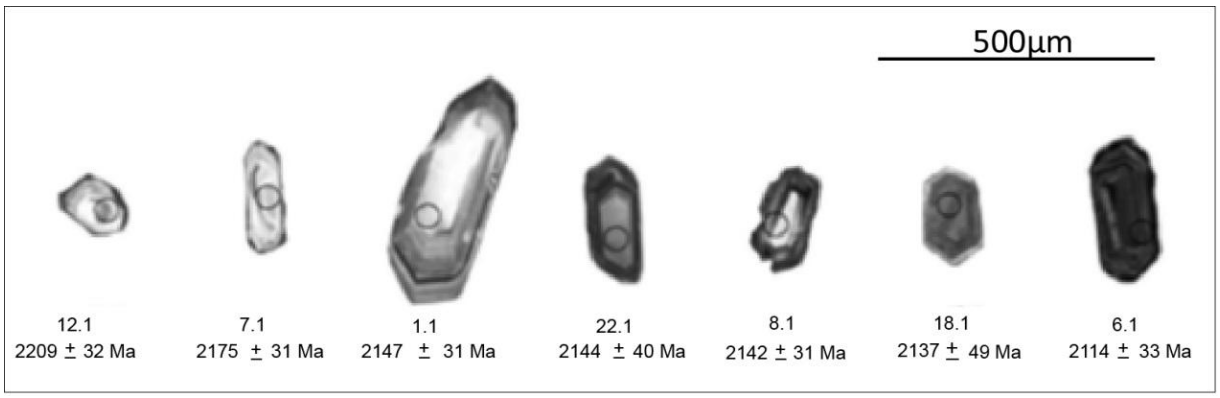


**Figure 7**. Cathodoluminescence images of selected zircons from meta-andesitic basalt sample CB-13A. The circle locates the spot of the analysis in the zircons and the corresponding age.

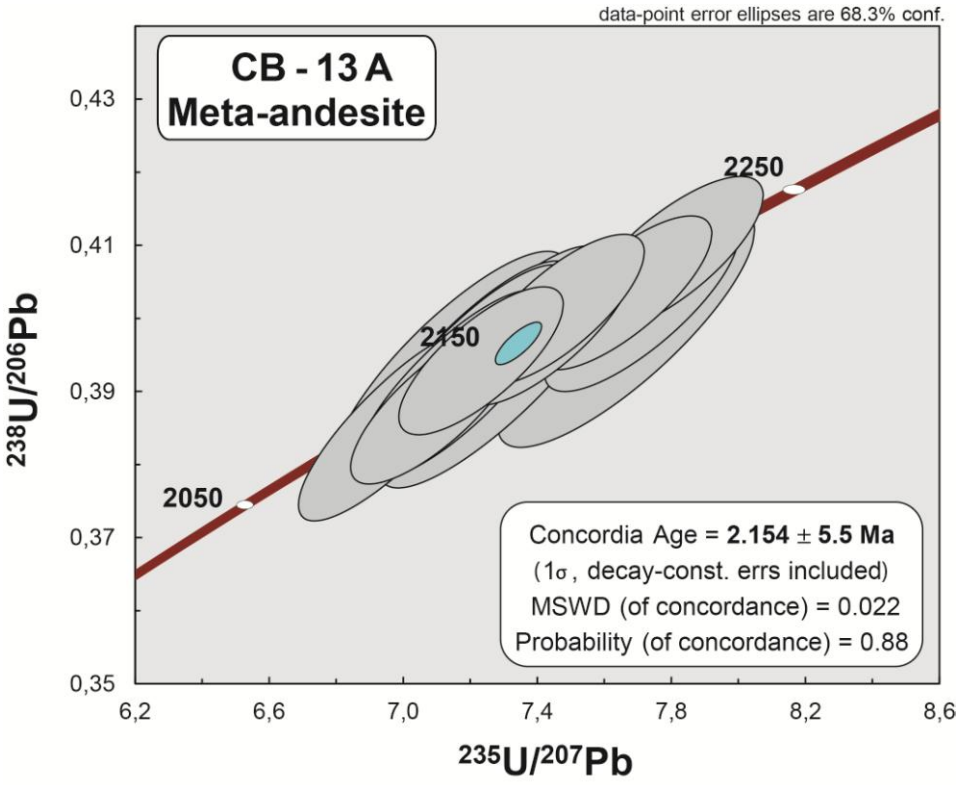


**Figure 8**. Concordia diagram for analyzed zircons from meta-andesitic basalt CB-13A (n=18).

| Spot | $^{207}Pb/^{235}U$ | 1σ | $^{206}Pb/^{238}U$ | 1σ | *rho* | $^{238}U/^{206}Pb$ | 1σ | $^{207}Pb/^{206}Pb$ | 1σ | $^{208}Pb/^{206}Pb$ | 1σ | $^{206}Pb/^{238}U$ Age (Ga) | Error Ga | $^{207}Pb/^{235}U$ Age (Ga) | Error Ga | $^{207}Pb/^{206}Pb$ Age (Ga) | Error Ga | Conc. % $^{206}Pb/^{238}U$ $^{207}Pb/^{206}Pb$ |
|---|---|---|---|---|---|---|---|---|---|---|---|---|---|---|---|---|---|---|
| 3,1 | 7,4255 | 0,1699 | 0,3996 | 0,0073 | 0,80 | 2,5022 | 0,0458 | 0,1348 | 0,0010 | 0,2856 | 0,2407 | 2,167 | 0,034 | 2,164 | 0,020 | 2,158 | 0,012 | 100 |
| 4,1 | 7,7082 | 0,1908 | 0,4019 | 0,0079 | 0,79 | 2,4885 | 0,0488 | 0,1363 | 0,0010 | 0,3008 | 0,2535 | 2,178 | 0,036 | 2,198 | 0,022 | 2,177 | 0,012 | 100 |
| 6,1 | 7,0951 | 0,1673 | 0,3881 | 0,0072 | 0,78 | 2,5769 | 0,0476 | 0,1314 | 0,0009 | 0,2981 | 0,2512 | 2,114 | 0,033 | 2,123 | 0,021 | 2,114 | 0,012 | 100 |
| 7,1 | 7,4635 | 0,1671 | 0,4012 | 0,0068 | 0,76 | 2,4926 | 0,0425 | 0,1343 | 0,0009 | 0,4337 | 0,3655 | 2,175 | 0,031 | 2,169 | 0,020 | 2,152 | 0,012 | 101 |
| 8,1 | 7,2306 | 0,1615 | 0,3942 | 0,0067 | 0,76 | 2,5369 | 0,0432 | 0,1334 | 0,0010 | 0,4056 | 0,3418 | 2,142 | 0,031 | 2,140 | 0,020 | 2,139 | 0,012 | 100 |
| 10,1 | 7,4291 | 0,1685 | 0,3987 | 0,0070 | 0,78 | 2,5081 | 0,0443 | 0,1346 | 0,0010 | 0,3667 | 0,3092 | 2,163 | 0,032 | 2,164 | 0,020 | 2,155 | 0,012 | 100 |
| 12,1 | 7,8017 | 0,1789 | 0,4088 | 0,0071 | 0,75 | 2,4463 | 0,0422 | 0,1381 | 0,0010 | 0,2909 | 0,2451 | 2,209 | 0,032 | 2,208 | 0,020 | 2,199 | 0,012 | 100 |
| 13,1 | 7,6574 | 0,1726 | 0,4035 | 0,0070 | 0,77 | 2,4783 | 0,0428 | 0,1363 | 0,0010 | 0,2894 | 0,2440 | 2,185 | 0,032 | 2,192 | 0,020 | 2,177 | 0,012 | 100 |
| 16,1 | 7,1434 | 0,1877 | 0,3910 | 0,0085 | 0,83 | 2,5575 | 0,0555 | 0,1317 | 0,0015 | 0,7931 | 1,1297 | 2,128 | 0,039 | 2,129 | 0,023 | 2,117 | 0,020 | 100 |
| 17,1 | 6,9714 | 0,1885 | 0,3853 | 0,0087 | 0,84 | 2,5952 | 0,0587 | 0,1311 | 0,0014 | 0,9701 | 1,3816 | 2,101 | 0,040 | 2,108 | 0,024 | 2,110 | 0,019 | 100 |
| 18,1 | 7,1378 | 0,2324 | 0,3931 | 0,0106 | 0,83 | 2,5438 | 0,0686 | 0,1336 | 0,0015 | 0,7869 | 1,1221 | 2,137 | 0,049 | 2,129 | 0,029 | 2,142 | 0,019 | 100 |
| 19,1 | 7,3070 | 0,1933 | 0,3968 | 0,0086 | 0,82 | 2,5201 | 0,0549 | 0,1323 | 0,0015 | 0,5516 | 0,7857 | 2,154 | 0,040 | 2,150 | 0,023 | 2,125 | 0,019 | 101 |
| 21,1 | 7,2021 | 0,1901 | 0,3941 | 0,0087 | 0,84 | 2,5375 | 0,0562 | 0,1321 | 0,0015 | 0,4979 | 0,7092 | 2,142 | 0,040 | 2,137 | 0,023 | 2,123 | 0,019 | 101 |
| 22,1 | 7,2130 | 0,1920 | 0,3946 | 0,0087 | 0,83 | 2,5341 | 0,0559 | 0,1335 | 0,0015 | 0,9250 | 1,3174 | 2,144 | 0,040 | 2,138 | 0,023 | 2,142 | 0,019 | 100 |
| 24,1 | 7,6633 | 0,2522 | 0,3986 | 0,0108 | 0,82 | 2,5087 | 0,0679 | 0,1355 | 0,0016 | 0,3681 | 0,5246 | 2,163 | 0,050 | 2,192 | 0,029 | 2,166 | 0,021 | 100 |
| 25,1 | 7,2889 | 0,2382 | 0,3932 | 0,0109 | 0,85 | 2,5434 | 0,0704 | 0,1334 | 0,0016 | 0,6947 | 0,9906 | 2,138 | 0,050 | 2,147 | 0,029 | 2,140 | 0,020 | 100 |
| 26,1 | 7,1669 | 0,1881 | 0,3909 | 0,0085 | 0,83 | 2,5583 | 0,0555 | 0,1317 | 0,0014 | 0,3332 | 0,4745 | 2,127 | 0,039 | 2,132 | 0,023 | 2,118 | 0,019 | 100 |

**Table 1**. Summary of U-Pb zircon isotopic data by LA-MC-ICPMS for meta-andesitic basalt CB-13A. The data were collected with a routine spot size of 25 µm.

*4.3 Geochemistry*

The results of the geochemical analyses performed on 31 metabasite samples are shown in **Table 2.** The selected samples did not show evidence of weathering, hydrothermal or retrometamorphism alterations and had loss on ignition (LOI) values of 0.5% to 1.5% after ignition at 1,000 °C.

Based on the content analysis of major and trace elements (LILE, HFSE, and REE) and the arrangement of the analyzed samples in the classification and evaluation diagrams of the differentiation processes, two main compositional groups denominated $G_1$ and $G_2$-$G_3$-$G_4$ were singled out.

As in most of the Paleoproterozoic terranes, the polyphase metamorphism that affected the VNGB rocks can remobilize the mobile elements of the metabasites and modify the composition of the protoliths. In order to evaluate this possibility, igneous trend models formulated by Beswick & Soucie (1978) based on the logarithmic molecular ratios of major elements in unaltered Phanerozoic igneous rocks were used. As observed in **Figure 9**, the VNGB metabasites have preserved igneous trends. Samples that lie to the right of the igneous field in diagram 5D, identify $K_2O$ gain.

| Group/ Subgroup | G1 | | | | | | | | G2 | | | | | G3 | | |
|---|---|---|---|---|---|---|---|---|---|---|---|---|---|---|---|---|
| Sample | PIA-12 | ANT-57 | ANT-59 | CB-31 | CB-08 | VNG-56 | VNG-57 (CX66) | VNG-45 | VNG-32 | VNG-33 | VNG-57 (CX48) | VNG-38 | VNG-44 | VNG-20 | VNG-28 (CX32) | VNG-28 (CX33) |
| SiO2 | 45.23 | 48.46 | 48.47 | 49.69 | 48.99 | 49.23 | 48.02 | 49.92 | 46.53 | 51.97 | 46.63 | 54.51 | 53.99 | 51.74 | 54.78 | 50.55 |
| Al2O3 | 16.2 | 13.66 | 15.07 | 13.82 | 14.58 | 5.81 | 6.83 | 14.04 | 13.5 | 12.68 | 14.83 | 13.91 | 14.16 | 13.67 | 13.3 | 13.48 |
| Fe2O3 | 15.65 | 16.02 | 14.71 | 15.7 | 15.14 | 12.59 | 12.86 | 14.8 | 9.23 | 10.89 | 12.79 | 9.77 | 10.14 | 11.26 | 12.58 | 13.59 |
| MgO | 5.65 | 4.07 | 5.75 | 4.65 | 5.93 | 17.34 | 17.2 | 5.29 | 9.91 | 8.38 | 7.83 | 8.94 | 7.35 | 8.99 | 6.67 | 7.84 |
| CaO | 8.45 | 11.62 | 7.5 | 9.88 | 8.13 | 8.51 | 7.92 | 9.4 | 16.01 | 12.64 | 7.66 | 6.49 | 9.23 | 8.43 | 7.56 | 8.78 |
| K2O | 0.87 | 0.05 | 0.12 | 0.12 | 0.15 | 2.77 | 2.85 | 0.86 | 0.78 | 0.25 | 4.35 | 2.58 | 1.4 | 0.28 | 0.74 | 1.1 |
| Na2O | 2.7 | 0.64 | 3.23 | 1.71 | 3.04 | 0.32 | 0.38 | 2.7 | 0.15 | 0.61 | 0.63 | 1.15 | 1.2 | 3.48 | 2.19 | 2.13 |
| TiO2 | 2.68 | 3.06 | 2.84 | 2.92 | 2.63 | 1.04 | 1.32 | 1.41 | 0.63 | 0.71 | 1.15 | 0.57 | 0.65 | 0.79 | 0.77 | 0.9 |
| P2O5 | 0.27 | 0.39 | 0.43 | 0.38 | 0.34 | 0.09 | 0.14 | 0.34 | 0.2 | 0.26 | 0.12 | 0.07 | 0.08 | 0.04 | 0.05 | 0.05 |
| MnO | 0.2 | 0.22 | 0.18 | 0.17 | 0.18 | 0.18 | 0.18 | 0.19 | 0.33 | 0.32 | 0.28 | 0.17 | 0.18 | 0.16 | 0.22 | 0.25 |
| Sum | 99.76 | 99.76 | 99.81 | 99.77 | 99.76 | 99.81 | 99.83 | 99.8 | 99.74 | 99.84 | 99.78 | 99.87 | 99.81 | 99.85 | 99.85 | 99.84 |
| LOI | 1.8 | 1.5 | 1.5 | 0.7 | 0.6 | 1.7 | 1.9 | 0.8 | 2.3 | 1,0 | 3.5 | 1.7 | 1.4 | 1,0 | 1,0 | 1.2 |
| Cr2O3 | 0.01 | 0.012 | 0.025 | 0.01 | 0.01 | 0.143 | 0.117 | 0.012 | 0.122 | 0.156 | 0.039 | 0.031 | 0.022 | 0.005 | 0.004 | 0.002 |
| Ba | 281 | 72 | 68 | 62 | 150 | 491 | 348 | 154 | 247 | 49 | 349 | 188 | 136 | 29 | 58 | 56 |
| Co | 53.4 | 38.6 | 40.1 | 45.9 | 45.3 | 80.9 | 82.4 | 50.7 | 44.2 | 51,0 | 45.3 | 39.2 | 48.4 | 44.9 | 45.6 | 49,0 |
| Hf | 4.9 | 4.2 | 3.9 | 4.3 | 3,0 | 2.5 | 2.6 | 1.6 | 2.2 | 2.1 | 1.7 | 1.5 | 2,0 | 1.4 | 1.5 | 1.4 |
| Nb | 8.8 | 13.6 | 10.5 | 14.5 | 13.3 | 14,0 | 16,0 | 2.9 | 3.2 | 4.1 | 3,0 | 4.5 | 5.4 | 1.5 | 1.7 | 1.9 |
| Rb | 18.8 | 1.6 | 2.3 | 0.5 | 3.6 | 98.8 | 134.6 | 19.9 | 26.4 | 5.8 | 133.9 | 95.8 | 47.5 | 11.1 | 43.7 | 45.9 |
| Sc | 38 | 35 | 26 | 31 | 28 | 14 | 15 | 29 | 24 | 33 | 35 | 30 | 30 | 49 | 44 | 48 |
| Sr | 244.9 | 453.5 | 301.9 | #### | 530.5 | 64.5 | 86.7 | 262.1 | 929.4 | 209.1 | 132.3 | 73.4 | 163.9 | 155.5 | 263,0 | 204.1 |
| Ta | 0.7 | 0.9 | 0.7 | 0.7 | 0.8 | 0.8 | 1.3 | 0.3 | 0.2 | 0.2 | 0.3 | 0.2 | 0.4 | <0.1 | <0.1 | <0.1 |
| Th | 3.6 | 3.5 | 2.7 | 3.3 | 3.4 | 4.1 | 5.5 | 1.9 | 1.7 | 3.5 | 0.6 | 1.4 | 1.4 | <0.2 | 0.2 | 0.2 |
| V | 482 | 406 | 318 | 400 | 360 | 136 | 173 | 283 | 178 | 205 | 229 | 187 | 213 | 313 | 315 | 349 |
| Y | 31.1 | 30.9 | 23,0 | 31.8 | 28.7 | 12.5 | 13.7 | 17.2 | 13.9 | 16.1 | 21,0 | 18,0 | 20.3 | 16.9 | 15.6 | 17,0 |
| Zr | 157.1 | 170.5 | 127.3 | 175.2 | 159.8 | 92,0 | 106.4 | 68.5 | 90.8 | 93.9 | 78.4 | 69.6 | 77.8 | 42.9 | 39.8 | 45.2 |
| Cu | 50.8 | 41,0 | 75,0 | 81.4 | 83.3 | 73.9 | 29.4 | 165,0 | 25.2 | 23.3 | 375.9 | 22,0 | 203.1 | 152.5 | 37.9 | 29.5 |
| Ni | 44.8 | 31.7 | 47,0 | 39.8 | 58.9 | 507.2 | 541.2 | 72.7 | 184.9 | 30.4 | 95.3 | 56.1 | 45.1 | 15.6 | 27.9 | 18.2 |
| La | 13.3 | 27.7 | 19.8 | 21.7 | 21.7 | 22.3 | 24.4 | 28.8 | 22,0 | 36.4 | 6.1 | 6.1 | 8.6 | 2.9 | 2.6 | 2.8 |
| Ce | 29.6 | 57.8 | 40.7 | 49.2 | 47.3 | 43.1 | 49.2 | 52.9 | 50.1 | 78.7 | 13,0 | 15.3 | 18.7 | 8.1 | 6.6 | 7,0 |
| Pr | 3.98 | 7.21 | 5.31 | 6.3 | 6,00 | 5.21 | 6.2 | 6.51 | 6.55 | 9.68 | 1.94 | 2.02 | 2.42 | 1.06 | 1,00 | 1.04 |
| Nd | 19.4 | 30.6 | 24.8 | 31,0 | 26.1 | 20.5 | 25.3 | 25.9 | 29.9 | 39.7 | 8.7 | 8.8 | 10.8 | 5.8 | 4.9 | 5.1 |
| Sm | 5.18 | 7.28 | 5.51 | 6.94 | 6.04 | 3.84 | 4.66 | 4.46 | 5.06 | 6.94 | 2.5 | 2.31 | 2.51 | 1.89 | 1.48 | 1.64 |
| Eu | 1.77 | 2.78 | 2.17 | 2.47 | 2.16 | 1.02 | 1.26 | 1.61 | 1.7 | 2.1 | 1,00 | 0.71 | 0.87 | 0.72 | 0.67 | 0.82 |
| Gd | 5.91 | 7.2 | 5.3 | 6.61 | 6.56 | 3.29 | 3.61 | 4.25 | 3.83 | 4.83 | 3.25 | 3.05 | 3.52 | 2.61 | 2.33 | 2.56 |
| Tb | 1.08 | 1.1 | 0.9 | 1.06 | 0.95 | 0.44 | 0.53 | 0.59 | 0.48 | 0.72 | 0.56 | 0.48 | 0.57 | 0.48 | 0.4 | 0.46 |
| Dy | 6.87 | 6.66 | 5.14 | 5.74 | 5.78 | 2.28 | 3.38 | 3.46 | 2.92 | 3.85 | 3.43 | 3.18 | 4.06 | 3.22 | 2.84 | 2.82 |
| Ho | 1.37 | 1.22 | 0.97 | 1.13 | 1.14 | 0.41 | 0.53 | 0.7 | 0.54 | 0.59 | 0.76 | 0.69 | 0.81 | 0.65 | 0.56 | 0.67 |
| Er | 3.58 | 3.39 | 2.58 | 3.11 | 3.22 | 1.35 | 1.32 | 2.11 | 1.44 | 1.76 | 2.31 | 2.02 | 2.55 | 2.03 | 1.86 | 1.85 |
| Tm | 0.49 | 0.46 | 0.33 | 0.44 | 0.45 | 0.16 | 0.2 | 0.29 | 0.2 | 0.26 | 0.32 | 0.33 | 0.34 | 0.31 | 0.29 | 0.29 |
| Yb | 2.85 | 2.85 | 2.07 | 2.9 | 2.53 | 1.01 | 1.21 | 1.92 | 1.23 | 1.58 | 2.05 | 1.92 | 2.07 | 2.03 | 1.8 | 1.78 |
| Lu | 0.44 | 0.4 | 0.34 | 0.45 | 0.36 | 0.14 | 0.15 | 0.27 | 0.2 | 0.27 | 0.32 | 0.27 | 0.36 | 0.31 | 0.28 | 0.31 |

Continue Table 2.

| Group/ Subgroup | G3 | | | G4 | | | | | | | | | | | |
|---|---|---|---|---|---|---|---|---|---|---|---|---|---|---|---|
| Sample | VNG-57 (CX68-A) | VNG-36 | VNG-57 (CX68-B) | VNG-15 | VNG-16 | VNG-18 | VNG-35 | VNG-42 | VNG-57 (CX67) | VNG-26 | CB-19 | VNG-12 | VGN-14 | VNG-51 | VNG-55 |
| SiO2 | 49.63 | 51.84 | 49.96 | 53.82 | 50.68 | 44.14 | 49.02 | 48.94 | 52.31 | 53.59 | 50.41 | 47.46 | 50.38 | 50.84 | 51.27 |
| Al2O3 | 13.41 | 14.3 | 12.03 | 9.31 | 12.5 | 12.01 | 9.56 | 10.27 | 13.16 | 6.56 | 12.92 | 6.04 | 6.47 | 7.45 | 13.61 |
| Fe2O3 | 13.68 | 11.18 | 12.54 | 11.63 | 10.82 | 13.65 | 11,00 | 12.31 | 12.85 | 10.17 | 9.81 | 14.42 | 10.53 | 11.61 | 9.99 |
| MgO | 12.83 | 10.06 | 10.47 | 10.61 | 11.54 | 15.66 | 14.56 | 12.76 | 8.58 | 16.49 | 9.07 | 11.8 | 12.82 | 16.46 | 9.39 |
| CaO | 4.4 | 6.31 | 10.11 | 10.59 | 7.21 | 9.15 | 12.12 | 10.83 | 7.62 | 10.04 | 12.63 | 16.82 | 15.44 | 10.23 | 10.44 |
| K2O | 1.43 | 1.77 | 0.13 | 0.25 | 2.27 | 0.57 | 0.47 | 0.97 | 0.16 | 0.51 | 0.54 | 0.3 | 0.66 | 0.21 | 0.55 |
| Na2O | 2.35 | 1.52 | 2.52 | 1.66 | 0.79 | 0.98 | 0.6 | 1.43 | 3.69 | 0.27 | 2.63 | 0.68 | 0.28 | 0.52 | 2.41 |
| TiO2 | 0.61 | 0.65 | 0.55 | 0.42 | 0.53 | 0.52 | 0.4 | 0.62 | 0.61 | 0.23 | 0.42 | 0.6 | 0.29 | 0.33 | 0.41 |
| P2O5 | 0.04 | 0.07 | 0.04 | 0.04 | 0.04 | 0.05 | 0.03 | 0.05 | 0.04 | 0.02 | 0.04 | 0.01 | 0.03 | 0.04 | 0.04 |
| MnO | 0.17 | 0.16 | 0.18 | 0.24 | 0.26 | 0.24 | 0.22 | 0.23 | 0.18 | 0.19 | 0.3 | 0.33 | 0.34 | 0.27 | 0.28 |
| Sum | 99.83 | 99.89 | 99.78 | 99.89 | 99.87 | 99.89 | 99.88 | 99.87 | 99.81 | 99.9 | 99.84 | 99.89 | 99.87 | 99.91 | 99.87 |
| LOI | 1.2 | 2,0 | 1.2 | 1.1 | 3.1 | 2.7 | 1.7 | 1.3 | 0.5 | 1.7 | 0.9 | 1.1 | 2.2 | 1.6 | 1.4 |
| Cr2O3 | 0.05 | 0.022 | 0.088 | 0.145 | 0.114 | 0.195 | 0.141 | 0.131 | 0.033 | 0.118 | 0.122 | 0.228 | 0.329 | 0.246 | 0.08 |
| Ba | 169 | 55 | 277 | 10 | 182 | 16 | 94 | 159 | 50 | 15 | 136 | 17 | 36 | 13 | 33 |
| Co | 58,0 | 43.1 | 60.9 | 62.3 | 61.3 | 80.3 | 63.3 | 68.4 | 54.7 | 55.9 | 68.3 | 74.9 | 91.8 | 92.6 | 47.9 |
| Hf | 1.7 | 0.8 | 0.8 | 0.8 | 1,0 | 0.9 | 0.6 | 1.1 | 1.3 | 0.2 | 0.4 | 1.2 | 0.6 | 0.4 | 0.7 |
| Nb | 1.1 | 1.2 | 1.2 | 1.2 | 1.4 | 1.4 | 0.9 | 1.4 | 0.8 | 0.3 | 1.5 | 2.4 | 0.9 | 0.4 | 0.8 |
| Rb | 57.5 | 44.7 | 1.5 | 5,0 | 90.3 | 15.6 | 15.8 | 33.4 | 2.4 | 22.3 | 7.7 | 1.1 | 26.6 | 6.8 | 16.6 |
| Sc | 39 | 44 | 38 | 31 | 34 | 36 | 26 | 33 | 39 | 20 | 48 | 30 | 21 | 24 | 37 |
| Sr | 222.8 | 79.9 | 495.9 | 85.7 | 88.6 | 23.6 | 134,0 | 112.8 | 524.9 | 40.4 | 315.6 | 28.6 | 78.3 | 18.7 | 128.2 |
| Ta | <0.1 | 0.1 | <0.1 | <0.1 | 0.1 | <0.1 | <0.1 | <0.1 | <0.1 | <0.1 | <0.1 | 0.1 | <0.1 | <0.1 | <0.1 |
| Th | 0.3 | <0.2 | 0.3 | 0.2 | 0.4 | 0.3 | 0.4 | 0.4 | 0.3 | <0.2 | 0.3 | <0.2 | <0.2 | <0.2 | 0.2 |
| V | 234 | 269 | 220 | 180 | 211 | 209 | 156 | 201 | 228 | 112 | 237 | 181 | 112 | 130 | 205 |
| Y | 13.9 | 14.2 | 13.5 | 6.3 | 8.7 | 9.4 | 7.9 | 10.9 | 14.1 | 6.2 | 13.3 | 11.3 | 5.5 | 6.9 | 11.3 |
| Zr | 43.4 | 35.8 | 39.1 | 24.9 | 35.2 | 32,0 | 23.5 | 38.1 | 40.5 | 12.6 | 28.6 | 36.2 | 18.7 | 16.9 | 25,0 |
| Cu | 16.4 | 30.2 | 275.4 | 81.2 | 30,0 | 97.6 | 53.6 | 23.6 | 138.7 | 39.6 | 19.7 | 51.7 | 67.4 | 9,0 | 197.5 |
| Ni | 63.4 | 47.2 | 109 | 98.7 | 214.3 | 275.5 | 295.2 | 101.2 | 56.3 | 62.1 | 79.8 | 232.8 | 855.6 | 256.2 | 77.9 |
| La | 2.5 | 2,0 | 2.8 | 2.6 | 2.6 | 3.1 | 2.7 | 2.5 | 3.5 | 1.8 | 4,0 | 2.5 | 2.3 | 3.3 | 2.7 |
| Ce | 6.8 | 4.9 | 6.7 | 4.1 | 5.5 | 6.2 | 5,0 | 5.3 | 7.2 | 3.6 | 7.1 | 6.2 | 4.2 | 6.2 | 5.3 |
| Pr | 0.91 | 0.8 | 0.9 | 0.6 | 0.79 | 0.88 | 0.7 | 0.77 | 0.93 | 0.41 | 1.07 | 0.98 | 0.54 | 0.8 | 0.67 |
| Nd | 5.4 | 3.7 | 4.6 | 2.9 | 3.3 | 4,0 | 3.3 | 3.6 | 4.6 | 2,0 | 3.9 | 5.2 | 2.8 | 3.7 | 2.8 |
| Sm | 1.57 | 1.46 | 1.38 | 0.83 | 1.13 | 1.15 | 0.96 | 1.19 | 1.54 | 0.6 | 1.32 | 1.81 | 0.72 | 0.98 | 0.9 |
| Eu | 0.53 | 0.54 | 0.35 | 0.27 | 0.45 | 0.47 | 0.4 | 0.32 | 0.58 | 0.43 | 0.43 | 0.5 | 0.5 | 0.58 | 0.4 |
| Gd | 2.16 | 2.02 | 1.87 | 1.07 | 1.48 | 1.6 | 1.38 | 1.78 | 2.16 | 0.93 | 1.48 | 2.17 | 0.98 | 1.11 | 1.46 |
| Tb | 0.37 | 0.39 | 0.36 | 0.18 | 0.25 | 0.25 | 0.22 | 0.3 | 0.38 | 0.16 | 0.3 | 0.36 | 0.18 | 0.2 | 0.26 |
| Dy | 2.59 | 2.47 | 2.41 | 1.27 | 1.78 | 1.91 | 1.62 | 1.94 | 2.71 | 1.17 | 2.19 | 2.1 | 1.12 | 1.53 | 1.93 |
| Ho | 0.51 | 0.61 | 0.61 | 0.25 | 0.35 | 0.41 | 0.34 | 0.38 | 0.62 | 0.26 | 0.57 | 0.39 | 0.27 | 0.29 | 0.39 |
| Er | 1.67 | 1.74 | 1.64 | 0.81 | 1.03 | 1.34 | 0.93 | 1.18 | 1.93 | 0.84 | 1.29 | 1.14 | 0.88 | 0.97 | 1.39 |
| Tm | 0.24 | 0.25 | 0.27 | 0.12 | 0.17 | 0.19 | 0.14 | 0.2 | 0.27 | 0.13 | 0.22 | 0.16 | 0.11 | 0.14 | 0.2 |
| Yb | 1.74 | 1.64 | 1.66 | 0.84 | 1.08 | 0.97 | 0.92 | 1.03 | 1.84 | 0.88 | 1.67 | 1.05 | 0.8 | 1.02 | 1.33 |
| Lu | 0.27 | 0.26 | 0.26 | 0.12 | 0.19 | 0.17 | 0.14 | 0.18 | 0.27 | 0.16 | 0.27 | 0.16 | 0.13 | 0.16 | 0.25 |

**Table 2**. Litogeochemistry data from analyzed metabasites of the Vila Nova greenstone belt.

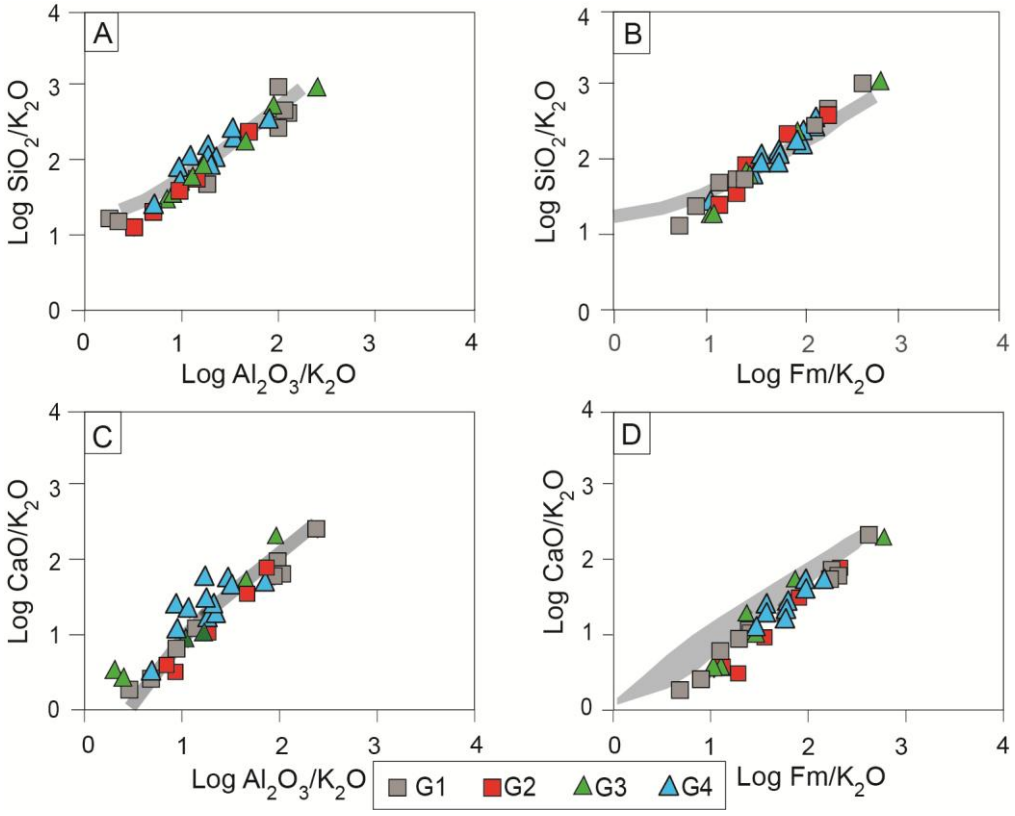


**Figure 9**. Logarithmic molecular binary diagrams of Beswick & Soucie (1978) for evaluation of metasomatic effects on VNGB metabasites. Fm = FeOT + MgO + MnO.

*Differentiation Processes*

The arrangement of the major elements shows that most of the metabasites present a basic composition, with $SiO_2$ content ranging from 45.23% to 54.78%, with only one metaultrabasite ($SiO_2$=44.15%). The $G_1$ group samples exhibit moderate concentrations of MgO (4.07-5.93%), and reach higher values of $TiO_2$ (2.63-3.06%), $Al_2O_3$ (13.66-16.20%), $FeO_t$ (14.71-16.02%) and $P_2O_5$ (0.27-0.43). The $FeO_t$/MgO ratio > 1.75 allows classifying these samples as Fe-Ti basalts (Melson *et al*., 1976; Sinton *et al.*, 1983). The most magnesian samples from this group shows lower contents of $Al_2O_3$ (5.81-6.83%), FeOt (12.59-12.86%), $TiO_2$ (1.04-1.32%) and $P_2O_5$ (0.09-0.14%) and higher concentrations of MgO (17.20-17.34%), characterized by a magnesium number (mg#) ratio [MgO/(MgO + $FeO_t$)]) with values from 72-73, much higher than the average values of the Fe-Ti basalts, from 33-43. The $G_2$-$G_3$-$G_4$

subgroups have lower contents of $TiO_2$ (0.23-1.15%), $FeO_t$ (9.23-14.42%), $P_2O_5$ (0.01-0.26) and variable content of MgO (6.67-16.43%). The mg# assumes values from 54-77 in $G_2$, 51-65 in $G_3$ and from 56-76 in $G_4$.

The binary diagrams using the relationship between the major and minor elements against MgO as the variation index are shown in **Figure 10 and 11.** The samples configure linear to curve trends, which reflects the little change by the action of post-magmatic processes. Despite the dispersion of the major elements, there are differences between the $G_1$ and $G_2$-$G_3$-$G_4$ groups. The $G_1$ samples show enrichment of CaO, $Fe_2O_3$, $TiO_2$,$P_2O_5$ with fractionation (with the decrease of MgO). The $K_2O$ oxide decreases with differentiation, whereas $SiO_2$ and $Na_2O$ do not form defined trends. $Al_2O_3$ shows low values in the most magnesian samples and higher values in the other samples with decrease from 5% MgO. In the samples of group $G_2$-$G_3$-$G_4$, the contents of $SiO_2$, $TiO_2$, $P_2O_5$, $Na_2O$ and $K_2O$ increase with differentiation. In this group, the $TiO_2$ and $P_2O_5$ oxides form linear trends with incipient enrichment in the later phases of the differentiation. The $Fe_2O_3$ contents increase with the fractionation in subgroup $G_2$ and show relative dispersion in the other subgroups. Meanwhile, in subgroups $G_2$ and $G_4$, it is not possible to clearly identify the behavior of CaO, and in G3, it presents enrichment with magmatic differentiation.

In the binary diagrams with minor elements, the decrease of Co, $Cr_2O_3$ and Ni is observed with magmatic fractionation in all groups, attesting the compatible character of these elements **(Figure 11)**. Sr and Eu show a rectilinear and more enriched pattern in subgroups $G_1$ and $G_2$, when compared to $G_3$ and $G_4$, with the advance of the crystallization. The elements Zr, Sc and V are incompatible and show enrichment with magmatic fractionation in all groups.

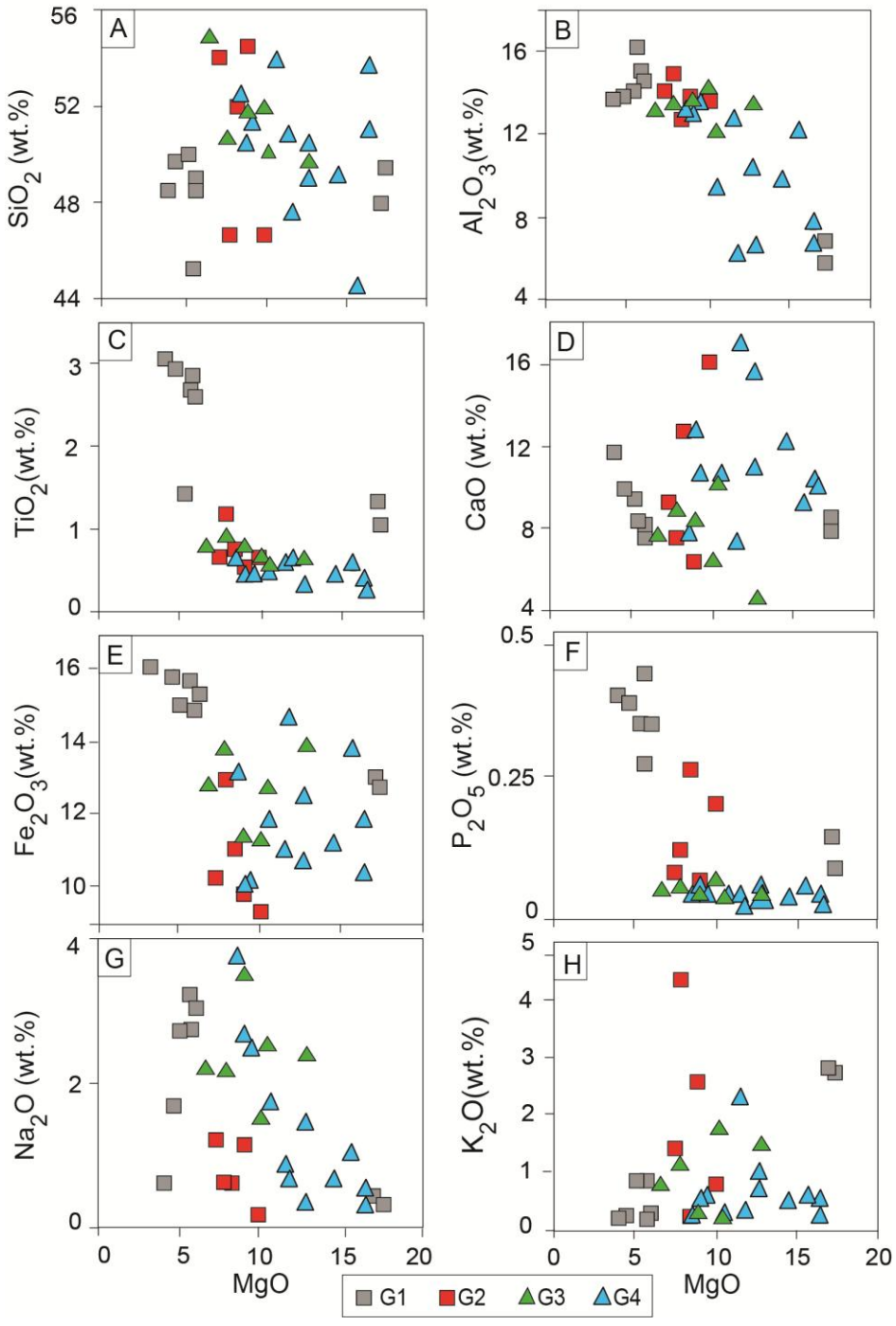


**Figure 10**. Diagrams of variation between the major elements (% by weight) and the MgO content (% by weight) for the VNGB metabasites.

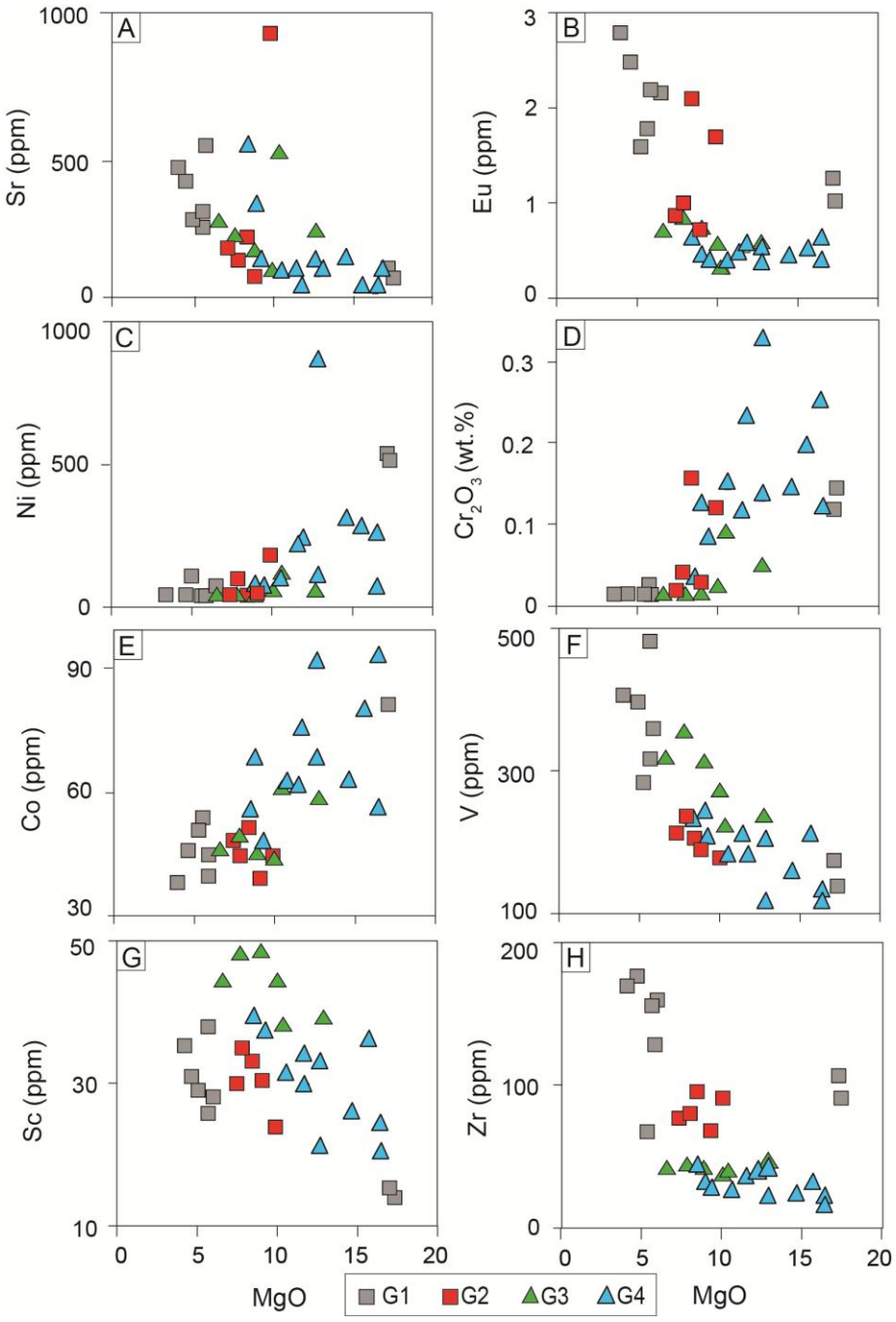


**Figure 11**. Diagrams of variation between the minor elements (ppm) and the MgO content (% by weight) for the VNGB metabasites.

*Classification Diagrams*

The arrangement of the VNGB metabasites in the Le Maitre (1989) TAS diagram characterizes the protoliths as basalts ($G_1$) and andesitic basalts ($G_2$-$G_3$-$G_4$), subalkaline in nature **(Figure 12A)**. In the AFM diagram by Irvine & Baragar (1971) the analyzed metabasites showed a dominant trend with Fe enrichment,

characteristic of the tholeiitic series **(Figure 12B)**. When arranged in the Jensen diagram (1976), the $G_1$ group metabasites are composed of high-Fe basalts and komatiites **(Figure 12C)**. The $G_2$ and $G_3$ samples plot in the field defined for high-Mg tholeiitic basalts. The $G_4$ group samples make up a continuous alignment that extends between the field of the komatiites and komatiite basalts, finalizing in the tholeiitic basalts with high magnesium. In the Winchester and Floyd diagram (1977), which uses the $Zr/TiO_2$ *vs* Nb/Y ratio, most of the samples are located in the field of basalts and subalkaline andesites, with two G1 samples falling in the field of alkaline basalts **(Figure 12D).**

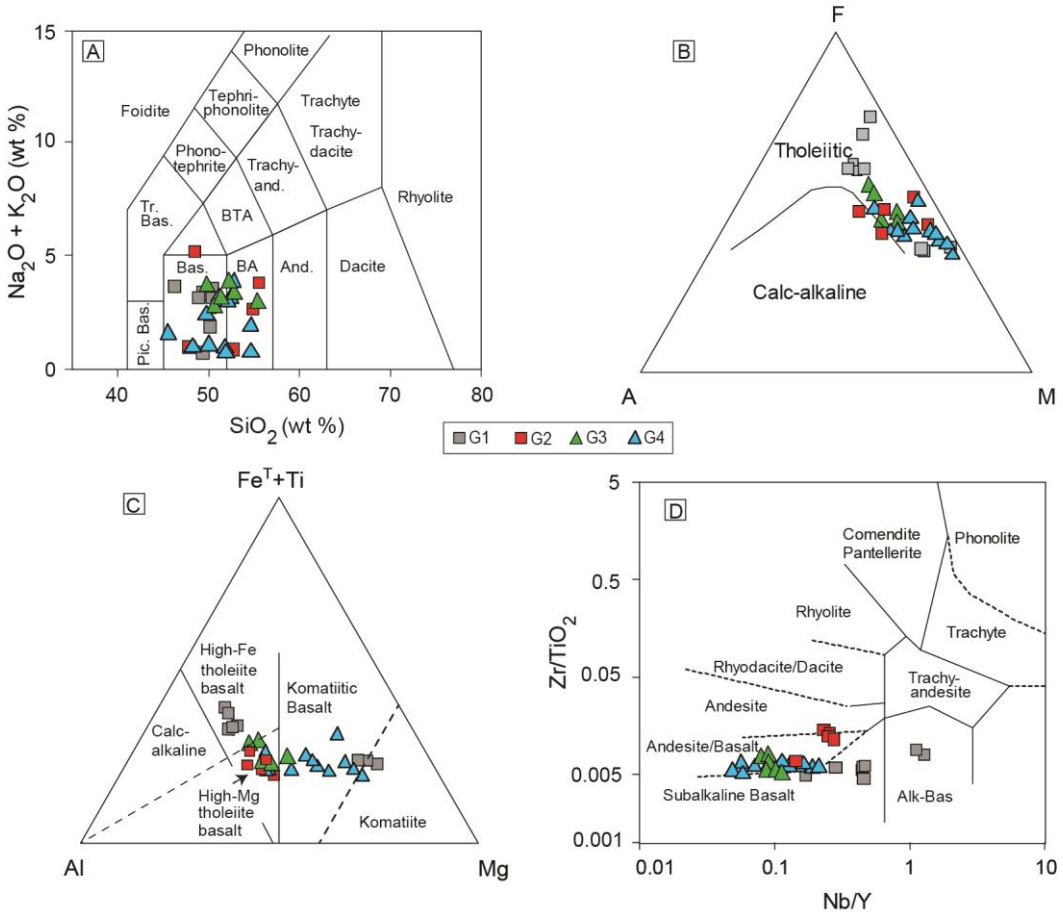


**Figure 12**. Representation of the VNGB metabasites in the classification diagrams. A) TAS ($Na_2O+K_2O$)-$SiO_2$) from Le Maitre (1989), B) Irvine & Baragar AFM (1971), C) Jensen (1976) and D) Winchester & Floyd (1977).

*Magma Sources*

The MORB-normalized multi-element diagrams (Pearce, 1983) and chondrite-normalized REE patterns (Boynton, 1984) allow the individualization of the sample set into four distinct groups (**Figures 13**). The rocks of group $G_1$ show higher total REE levels and an enriched light REE pattern with positive anomalies incipient or absent and negative Eu anomalies. The rocks of group $G_2$ show lower REE levels, with a moderately enriched LREE pattern. The samples of groups $G_3$ and $G_4$ show straight REE patterns and lower levels than those of chondrite. The distribution of the VNGB metabasites in *MORB*-normalized multi-element diagrams also identifies enrichment in *LILE* in all groups. However, groups G1 and G2 have higher overall levels of minor elements than *MORB*, while subgroups $G_3$ and $G_4$ exhibit lower levels of *HFS* and heavy REE than those of MORB.

The Fe-Ti basalts of $G_1$ are enriched in Sr, Ba and Th and depleted in K and Rb relative to MORB. Compared to the other analyzed groups, they have the highest levels of HFSE elements, with moderate enrichment. The Fe-Ti basalts exhibit strong to moderate positive Th, Ce and Ti anomalies and moderate to weak negative anomalies of Nb, Ta, Y and Yb. The high-Fe tholeiitic basalt sample presents Nb and Ta values very close to MORB values and strong Ce positive anomalies, negative Nb-Ta anomalies and incipient negative anomalies of Ti, Y, and Yb.

The high-Mg tholeiitic basalts of the $G_2$ group show K, Rb and Ba enrichment and Sr concentrations close to the MORB pattern. The Nb, Ta and Ce contents show slight to moderate enrichment, with an incipient negative Nb anomaly and weak to strong positive Ce anomalies. The remaining HFSE elements in general exhibit slight depletion, with weak negative Hf, P, Ti and Yb anomalies and mild to moderate positive Sm and Zr anomalies.

The high-Mg tholeiitic basalts and the $G_3$ group komatiite basalts are enriched in LILE (Sr, K, Rb and Ba), with strong positive Rb anomalies. The HFSE elements (Ta, Nb, Ce, P, Zr, Hf, Sm, Ti, Y and Yb) are moderately depleted compared to MORB and show positive Ce anomalies, varying Hf anomalies and negative P and Ta anomalies.

The $G_4$ group samples are characterized by compositions of komatiites to high-Mg tholeiitic basalts. They present variable enrichment in LILE elements, generally with strong to slight positive anomalies of Rb and Ba and slight to moderate negative anomalies of Sr. The HFSE elements are slightly depleted relative to the MORB, and have positive Ce anomalies and negative Nb and P anomalies.

The samples of group $G_1$ are characterized by the highest total REE levels of the analyzed groups, with a (La/Lu)n ratio between 3.13 to 7.19 in Fe-Ti basalts, from 11.07 to 14.00 in komatiites and 11.07 in high-Fe tholeiitic basalt. The rocks of group $G_2$ show a concentration of total REE higher than chondrite values, with moderate to high fractionation of heavy rare earth elements (HREE) and (La/Lu)n ratio between 1.98 and 14. The $G_3$ group showed slightly enriched REE contents compared to chondrite values, and low (La/Lu)n ratio with values ranging from 0.79 to 1.11. Group $G_4$ shows slightly enriched concentrations compared to the chondrite values, with (La/Lu)n ratio between 1.12 and 2.25. The $G_4$ samples show depletion in medium REE with positive Eu anomalies ranging from weak (komatiitic basalts to high-Mg tholeiitic basalts) to strong basalts (komatiites to komatiitic basalts), and weak negative anomalies for the samples of komatiitic basalts.

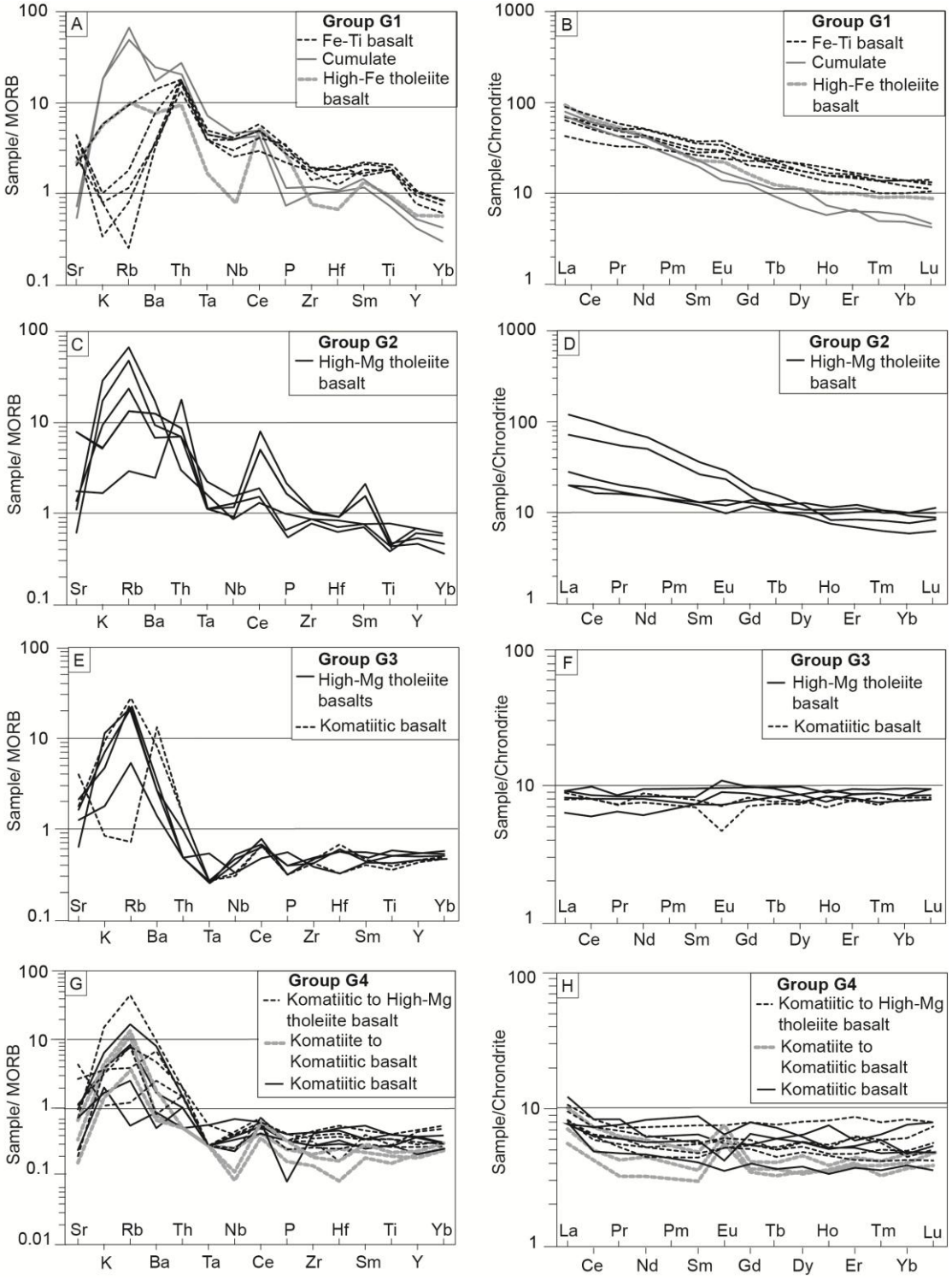


**Figure 13**. A, C, E and G) Multi-element diagrams standardized by MORB (Pearce, 1983) and B, D, F and G) chondrite-normalized ETRs (Boynton, 1984) for the VNGB metabasite groups.

*Metamorphism and Deformation*

The successive stages of deformation and metamorphism are commonly preserved in metamorphic rocks. The recognition and correct interpretation of the

relations between the foliations and the porphyroblasts are essential for the understanding of the evolution of the metamorphic conditions.

Two major metamorphic events were recognized, an orogenic metamorphism event, and a contact metamorphism one. In the orogenic metamorphism event, the $S_1$, $S_2$ foliations, and a fine and discontinuous $S_3$ schistosity were recognized. The $S_1$ schistosity is partially preserved as $F_2$ intrafolial folds, enveloped and transposed by the of $S_2$ crenulation cleavage, both generated between metamorphic conditions of the greenschist and lower to medium amphibolite facies. The $S_3$ foliation is defined by fracture cleavage, locally fine schistosity. The cleavage is filled by fine quartz and carbonate veins, associated with a retrometamorphic event under greenschist facies conditions.

The contact metamorphism event is identified by the overlaying of textures with no mineral orientation, by the massive structure and the acicular and fine decussate textures (<0.1 mm). The association of chlorite and clinochlorite and hornblende, tremolite and plagioclase observed in the mafic cornubianites shows a thermal metamorphism generated under variable conditions between the ab-ep hornfels and Hbl hornfels facies, while the diopside and hornblende paragenesis characterizes the pyroxene hornfels facies and marks the maximum temperature peak. The main microstructures and metamorphic events are summarized in Table 3.

| Rock | Mineral Paragenesis/Tectonic event | | Temporal Relation | Metamorphic Facies | Microstructural/textural features | |
|---|---|---|---|---|---|---|
| Amphibolites | Hbl + Pl + Grt (Di) | MO | syntectonic | Upper Amphibolite | Intrafolial folds and crenulation cleavage | S1, S2 |
| Amphibolites | Chl + Ser + Ep | MO | tardi-tectonic | Greenschist | Retrograde metamorphism on fractures | S3 |
| Amphibole schists | Bt + Tr | MO | syntectonic | Amphibolite | Mineralogical orientation | S1,S2 |
| Amphibole schists | Hbl + Chl + Clc | MO | syntectonic | Upper Greenschist | Mineralogical orientation | S1,S2 |
| Amphibole schists | Hbl + Tr | MO | syntectonic | Amphibolite | Mineralogical orientation | S1,S2 |
| Mafic-Hornfels | Di + Hbl | MC | post-tectonic | Px-Hornfels | Decussate texture | - |
| Mafic-Hornfels | Hbl + Pl | MC | post-tectonic | Hb-Hornfels | Decussate texture | - |
| Meta-ultramafites | Tr | MO | syntectonic | Amphibolite | Intrafolial folds and crenulation cleavage | S1, S2 |

**Table 3**. Relationship between the main microstructures and metamorphic events observed in the VNGB units. Legend: OM= orogenic metamorphism, CM= contact metamorphism; $S_1$= schistosity, $S_2$= crenulation cleavage, $S_3$= fracture cleavage. Minerals: Hb= hornblende, Pl= plagioclase, Grt= garnet, Di= diopside, Chl= chlorite, Ser= sericite, Ep= epidote, Trem= tremolite, Bt= biotite, Qz= quartz.

## 5. Discussion

The metabasites of the Vila Nova greenstone belt were affected by an orogenic metamorphism that transformed the volcanic rocks into amphibole schists and amphibolites. The mineral associations indicate that the transformations occurred under conditions between the upper green schists and medium amphibolite facies, and under intermediate pressure conditions. The structural relationships observed in the VNGB rocks indicate that the metamorphism occurred associated with three deformation events related to compressive tectonics. The relationships between the foliations and metamorphic and stretching lineations indicate frontal collisional kinematics, generating low-angle shear zones in the areas of maximum deformation. These zones are responsible for the contacts between the metavolcano-sedimentary rocks of the Vila Nova greenstone belt and the orthogneisses and metagranites of the Tumucumaque Complex, which represent the Archean basement. The internal relationships between the VNGB rocks were also affected

mainly by the VNSZ, which puts in contact a lower domain composed mainly of metavolcanic rocks and an upper domain composed of metasedimentary rocks.

*Magmatic Evolution*

The compositional differences observed among the samples of groups $G_1$, $G_2$, $G_3$ and $G_4$ based on the analysis of the bivariate diagrams of major elements indicate that the magmatic evolution occurred through fractional crystallization from distinct differentiation lines for $G_1$ compared to the other groups. In $G_1$, the strong enrichment in Fe and Ti with the advancement of crystallization is characteristic of magmas generated under reducing conditions. In these environments, the low $fO_2$ inhibits the early crystallization of oxides such as magnetite and chromite/ilmenite, leading to the enrichment of Fe and Ti. In more oxidizing environments, the addition of water favors the early crystallization of free Si oxides, such as chromite and iron-magnesium minerals with low Si (olivine). Consequently, the samples show slight or no enrichment in FeOt and $TiO_2$, increase in $SiO_2$ and decrease in the contents of $Cr_2O_3$ with the advancement of crystallization similar to the metabasites related to $G_2$, $G_3$ and $G_4$.

Besides the differences in the contents and patterns identified in the binary variation diagrams, the decrease of Ni, Cr, and Co with the magmatic fractionation observed in all groups suggests that the crystallization of olivine played a fundamental role in the evolutionary process of these magmas. In comparison with $G_1$, the $G_2$, $G_3$ and $G_4$ groups show evidence of depletion in $Cr_2O_3$ with fractionation, which suggests greater effectiveness in the crystallization of chromite. Though less pronounced, other considerations can be made. In $G_1$, the strong enrichment in Sr and Eu combined with the decrease of MgO suggest an incipient fractionation of plagioclase. However, in the other groups, the crystallization of plagioclase is inferred

in the initial stages by the patterns of Sr and Eu, followed by a change in the petrogenetic order, causing enrichment of these elements in the late phases.

In evolutionary terms, the magnesium number (mg#) with relatively low values (33 and 43) attests the Fe-Ti basalts of $G_1$ as derived from a mantle more enriched in Fe. The $G_2$ (54-68), $G_3$ (51-65) and $G_4$ (56-76) samples show mg# values of moderately or slightly fractionated magmas. The metabasites of group $G_4$ that have Ni > 250 ppm and magnesium number from 69 to 76 may represent very primitive liquids.

*Tectonic environment of the VNGB Metabasites*

The precise definition of the tectonic environment of formation of the volcanic rocks is based on field association and, mainly, on the compositional characteristics of the magmatism. In this aspect, the composition of the major elements, trace elements and rare earths was used to establish the parameters (diagrams) that define the tectonic environments of the main associations of Phanerozoic volcanic rocks (Shervais 1982; Pearce 1982; Pearce, 2008).

Shervais (1982) certifies that the Ti/V ratios are intrinsic to the magma-forming tectonic environment, since the V compatibility is controlled by the $fO_2$, as well as the partial melting degree and consequent fractional crystallization. The element Ti presents incompatible behavior regardless of the oxy-reducing conditions. This author has shown that the partition coefficient of V is affected by the increase of $fO_2$ in oxidizing environments, such as island arcs and continental margin. The magmas generated by conditions between 20 and 30% partial melt have a Ti/V ratio between 10 and 20. In tectonic environments with reducing conditions, such as the mid-ocean ridges, magmas generated with a similar degree of melt have Ti/V ratios between 20 and 50, while ratios higher than 50 are characteristic of alkaline rocks. In back-arc

basins, the Ti/V ratio shows values between 10 and 50. This wide variation can occur due to the interaction between the mantle (depleted or enriched) and the input of fluids due to the dehydration of the oceanic lithosphere during the subduction process.

In the diagram in **Figure 14A,** the samples of the $G_2$ (18-30), $G_3$ (14-15) and $G_4$ (10-19) groups show similar composition to the basalts of island arcs, while the samples of group $G_1$ are similar to basalts generated in back-arc and/or mid-ocean ridge basins. The VNGB metabasites show features of a poorly developed subduction environment, such as in island arc and back-arc basins. However, the extraction of magma in a ridge from a previously metasomatized mantle (with inherited subduction components) should also be considered. Similar behavior is observed in the Pearce (1980) diagram, based on Ti *vs.* Zr **(Figure 14B)**. However, the Fe-Ti basalts of the $G_1$ group are similar in composition to the intraplate basalts.

Pearce & Stern (2006) indicate that the main characteristics of basalts generated in retro-arc basins are the depletion in HFSE (Zr, Ta, Nb, P, Ti and Zr) and enrichment in LILE (Sr, K, Rb and Th). According to the authors, these characteristics are related to the addition of aqueous fluids derived from the dehydration of the oceanic plate during subduction. In the MORB-normalized multi-element diagrams, the metabasites of the $G_3$ and $G_4$ groups show LILE enrichment (Sr, K, Rb, Ba) and moderate depletion in HFSE, with negative anomalies of Nb, Ta, P, Ti and Zr, which corroborate this interpretation. The $G_1$ and $G_2$ samples also show moderate enrichment of LILE elements (Sr, Rb, Ba and K), however, they show a higher content of HFSE (Zr, P and Ti), with slight positive anomalies of Nb and Ta, suggesting interaction with a more enriched source.

The selective depletion of middle REEs, as observed in the $G_4$ samples, is attributed by some authors (Agafonov & Erkushev, 1985; Gruau, 1985; Lesnov, 2010)

to the serpentinization of ultramafics in seafloor metamorphism. According to Lesnov (2010), the selective enrichment of light REEs can occur from the interaction of the rock with marine fluids or fluids segregated from later granitic intrusions. Invariably, the patterns observed in the metabasites of the G4 group appear to have been modified by the influence of the metamorphic processes.

Most of the metabasites of the $G_1$ subgroup are characterized by high levels of $TiO_2$ (>2%) and $FeO_t$ (>12%), similar to the basalts generated in propagation expansion centers. These basalts were named by Sinton et al. (1983) as Fe-Ti type basalts. These expansion centers originate at the extremities of the extension plate boundaries that progressively spread through the rigid lithosphere, occurring within continents (Courtillot, 1982), oceans (Hey et al., 1989), magmatic arcs and retro-arc basins (Parson & Wright, 1996). The low mg# values associated with Fe-Ti basalts suggest they are generated from a high degree of parent magma fractionation. Based on petrographic criteria of texture and mineral composition, the $G_1$ samples plotted on the komatiitic fields in the Jensen diagram (1976) can be reported as cumulate rocks. The high enrichment in light REEs, characteristic of low melting conditions, favors the interpretation that these rocks have a residual origin.

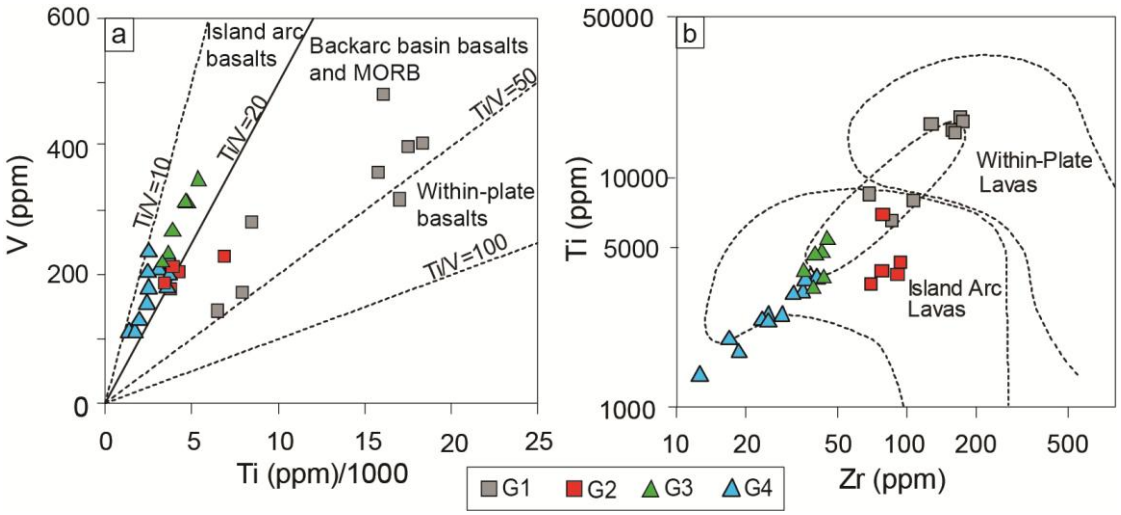


**Figure 14**. Representation of the GBVN metabasites in tectonic ambience diagrams of mafic rocks. A) V *vs.* Ti (Shervais, 1982), B) Ti *vs.* Zr (Pearce, 1980).

*Mantle Sources and Contamination*

The variation of the Ti/Yb ratio is sensitive to the depth of the partial melting that gave rise to the basic magmas, whereas the Nb/Yb ratio can be used to characterize the mantle fertility (Pearce, 2008). The Nb/Yb-$TiO_2$/Yb ratio values in diagrams proposed by Pearce (2008) show different mantle reservoirs for the VNGB metabasite groups. The high values of Nb and $TiO_2$ (normalized by Yb) attributed to Fe-Ti basalts and to $G_1$ cumulates identify deeper sources, originating from the asthenospheric mantle, in a likely interaction of plume and mid-ocean ridge **(Figure 15A)**. The Ce/Yb ratio, ranging from 10.38 to 20.28 for the Fe-Ti metabasalts of $G_1$, can be attributed to low degrees of melting at high depths and/or the presence of garnet as a residual phase, which corroborates a genesis model of associated with the influence of mantle plume.

The lower concentrations of Nb and $TiO_2$ (normalized by Yb) identified in $G_2$, $G_3$ and $G_4$ suggest shallow melt generation in the normal to slightly enriched mantle region at mid-ocean ridge seafloor spreading zones **(Figure 15A)**. The lower Ce/Yb ratios in part of the $G_2$ group (6.34 - 9.03), and in the $G_3$ (2.98 - 4.03) and $G_4$ (3.91 -

6.39) groups, may have originated from a high degree of melting and/or the presence of spinel as a residual phase.

The Th/Yb *vs.* Nb/Yb ratio variations are sensitive to the composition of the source of basic magmas and the effects of crustal contamination or related to the subduction components, independent of fractional crystallization and/or partial melting (Pearce, 2008). Thus, the basaltic magmas derived from the depleted mantle, asthenospheric plume and lithospheric mantle enriched by a low-degree asthenosphere melt, are positioned within or very close to the diagonal field defined by constant Th/Nb ratios **(Figure 15B)**. Since Th is a mobile element in the hydrated mantle, the mantle sources metasomatized by processes related to subduction or crustal contamination are enriched in Th relative to Nb, resulting in Th/Yb ratios higher than Nb/Yb. In general, the $G_2$ and $G_4$ samples are close but slightly above the field defined for MORB-OIB rocks. However, in the $G_2$ and $G_3$ samples, there is a vertical trend, common to volcanic arc associations. The enrichment of LILE, with the depletion of HFSE and the negative anomalies of Nb and P, observed in the MORB-normalized multi-element diagrams, suggests that the increase of Th is related to the subduction. The $G_1$ group metabasites identify crustal components, but are associated with higher Nb values, and require a more enriched source.

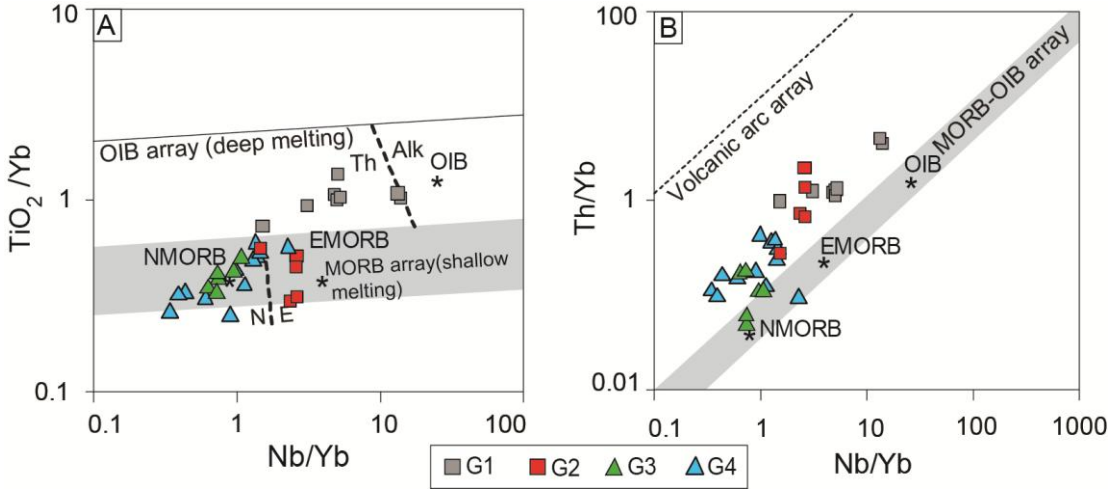


**Figure 15**. A) $TiO_2$/Yb *vs.* Nb/Yb (Pearce, 2008) and B) Ti/Yb *vs.* Nb/Yb (Pearce, 2008). N-MORB: normal meso-oceanic basalts; E-MORB: enriched meso-oceanic basalt and OIB: basalts of oceanic islands.

Comparing the Nb / Yb and Th / Yb ratios of the GBVN metabasites samples from East Scotia Ridge basalts and South Sandwich Island Arc basalts (data from Fretzdorff et al., 2002), the G1 samples show trend towards vertex A, represented by Bouvet Island, a recognized plume environment influenced. The G2 samples show a parallel trend to vertex B, which can be understood as subducted slab-released components from sediments. The G3 and G4 plot very close to the delimited field for samples of South Sandwich Island Arc (vertex C). This trend is suggested to be generated from sub-arc mantle modified by subduction-related components from the downgoing slab **(Figure 16)**. Thus, the East Scotia Ridge basalts could represent a modern analogue to explain the geochemical variation observed in the metabasites of GBVN.

The coexistence of Fe-Ti basalts ($G_1$) with basalts and andesitic basalts ($G_2$, $G_3$ and $G_4$), with characteristics of ridges in spreading centers with subduction components, points to a model of island arcs associated with propagation from a mid-ocean ridge in a back-arc basin **(Figure 17)**.

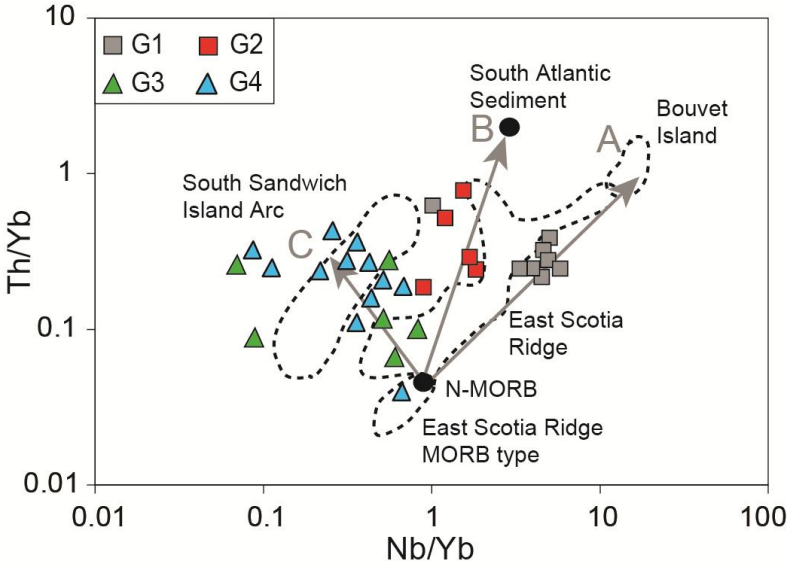


**Figure 16**. Variation of Th/Yb vs. Nb/Yb for the East Scotia Ridge lavas (modified from Fretzdorff et al., 2002) compared with the metavolcanic rocks of VNGB**.**

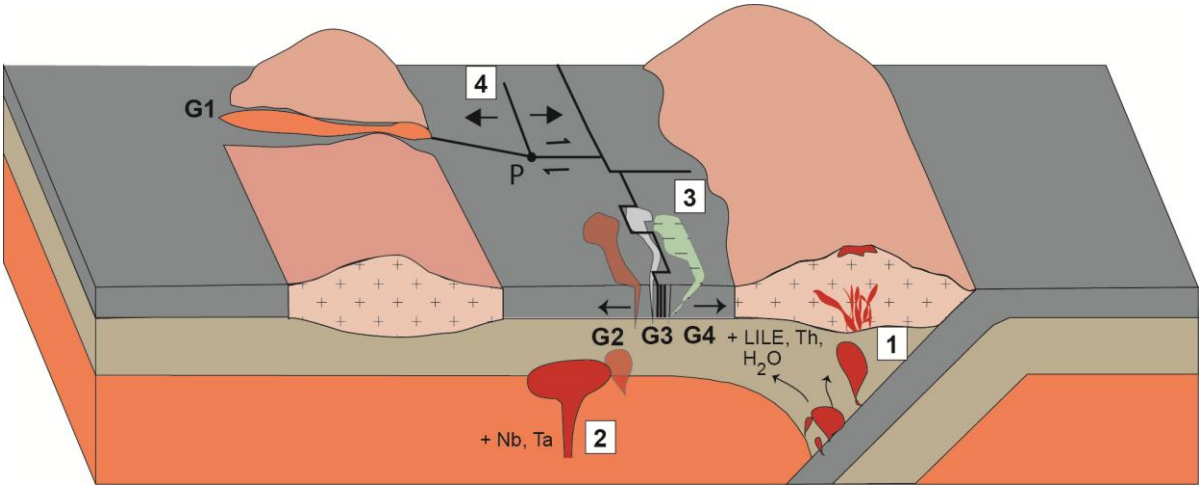


**Figure 17**. Block diagram illustrating the probable tectonic environment of the formation of themetabasites of Vila Nova Greenstone Belt and the sources of the mantle heterogeneity in back-arc basins. 1) Interaction of the subduction components with the depleted upper mantle, 2) Interaction of the upper mantle with asthenospheric source, 3) Interaction with sea water and 4) Propagating rift structures and origin of Fe-Ti basalts.

## 6. Conclusions

The metamorphic rocks of the VNGB present petrographic and geochemical characteristics compatible with basalts and andesitic basalts of tholeiitic composition, which were transformed by an event of polycyclic orogenic metamorphism. The

available ages indicate that the VNGB volcanism occurred between 2.17 and 2.15 Ga, while the intrusive granites responsible for the contact metamorphism were positioned between 2.06 and 1.99 Ga. Therefore, the orogenic metamorphism affected these units between 2.15 and 2.07 Ga. This metamorphic event is responsible for the structuring of the VNGB units and for the generation of the Vila Nova, Ipitinga and Serra do Navio shear zones.

The geochemical signatures of the VNGB metabasites correspond to island-arc basalts (groups $G_2$, $G_3$ and $G_4$) and back-arc basalts (Fe-Ti basalts, group $G_1$). The composition of the minor elements indicates that the formation of the metabasites involved the interaction between enriched MORB ($G_2$) and normal MORB ($G_3$, $G_4$) type sources with subduction components. However, the U-shaped pattern observed in multi-element diagrams of the $G_4$ group samples, as well as the slight selective enrichment in LREE, may suggest that these rocks were affected by seafloor metamorphism.

**Acknowledgments**

We thank the *Conselho Nacional de Desenvolvimento Científico e Tecnológico* (CNPq) for the research scholarships granted to the second and third authors; the Amapari Mining Company for field logistics and making geologic and drill core data available. We thank the reviewers for their critical suggestions.

**References**

Agafonov, L.V. and Erkushev, Y.A., 1984. Rare Earth Element Distribution in Rocks from Shavaryn Tsaram Volcano, Mongolia. *Geol. Geofiz*, (6), pp.65-76.

Avelar, V.D., Lafon, J.M., Delor, C., Guerrot, C. and Lahondère, D., 2003. Archean crustal remnants in the easternmost part of the Guiana Shield: Pb–Pb and Sm–Nd geochronological evidence for Mesoarchean versus Neoarchean signatures. *Géologie de la France*, *2*, pp.3-4.

Barbosa, J.P.O., Costa Neto, M.C., Rosa-Costa, L.T., Anjos, G.C., Chaves, C.L., 2013. Projeto Folha Macapá - NA.22-Y-D. Mapa Geológico (1:250.000). CPRM, Belém.

Belousova, E., Griffin, W.L., O'Reilly, S.Y. and Fisher, N.L., 2002. Igneous zircon: trace element composition as an indicator of source rock type. *Contributions to mineralogy and petrology*, *143*(5), pp.602-622.

Beswick, A.E. and Soucie, G., 1978. A correction procedure for metasomatism in an Archean greenstone belt. *Precambrian Research*, *6*(2), pp.235-248.

Borghetti, C.; Philipp, R.P.; Basei, M.A.S.; Mandetta, P. 2014. New ages from Vila Nova and Tumucumaque Complex in the Cupixi region, Porto Grande, Amapá, Brazil.9th South American Symposiumon Isotope Geology.Boletim de Resumos Expandidos, São Paulo, Brasil.

Borghetti, C.; Philipp, R.P. 2017. Geologia e geofísica do greenstone belt Vila Nova, porção NE do Cráton Amazônico, Amapá, Brasil. Geol. USP, Sér. cient., São Paulo, 17(1):109-127.

Borghetti, C.; Philipp, R.P.; Basei, M.A.S.; Mandetta, P.; Hoffmann, I. B. 2017a. Geology and U-Pb zircon geochronology of the Vila Nova greenstone belt, Amapá, Brazil: arc related basin and tectonic implications for a Rhyacian orogeny in the NE domains of the Amazonian Craton.Precambrian Research. Submitted.

Borghetti, C.; Philipp, R.P.; Basei, M.A.S.; Mandetta, P.; Hoffmann, I. B. 2017b. Geochronology of the Tumucumaque Complex: an Archean nucleus in the NE portion

of the Amazon Craton, Vila Nova-Serra do Navio region, Amapá State, Brazil. Brazilian Journal of Geology. Submitted.

Boynton, W.V., 1984. Geochemistry of the rare earth elements: meteorite studies. W: Rare earth element geochemistry.(red. P. Henderson): 63–114.

Chemale, F., Philipp, R.P., Dussin, I.A., Formoso, M.L.L., Kawashita, K. and Berttotti, A.L., 2011. Lu–Hf and U–Pb age determination of Capivarita Anorthosite in the Dom Feliciano Belt, Brazil. *Precambrian Research*, *186*(1), pp.117-126.

Cordani, U.G. and Neves, B.B., 1982.The geologic evolution of South America during the Archean and Early Proterozoic. *Brazilian Journal of Geology*, *12*(1-2-3), pp.78-88.

Courtillot, V., 1982.Propagating rifts and continental breakup. *Tectonics*, *1*(3), pp.239-250.

deWit, M.J. and Ashwal, L.D., 1986. Workshop on Tectonic Evolution of Greenstone Belts. LPI Tech. Rpt. 86-10. Lunar and Planetary Institute, Houston. 227 pp.

Elholou, S., Belousova, E., Griffin, W.L., Pearson, N.J. and O'Reilly, S.Y., 2006. Trace element and isotopic composition of GJ-red zircon standard by laser ablation. *Geochimica et Cosmochimica Acta*, *70*(18), p.A158.

Fretzdorff, S., Livermore, R.A., Devey, C.W., Leat, P.T. and Stoffers, P., 2002. Petrogenesis of the back-arc east scotia ridge, south Atlantic ocean. *Journal of Petrology*, *43*(8), pp.1435-1467.

Grant, F.S., 1984. Aeromagnetic, geology and ore environments: II Magnetite and ore environments.Geoexploration, 24. pp. 335-362.

Gruau, G., Martin, H., Leveque, B., Capdevila, R. and Marot, A., 1985. Rb—Sr and Sm—Nd geochronology of lower Proterozoic granite—greenstone terrains in French Guiana, South America. *Precambrian Research*, *30*(1), pp.63-80.

Heubeck, C. and Lowe, D.R., 1994. Depositional and tectonic setting of the Archean Moodies Group, Barberton greenstone belt, South Africa. *Precambrian Research*, *68*(3-4), pp.257-290.

Hey, R.N., Sinton, J.M. and Duennebier, F.K., 1989. Propagating rifts and spreading centers. *The Geology of North America*, pp.161-176.

Irvine, T.N.J. and Baragar, W.R.A.F., 1971. A guide to the chemical classification of the common volcanic rocks. *Canadian journal of earth sciences*, *8*(5), pp.523-548.

Jackson, S.E., Pearson, N.J., Griffin, W.L. and Belousova, E.A., 2004. The application of laser ablation-inductively coupled plasma-mass spectrometry to in situ U–Pb zircon geochronology. *chemical Geology*, *211*(1), pp.47-69.

Janoušek, V., Farrow, C.M. and Erban, V., 2006. Interpretation of whole-rock geochemical data in igneous geochemistry: introducing Geochemical Data Toolkit (GCDkit). *Journal of Petrology*, *47*(6), pp.1255-1259.

Jensen, L.S., 1976. *A new cation plot for classifying subalkalic volcanic rocks*.Ont. Div. Mines, Misc. Pap. No. 66, pp. 21

Jost, H., Carvalho, M.J., Rodrigues, V.G. and Martins, R., 2014. Metalogênese dos greenstone belts de Goiás. *Metalogênese das províncias tectônicas brasileiras, Belo Horizonte, CPRM*, pp.141-168.

Kusky, T.M. and Polat, A., 1999. Growth of granite–greenstone terranes at convergent margins, and stabilization of Archean cratons. *Tectonophysics*, *305*(1), pp.43-73.

Le Maitre, R.W.B., Dudek, P., Keller, A., Lameyre, J., Le Bas, J., Sabine, M.J., Schmid, P.A., Sorensen, R., Streckeisen, H., Woolley, A. and Zanettin, A.R., 1989. *A classification of igneous rocks and glossary of terms: Recommendations of the International Union of Geological Sciences, Subcommission on the Systematics of Igneous Rocks* (No. 552.3 CLA). International Union of Geological Sciences.

Lesnov, F.P., 2010. *Rare Earth Elements in Ultramafic and Mafic Rocks and their Minerals: Main types of rocks. Rock-forming minerals*. CRC Press.

Lobato, L., Ribeiro-Rodrigues, L., Zucchetti, M., Noce, C., Baltazar, O., Da Silva, L. and Pinto, C., 2001. Brazil's premier gold province. Part I: The tectonic, magmatic, and structural setting of the Archean Rio das Velhas greenstone belt, Quadrilátero Ferrífero. *Mineralium Deposita*, *36*(3), pp.228-248.

Lowe, D.R. and Byerly, G.R. eds., 1999. *Geologic evolution of the Barberton greenstone belt, South Africa* (Vol. 329).Geological Society of America, 329, pp. 1-36.

Magalhães, L.A., Souza Filho, C.R. & Silva, A.M. (2007). Caracterização geológica – geofísica da porção central do Amapá com base em processamento e interpretação de dados aerogeofísicos. Revista Brasileira de Geociências. 37(3), pp 464-477.

McReath, I. and Faraco, M.T.L., 2006. Paleoproterozoic greenstone-granite belts in northern Brazil and the former Guyana Shield-West African craton province. *Geologia USP. Série Científica*, *5*(2), pp.49-63.

Melson, W.G., Vallier, T.L., Wright, T.L., Byerly, G. and Nelen, J., 1976. Chemical Diversity of Abyssal Volcanic Glass Erupted Along Pacific, Atlantic, and Indian Ocean Sea Floor Spreading Centers. *The geophysics of the Pacific ocean basin and its margin*, pp.351-367.

Noce, C.M., Pedrosa-Soares, A.C., Silva, L.C., Alkmim., F.F. 2007. O embasamento Arqueano e Paleoproterozóico do Orógeno Araçuaí. Geonomos, 15 (1), pp. 17-23.

Parson, L.M. and Wright, I.C., 1996. The Lau-Havre-Taupo back-arc basin: A southward-propagating, multi-stage evolution from rifting to spreading. *Tectonophysics*, *263*(1-4), pp.1-22.

Pearce, J.A., 1982. Trace element characteristics of lavas from destructive plate boundaries. *Andesites*, *8*, pp.525-548.

Pearce, J.A., 1983. Role of the sub-continental lithosphere in magma genesis at active continental margins. In: Hawkesworth, C.J., Norry, M.J. (Eds.), Continental Basalts and Mantle Xenoliths. Shiva Publishing, Nantwich, pp. 230–249.

Pearce, J.A. and Stern, R.J., 2006. Origin of back- arc basin magmas: Trace element and isotope perspectives. *Back-Arc Spreading Systems: Geological, Biological, Chemical, and Physical Interactions*, pp.63-86.

Pearce, J.A., 2008. Geochemical fingerprinting of oceanic basalts with applications to ophiolite classification and the search for Archean oceanic crust. *Lithos*, *100*(1), pp.14-48.

Pimentel, M.M., Spier, C.A. and Ferreira Filho, C.F., 2002. Estudo Sm-Nd do Complexo Máfico-Ultramáfico Bacuri. Amapá: Idade da Intrusão, Metamorfismo e Natureza do Magma Original.*Revista Brasileira Geociências 32,* pp. 371-376

Rosa-Costa, L.D., Ricci, P.S.F., Lafon, J.M., Vasquez, M.L., Carvalho, J.M.A., Klein, E.L. and Macambira, E.M.B., 2003. Geology and geochronology of Archean and Paleoproterozoic domains of the southeastern Amapá and northwestern Pará, Brazil–southeastern Guiana Shield. *Géologie de la France*, *2*(3), pp.4.

Rosa-Costa, L.T., Lafon, J.M. and Delor, C., 2006. Zircon geochronology and Sm–Nd isotopic study: further constraints for the Archean and Paleoproterozoic geodynamical evolution of the southeastern Guiana Shield, north of Amazonian Craton, Brazil. *Gondwana Research*, *10*(3), pp.277-300.

Rosa-Costa, L.T., Silva, C.M.G., Barbosa, J.P.O. and Costa Neto, M.C., 2012. Projeto Folha Rio Araguari e NA. 22-YB. *Mapa Geológico (1: 250.000). CPRM, Belém*.

Santos, J.O.S.; Hartmann, L.A.; Gaudette, H.E.; Groves, D.I.; Mcnaughton, N.J.; Fletcher, I.R. 2000. A new understanding of the provinces of the Amazon Craton based on integration of field mapping and U-Pb and Sm-Nd geochronology.*Gondwana Research*, 3(4), pp. 453-488.

Serviço Geológico do Brasil (CPRM). (2004). Programa Geologia do Brasil, Projeto Aerogeofísico Rio Araguari, *Relatório Final do levantamento e processamento dos dados magnetométricos e gamaespectrométricos*. Rio de Janeiro: Lasa Engenharia e Prospecções S/A. (Texto Técnico, I),p.p 136

Shervais, J.W., 1982. Ti-V plots and the petrogenesis of modern and ophiolitic lavas. *Earth and planetary science letters*, *59*(1), pp.101-118.

Sinton, J.M., Wilson, D.S., Christie, D.M., Hey, R.N. and Delaney, J.R., 1983.Petrologic consequences of rift propagation on oceanic spreading ridges. *Earth and Planetary Science Letters*, *62*(2), pp.193-207.

Spier, C.A. and Ferreira Filho, C.F., 1999.Geologia, Estratigrafia e Depósitos Minerais do Projeto Vila Nova, Escudo das Guianas, Amapá, Brasil. *Revista Brasileira de Geociências*, *29*(2), pp.173-178.

Tassinari, C.C. and Macambira, M.J., 1999. Geochronological provinces of the Amazonian Craton. *Episodes-Newsmagazine of the International Union of Geological Sciences*, *22*(3), pp.174-182.

Tassinari, C.C.G.; Bettencourt, J.S.; Geraldes, M.C.; Macambira, M.J.B.; Lafon, J.M. 2000.The Amazonian Craton. In: Cordani, U.G.; Milani, E.J.; Filho, A.T.; Campos, D.A. (eds.) Tectonic Evolution of South America. Rio de Janeiro, *31º International Geological Congress*, SBG. pp. 41-95.

Teixeira, W., Tassinari, C.C.G., Cordani, U.G. and Kawashita, K., 1989. A review of the geochronology of the Amazonian Craton: tectonic implications. *Precambrian Research*, *42*(3-4), pp.213-227.

Winchester, J.A. and Floyd, P.A., 1977. Geochemical discrimination of different magma series and their differentiation products using immobile elements. *Chemical geology*, *20*, pp.325-343.

Zeh, A., Gerdes, A. and Barton Jr, J.M., 2009. Archean accretion and crustal evolution of the Kalahari Craton—the zircon age and Hf isotope record of granitic rocks from Barberton/Swaziland to the Francistown Arc. *Journal of Petrology*, *50*(5), pp.933-966.

Zeh, A., Gerdes, A. and Heubeck, C., 2013. U–Pb and Hf isotope data of detrital zircons from the Barberton Greenstone Belt: constraints on provenance and Archaean crustal evolution. *Journal of the Geological Society*, *170*(1), pp.215-223.

| ANEXO I |
| --- |
| Título da Dissertação/Tese: |
| ***"EVOLUÇÃO GEOTECTÔNICA DOS COMPLEXOS VILA NOVA E TUMUCUMAQUE NA PORÇÃO NORDESTE DO CRÁTON AMAZÔNICO, AMAPÁ"*** |
| Área de Concentração: Geoquímica |
| Autor: **Cristiano Borghetti** |
| Orientador: Prof. Dr. Ruy Paulo Philipp |
| Examinador: Prof. Dr. Roberto Sacks de Campos |
| Data: 14/09/2018 |
| Conceito: A (EXCELENTE) |
| PARECER: |
| PARECER EM ANEXO. |

Assinatura: Data: 14/09/2017

Ciente do Orientador:

Ciente do Aluno:

**ANEXO I**

Título da Dissertação/Tese:

***"EVOLUÇÃO GEOTECTÔNICA DOS COMPLEXOS VILA NOVA E TUMUCUMAQUE NA PORÇÃO NORDESTE DO CRÁTON AMAZÔNICO, AMAPÁ"***

Área de Concentração: Geoquímica

Autor: **Cristiano Borghetti**

Orientador: Prof. Dr. Ruy Paulo Philipp

Examinador: Prof. Dr. Edinei Koester

Data: 14 de setembro de 2018

Conceito: "A" (Excelente)

PARECER:

A tese acima mencionada apresenta sob ponto de vista de forma algumas melhorias que podem ser observadas principalmente na parte introdutória do trabalho, mas que não desmerecem a qualidade do trabalho. A apresentação oral do candidato foi excelente, auxiliando o "leitor" no entendimento do trabalho. Sob ponto de vista de conteúdo, o candidato apresenta conteúdos de campo, geofísica, estrutural, petrografia, e dados isotópicos U-Pb e Lu-Hf, interagindo com dados da literatura de geoquímica. Aliado a grande quantidade de dados sugere-se integrar e discutir os mesmos, envolvendo o cenário geológico da região do Cráton Amazônico. Assim considero o candidato "Aprovado".

Assinatura: Data: 14/09/2018

Ciente do Orientador:

Ciente do Aluno:

| ANEXO I |
| --- |
| Título da Dissertação/Tese: |
| ***"EVOLUÇÃO GEOTECTÔNICA DOS COMPLEXOS VILA NOVA E TUMUCUMAQUE NA PORÇÃO NORDESTE DO CRÁTON AMAZÔNICO, AMAPÁ"*** |
| Área de Concentração: Geoquímica |
| Autor: **Cristiano Borghetti** |
| Orientador: Prof. Dr. Ruy Paulo Philipp |
| Examinador: Prof. Dr. Rômulo Machado |
| Data: 14/09/18 |
| Conceito: A (EXCELENTE) |
| PARECER: ANEXO |

# PARECER

*Assunto*: Tese de Doutorado de **Cristiano Borghetti** "Evolução Geotectônica dos complexos Vila Nova e Tumucumaque na porção nordeste do Cráton Amazônico, Amapá"

*Examinador*: Prof. Dr. Rômulo Machado, Instituto de Geociências da USP.

A Tese de Doutorado do candidato acha-se organizada em formato de artigos e apresenta conteúdo de excelente qualidade. O trabalho objetiva caracterizar a evolução geotectônica das unidades dos complexos Vila Nova e Tumucumaque, no Amapá. Para isso, o autor valeu-se de informações de campo (mapeamento geológico e integração de dados geofísicos), análises estratigráficas de furos de sondagem, dados petrográficos, estruturais, geoquímicos (elementos maiores, traços e terras raras) e análises geocronológicas pelos métodos U-Pb e Lu-Hf (em zircão). Os dados são tratados adequadamente e sustentam as conclusões apresentadas nos artigos.

A tese estruturada em formato de artigos pode ser dividida em duas partes: a primeira contempla uma introdução sobre o tema, incluindo localização da área estudada, contexto geotectônico, resumo dos quatro artigos que integram a teste e conclusões. A segunda parte inclui a cópia dos quatro artigos: três deles já publicados - um na Revista Geologia USP e dois no *Journal South America Earth Sciences*- e o quarto foi submetido na *Precambrian Research*.

O primeiro artigo intitula-se '*Geologia e geofísica do greenstone belt Vila Nova, porção NE do Cráton Amazônico, Amapá, Brasil*', e contempla a integração de dados aerogeofísicos (magnetometria e gamaespectroscopia) com dados de campo oriundos de mapeamenento geológico. Os resultados permitiram separar as unidades metavulcano-sedimentares do *greentone belt* Vila Nova das unidades do embasamento (Complexo Tumucumaque), bem como definir lineamentos nas imagens, os quais correspondem no terreno a zonas de cisalhamento dúcteis com movimentação sinistral com componente inversa.

O segundo artigo, intitulado '*Geochronology of the Archean Tumucumaque Complex, Amapá Terrane, Amazonian Craton, Brazil*', apresenta estudos isotópicos pelos métodos U-Pb e Lu-Hf em zircão, a partir de ortognaisses, metagranodioritos e gabros do Complexo Tumucumaque. Foram obtidas idades de cristalização entre 2,8 e 2,6 Ga, sugerindo a existência de eventos magmáticos orogênicos durante o Arqueano. Os dados de Lu-Hf sugerem rochas formadas principalmente por retrabalhamento crustal.

O terceiro artigo intitula-se '*U-Pb zircon geochronology and Lu-Hf isotopes of the Vila Nova greenstone belt: arc-related association of the Rhyacian orogeny in the northern Amazonian Craton*' e contempla a caracterização isotópica pelos métodos U-Pb e Lu-Hf em zircão de rochas metavulcânicas (andesitos) e metassedimentares (quartzito e metaconglomerado) do Complexo Vila Nova (CVN). Inclui também dados estruturais e a integração de dados aerogeofísicos (magnetometria e gamaespectroscopia). As idades obtidas (2,17 e 2,15 Ga) sugerem que a Bacia Vila Nova evoluiu durante o Riaciano, e foi afetada por metamorfismo orogênico entre 2,15 e 2,07 Ga. Os zircões detríticos (entre 3,6 e 3,0 Ga) indicam proveniência a partir da erosão de rochas do embasamento (complexos Tumucumaque e Guianense).

O quarto artigo intitulado '*Geochemistry and origin of the tholeiitic metabasalts from the 2.15 Ga Vila Nova greenstone belt, Guiana Shield, Brazil*' envolveu a integração de mapeamento geológico e estrutural, com análises estratigráficas de furos de sondagem selecionados, análises petrográficas, geoquímicas e isotópicas pelos métodos U-Pb e Lu-Hf em zircão de rochas metavulcânicas (basaltos e basalto andesítico) do Complexo Vila Nova (CVN). Este artigo investigou principalmente a origem das rochas metavulcânicas no referido complexo. Os resultados indicam vulcanismo entre 2,17 e 2,15 Ga, seguido por metamorfismo orogênico entre 2,15 e 2,17 Ga. Os metabasaltos teriam sido originados em ambientes tectônicos de arcos de ilha e de retro-arco (grupo rico em Fe-Ti).

Por fim, conclui-se que a Tese de Doutorado do **Cristiano Borghetti** representa uma inestimável contribuição ao estudo geotectônico dos complexos Vila Nova e Tumucumaque, no Amapá. O candidato valeu-se do uso de diferentes metodologias, mapeamento geológico, integração de dados aerogeofísicos (magnetometria e gamaespectroscopia), análises estratigráficas de furos de sondagem, descrições petrográficas, dados estruturais, geoquímicos e datações isotópicas pelos métodos U-Pb e Lu-Hf em zircão. Os resultados apresentados para estes complexos são compatíveis com um modelo tectônico de formação de um proto-oceano no Riaciano, e geração de magmatismo básico e sedimentos siliciclásticos maturos de margem passiva. Após isso, houve o fechamento do oceano entre 2,18 e 2,13 Ga, produzindo um magmatismo orogênico pouco evoluído, caracterizado pela formação de arcos intra-oceânicos e sequências vulcano-sedimentares relacionadas à bacias de arco. As zonas de cisalhamento teriam sido geradas após colisão e metamorfismo entre os dois blocos arqueanos.

Face ao exposto, considero o candidato aprovado e habilitado para que lhe seja conferido o título de Doutor em Geociências da Universidade Federal do Rio Grande do Sul.

São Paulo, 13 de setembro de 2018.

Rômulo Machado
Professor Titular do Instituto de Geociências da USP

Assinatura: Data:

Ciente do Orientador:

Ciente do Aluno: